Romanian Journal of MINERALOGY

continuation of

DĂRI DE SEAMĂ ALE ŞEDINŢELOR INSTITUTULUI DE GEOLOGIE ŞI GEOFIZICĂ
COMPTES RENDUS DES SÉANCES DE L'INSTITUT DE GÉOLOGIE ET GÉOPHYSIQUE
(1. Mineralogie–Petrologie)

Founded 1906 by the Geological Institute of Romania

ISSN 1220-5621

Vol. 76
Part 1

CONTENTS

(Contents continued on outside back cover)

Institutul de Geologie şi Geofizică
Bucureşti – 1993

Romanian Journal of MINERALOGY

Published annually by the Institute of Geology and Geophysics, Bucharest
Director Ion Rădulescu

Editorial Office:
Institute of Geology and Geophysics
Str. Caransebeş 1
78344 Bucureşti–32, Romania
Tel. 65 75 30; 65 66 25
Fax. 010-40-0-12 84 44

The manuscripts should be sent to the scientific editor and/or executive secretary and the correspondance concerning advertisements, announcements and subscriptions to the executive secretary.

This journal follows the rules of the Commission on New Minerals and Mineral Names of the IMA in all matters concerning mineral names and nomenclature.

The **Romanian Journal of Mineralogy** (Rom. J. Mineralogy) is now at its first volume in the new form. However, the publication goes back to 1910, as the first volume of the "Dări de seamă ale Şedinţelor"(D.S.) has appeared as proceedings of geologists working with the Geological Institute of Romania. The journal (D.S.) appeared initially as a single volume (till volume 54, 1969), then with five series, the present issue being a direct continuation of the D.S./series 1(Mineralogy and Petrology).

The editor has changed the name as follows: Institutul Geologic al României (vol. I–XXXVI, 1910–1952), Comitetul Geologic (vol. XXXVII–LII/1, 1953–1966), Comitetul de Stat al Geologiei (vol. LII/2–LV/1, 1967–1969), Institutul Geologic (vol. LV/2–LX, 1970–1974), Institutul de Geologie şi Geofizică (vol. LXI–74, 1975–1990).

The **Institute of Geology and Geophysics** is now publishing the following periodicals:

Romanian Journal of Mineralogy
Romanian Journal of Petrology
Romanian Journal of Mineral Deposits
Romanian Journal of Paleontology
Romanian Journal of Stratigraphy
Romanian Journal of Tectonics and Regional Geology
Romanian Journal of Geophysics

as well as other publications.

Classification index for libraries 55(058)

Printed by the Institute of Geology and Geophysics

ANUNŢ

Societatea Mineralogică a României, înfiinţată cu ocazia primului simpozion naţional de mineralogie (Cluj-Napoca, octombrie 1992), cu personalitate juridică din luna martie 1993, a fost primită în rîndurile membrilor Uniunii Mineralogice Europene (EMU) şi Asociaţiei Internaţionale de Mineralogie (IMA).

Pentru a realiza o legătură directă şi permanentă între IMA, EMU şi mineralogii români, *Rom J. Mineralogy* devine şi Buletinul Societăţii Mineralogice a României, editorul revistei rămînînd Institutul de Geologie şi Geofizică.

Prin afilierea societăţii noastre la IMA şi EMU, toate recomandările privind nomenclatura mineralogică devin obligatorii pentru cei care doresc să publice lucrări în *Rom. J. Mineralogy*. Începem cu acest număr publicarea acestor recomandări prin reproducerea integrală a articolului "Solid Solutions in Mineral Nomenclature", pentru care am primit acordul autorului, Dr. E. H. Nickel. În partea a doua a volumului 76 va fi reprodusă lucrarea "Procedures Involving the IMA Commission on New Minerals and Mineral Names, and Guidelines on Mineral Nomenclature", autorii fiind E. H. Nickel şi J. A. Mandarino (vicepreşedinte, respectiv preşedintele Comisiei de Minerale Noi şi Denumiri de Minerale a IMA).

Ne exprimăm şi pe această cale gratitudinea faţă de Prof. Dr. Stefan Hafner, secretarul general al IMA, Prof. Dr. G. Ferraris, preşedintele EMU, precum şi consiliilor de conducere ale IMA şi EMU pentru înţelegerea şi sprijinul acordate Societăţii Mineralogice a României în vederea obţinerii, fără eforturi financiare, a calităţii de membru al celor două organisme mineralogice.

NOTICE

The Mineralogical Society of Romania has been founded on the occasion of the first national symposium on Mineralogy, held in Cluj-Napoca (October 1992). Thereafter (March 1993) the society has achieved the legal status of a non-profit organization and became member of the EMU and IMA.

In order to ensure a direct and permanent liaison between IMA, EMU and the Romanian mineralogists, the *Rom. J. Mineralogy* becomes also the Bulletin of the Mineralogical Society of Romania. The main editor remains, however, the Institute of Geology and Geophysics.

The application at IMA implies that all recommendations concerning mineral nomenclature become compulsory for everybody wishing to publish papers in *Rom. J. Mineralogy*. To facilitate this, we commence now the publications of such recommendations with the paper "Solid Solutions in Mineral Nomenclature", for which the author's (Dr. E. H. Nickel) permission has been achieved. In part two of the vol. 76 of *Rom. J. Mineralogy* the paper "Procedures Involving the IMA Commission on New Minerals and Mineral Names, and Guidelines on Mineral Nomenclature", will also published; the authors are E. H. Nickel and J. A. Mandarino, vice-president and president, respectively, of the IMA Commission on New Minerals and Mineral Names.

We wish to express here our gratitude to Prof. Stefan Hafner, secretary of IMA and to Prof. G. Ferraris, president of EMU as well as to the IMA and EMU councils for the assistance in obtaining the IMA and EMU memberships, which in the next years shall be free-of-charge for the Mineralogical Society of Romania.

Dr. G. Udubaşa

Reprezentant naţional al României la IMA — IMA National Representative for Romania

Gh. Ilinca

Secretar ad-interim al Societăţii Mineralogice a României — Secretary(ad-interim) of the Mineralogical Society of Romania

IMA '94
16th General Meeting
of the
International Mineralogical Association

Pisa, Italy
Palazzo dei Congressi
3-8 September, 1994

Sponsored by:

Società Italiana di Mineralogia e Petrologia
European Mineralogical Union
Consiglio Nazionale delle Ricerche

Adresa pentru corespondenţă:
Prof. Stefano Merlino
Organizing Committe IMA'94
Dipartimento di Science della Terra
Università di Pisa
Via S. Maria 53
I-56126 Pisa
Italia
Fax: 39-(0)50-40976

Informaţii privind Congresul IMA'94 pot fi obţinute şi de la sediul Societăţii Mineralogice a României, Bucureşti-32, 78 344 Str. Caransebeş 1 (Dr. G. Udubaşa, Gh. Ilinca).

Rom. J. Mineralogy, 1993, 76, 1, p. 3–5

SOLID SOLUTIONS IN MINERAL NOMENCLATURE

Ernest H. NICKEL

Vice-chairman, Commission on New Minerals and Mineral Names, International Mineralogical Association

Divisoin of Mineral Products, CSIRO, Private Bag, Wembley, WA 6014, Australia

Key words: Solid solution. Order-disorder. Nomenclature.

Abstract: The paper comprehensively covers the aspect of mineral nomenclature of the members of solid-solution series, which include three categories, i.e. (1) complete solid-solutions without structural ordering, (2) solid-solutions with structural ordering, and (3) partial solid-solution series. As the matter has the approval of the CNMMN, the mineralogists wishing to publish papers in this journal are advised to adhere to the recommendations discussed below.

Introduction

Guidelines for mineral nomenclature recommended by the Commission on New Minerals and Mineral Names (CNMMN) of the International Mineralogical Association were summarized by Nickel and Mandarino (1987–1989) and published in most of the international mineralogical journals.

One aspect of mineral nomenclature that was not covered in the guidelines was the question of how members of solid-solution series should be named. This matter was initially discussed by the Nomenclature Subcommittee of the CNMMN, and the recommendations of that body were subsequently considered and modified by the full CNMMN membership. These deliberations culminated in a general consensus that is embodied in this paper. Although similar to brief recommendations have been published by the Commision on New Minerals and Minerals Names of the All-Union Mineralogical Society of the USSR Academy of Sciences (*Zap. Vses. Min. Ob.*, 1977, 106, p. 686–688), it is considered appropriate to publish this paper because it covers the subject more comprehensively and because it has the approval of the CNMMN.

Mineralogists wishing to give names to members of known solid-solution series are advised to adhere to the recommendations in this paper. However, to avoid confusion, mineral names or definitions already in the literature that contravene the recommendations should not be changed unless there are compelling reasons to do so, and then only if approved by a formal vote of members of the CNMMN.

Although general guidelines are recommended, readers will note that a certain degree of flexibility is permitted in the case of partial solid-solution series. Proposals for mineral names in this category will be judged by members of the CNMMN on the merits of each particular case.

Solid solutions can be considered in terms of three categories: complete solid solutions without structural ordering, solid solutions with structural ordering, and partial solid solutions. Mineral nomenclature in each of these categories is discussed below.

1. Complete solid-solutions without structural ordering

For purposes of nomenclature, a complete solid-solution series without structural ordering of the ions defining the end members is arbitrarily divided at 50 mole %, and the two portions are given different names, with each name applying to the compositional range from the end member to the 50 % mark. For the sake of brevity this will be called the '50 % rule'. In Figure 1, one name applies to the range A–c, and the other to the range c–B. A mineralogical example of this is the forsterite-fayalite series, $(Mg,Fe)_2SiO_4$, in which the name forsterite applies to the compositional range from Mg_2SiO_4 to $MgFeSiO_4$, and the name fayalite applies from Fe_2SiO_4 to $MgFeSiO_4$.

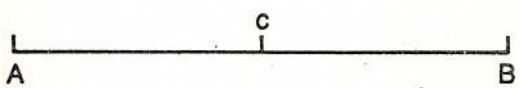

Fig. 1 – Diagrammatic representation of a complete binary solid-solution series. A and B represent the two end members, and c represents the mid-point (50 %).

Analogously, the 50 % rule applied to members of ternary solid-solution series implies that mineral names should be given only to the three end members, each name should apply to the compositional range from the end member to the nearest right bisectors of the sides of the composition triangle, as shown in Figure 2. For example, in the apatite series, $Ca_5(PO_4)_3(F,OH,Cl)$, the apices of the compositional triangle (Fig. 2) can be represented by F, OH and Cl, respectively, making A = fluorapatite, B = hydroxylapatite, and C = chlorapatite.

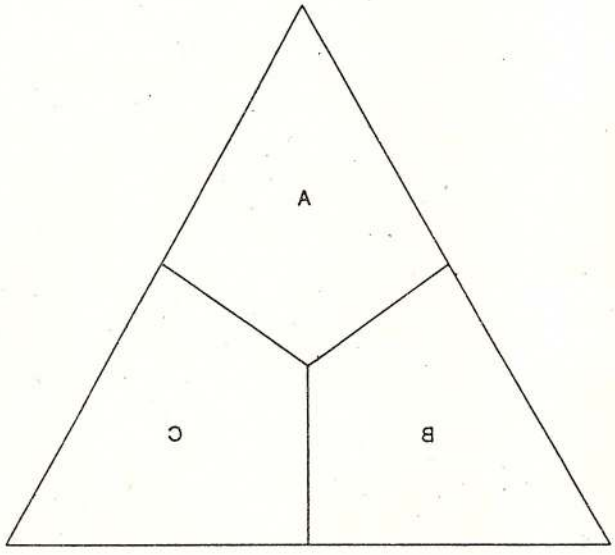

Fig. 2 – Diagrammatic representation of a complete ternary solid-solution series. A, B and C represent the three compositional fields, each of which merits a mineral name.

According to the same principle, in a multicomponent solid-solution series different mineral names can be given to isostructural or isotypic phases that have different chemical elements dominant in specified structural sites. An example of this is provided by minerals of the monazite series in which a number of different rare-earth elements can predominate in the cation structural site. The dominant element then specifies the appropriate "Levinson" suffix, e.g. monazite-(La).

2. Solid-solutions with structural ordering

If there is structural ordering of the ions that define the end members within an otherwise disordered solid-solution series, the ordered phase may be given a mineral name different from those of the end members. An example is provided by dolomite, $CaMg(CO_3)_2$, in which ordering of the Ca and Mg ions results in a crystal structure distinct from those of calcite and magnesite, the Ca and Mg end-members, respectively, of the (Ca, Mg)CO_3 series. It is recommended that the name of a newly-described ordered phase discovered in an existing solid-solution series be derived from, or related to, the name of the solid solution or one of the end members, although the author of the name is not obligated to do so.

3. Partial solid-solution series

If there is limited solid solution at one or more of the end members, and the solid solution does not extend to the 50 % mark, the 50 % rule is generally applied. Therefore, in Figure 3, the name of end-member A applies to the compositional range A–c and the name of end-member B applies to the range c–B, even if known compositions extend only to A′ or B′; this is to allow for the possibility of new chemical data extending compositions toward c. For purposes of nomenclature, it does not matter whether or not A and B are isostructural.

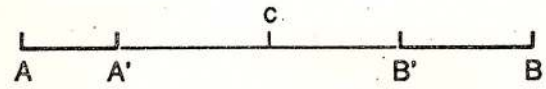

Fig. 3 – Diagrammatic representation of a partial binary solid-solution series in which A′–B′ represents the miscibility gap.

If the miscibility gap is one side of the 50 % mark, as in Figure 4, and if the phases represented by A–A′ and B–B′ are not isostructural, a separate name should not be given for the range B′c if it is very small, but if it is of substantial extent, then a separate name might be justified. The dividing line between a "small" range and a "substantial" one, in this case and others given below, can be taken as about 10 mole %, although each situation should be regarded on its own merits.

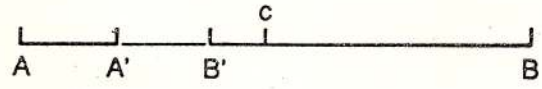

Fig. 4 – Diagrammatic representation of a partial binary solid-solution series in which A′–B′ represents the miscibility gap, and the range B–B′ encompasses the mid-point, c.

Similar considerations should apply to ternary or higher-order partial solid-solution series. Therefore, in a situation like that depicted in Figure 5, the field defined by composition FGED does not warrant a separate name if it is very small, but may be given a separate name if it is of substantial size.

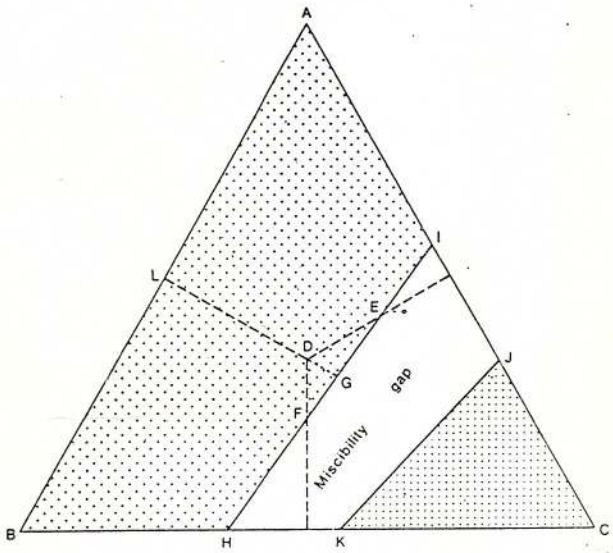

Fig. 5 – Diagrammatic representation of a partial ternary solid-solution series in which the area HKJI represents the miscibility gap, and D represents the mid-point of the triangle.

If the known compositions embrace the 50 % mark, but do not appear to extend to either end member (Fig. 6), only one name should apply to the compositional range. However, here again, the compositional range should be taken into account; if it is very small, then only one name should be given, but if it is large, consideration may be given to two names. An example of a mineral in this category is pentlandite, $(Ni,Fe)_9S_8$, the composition of which centres around Ni:Fe = 1:1, and compositions near the Ni and Fe end-members are not known.

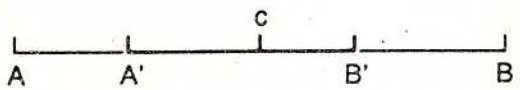

Fig. 6 – Diagrammatic representation of a partial binary solid-solution series in which the solid solution is limited to the region A′–B′.

The analogous situation in a ternary solid solution can be represented by Figure 7, in which known compositions cluster about a geometric boundary or boundaries. If the scatter of compositional points is small, only one name should be given to the cluster, but if the scatter is large, consideration can be given

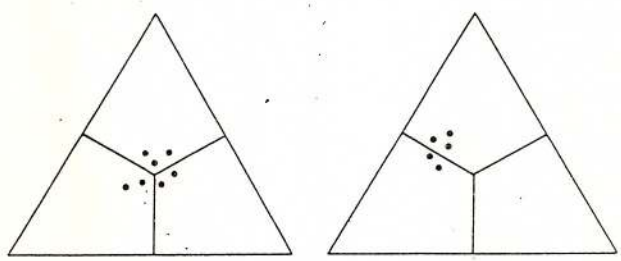

Fig. 7 – Diagrammatic representation of ternary solid solution series in which known compositions cluster about geometric boundaries.

to more than one name.

In cases such as those illustrated by Figures 6 and 7, one particular composition of a type specimen should be nominated as the type, because later work might well reveal a wider range of compositions justifying two (or more) names. One of these should be the name already in existence.

Reference

Nickel E. H., Mandarino J. A.: Procedures involving the IMA Commission on New Minerals and Mineral Names, and guidelines on mineral nomenclature. *Acta Petrol. Min.* 6 (1987), p. 252–278 (in Chinese); *Amer. Min.* 72 (1987), p. 1031–1042; *Bol. Soc. Esp. Min.* 12 (1989), p. 1–30 (in Spanish); *Bull. Min.* 110 (1987), p. 717–741; *Can. Min.* 25 (1987), p. 353–377; *Fortsch. Min.* 65 (1987), p. 175–196; *Indian J. Earth Sci.* 14 (1987), p. 152–188; *Min. J.* 13 (1987), p. 505–532; *Min. Mag.* 52 (1988), p. 275–292; *Min. Petrol.* 37 (1987), p. 157–179; *Min. Zhurnal* 11 (1) (1989), p. 51–86 (in Russian); *Rend. Soc. Ital. Min. Petrol.* 4 (1987), p. 27–53 (in Italian); *Riv. Min. Ital.* (1988), Supplemento al no. 1, p. 5–31 (in Italian); *Schweiz. Min. Petrogr. Mitt.* 67 (1987), p. 185–210.

Rom. J. Mineralogy, 1993, 76, 1, p. 7–13

PTX CONSTRAINTS OF ORE PARAGENESES WITH SOME CASE STUDIES

Gheorghe UDUBAŞA

Institutul de Geologie şi Geofizică. Str. Caransebeş 1, 78344 Bucureşti 32.

Key words: Paragenesis. Mineral assemblages. P-T conditions. Solid solution. Isotopes. Sulfur. Oxides. South Carpathians – Leaota Mountains.

Abstract: A hierarchy is proposed concerning the three "mineral units" already separated, i.e. mineral association (MAT), mineral paragenesis (MP) and mineral assemblage (MAG). In addition, the inherited paragenesis, the remote parageneses and apparent parageneses are defined, for which examples are given to support the classification proposed. Thus, case studies of the Co-Ni-Bi-Ag-U ores in the Leaota Mts and of the Fe-Ti oxide minerals in rocks and ores are presented as well as some comments on the relationships between parageneses and solid solution series and paramorphs or pseudomorphs.

1. General Remarks

The concept of mineral parageneses (MP) has been for many years matter of interesting discussions with different, partly controversial views (see Rösler et al., 1968; Craig et al., 1986; Commission on Paragenesis at the 8^{th} IAGOD Symposium, Ottawa, 1990). However, a generally accepted definition of the term still does not exist and thus further discussion on the topic seems to be necessary.

It is likely that the best way of defining the MP is to combine all the available data, experimental included, concerning the mineral species found together in a rock or ore sample or in a geological body. Subtle properties of the minerals such as their stable isotope compositions must be taken into consideration in order to test if all kinds of the equilibrium were attained.

A geological body, of rocks or ores, rarely appears as a result of a single or unique geological process. The minerals evolve in time and their changes are related to changes of the environment parameters. Generally speaking, as long as the PTX changes do not overstep the stability fields of the minerals, the coexisting minerals continue to form a MP, i.e. an association of minerals being under equilibrium conditions. If either of the minerals or some main properties of the minerals involved change, then it is appropriate to speak of "inherited parageneses". Parageneses formed under conditions of a metastability state, which is a form of equilibrium (Scott, 1974), are also included here.

The coexisting minerals can be formally identified by direct observations. However, for establishing if they really form a paragenesis, stability diagrams must be used in order to depict the PTX conditions and special analyses are needed, such as minor elements analyses, isotope analyses etc, in order to test if the equilibrium was attained.

Thus it is possible to trace the equilibrium trends in a geological body and also to identify the "remote parageneses", i.e. minerals formed at the same time but in different parts of the geological body by natural, continuous changes of the environment parametres. The term "remote parageneses" can eventually be extended over parageneses directly related to a genetical point of view, e.g. the copper and iron minerals in the copper porphyries such as chalcopyrite + pyrite + magnetite + bornite in the proper mineralized porphyries and enargite + luzonite + chalcocite in veins around them, which almost always form in direct relation to the porphyry copper systems.

The increasing state of knowledge decisively enlarges the possibility to discover new minerals and consequently new parageneses. In this respect it is perhaps not superfluous to speak of "apparent parageneses", when for example minerals of special composition are (mis)taken for common minerals. It is the case of the recently described chlorine-bearing PbSb sulfosalts (ardaite, dadsonite etc), the properties of which are similar to those of semseyite, boulangerite etc. Generally, in the solid solution or homologous series only small changes of one parameter may induce compositional and structural changes defining new minerals and thus new parageneses. Subtle varia-

tions of the sulfur fugacity produce transformation of jamesonite in robinsonite; the presence of water stabilizes the whole plagionite series towards high temperature (Moëlo, 1979, 1982). That is why the parageneses of the sulfosalts are so variable and are found together without any (apparent) special reason.

Stabilizing effects of the minor elements play also an important role in the formation of the manganese-bearing humites whose structure and composition are very closely related. Fluorine and zinc stabilize the leucophoenicite structure whereas zinc alone is a typical and compulsory element for sonolite (Dunn, 1985). Mixed layering structures such as those frequently encountered by the clay minerals and those more rarely found, e.g. at the leucophoenicite-jerrygibbsite (Yau and Peacor, 1986) show that either the minerals have very narrow stability fields or the changing parameters were not able to completely instabilize the older mineral(s).

From such cases the problem arose if a hierarchy may be made regarding the modes of coexistence of minerals. According to the older proposals of the author (Udubaşa, 1986, 1990) there may be separated the following units:

(1) Mineral association (MAT), including all the minerals that exist in a geological body, regardless of their age and equilibrium state. The "apparent parageneses" certainly belong here.

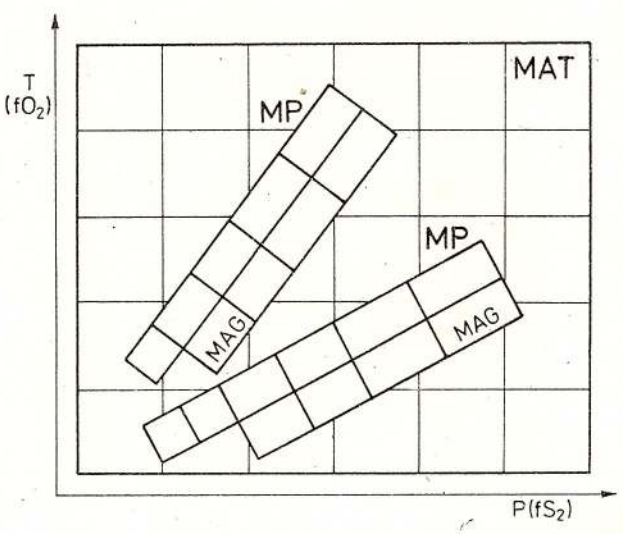

Fig. 1 – Schematical representation of mineral association (MAT), mineral paragenesis (MP) and mineral assemblage (MAG) in a theoretical TP or fO_2/fS_2 space.

(2) Mineral paragenesis (MP), consisting of minerals formed under equilibrium conditions or completely re-equilibrated in time by continuous changes of the PTX parameters; that is, the minerals remain within their stability fields and/or metastable extensions. Subunits: inherited paragenesis, remote parageneses. A still unsolved problem is that of the polytypes, which may be treated either as mineral species or as mixed layer structures (e.g. the pyrrhotite group).

(3) Mineral assemblage (MAG), including minerals having direct boundaries or can be seen together in a thin or polished section. The incompletely re-equilibrated parageneses belong here.

Although the MAT, MP and MAG seem to be well-defined terms, it is quite clear that the limits between them must be regarded as being mobile, a fact primarily related to the state of knowledge. The inherited parageneses actually form a "bridge" between MP and MAG as the relict minerals do not always exhibit changes which can easily be depicted by usual methods. The relationships among the three units separated are schematically represented in Figure 1.

2. Some case studies

2.1. The Co-Ni-Ag-Bi-U association in the Leaota Mts

The crystalline massif of Leaota lies in the south-eastern part of the South Carpathians in Romania and consists of medium grade metamorphics of Upper Precambrian age belonging to the so-called Leaota Group. There are numerous ore occurrences irregularly distributed over the area. The ores form either stratabound lense-shaped bodies or veins of limited size. Their composition is extremely different. The main occurrences belong to the Schneiderhöhn's Co-Ni-Bi-Ag-U association. However, there also exist occurrences consisting of Fe-Cu sulfides, Pb-Zn sulfides and of Au with galena and some Bi. Controversial views are held as to the origin of the Leaota ores. Some people advocate the syngenetic character (Gurău et al., 1983, unpubl. data; Zincenco, 1985, unpubl. data) having in mind the stratabound development of some ore bodies. Opinions were also expressed favouring the epigenetic nature of all ores (Vlad, Dinică, 1984). However, convincing arguments supporting both opinions are lacking due to the fact that the main occurrences show mixed features.

Careful analysis of the mineral composition of the ore occurrences first led to a grouping of ores including ten types. Minor elements analyses and especially the sulfur isotope analyses showed that the typology of ores and ore bodies is much simpler and the number of the ore types has been reduced to five. Their main characteristics are given in Table 1. Although similar in some instances and often associated in space, the five occurrence types finally separated have distinctive features that do not allow acceptance of a single mineralizing process.

Depending on their supposed age, the ore types are the following:

Table 1
The Main Characteristics of the Leaota Ore Occurrences

Ore type	Mineral parageneses	Ass.nonmetallic minerals	Typical minor elements	Host rocks
GBR (veins; arg. alter.)	pyrite, sphalerite[x], galena, chalcopyrite, marcasite, (gold, pyrrhotite, wittichenite)	quartz calcite ankerite	Bi Ag	V,L[xx]
U (fracture veins)	uraninite, (pyrite, marcasite)	carb. matter		L, C
ND (discordant lenses in TT ores)	safflorite, tetrahedrite, chalcopyrite, sphalerite[x], galena, pyrite	calcite ankerite	Au	L, C
TT (fahlbands on mylonite planes)	pyrrhotite, pyrite, chalcopyrite, rutile, sphalerite[x], bismuth, bismuthinite, molybdenite	calcite	Bi	L, C
GP (shear-zone related quartz bodies)	pyrite, galena, gold, rutile, sphalerite[x], (chalcopyrite)	quartz (calcite)	Bi Ag	V–L, C
Syngenetic metallic minerals	pyrite – isolated grains or small lenses	quartz	Ni Co	V, L, C
	magnetite – porphyroblasts			L
	hematite-ilmenite sol sol -scattered grains			L, C

[x] Iron poor; In brackets – accessory or minor minerals.

[xx] Acc. to Gheuca and Dinică (1984, unpubl. data), the Leaota Group consists of three formations with different lithologies: Voineşti (V) Fm (gneisses dominated; amphibolites); Lereşti (L) Fm (partly retrogressed micaschists with albite and magnetite porphyroblasts; gneisses); Căluşu (C) Fm (ditto, more intensely retrogressed; greenschists with hematite–ilmenite). At the boundary between the Voineşti and Lereşti formations there exist granite bodies intruded on a shear plane of Hercynian age (Tatu, Săbău, 1987).

(1) GP-type (Ghimbav-Păltineţ). Shear-zone related quartz bodies with gold and sulfides forming nests and/or scattered grains. The ratio quartz (+calcite) : sulfides (+gold) is about 9:1. Alterations lack.

(2) TT-type (Tîncava-Tîbra). Iron and copper sulfides located in retrogressed rocks, reminiscent of the Skandinavian fahlbands. They appear in relation to shear planes containing black mylonites. The ore minerals are always enveloped in carbonate minerals, mostly calcite. Typical of these ores is their localization at different lithostratigraphic levels and the lack of alterations. A narrow range of sulfur isotope composition (average $\delta^{34}S$ of about –23 ‰) is also very typical. Worth mentioning is the presence of pyrite bands below and above the fahlbands-like lenses with a sulfur isotope composition distinct of the fahlbands. The pyrite bands are situated outside the mylonite planes but in their zone of influence.

(3) ND-type (Neguleţ-Dăniş). Veins or lenses cutting across the TT-type lenses, with which they always are spatially associated, a feature strongly suggesting again the resemblance with the fahlbands. The mineral composition is very complex. The most frequent assemblage consists of safflorite (an iron-rich intermediate member of the safflorite-löllingite solid solution series, sometimes with safflorite nuclei), chalcopyrite and tetrahedrite (with a Sb:As ratio of about 3:1). The alterations are slight or even lacking.

(4) U-type (many occurrences). Fracture fillings, sometimes spatially associated with the fahlbands. The uraninite fine grains are embedded in a partly anisotropized carbonaceous matter reminiscent of thucolite. The U-ores are probably the youngest among the Leaota mineralizations (may be of Alpine age). The relationships with the fahlbands are shown in Figure 2.

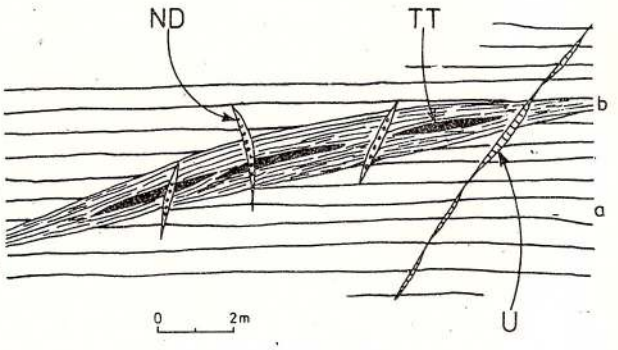

Fig. 2 – Relationships between the fahlband-like ores (TT-Tibra-Tincava) + ND (Neguleţ-Dăniş) and the late (Alpine?) uranium mineralization (U – pitchblende-thucholite) in the Leaota Mts. Country rocks are (a) micaschists and paragneisses with (b) sheared counter parts.

have quite different sulfur isotope compositions (Fig. 3). Formally, mineral associations exhibiting a range of the $\delta^{34}S$ values of about 40 ‰ are unlikely to have formed as a result of an unique mineralizing process. Such ores represent merely products of superposed processes and therefore contain overlapping mineral parageneses. The sulfur isotope composition of the TT-type ores is very striking, with a variation range from −33 ‰ to −19 ‰. A further interval from −15 ‰ to 10 ‰ corresponds to the values obtained for the pyrite forming bands or disseminations in quartz- or chlorite-rich rocks which accompany the fahlbands. The other ore types exhibit rather different isotope ratios, as a rule with positive values of the $\delta^{34}S$ (Fig.3).

On the fS_2/fO_2 diagram the main ore types occupy different fields suggesting again that the ores have formed under various conditions (Fig. 4). Scarcely occurring syngenetic pyrite grains or small lenses isotopically differ from the pyrite of the TT-type. On

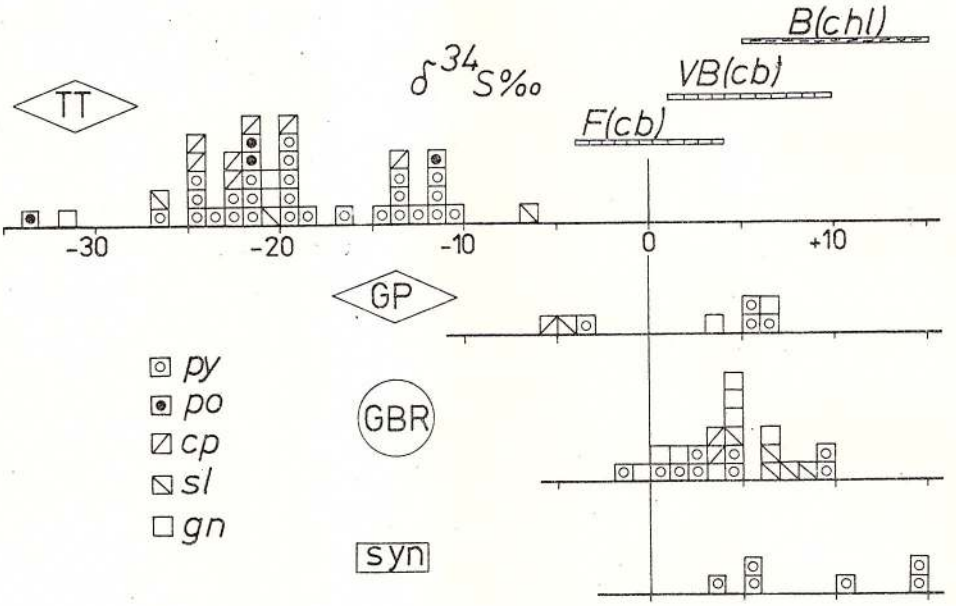

Fig. 3 – Sulphur isotope analyses of different ore types in the Leaota Mts (TT-Tibra-Tincava, GP-Ghimbav-Păltineţ, GBR-Grui-Brusture-Roşu, syn.syngenetic pyrite) as compared with the regionally metamorphosed ores in the East Carpathians (B-Bălan, in chlorite-rich rocks/chl; VB-Blazna Valley and F-Făgăraş Mts in carbonate-rich sequences).
Abbreviations: py, pyrite; po, pyrrhotite; cp, chalcopyrite; sl, sphalerite; gn, galena.

(5) GBR-type (Grui-Brusture-Roşu). Veins of limited development inlayed in rock sequences belonging to all the three formations of the Leaota Group. Significant alteration, especially argillic, occurs along the fracture veins. Nearby small pockets or lenses with massive fluorite or amethyst crystals may be found.

Beside the differences in the mineral composition and in the relationships to the host rocks, the ore types the diagram such pyrites are situated at rather high fO_2, suggested by the presence of the ilmenite-hematite solid solution in the host rocks. The isotopic difference between the syngenetic pyrite and the fahlbands-related one is too large, thus excluding a common origin.

Therefore it can be concluded that the Leaota ore types have formed under different conditions and at

different moments of the Phanerozoic evolution of the metamorphic rock pile.

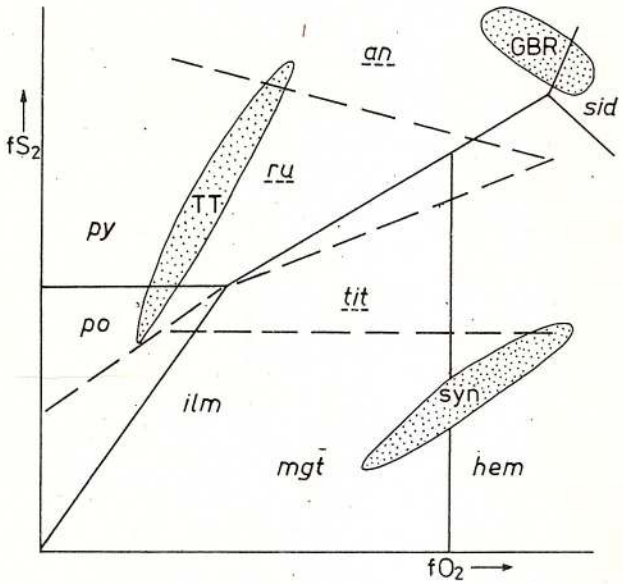

Fig. 4 – Position of different ore types in the Leaota Mts on the fS_2/fO_2 diagram of iron and titanium minerals (see Udubaşa, 1982 for details concerning the two superposed diagrams). See Fig. 3 for abbreviated ore types. Abbreviations: an, anatase; hem, hematite; ilm, ilmenite; mgt, magnetite; po, pyrrhotite; py, pyrite; ru, rutile; sid, siderite; tit, titanite.

Emplacement of some granite bodies on a generalized shear plane during Hercynian time is likely synchronous with the first phase ore accumulation (GP-type). The shear planes have been partly healed by quartz, thus preventing further motion. The second event is represented by fahlbands generation on locally developed shear planes with carbonates as residual products of shearing. Repeated movements on such planes led to abundant mylonite formation and the development of the Co-Ni-Cu ore veins, typically inlayed on the TT-type sulfide lenses (Fig. 2). Later thrusting resulted in the filling with U-ores of fractures of Alpine age or of Alpine reactivated shear planes. Their composition is restrictive and the abundance of carbonaceous matter poses the problem of its provenance from the overthrust sedimentary rocks of Cretaceous age.

Concluding, it can be said that the Leaota ore occurrences contain overlapping mineral parageneses with rather different compositions formed during a relatively long time interval. As most of the ore minerals shows isotopic disequilibrium, due to the repeated tectonic movements, the isotopic geothermometer cannot be applied and thus the formation temperatures are only indirectly deduced. For the TT-type ores it may be assumed that the (re)equilibration temperature did not reach 271^0 C, which is the melting point of bismuth. The absence of the reaction chalcopyrite + pyrrhotite $\rightleftharpoons$ pyrite + high cubanite taking place at 334^0 C (Yund and Kullerud, 1966) represents a further limitation towards higher temperatures. Such data severely contradict the temperature estimate of the peak metamorphism of the host rocks, for which the presence of grains of hematite-ilmenite solid solution indicate temperatures in excess of 600^0 C. For the ND-type (Co-Ni-Cu veins) temperatures of about 400^0 C may be deduced from the composition of the safflorite-löllingite solid solution. The contrasting conditions of the main ore types, crudely corresponding to mineral parageneses, are given in Table 2.

The overlapping mineral parageneses in the area studied nicely explain the lack of any regional zoning of ore occurrences, which is due to the non-uniform behaviour of the host rocks during sequential shearing and/or fracture opening.

Table 2
Estimation of formation conditions of the ore types

Ore type	fS_2	a_{As}	fO_2	T, ^{0}C	P_{CO_2}
BGR	high	–	low	medium	high
U	low	–	high	low	–
ND	low	high	low	medium	high
TT	medium	–	medium	low	medium
GP	medium	–	medium	medium	low
syng.py	v. low	low	high	medium	high

2.2 Parageneses of Fe-Ti oxide minerals

The analysis of the Fe-Ti oxide minerals distribution in various types of rock and ores allowed an empirical diagram to be drawn, which has been superposed on the known diagram of the iron minerals (Udubaşa, 1982). On this combined diagram (Fig. 5) some specific fields are traced for (a) thermic contacts of intrusive rocks with black shales, (b) porphyry copper systems and (c) epithermal gold-quartz veins. The typomorph significance is high, which is an important property of a paragenesis. Besides the main minerals shown in Table 3 there also appear other minerals such as chalcopyrite in (a), bornite in (b) and gold in (c) which, however, may lack. Such parageneses include only Fe-Ti oxides and iron sulfides and they would be better designated as partial parageneses (Teilparagenesen).

The accessory oxide minerals in magmatic rock have been comprehensively treated by Haggerty (1976). In addition, some supplementary data were obtained as concerns the behaviour of magnetite and ilmenite in the lava flows and the non-erupted rock bodies (Udubaşa, 1984). The difference consists in abundant development of maghemite and/or titanomaghemite at the expense of primary magnetites in the lava flows and of titanite at the expense of ilmenite in the non-erupted

rocks. Two inherited parageneses, i.e. magnetite + maghemite and magnetite + ilmenite + titanite, have been thus depicted bearing a high typomorph significance. They may be of help in the study of complex volcanic and volcano-plutonic structures.

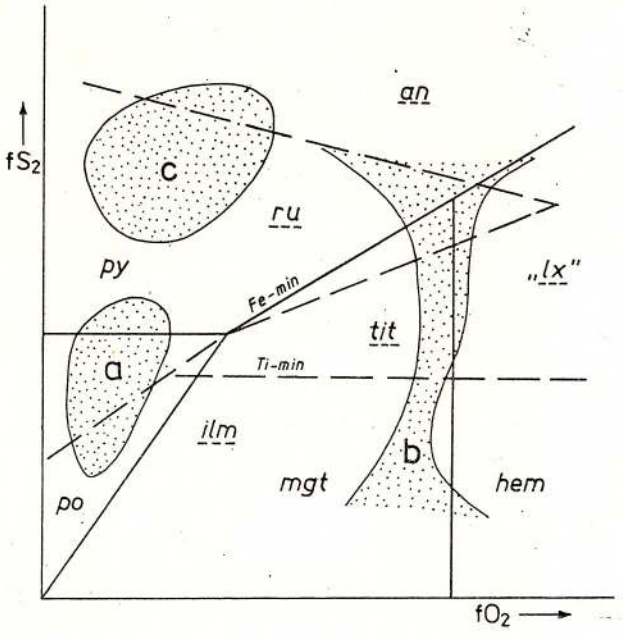

Fig. 5 – Stability field of titanium minerals parageneses from contact metamorphic rocks (a), porphyry coppers, (b) and epithermal gold ores, (c).
Abbreviations: see Figure 4; "lx" means "leucoxene".

Table 3
Some parageneses of the Fe-Ti oxide minerals

Magmatic rocks	
– lava flows	magnetite, maghemite
– non-erupted rocks	magnetite, ilmenite, titanite
Postmagmatic formations[x]	
– thermic contacts	pyrrhotite, rutile, chalcopyrite[xx]
– porphyry coppers	magnetite, hematite, titanite, rutile, pyrite, chalcopyrite
– gold-quartz veins	pyrite, rutile

[x] See diagram in the Figure 5

[xx] The whole paragenesis (po, ru, cp) occurs only in the contacting intrusive bodies, giving sometimes suggestions of a pervasive mineralization. In the hornfelsized black shale there are also pseudomorphs of pyrrhotite after framboidal pyrite, the coexisting minerals – po, ru, py – forming an "inherited paragenesis".

3. Discussion

The meaning of mineral paragenesis as used here is basically according to the final statement of the Breithaupt Colloquium 1966 (Rösler et al., 1968). The use of minor elements and of stable isotopes is really an important way in deciding if the associated minerals in a given geological body form a paragenesis or not. Attaining or destroying the isotopic equilibrium is a main feature of a true paragenesis and of an inherited paragenesis, respectively. The second term seems to be necessary as in some cases the mineral species remain the same but the isotopic composition changes significantly. Such examples are discussed by Udubaşa (1986); some hydrothermal base metal ore veins in Romania are locally affected by directional faulting. The sulfur isotope compositions of the affected and not affected sulfides show significant differences. The primary sulfide paragenesis of the hydrothermal veins (pyrite, galena, sphalerite, chalcopyrite) is accompanied by a new paragenesis consisting of the same sulfides but with different sulfur isotope ratios; in addition, the sphalerite becomes iron-poorer.

The term "remote parageneses" may be of importance in defining the simultaneously formed minerals in different parts of a geological body, say a vein, as a result of a monoascendent deposition. Interesting is the case of the paragenesis enargite + luzonite + chalcocite that practically appears only in the close vicinity of the porphyry copper systems and genetically directly connected with them. Such relationships may have also practical importance in discovering the blind porphyry systems.

Parageneses including solid solutions or homologous series are also a provoking matter of discussion, as their intermediate members develop by only very subtle changes of the environment parameters. Such changes escape the routine observations. If a slight doubt arises as to the correct identification of the minerals, then it would be better to use the term "apparent paragenesis".

The paramorphs and the pseudomorphs in relation to the associated minerals express the PTX controls outside and inside the composition fields of the minerals, respectively. Preserving the crystal morphology of the primary minerals, the paramorphs and pseudomorphs pose again the use of the term inherited parageneses, typically showing small compositional changes. In this respect, the regionally metamorphosed iron sulfide ores from the Cerna Valley in the South Carpathians offer a good example. Pseudomorphs of pyrrhotite after pyrite porphyroblasts, initially embedded in a matrix of fine grained pyrrhotite, have been interpreted as being produced by thermic effect related to granitoids. Two overlapping parageneses (two pyrrhotites with the corresponding pyrites)

form here an apparently simple ore but with a complex evolution.

Paramorphs of rutile after brookite have been described by Balintoni and Chiţimuş (1973) in the Lower Cambrian Tulgheş Group in the Eastern Carpathians, Romania. The depicted parageneses including the two polymorphs of TiO_2 helped to confirm the polymetamorphic evolution of the metamorphic rocks.

The proposed hierarchy including mineral association (MAT), mineral paragenesis (MP) and mineral assemblage (MAG) (Udubaşa, 1986, 1990) was intended to delineate coexisting minerals with different relationships among them, regarding the state of equilibrium, age relations, overlapping parageneses, inherited parageneses, polyascendent ore deposition etc. This proposal must be considered as matter of discussion in order to find out outstanding definitions of the term(s) – MAT, MP, MAG (if generally accepted). Such terms may be of help in studying the rocks and ores different genesis and evolution.

References

Balintoni I., Chiţimuş V. (1973) Prezenţa paramorfozelor de rutil după brookit în cristalinul seriei de Tulgheş (Carpaţii Orientali). *Stud. cerc. geol., geofiz., geogr., Seria Geologie*, 18, p. 329–334, Bucureşti.

Craig J. R., Hagni R. D., Kiesl W., Lange I. M., Petrovskaya N. V., Shadlun T. N., Udubaşa G., Augustithis S. S. (eds.) (1986) Mineral parageneses Theophrastus Publ., Athens, 696 p.

Dunn P. J. (1985) Manganese humites and leucophoenicites from Franklin and Sterling Hill, New Jersey: parageneses, compositions and implications. *Amer. Mineralogist*, 70, p. 379–387.

Haggerty S. E. (1976) Opaque mineral oxides in terrestrial igneous rocks. In: D. Rumble III (ed.) Oxide Minerals. Mineralog. Soc. America Short Course Notes 3, p. Hg 101–Hg 300.

Moëlo Y. (1979) Quaternary compounds in the system Pb-Sb-S-Cl: dadsonite and synthetic phases. *Canad. Mineralogist*, 17, p. 575–600, Toronto.

– (1982) Genesis of lead sulfosalts: some general principles. 13^{th} Gen. Meeting IMA '82, Varna. Abstracts of papers, p. 71, Publ. House Bulg. Acad. Sci.

Rösler H. J., Baumann L., Leeder O., Pfeiffer L., Starke R., Wolf M. (Red.) (1968) Probleme der Paragenese von Mineralen, Elementen und Isotopen. Breithaupt-Kolloquium 1966 in Freiberg. Teil II. *Freib. Forschungshefte* C 231, 299 p.

Scott S. D. (1974) Experimental methods in sulfide synthesis. In: P. H. Ribbe (ed.) Sulfide mineralogy. Mineralog. Soc. America. Short Course Notes 1, p. S 1-S 38.

Tatu M., Săbău G. (1987) The Albeşti granite: petrogenetic considerations. *D. S. Inst. Geol. Geofiz.*, 72-73/1, p. 275–286, Bucureşti.

Udubaşa G. (1982) Rutile of postmagmatic mineral formation. In: Amstutz G. C., Goresy A. El., Frenzel G., Kluth C., Moh G., Wauschkuhn A., Zimmermann R. A. (eds.) Ore genesis – the state of the art. Springer Berlin-Heidelberg, p. 784–793.

– (1984) Typomorphism of some ore minerals and a PvT classification of certain ore deposits. *An. Inst. Geol. Geofiz.*, LXIV, p. 141–152, Bucureşti.

– (1986) Parageneses of some opaque minerals in rocks and ores. In: Craig J. R. et al. (eds.) Mineral Parageneses. Theophrastus Publ., Athens, p. 55–74.

– (1990) Associations, paragenese and assemblages of ore minerals. 8^{th} Symp. IAGOD, Ottawa, august 12–18, 1990. Program with Abstracts, p. 166.

Vlad Ş., Dinică I. (1984) Vein mineralization of the Leaota Mountains; Preliminary considerations. *Rev. roum. géol., géophys., géogr., Série de géologie*, 28, p. 35–41, Bucureşti.

Yau Yu-Chyi, Peacor D. R. (1986) Jerrygibbsite-leucophoenicite mixed layering and general relations between the humite and leucophoenicite families. *Amer. Mineralogist*, 71, p. 985–988.

Yund R. A., Kullerud G. (1966) Thermal stability of assemblages in the Cu-Fe-S system. *Jour. Petrology*, 7, p. 454–488, Oxford.

Paper presented at the Breithaupt Colloquium, Sept. 16–18, 1991, Freiberg, Germany

Rom. J. Mineralogy, 1993, 76, 1, p. 15–21

MINERALOGY OF THE Fe–Mn ORE DEPOSIT AT RĂZOARE, PRELUCA MTS. I. TEPHROITE AND MANGANESE–BEARING HUMITES

Paulina HÂRTOPANU, Gheorghe UDUBAŞA, Constanţa UDRESCU, Corina CRISTEA

Institutul de Geologie şi Geofizică. Str. Caransebeş 1, 78344 Bucureşti 32.

Erna CĂLINESCU

"PROSPECŢIUNI" S.A. Str. Caransebeş 1, 78344 Bucureşti 32.

Key words: Nesosilicates. Olivine. Tephroite. Sonolite. Leucophoenicite. Alleghanyite. Retrograde metamorphism. Polymetamorphism. Mineral data. X-ray data. Infrared spectra. Preluca Mountains.

Abstract: Among the six mineral assemblages of the Răzoare Fe–Mn deposit, the tephroite + manganese-bearing humites one is the most typical, occurring in the lower, carbonate rich part of the ore-bearing sequence, which is silica-undersaturated. Sonolite, leucophoenicite and probably alleghanyite and ribbeite are intimately intergrown with tephroite giving as a rule mixed X-ray spacings. The most conspicuous feature of the manganese-bearing humites from Răzoare is their boron content reaching 2500 ppm. The assemblage tephroite + manganese-bearing humites reveals a lower grade, retromorphic phase in the evolution of the Precambrian ore-bearing metamorphic sequence. Its polymetamorphic character is suggested by the higher grade assemblage consisting of manganoan fayalite + orthopyroxene + calderitic spessartine.

Introduction

The manganese-iron deposit at Răzoare, Preluca Mts, Romania, is a stratiform concentration of iron-manganese minerals showing evidence of regional metamorphism under conditions of the upper amphibolite facies (Udubaşa et al., in press, 1993). The ores contain about 60 mineral species among which the recently identified manganese-bearing humites constitute characteristic phases of the deposit. The complex mineralogical composition of the ore suggests a polyphase metamorphic evolution; besides manganoan fayalite and ortopyroxene, many generations of pyroxmangite and dannemorite have formed as well as different types of magnetite. At least six mineral assemblages (some of them being typical parageneses) have been recognized at Răzoare; they differ in their position in the lithostratigraphical column of the ore sequence, in their belonging to the different metamorphic events and consequently in their composition. The leading minerals of the six assemblages are (1) manganoan fayalite, (2) tephroite-manganese-bearing humites; (3) pyroxmangite; (4) dannemorite; (5) spessartine and (6) rhodochrosite.

Mode of Presentation

The assemblage thephroite-manganese-bearing humites (further on MBH) forms bands or lenses up to 1.5 m thick especially within the lower, carbonate-rich part of the ore sequence (Fig. 1)

The most striking feature of this assemblage is its restrictive chemical and mineralogical compositions. The iron content is negligible as compared to the other assemblages. In addition, the tephroite and the MBH do not occur within the other assemblages and no fayalite, pyroxmangite, garnet or dannemorite have been observed within the tephroite–MBH assemblage. Coarse to medium aggregates of tephroite + MBH of reddish, reddish-brown to pinkish colour typically contain disseminations of black, subhedral or euhedral jacobsite grains reaching 2–5 mm in size. Generally, the leading minerals of the assemblage are the MBH. However, the jacobsite locally becomes the dominant species reaching up to 90 volume percent of the mineral aggregates. Apatite and/or carbonate fluorapatite are intimately intergrown with silicates and with the host rhodochrosite.

Commonly, the aggregates are massive with no bed-

ding which is typically developed in the other assemblages. Slight bedding may be sometimes observed only under the microscope as being due to grain flattening and/or twin planes orientation on metamorphic S – planes.

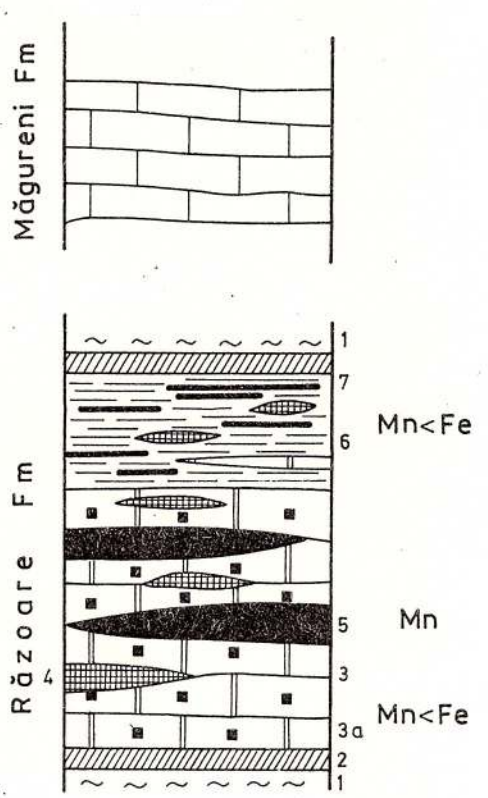

Fig. 1 – The lithostratigraphic column of the Răzoare Formation (thickness up to 60–70 m) showing the lower, carbonate rich part, silica subsaturated and the upper, amphibole-rich part, silica saturated (partly). 1, paragneisses and micaschists; 2, quartzites; 3, rhodochrosite matrix with jacobsite dissemination, lacking at the footwall (3a); 4, manganoan fayalite-rich lenses and pods; 5, tephroite + manganese-bearing humites: 6, dannemorite; 7, magnetite and/or pyrrhotite bands.

The abundance of the MBH at Răzoare is somewhat uncommon as in other regionally metamorphosed manganese deposits they occur only as accessory constituents. In Romania, Bălan (1976) has described only few microscopic grains of sonolite and alleghanyite in the Iacobeni manganese deposit, East Carpathians.

Physical and Optical Properties

The grain size of the tephroite and MBH varies between 0.1 and 1.0 cm. The grains are generally isometric, sometimes slightly flattened or have a lamellar development. The colour is highly variable from grey-lilac (typical of tephroite dominated aggregates) to red, reddish-orange, brownish red, rose or pink (the MBH aggregates). The grains are brittle and show a glassy luster and uneven fracture.

Microscopically, the minerals are quite similar, occurring as colourless grains of different dimensions, sometimes exhibiting a slight developed cleavage. The birefringence is high with bright colours but without specific teints. The 2 V angle is always negative with values of 70–72^0 for the MBH and of 50–60^0 for tephroite. Polysynthetic twins may be always observed at MBH (Pl. I, Figs. 1–4), sometimes with a symmetrical development. The tephroite grains are in places mantled by MBH, a feature observed also under the binocular microscope. Twinned "islands" of MBH occur also within the larger tephroite grains. Intergrowths of tephroite with carbonate fluorapatite are frequently encountered (Pl. I, Fig. 5). Some MBH samples gelatinize when treated with HCl, a feature known as characteristic of leucophoenicite (Winchell, Winchell, 1951).

Due to the advanced intergrowth state the MBH may commonly be identified only as mineral group and at first sight they may be mistaken for pyroxmangite. This is probably why the MBH have not been identified at Răzoare till now.

Age Relations

The tephroite seems to be the oldest mineral of the assemblage whereas the jacobsite is younger, tending to cement the silicate grains. The jacobsite forms also anhedral grains interrupting the MBH twins (Pl. I, Figs. 6, 7). Similar relationships to silicates show the phosphates (apatite and carbonate fluorapatite).

The associated carbonate is a rhodochrosite with low to very low contents of Fe, Mg and Ca (Tab. 1). It appears intergrown with silicates, sometimes substituting them; veining of silicates by a younger rhodochrosite generations has been observed too.

Table 1
Partial analyses of carbonates hosting the tephroite-MBH assemblage (%)

	MnO	FeO	CaO	MgO
1	52.18	–	4.87	1.56
2	54.82	–	2.41	0.70
3	53.15	–	2.34	1.80

The tephroite shows slight alterations to secondary manganese minerals such as bementite, pennantite and neotokite whereas the humites do not.

Table 2

Wet chemical analyses of tephroite (1), sonolite (2–3) and leucophoenicite (4–5) from Răzoare

	1	1^{x}	2	2^{x}	3	4	4^{x}	5	5^{x}
SiO_2	25.97	16.10	23.15	23.15	23.06	22.41	22.41	22.33	22.33
TiO_2	0.13	0.13	–	–	–	–	–	–	–
Al_2O_3	0.60	0.60	–	–	–	–	–	–	–
Fe_2O_3	–	–	0.05	–	–	0.83	–	1.40	–
FeO	–	–	0.61	0.61	–	–	–	–	–
MnO	62.20	36.98	62.89	62.87	64.98	59.92	59.55	62.89	62.27
MgO	1.19	1.19	1.08	1.08	1.21	2.37	2.37	1.71	1.71
CaO	0.09	0.03	1.07	0.78	0.86	1.74	1.19	0.78	0.78
P_2O_5	0.09	–	0.44	–	–	0.84	–	0.04	–
K_2O	0.01	0.01	0.05	0.05	–	0.06	0.06	0.05	0.05
Na_2O	0.08	0.08	0.03	0.03	0.04	0.04	0.04	0.04	0.04
H_2O	0.75	–	–	1.81^{xx}	2.26^{xxx}	2.27	2.23	2.58	2.32^{xx}
Number of ions on the basis of 4 O (1); 18 (O,OH)(2–3) and 14 (O,H)(4–5)									
Z site									
Si^{4+}		0.9660		3.8369	3.7726		2.9163		2.8787
Al^{3+}		0.0424		–	–		–		–
		1.0084		3.8369	3.7726		2.9163		2.8787
Y site									
Ti^{4+}		0.0059		–	–		–		–
Fe^{2+}		–		0.0845	–		–		–
Mn^{2+}		1.8793		8.8258	9.0042		6.5339		6.7995
Mg^{2+}		0.1064		0.2668	0.2951		0.4597		0.3286
Ca^{2+}		0.0019		0.1385	0.1507		0.1659		0.1077
K^{+}		0.0008		0.0106	–		0.0100		0.0082
Na^{+}		0.0093		0.0096	0.0127		0.0101		0.0100
		2.0036		9.3358	9.4627		7.1796		7.2540
	OH^{-}	–		2.0000	2.0000		1.9358		2.0000
Me^{2+}:Si		1.99		2.42	2.50		2.45		2.52

^{x} Recalculated analyses by eliminating P_2O_5 as $Ca_5(PO_4)_3(OH)$ and Fe_2O_3 as $MnFe_2O_4$.

^{xx} Calculated H_2O

^{xxx} Calculated value: 1.83

Calculated formulae:

1^{x} $(Mn_{1.88}Mg_{0.11}Ca_{0.002})_{2.013}(Si_{0.96}Al_{0.04})O_4$

2^{x} $(Mn_{8.83}Fe_{0.08}Mg_{0.27}Ca_{0.14})_{9.33}(Si_{0.96}O_4)_2(OH)_2$

3^{x} $(Mn_{9.00}Mg_{0.24}Ca_{0.15})_{9.46}(Si_{0.94}O_4)_2(OH)_2$

4^{x} $(Mn_{6.53}Mg_{0.46}Ca_{0.17})_{7.18}(Si_{0.97}O_4)_3(OH)_{1.94}$

5^{x} $(Mn_{6.80}Mg_{0.33}Ca_{0.11})_{7.25}(Si_{0.96}O_4)_3(OH)_2$

Chemical Analyses

For the time being only wet chemical analyses are available for the most uniformly coloured monomineralic samples. The results are given in Table 2. Due to the advanced intergrown state, the analyses had to be corrected for the formula calculation using a special programme created by G. Ilinca. In spite of correction the formulae are undersaturated with respect to Si and oversaturated with respect to Y site cations. Such features also appear by calculating the published analyses for sonolite (Cook, 1969) and leucophoenicite (Dunn et al., 1984). More reliable data were obtained for tephroite (no. 1 in Table 1) which can be compared with the published analyses of Peters et al. (1973). However, the calculated ratio Me^{2+} = Si for the MBH from Franklin is of 2.26 and 2.23, i.e. typical of sonolite (theoretical value 2.25) whereas for all chemical analyses from Răzoare the ratio Me^{2+}:Si varies between 2.42 and 2.52, near the theoretical value for the ribbeite-alleghanyite pair, i.e. 2.5, and slightly overpassing it, towards the still unknown equivalent(s) of norbergite, having the ratio Me^{2+}:Si of 3.

This chemical feature of the Răzoare MBH raises the problem of correct identification. However, the X-ray diffraction analyses indicate that the most frequently encountered powder pattern is that of sonolite. It is hoped that the microprobe analyses now in progress,

will help in elucidating this intriguing problem.

Minor Elements

The minor elements were determined by means of emission spectrography using synthetic standards with 77% MnO_2 and 23% SiO_2. Analytical errors are of about = 10%. The results are given in Table 3, which also includes some major elements (Mg, Fe, Ca) showing contents of 1–3 percent not differing much as compared with the wet chemical determinations (Tab. 2). There are few identified minor elements most of them being below the detection limit. The main conspicuous feature of the Răzoare MBII is the presence of boron, showing a large variation interval i.e. between 80 and 2500 ppm. However, there are two marked intervals of content variations: 80–240 and 1600–2500 ppm. Such discontinuous variations also show the Ni contents (4.5–26.0 and 58–75 ppm) (Fig. 2), not for the same samples as in case of boron. Noteworthy, the zinc content is below detection limit (100 ppm) in all the analysed samples. Higher Zn contents were recognized only in samples of pyroxmangite (140–400 ppm), seemingly the only Zn-bearer at Răzoare.

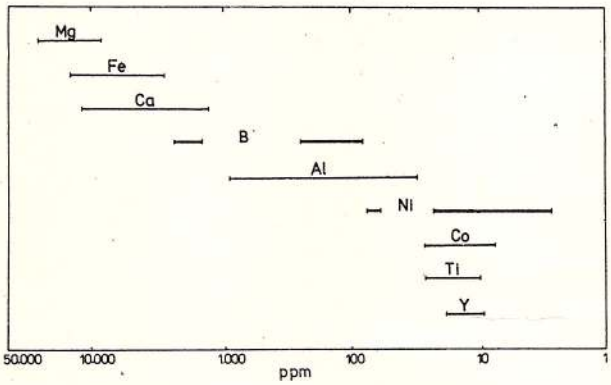

Fig. 2 – Variation intervals of spectrographically analysed elements.

Table 3
Emission spectrography analyses on manganese-bearing humites from Răzoare (ppm)

Sample number	Mineral	Mg	Fe	Ca	Al	B	Y	Ni	Co
114	L	1.8%	9200	7200	320	2500	–	11	17
10	L	2.7%	5000	1.3%	115	1600	–	6	8
79	L	2.1%	6500	5400	560	82	13	–	12
52	L	1.1%	1.7%	7500	420	170	10	7	7
52a	L	1.9%	6500	1.1%	380	230	12	5.5	6.5
42a	S	1.1%	1.1%	7200	900	180	12	75	25
139	S	1.0%	6700	8200	160	120	12	12	27
105A	S	2.0%	3000	1900	–	210	–	3.5	9.5
42C	S	9500	1.0%	6200	800	200	17	58	23

Below detection limit: Y(10), Ni(3), Al(3), V(5), Cr(30), Sc(5), Ga(10), Ge(10), Cu(3), Zr(10), Zn(100 ppm). S – sonolite; L – leucophoenicite.

X-ray Diffraction Powder Patterns

Although relatively coarse-grained the tephroite and associated MBII from Răzoare give generally mixed X-ray powder patterns. Over 30 X-ray diffraction charts have been obtained on different samples. Most of them constantly show well resolved peaks at d of 3.6x, 2.8x and 1.8x Å with variable intensities. Clearly two-phase samples have splited peaks, especially at 2.8x and 1.8x Å, suggesting the probable submicroscope intergrowths of MBII. However, some purer samples exhibit diffraction patterns characteristic of tephroite, sonolite and leucophoenicite and for reason of being directly compared the data are graphically presented (Fig. 3). Small and/or ill defined peaks characteristic of alleghanyite and ribbeite have occurred in some few samples analysed. However, these phases could not be definitely identified. The main MBII at Răzoare remain thus the sonolite and the leucophoenicite. Patterns with well developed peaks at 5.30, 3.62, 2.86, 2.60, 2.55 and 1.80 Å are typical of tephroite (Fig. 3A). Slight transformation of tephroite to sonolite leads to

change of peak intensities and to the appearance of the sonolite peak at 1.74 Å(Fig. 3B). The latter peak is better developed in the sonolite-dominated samples, with inherited tephroite (Fig. 3C); here a group of peaks, i.e. at 2.61, 2.65 and 2.70 characteristically develop. For the leucophoenicite-dominated samples the X-ray powder pattern exhibits two peaks, i.e. at 2.87 and 2.70 of nearly equal intensities (Fig. 3D). The following chart (Fig. 3E) shows some peaks suggesting the presence of alleghanyite (i.e. at 3.13, 3.02, 1.76Å etc), in which, however, the leading pattern is that of sonolite.

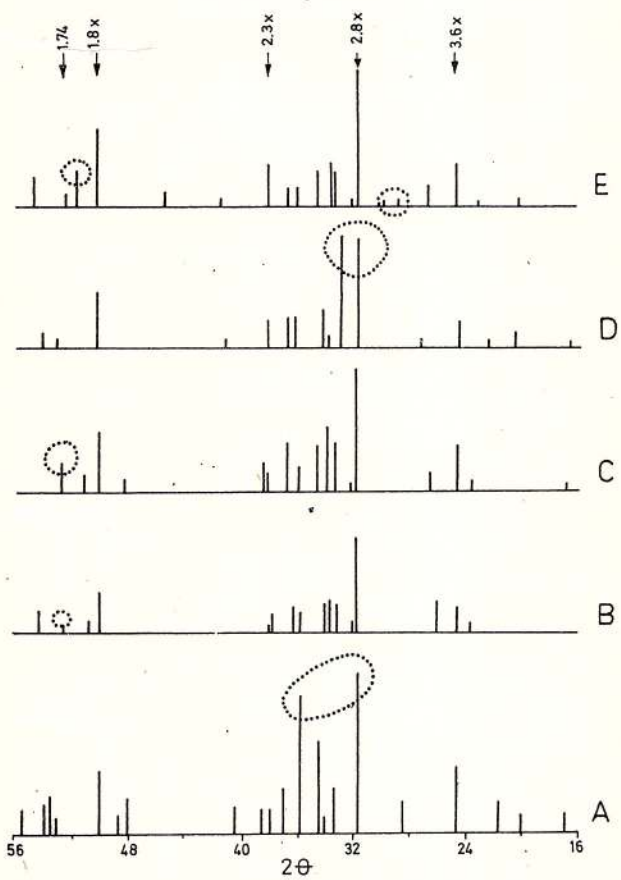

Fig. 3 - X-ray diffraction charts of the most typical samples of the tephroite-MBII assemblage.
A, tephroite; B, slightly "sonolitized" tephroite; C, sonolite with tephroite relics; D, leucophoenicite with sonolite; E, sonolite pattern with subordonate alleghanyite peaks.

IR Data

No standard IR curves seem to exist for the MBII yet. Although of similar appearance, the curves presented in Figure 4 show some differences. Tentatively, they may be interpreted as being characteristic of the two leading MBII species existing at Răzoare, i.e. sonolite and leucophoenicite. The IR spectra of the MBII show supplementary absorbtion peaks as compared to those of tephroite; they are at 452, 674, 918 cm^{-1} for both MBII species and particularly at 1085 cm^{-1} for sonolite. The absorption peaks at 3500 cm^{-1} indicating the structurally bounded OH groups are also characteristically developed for the MBH species as compared to that of tephroite.

Discussion

As part of a study of the manganese-iron minerals from Răzoare, Preluca Mts, Romania, we examined many specimens containing prevailingly MBH and jacobsite. The whole assemblage (tephroite, MBH, carbonate-fluorapatite, apatite) practically contain no iron, except jacobsite, a feature which contrasts with the other assemblages occurring within the deposit. The tephroite-MBH assemblage is developed in the lower, carbonate-rich part of the Mn-Fe-bearing metamorphic sequence, which is silica-undersaturated. Like the whole deposit, the tephroite-MBH assemblage is also poor in Mg and Ca.

The MBH belong to the morphotropic series of humites (Fleischer, 1983) with the general formula of

$$nMn_2SiO_4.Mn(OH)_2$$

where n=1, 2, 3, 4, giving three polymorphs pairs (Tab. 4). At the same time, the MBH include two structurally distinct groups or families, i.e. the manganhumite and the leucophoenicite groups (Moore, 1970; Dunn, 1985; Dunn et al., 1984; Peacor et al., 1987). The Răzoare ores seem to contain only the monoclinic members and thus representatives of both groups.

Preliminary data on the Răzoare material showed intimate intergrowths of tephroite with sonolite and leucophoenicite. Some evidences suggest the presence of alleghanyite too, as well as the probable existence of ribbeite. For the time being only wet chemical analyses are available, carried out on relatively uniformly coloured materials. The X-ray diffraction date show the predominance of the sonolite and leucophoenicite powder patterns with either relics of tephroite or "satellite" reflection characteristic of alleghanyite and to a lesser extent of ribbeite. The mixed X-ray spacings are probably due to insufficiently purified analysed material; such data may, however, indicate a generalized state of mixed layering as Yau and Peacor (1986) have demonstrated for jerrygibbsite-leucophoenicite.

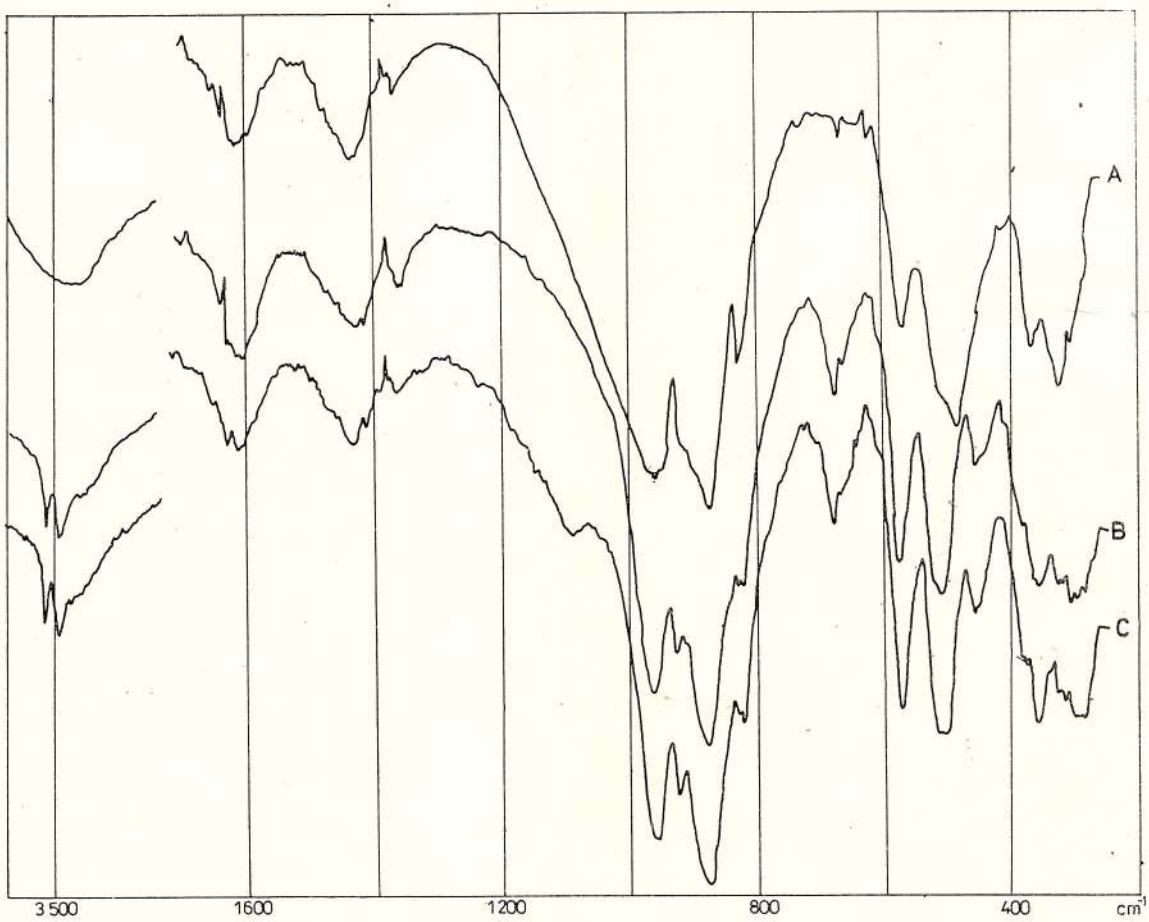

Fig. 4 – IR absorbtion charts of tephroite (A), leucophoenicite (B) and sonolite (C).

The Răzoare MBH do not show significant F (some few analyses gave only 0.04–0.08 percent F) and Zn contents, typically identified by Dunn (1985) as having stabilizing effects on the MBH structures. However, Yau and Peacor (1986) suggested that leucophoenicite group minerals formed in absence of F. Instead, the MBH of Răzoare constantly shows significant boron contents, seemingly higher in the leucophoenicite-dominated samples (up to 2500 ppm). It is likely that boron may play a critical role in the composition/structure of the MBH from Răzoare, in a way difficult to be clarified. It is a matter of further research.

The appearance frequency of the MBH identified at Răzoare by all the methods used up to now increases in the following succession: alleghanyite (?) – leucophoenicite – sonolite, suggesting their probable order of succession by formation at the expense of tephroite. This is a possible explanation of the gradual disappearance of the earliest formed phase (alleghanyite) with an intriguing inheritance of its Me^{2+}:Si ratio.

The tephroite-alleghanyite (?)-leucophoenicite-sonolite assemblage represents a typical feature of the Răzoare ores. Although not previously described here, these mineral species have a wide distribution within the ore lenses. Macroscopically the rose-red-brown granular aggregates of tephroite-MBH resemble much the pyroxmangite-rich assemblage, in which, however, jacobsite is lacking. As compared to the higher grade assemblage of manganoan fayalite-orthopyroxene cal-

Table 4
Systematics of manganese-bearing humites[x]

		Formula	Me^{2+}:Si	Stabilizing elements[xx]
Tephroite		Mn_2SiO_4	2	
Orthorhombic Series Pbnm	Monoclinic Series $P2_1b$			
Unknown in nature		$Mn_3(SiO_4)(OH)_2$	3.0	
Ribbeite	Alleghanyite	$Mn_5SiO_42OH_2$	2.5	F, Zn
Manganhumite	*Leucophoenicite*	$Mn_7(SiO_4)_3(OH)_2$	2.33	Ca, Zn
Jerrygibbsite	Sonolite	$Mn_9(SiO_4)_4(OH)_2$	2.55	Zn
Manganese humites from Răzoare			2.42	B(?)[xxx]

Italics – the leucophoenicite group or family.
[x] The classification proposed by Dunn (1985) includes three groups, i.e. humite group (norbergite, chondrodite, humite and clinohumite), Mn-humite (alleghanyite, manganhumite and sonolite) and leucophoenicite group (leucophoenicite, jerrygibbsite, to which ribbeite adds, acc. to Peacor et al., 1987). In the last two groups members with Me^{2+}:Si of 3:1, i.e. the equivalents of norbergite, are still lacking in nature.
[xx] Acc. to Dunn (1985).
[xxx] This study.

deritic spessartine, the tephroite + MBH + jacobsite assemblage has formed during a later, retrograde metamorphic phase. Among many still unsolved problems of the Răzoare deposits, the presence of the tephroite-MBH assemblage is an intriguing one; it seems to have evolved in a nearly closed system containing iron linked practically only in jacobsite. The metamorphic evolution of the Mn-rich parts of the "stratified" protolith from Răzoare parallels that of iron-richer ones but shows some differences. Petrology of the deposit is, however, the matter of a future paper.

References

Bălan M. (1976) Mineralogia zăcămintelor manganifere de la Iacobeni. Edit. Acad. Române, 123 p., Bucureşti.

Cook D. (1969) Sonolite, alleghanyite and leucophoenicite from New Jersey. *Amer. Miner.*, 54, p. 1392–1398, Washington.

Dunn P. J. (1985) Manganese humites and leucophoenicites from Franklin and Sterling Hill, New Jersey: parageneses, compositions and implications for solid solution limits. *Amer. Miner.*, 70, p. 379–387, Washington.

– , Peacor D. R., Simmons W. B., Essene E. J. (1984) Jerrygibbsite, a new polymorph of $Mn_9(SiO_4)_4(OH)_2$ from Franklin, New Jersey, with new data on leucophoenicite. *Amer. Miner.*, 69, p. 546–552, Washington.

Fleischer M. (1983) Glossary of mineral species 1983. *Miner. Record Inc.*, 202 p., Tucson.

Moore P. B. (1970) Edge-sharing silicate tetrahedra in the crystal structure of leucophoenicite. *Amer. Miner.*, 55, p. 1146–1166, Washington.

Peacor D. R., Dunn P. J., Su S. C., Innes J. (1987) Ribbeite, a polymorph of alleghanyite and member of the leucophoenicite group from Kombat mine, Namibia. *Amer. Miner.*, 72, p. 213–216, Washington.

Peters T., Schwander H., Trommsdorff V. (1973) Assemblage among tephroite, pyroxmangite, rhodochrosite, quartz: experimental data and occurrences in the Rhetic Alps. *Contr. Miner. Petr.*, 42, p. 325–332, Berlin.

Udubaşa G., Hârtopanu P., Ilinca Gh., Valdman St. (in press, 1993) The regionally metamorphosed Mn-Fe deposit at Răzoare, Preluca Mts, Romania. *Rom. J. Miner. Dep.*, 76, Bucureşti.

Winchell A. N., Winchell H. (1951) Elements of optical Mineralogy. Wiley, New York.

Yau Yu-Chyi, Peacor D. R. (1986) Jerrygibbsite-leucophoenicite mixed layering and general relations between the humite and leucophoenicite families. *Amer. Miner.*, 71, p. 985–988, Washington.

Received: June 10, 1991
Accepted: June 12, 1991
Presented at the scientific session of the Institute of Geology and Geophysics: June 19, 1991

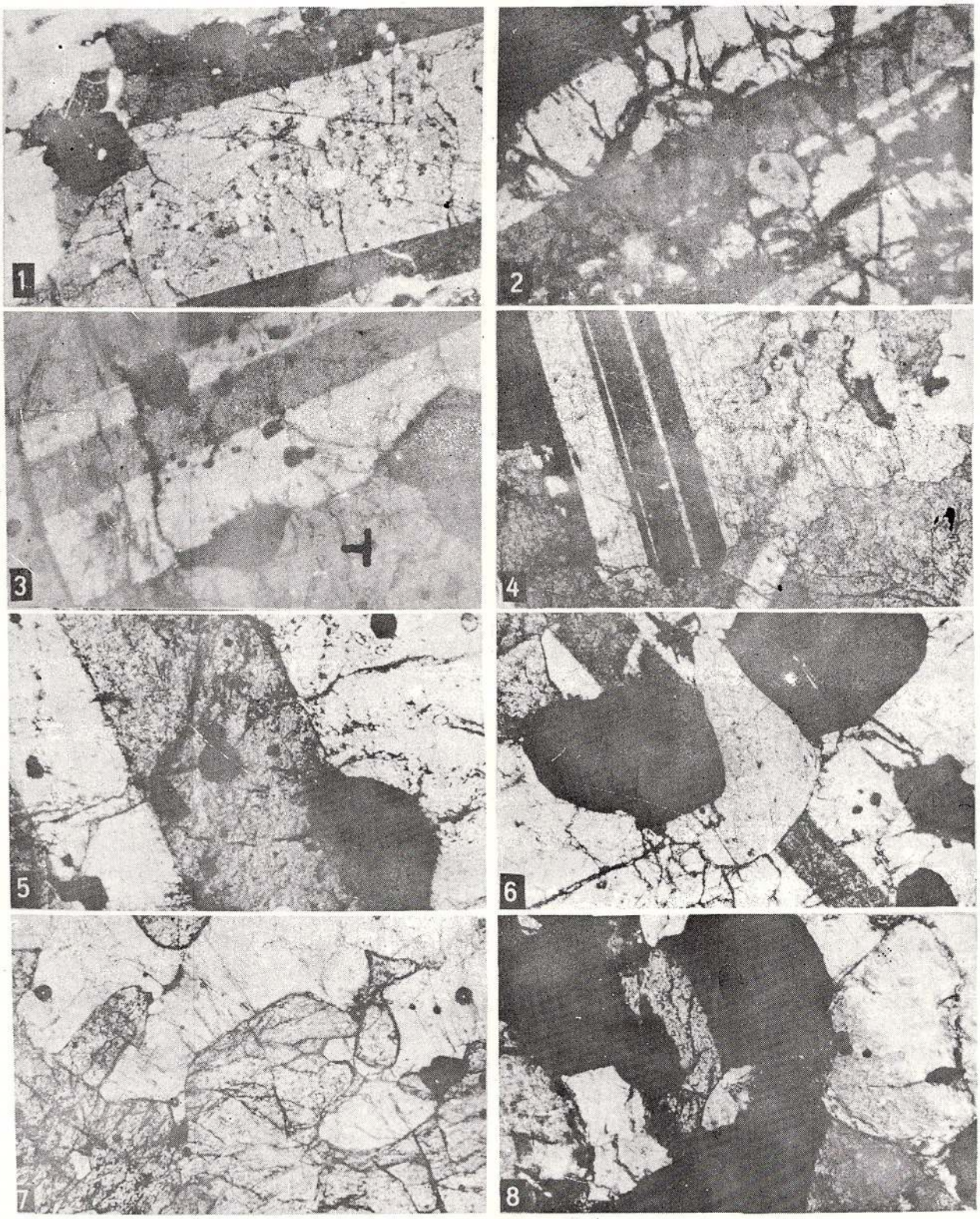

Plate

Fig. 1 – Twinned leucophoenicite grain with rhodochrosite inclusions. Jacobsite (black) cuts de twin. The coarse twinning is typical of leucophoenicite. Thin section, crossed polarizers, x 40.

Fig. 2 – Polysynthetically twinned sonolite with inclusions of carbonate fluorapatite. Crossed polarizers, x 40.

Fig. 3 – Tephroite (grey), associated with twinned leucophoenicites. Black is jacobsite. Crossed polarizers, x 40.

Fig. 4. – Twinned sonolite grain. Crossed polarizers, x 40.

Fig. 5 – A grain of manganese-bearing humite with alleghanyite type twin. Black is jacobsite. Crossed polarizers, x 40.

Fig. 6 – Sonolite twin interrupted by rhodochrosite (whitish grey) and jacobsite. Crossed polarizers, x 40.

Fig. 7 – Tephroite (grey) substituted by apatite (white), x 40.

Fig. 8 – Tephroite (middle of the photograph) included in jacobsite (black), associated with carbonate fluorapatite (shightly twinned). Crossed polarizers, x 40.

Rom. J. Mineralogy, 1993, 76, 1, p. 23–27

CONTRIBUTIONS TO THE STUDY OF THE FLUID INCLUSIONS IN THE MIAROLITIC QUARTZ INCLUSIONS IN THE DRĂGANULUI VALLEY

Ioan PINTEA

Institutul de Geologie şi Geofizică. C.P.181, 3400 Cluj-Napoca 1.

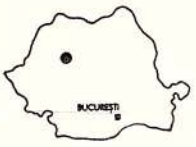

Key words: Fluid inclusions. Salinity. Density. Temperature. P-T conditions. Granite. Apuseni Mountains.

Abstract: The polyphase fluid inclusions from the miarolitic quartz crystals from the Drăganului Valley granite have a salinity of 50–70 per cent weight, density 1.09–1.57 g/cm^3, homogenization temperature ranging from 420 to more than 600^0 C and vapour pressure in the trapping moment of minimum 150 bars. Their coexistence with fluid inclusions rich in vapours suggests the fluids separation from the granitic melt and their subsequent dissolution by boiling.

Introduction

The druses in the granite cropping out in the Drăganului Valley, between its tributaries – Zărnii and Crăciunului valleys – were first described by Stoicovici and Gliszczynsky in 1944. Some aspects related to these formations were resumed by Giuşcă (1950), who also described some quartz crystals. They were also mentioned by Istrate (1978) and Ştefan (1980) but were not minutely described. Recently, when presenting generally the pneumatolitic phenomena associated with granites in Romania, Mârza (unpubl. data)[1] mentioned them again, giving a synthesis of all the data known so far. Thus, miarolites are especially located in microgranitic zones; they display spheroidal or elliptical shapes and consist of idiomorphous crystals of smoky and white quartz, orthose, albite, tourmaline, biotite, fluorite, metallic minerals and zeolites. Genetically, they are considered the result of a pneumatolitic process with an intensely alkaline metasomatosis which yielded the microgranitic facies.

1. Types of Fluid Inclusions in Quartz Crystals

The samples studied by us consisted of crystals of white and smoky quartz taken off from the whole outcropping area of granite (two of the samples are from the collection of I. Mârza). Several types of fluid inclusions have been emphasized which, according to their content at the ambient temperature, have been marked, as follows:

[1]I. Mârza – Pneumatolitic Mineralizations Associated with Granites (Granodiorites) in Romania.

1.1 *Type S.* Polyphase fluid inclusions which contain beside liquid and vapours several solid phases (Pl., Figs. 1–4).

1.2. *Type V.* Biphase fluid inclusions within which vapours prevail, the liquid phase representing only 5–10 per cent of the cavities volume (Pl., Fig. 5).

1.3. *Type SV.* Triphase fluid inclusions within which vapours prevail, liquid being subordinate, to which one or several solid phases are added (Pl., Fig. 6).

1.4. *Type L.* Biphase fluid inclusions within which the liquid phase occupies most of the cavities, the vapour phase subordinate.

With its varied morphological aspect from negative crystal to irregular shapes this type generally occupies planes of healed cracks; locally they are, however, spread within crystals. The smoky variety of quartz usually includes all types of fluid inclusions, whereas in the white variety types L and V predominate.

2. Polyphase Fluid Inclusions

These inclusions are characterized by several solid phases beside liquid and vapours, their study constituting the object of the present paper.

2.1 Identification of Solid Phases

The determination of the solid phases was based on the optical properties, solubility degree and microthermometric behaviour. In several cases favourable results have been obtained, in other cases because of the extremely reduced size the identification of some of the solid phases is uncertain or even impossible. The solid

phases taken into consideration are, as follows:

2.1.1. *Halite.* An omnipresent crystalline phase which is found as perfect or slightly rounded cubic crystals (Pl., Figs. 1–5), isotropic or colourless. At low temperature they react with the liquid yielding a hydrohalite that can be recognized after its birefringence and the low degree of solubility (Roedder, 1971). Volumetrically, it occupies the first place among the solid phases.

2.1.2. *Sylvite.* It represents the second solid phase identified positively. It differs from halite by its lower relief, octahedral aspect or obviously rounded, of a light-grey colour. Sylvite does not react with liquid at low temperatures (Pl., Figs. 1–4).

2.1.3. *Hematite.* It occurs as grains and hexagonal plates of a red, brown or black colour. It is not dissolved during the microthermometric tests (Pl., Figs. 1–4).

2.1.4. *Anhydrite.* It occurs as short or elongated prisms with a moderate birefringence and upright extinction. Its participation is more reduced and variable. The degree of solubility is fairly low (Pl., Figs. 1, 2, 4).

On the basis of these properties the last minerals were positively identified by a special Rx method by Zolensky and Bodnar (1982) in case of hematite and by Raman spectroscopy by Rosaco and Roedder (1979) in case of anhydrite.

2.1.5. *Magnetite.* It was identified in some cases on the basis of its magnetic properties. Magnetite occurs as inclusions of opaque edged grains.

2.1.6. *Unidentified solid phases.* They are represented by numerous nonmagnetic opaque grains associated or spread in inclusions or by transparent solid phases, with crystalline or noncrystalline forms, with a high relief and vivid birefringence colours (Pl., Figs. 1, 2, 3, 4, 6). Their identification only on the basis of the optical proprieties is difficult. Like anhydrite and hematite, they are not uniformely spread in inclusions and are never completely dissolved during the microthermometric tests. Thus, from all the solid phases mentioned only halite and sylvite belong to the "daughter" mineral group, the other phases being already formed at the moment of trapping.

2.2. Subtypes of Polyphase Fluid Inclusions

According to the arrangement within crystals, composition, shape, volumetric ratio between phases at the environmental temperature and the microthermometric behaviour, two subtypes of polyphase fluid inclusions can be distinguished:

2.2.1. *Subtype* S_1. Such inclusions are less frequently found. They generally consist of negative crystals shapes and are found as spatial groups or occupy evolute planes of healed cracks.

The volumetric ratio between phases shows constantly the following order: liquid, vapours, halite, sylvite, anhydrite, hematite and unidentified solid phases (Tabs. 1, 2). These phases are always accompanied by inclusions of type S and SV and, considering the homogenization way of the latter, they seem to be contemporaneous with them.

2.2.2. *Subtype* S_2. This subtype of inclusions occurs as rows which suggest healed cracks less developed than in the first case. The phase ratio is also constant but the order is changed (Tabs. 1, 2). It is of note a remarkable decrease of the vapours volume; sylvite usually occurs with geometric habit and occupies a volume almost equal to that of halite. The percentage of halite and of the unidentified solid phases also increases. The coexistence with types V and VS is much more obvious probably as a result of the inclusions formation from a heterogeneous (boiling) fluid.

Table 1

Filling of the polyphase fluid inclusions in the miarolitic quartz crystals in the Drăganului Valley at the ambient temperature

Composition	S_1 % volume	S_2 % volume
Aqueous solution	57.68	55.75
Vapours	26.43	4.07
Halite	12.41	25.06
Sylvite	2.51	13.63
Anhydrite	0.70	0.04
Hematite	0.13	0.95
Unidentified	0.14	0.50

2.3. Chemical Composition of the Polyphase Fluid Inclusions

The chemical composition of the polyphase fluid inclusions determinated based on the method of volume approximation (Roedder, 1971; Ramboz, 1979) as well as the data obtained are rendered in Table 2. The high salinity of the two subtypes of fluid inclusions is mainly given by the presence of Na and K chlorides, the other phases, vapours inclusive, representing only about 5 per cent of weight. Because CO_2 is lacking, the gases from inclusions are considered to consist only of water vapours and their mass was added to H_2O. The difference between the two subtypes is well marked also by the chemical composition determined as well as by the density values which point to a significant increase from S_1 to S_2.

2.4. Microthermometric Evolution

The microthermometric tests were carried out by means of microthermometric equipment built in the

laboratory of Fluid Inclusions of I.G.G. according to the norms presented in the relevant literature (e.g. Roedder, 1984).

Table 2

Chemical composition and density of the polyphase fluid inclusions of the miarolitic quartz crystals in the Drăganului Valley determinated on the basis of the method of volumetric approximation

Component	Subtype S_1		Subtype S_2	
	g/l	% weight	g/l	% weight
H_2O	505.54	47.26	485.04	30.78
NaCl	427.27	37.76	691.12	43.88
KCl	129.56	11.66	337.27	21.36
$CaSO_4$	19.42	1.79	49.73	0.07
Fe_2O_3	6.50	0.62	1.37	3.12
Unidentified	9.80	0.91	12.28	0.79
Density g/cm^3	1.098		1.576	

As anhydrite, hematite and the unidentified solid phases do not represent real "daughter" minerals we did not take them into consideration during our microthermometric tests. Thus, all the phase transitions recorded were included in the system H_2O-NaCl-KCl. The microthermometric behaviour of the two subtypes can be observed in the evolution sketch in Figure 1.

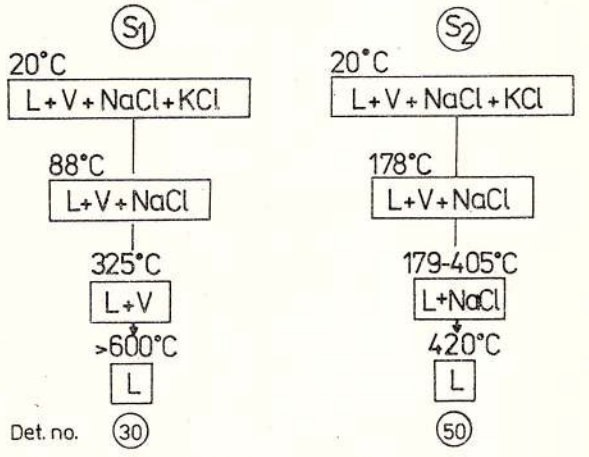

Fig. 1 – Microthermometric behavior of the polyphase fluid inclusions. The values represent the average temperatures for the 30, 50 cases, respectively. In case of subtype S_1 the final homogenization temperature could not be recorded because of the shortcomings of the apparata used; the final homogenization in liquid phase was inferred from the obvious decreasing tendency of the vapour bubble at 600^0 C in all cases.

As one can infer from these tests S_1 represents an initially homogeneous fluid (solution with saturated vapours) and, consequently, when characterizing it we used the diagram of the phase equilibrium of the system H_2O-NaCl-KCl (Roedder, 1984; Fig. 2). On the

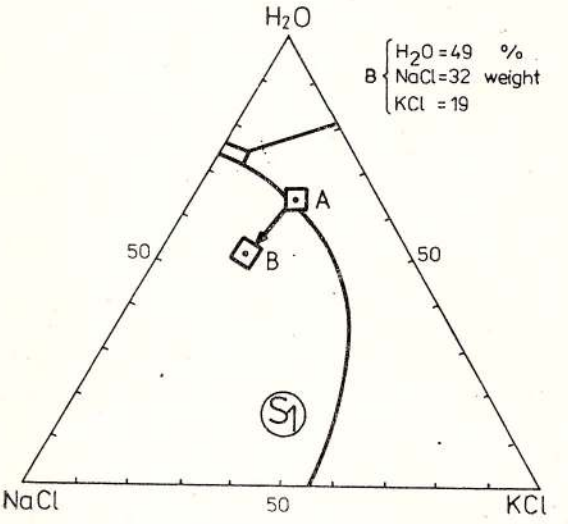

Fig. 2 – The plotting of the halite and sylvite dissolution temperature on the equilibrium diagram of the system H_2O-NaCl-KCl (from Roedder, 1984). A – average temperature of sylvite dissolution; B – the same value for halite. In the right top corner is mentioned the salinity of the inclusions S_1 determined by the plotting of point B on the triangle sides.

diagram point A represents the average of sylvite dissolution temperatures for 30 inclusions of this type. Point B represents the average of halite dissolution temperature and its position determines the chemical composition of this type of inclusions. The difference recorded using the two methods is not significant so that either value renders the chemical composition of the fluid inclusions. In case of the subtype S_2 the situation is different due to the anomalous homogenization way. The disappearance of the gas bubble before the halite cube suggests the origin of this type of inclusions in a heterogeneous fluid in course of boiling. As a matter of fact, the obvious coexistence with high-vapour (V or VS) inclusions represents a solid argument in favour of the above-mentioned facts. As the fluid included in S_2 was not in equilibrium with its vapours the equilibrium diagram of the system H_2O-NaCl-KCl could not be used and consequently one could not obtain another value of the chemical composition; NaCl dissolution temperature is regarded as minimum temperature of formation of this type. As for the formation pressure, for S_1 a volume of 100–150 bars has been obtained from the same diagram which represents the minimum value of the fluid vapour pressure at the moment of its trapping. In case of S_2 the pressure value has to be lower due to the higher concentration of salts (Roedder and Bodnar, 1980).

In conclusion, on the basis of the microthermometric behaviour one can infer that S_1 represents the initial fluid separated from the granitic melt in course of consolidation; this statement is based on the comparison of the homogenization temperature (higher than 600^0 C) with the consolidation temperature of the Zărnişoara Valley granite (ca. 700^0 C) determined by Ştefan (1980). It means that around this value the granitic melt coexisted with the hydrosaline melt, at the same time being separated by vesiculation and volatile phase (represented by inclusions of type V and SV). The much lower homogenization temperature of type S_2 (420^0 C) as well as the clear heterogeneous character of the trapping suggest the evolution of the initial fluid (represented by S_1) in the dissolution sense, which led to the superconcentration of the fluid phase and the further generation of the volatile phase (mainly water vapours). Similar phenomena have been minutely presented by several researchers (Ahmad and Rose, 1980; Ramboz et al., 1982; Ramboz, 1979; Weisbrod, 1981, a.s.o.). The formation of both types of fluid inclusions as well as of the associated ones took place under conditions of a significant decrease of the pressure, from 5 kb (value determined by A. Ştefan for granite consolidation conditions) to some hundreds of bars.

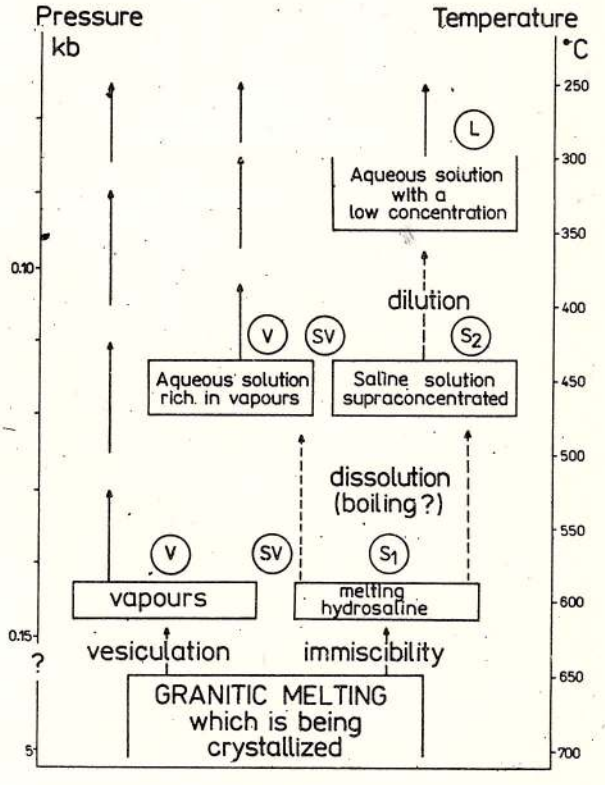

Fig. 3 – Probable post-magmatic evolution of the fluids associated to the miarolitic garnet in the Drăganului Valley (schematic representation).

3. Comments and Conclusions

The four types of fluid inclusions, especially in the smoky variety of quartz, point to a long and complex process of the quartz formation, quite shortly after the granite emplacement as a result of the interaction of the fluid phases with the mineral already crystallized. The formation of high-salinity fluid inclusions indicates two successive evolution moments. Thus type S_1 represents the initial fluid separated by the granitic melt in the course of crystallization (low-water content, high homogenization temperature, obvious primary character) and type S_2 represents a superconcentrated fluid resulting from the dissolution of the former. Either moment is characterized by the parallel generation of fluid phases, less dense, represented by inclusions V and VS. The formation of the two types of fluid inclusions took place under conditions of a significant decrease of the pressure. The final moment in the fluids evolution is marked by the pressure of inclusions L, which are not the object of the present paper. Figure 3 shows schematically the probable evolution way presented in this paper which can represent a work model for future researches. From this paper one can infer that the formation of the druses where quartz is always present took place during a long process (the term 'pneumatolitic' s.s. does not correspond any longer to the genesis conditions) which started from the magmatic stage and was controlled by the interaction between the fluid phases and the surrounding rocks.

References

Ahmad S. N., Rose A. W. (1980) Fluid Inclusions in Porphyry and Skarn Ore at Santa Rita, New Mexico. *Econ. Geol.*, 75, p. 229–250, New Haven.

Giuşcă D. (1950) Le massif eruptiv de la Vlădeasa. *An. Com. Geol.*, XXXII, p. 199–251, Bucureşti.

Istrate G. (1978) Petrologic study of the Vlădeasa massif (western part). *An. Inst. Geol. Geofiz.*, LIII, p. 179–289, Bucureşti.

Ramboz C. (1979) A fluid inclusion study of the copper mineralization in southwest Tintic district (Utah). *Bull. Min.*, 102, p. 622–632, Paris.

– , Pichavant M., Weisbrod A. (1982) Fluid immiscibility in natural processes: use and misuse of fluid inclusions data. II: Interpretation of fluid inclusions data in terms of immiscibility. *Chem. Geol.*, 37, p. 29–48, Amsterdam.

Roedder E. (1971) Fluid inclusion studies on the porphyry-type ore deposits at Bingham (Utah), Butte (Montana) and Climax (Colorado). *Econ. Geol.*, 66, 98–120, New Haven.

– , Bodnar R. J. (1980) Geologic pressure determination from fluid inclusion studies. *An. Rev. Earth Planet. Sci.*, 8, p. 263–301, Palo Alto.

– (1984) Fluid Inclusions. *Rev. in Min., Min. Soc. America*, 644 p., Blacksburg.

Rosaco G. J., Roedder E. (1979) Application of a new Raman microprobe spectrometer to nondestructive analysis of sulfate and other ions in individual phases in fluid inclusions in minerals. *Geochim. Cosmochim. Acta*, 43, p. 1907–1915, Cambridge.

Stoicovici E., Gliszczynsky S. V. (1944) Die Drusenvorkomen im Granit der Valea Drăganului, Rumänien. *N. Jahrb. f. Min. Geol. Paleont.* (A), 79, p. 129–160, Stuttgart.

Ştefan A. (1978) Petrographic study of the eastern part of the Vlădeasa eruptive massif. *An. Inst. Geol. Geofiz.*, LV, p. 210–314, Bucureşti.

Weisbrod A. (1981) Fluid inclusions in shallow intrusives. In: Hollister and Crawford (eds), Short course in fluid inclusions. *Min. Ass. Canada*, 6, p. 241–271, Ottawa.

Zolensky M. E., Bodnar R. J. (1982) Identification of fluid inclusions daughter crystals using Gandolfi X-ray techniques. *Am. Min.*, 67, 137–141, Washington.

Received: February 18, 1991
Accepted: February 18, 1991
Presented at the scientific session of the Institute of Geology and Geophysics: March 15, 1991

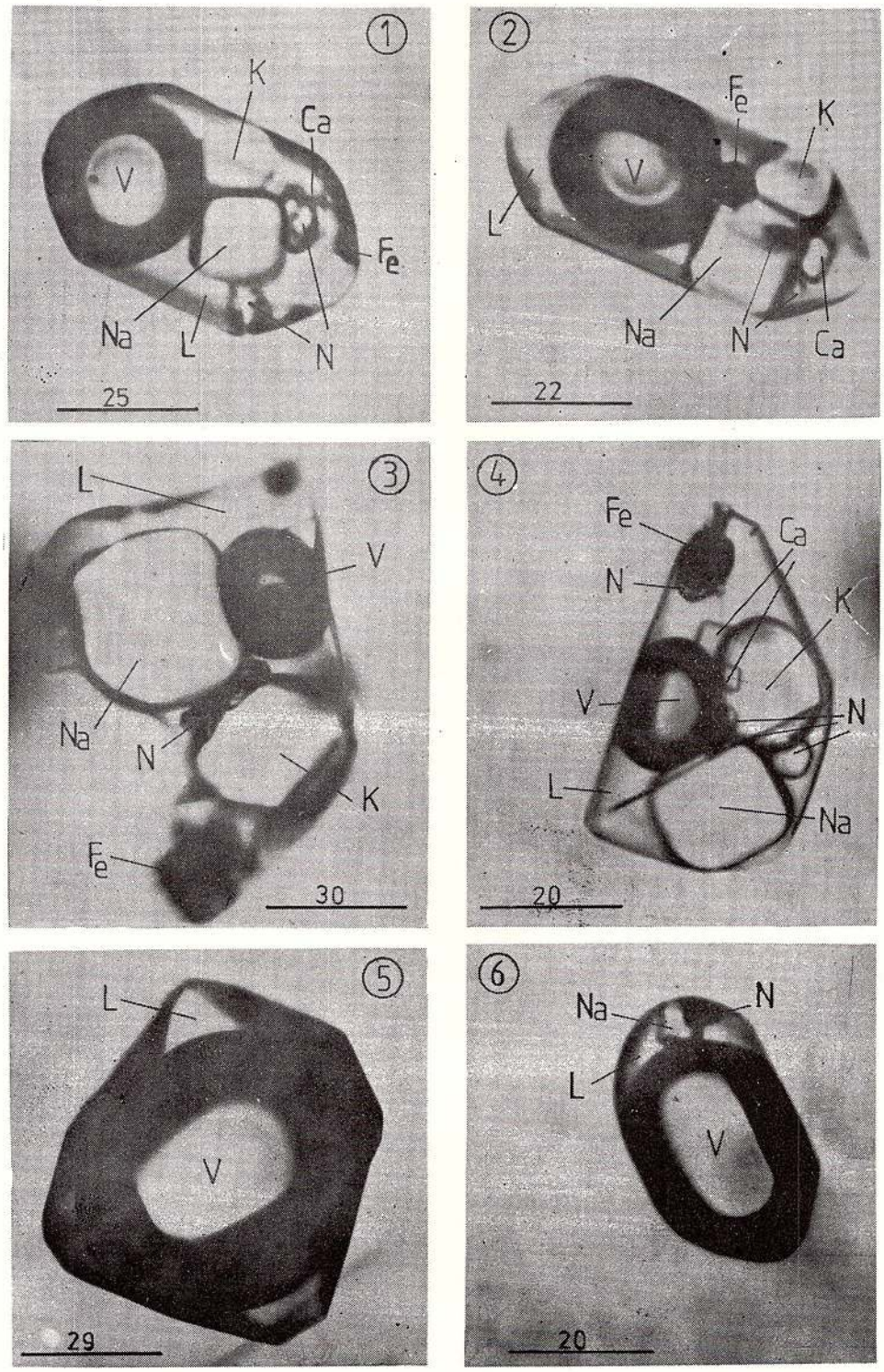

Plate

Figs. 1, 2 — Polyphase fluid inclusions S_1. It is of note the constant ratio between liquid, vapours, halite and sylvite. The presence of the other phases varies from one inclusion to the other.

Figs. 3, 4 — Polyphase inclusions S_2. They are characterized by their xenomorphous aspect; vapours percentage decreases, halite and sylvite occupy almost equal volumes in cavities. As in the above-mentioned case, anhydrite, hematite and the unidentified solid phases are differently distributed.

Fig. 5 — Biphase fluid inclusion in which vapours prevail (type V).

Fig. 6 — Mixed polyphase fluid inclusion SV. Two solid phases occur beside vapours and liquid phase in the moment of formation.

Rom. J. Mineralogy, 1993, 76, 1, p. 29–41

MINERALOGICAL DATA CONCERNING THE MAGNESIAN HORNFELS IN THE PIETROASA AREA (BIHOR MOUNTAINS)

Ştefan MARINCEA

Institutul de Geologie şi Geofizică. Str. Caransebeş 1, 78344 Bucureşti 32.

Key words: Carbonates. Borates. Nesosilicates. Sheet silicates. Hornfels. P-T conditions. Metasomatism. Mineral data. DTA data. Major elements. X-ray data. Apuseni Mountains – Bihor Mountains.

Abstract: A large area of magnesian hornfels is developed at the contact between the Pietroasa granitoid body and the Anisian dolostones belonging to the Ferice Unit, in the north-western part of the Bihor Mountains. The mineral assemblage which characterizes these hornfels includes, beside carbonates (calcite, dolomite), which constitute the background: forsterite, clinohumite, chondrodite, spinel, diopside, talc, tremolite, phlogopite, clinochlore, lizardite, brucite, as well as ludwigite, szaibelyite, magnetite, hematite and apatite. The presence of borates and of some minerals with potential fluorine contents (humite, phlogopite, tremolite, talc) points to a boron-fluorine metasomatism which locally affected the hornfels groundmass. This also occurs in case of some calcic hornfels in the vicinity, characterized by the abundance of an apophyllite with 49.28 mole per cent fluorapophyllite in solid solution. The optical properties of the minerals in magnesian hornfels area, as well as some other physical and chemical peculiarities, were used in order to establish some physico-chemical conditions which governed the evolution of this system during the thermometamorphism.

1. Introduction

In the north-western part of the Bihor Mountains, in the upper basin of the Crişul Pietros Valley, a large area of magnesian hornfels is developed at the contact between the Pietroasa granitoid body and the Anisian dolostones belonging to the Ferice Unit (Nappe). A weak boron-fluorine metasomatism locally affects the hornfels groundmass.

The Pietroasa granitoid body, with granite-granodiorite differentiations, was assigned to the second cycle of the banatitic magmatism in the Apuseni Mountains, Danian-Ypresian in age (Ştefan et al., 1988). It thermally affects a large area with carbonatic deposits referred to the Ferice Unit, but only the Anisian ones have a dolomitic nature, being the potentially pre-metamorphic rock of the study hornfels (Bordea, Bordea, 1973).

The widespreading of this hornfels area led us to investigate only few zones adjacent to the contacts in the Crişul Pietros, Sebişel and Aleului valleys, in the Giungitura Summit (Cărpineasa Valley) as well as two dolomite "roof pendants" located in Borului Hill and Măgura Guranilor areas (dotted area in Figure 1). All these areas are situated west of the Galbenii Fault.

Even if most of the premetamorphic rocks are "protodolomitic" in nature, the presence of alloclasts (quartz, micas, clay minerals: Bordea, Bordea, 1973) favourises the yielding of magnesian silicates as isochemically thermometamorphic products.

2. Mineralogical aspects

A previous petrographic study undertaken by Rafalet (1963) shows that the mineral assemblages in the Pietroasa magnesian hornfels include calcite, dolomite, brucite, forsterite, spinel, chondrodite, clinohumite, diopside, talc, tremolite, serpentines, ludwigite, magnetite and hematite. Szaibelyite (Stoicovici, Stoici, 1969), clinochlore, phlogopite (Marincea, 1992) and apatite also occur.

Such a mineralogy potentially indicates a weak and well-defined boron-fluorine metasomatism, which also affects some calcic hornfels in the vicinity.

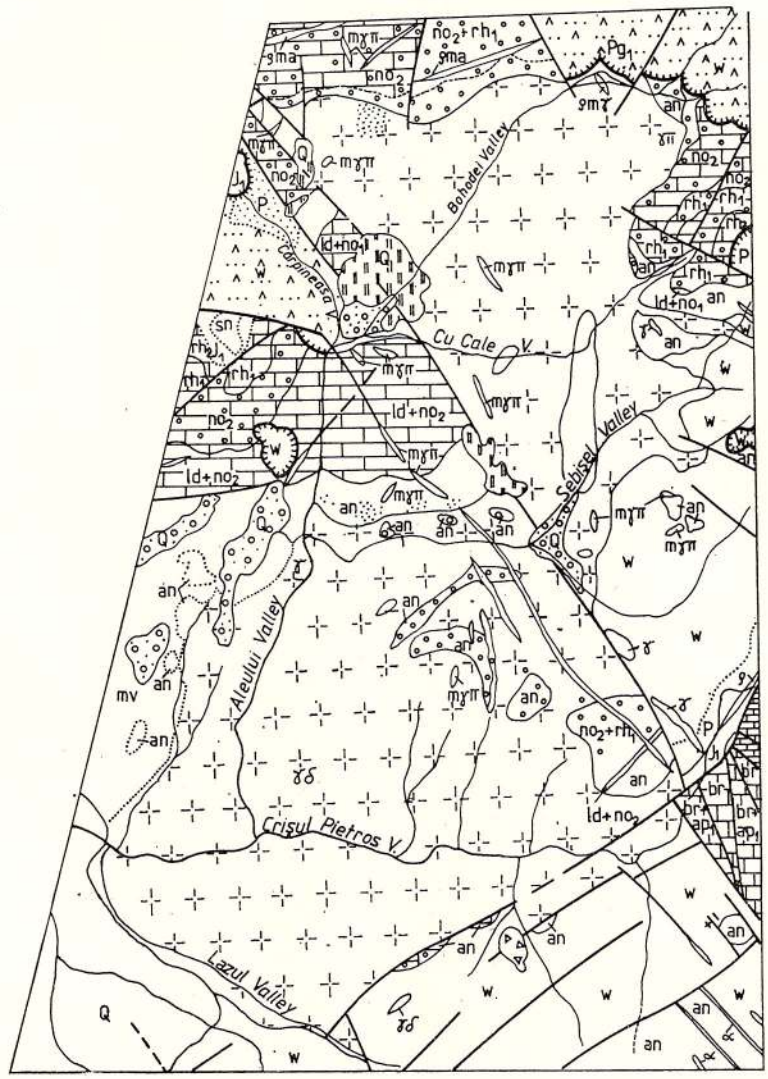

Fig. 1. – Sketch after the geological map of the study area, scale 1:50 000 (Pietroasa Sheet, Bleahu et al., 1985), with the distribution of the main areas of magnesian hornfels (dotted areas). p=Permian; w=Werfenian; an=Anisian; ld=Ladinian; no=Norian; rh=Rhetian; J_1=Lower Jurassic of the Ferice (p, w, an, ld-no_1, no_2-rh_1, J_1) and Arieşeni (w, an) units; br=Barremian; ap=Aptian (Bihor Unit); sn=Senonian (post-tectonic cover) α am; ρ; $\gamma\rho$; γ; mγ; ρm=hornblende quartz andesites; rhyolites; biotite + hornblende granodiorites; granites; porphyritic microgranites; microgranitic rhyolites, Maastrichtian-Paleocene in age (banatites); mv= Malvensian; Q=Quaternary (post-intrusive cover).

3. Mineralogy of the unmetasomatized and fluorine-metasomatized areas

3.1. Magnesian hornfels

Carbonates prevail in the premetamorphic rocks and they normally predominate in the contact area, too. In the magnesian hornfels calcite coexists with dolomite. The two carbonates can be distinguished with difficult by optical means (they are, however, differentiated by refringence) but their presence can be easily pointed out by thermal analyses. The main effects recorded on the DTA and DTG curves (Tab. 1) have been assigned to the following phase transformations:

a) 720–760^0 C on the DTA curve (710–755^0 C on the DTG curve): decomposition of $MgCO_3$ from dolomite;

b) 800–880^0 C on the DTA curve (790–875^0 C on the DTG curve): decomposition of $CaCO_3$ from dolomite;

c) 930–960^0 C on the DTA curve (925–950^0 C on the

Table 1
Thermal Analyses Data on Carbonates from Pietroasa Contact Area[x]

Sample Location	Character of the effect on the DTG and DTA curves	Thermal value on DTA curve (°C)	Thermal value on DTG curve (°C)	Loss in weight on TGA curve (%)	Identified mineral	I[xx]
153	endothermic	755	750	10.64	dolomite	
Sebişel Valley	endothermic	880	875	20.75	dolomite	1.05
	endothermic	940	935	50.00	calcite	
139	endothermic	720	710	13.12	dolomite	
Aleului Valley	endothermic	800	790	26.66	dolomite	0.97
	endothermic	960	950	49.00	calcite	
167	endothermic	760	755	14.75	dolomite	
Aleului Valley	endothermic	825	820	28.69	dolomite	1.06
	endothermic	930	925	43.00	calcite	

[x] analyst T. Drăghiciu, I.G.G.;
[xx] CO_2 in $MgCO_3/CO_2$ in $CaCO_3$, ratio, based on TGA curves of dolomitic phase.

Table 2
Magnesium Content in Carbonate Phases from Pietroasa Area,
Based on Variation of $(10\bar{1}4)$ Spacing (1)

Sample	Location	$d(10\bar{1}4)$ (Å)	$d(10\bar{1}4)$ (Å)	Associated minerals(3)	$MgCO_3$ %
A) Calcite					
133(2)	Sebişel Valley	3.027	0.008	fo, cl, ta, se, br, sz, lw, ch	2.73
139	Aleului Valley	3.021	0.014	fo, ch, se, br	4.78
160(2)	Aleului Valley	3.023	0.012	ph, br, se	4.10
167	Aleului Valley	3.020	0.015	fo, sp, ch, ph, se, br	5.12
173	Aleului Valley	3.027	0.008	di, fo, tr, se, br	2.73
179(2)	Aleului Valley	3.021	0.014	fo, ch, ta, br, se, cl, sz	4.78
210(2)	Aleului Valley	3.025	0.010	sp, fo, se, br	3.41
280	Crişul Pietros Valley	3.028	0.007	fo, sp, ch, se, br	2.39
292	Cărpineasa Valley	3.033	0.002	fo, sp, se, br, cl, ap	0.68
B) Dolomite					
139	Aleului Valley	2.8855	0.1495	fo, ch, se, br	51.02
153(2)	Sebişel Valley	2.8890	0.1460	ta, cl	49.83
167	Aleului Valley	2.8879	0.1470	fo, sp, ch, ph, se, br	50.20
292	Cărpineasa Valley	2.8870	0.1480	fo, sp, se, br, cl, ap	50.51
298	Cărpineasa Valley	2.8890	0.1460	fo, ta, se, br	49.83

(1) CuK_α radiation, λ=1.5418 Å; analyst C. Cristea (I.G.G.)
(2) Data for these samples are also given by Marincea (1992)
(2) Abbreviations in Fig. 5: sp=spinel; lw=ludwigite; sz=szaibelyite; cl=clinochlore; ap=apatite.

DTG curve): decomposition of $CaCO_3$ from calcite.

The dominance of c a l c i t e within the Pietroasa carbonatic association seems to be determined by the "protodolomitic" nature of the premetamorphic rock (which can be mineralogically regarded as a low-temperature magnesian calcite in equilibrium with dolomite). In magnesium-free marbles appeared as a result of the thermal metamorphism calcite develops as large monomineral masses which frequently contain non-carbonatic phases. Linear dolomitic segregations, which are disposed along the calcite perfect cleavage after $(10\bar{2}1)$, in angular unconformity with the polysynthetic twin planes $(02\bar{2}1)$, occur sporadically. These calcite-dolomite intergrowths are similar to those produced by exolution (Goldsmith, 1960; Carpenter, 1967). The X-ray method proposed by Goldsmith et al. (1955) was used in order to determine the $MgCO_3$ contents of some calcite samples. Using the standards proposed by Brown (1961) for pure carbonates ($d(10\bar{1}4)$=3.035

Å for calcite and d(10$\bar{1}$4)=2.742 Å for magnesite) the following equation for the relationship between (10$\bar{1}$4) spacing and composition has been obtained: X (mole percent $MgCO_3$)=341.29693Δd(10$\bar{1}$4), where Δd(10$\bar{1}$4)=d(10$\bar{1}$4) for the standard calcite -d(10$\bar{1}$4) for the analysed carbonate.

The magnesite contents determined on the basis of this method are presented in Table 2. The contents of Fe^{2+} and Mn^{2+} in marbles are very small (as can be seen in Table 3) and may be neglected as a source of error in this procedure.

has been pointed out based on the diffractometric evidence (Tab. 2) and confirmed by thermal analyses. The computation of the I ratio for the dolomitic phase, where I=(CO_2 from $MgCO_3$): (CO_2 from $CaCO_3$), deduced on the basis of the loss in weight marked on the TGA curves (Todor, 1972), pointed to values which define both calcic dolomites (I<1) and magnesian dolomites (I>1) with slight deviations from the ideal formula (I=1) (Tab. 1).

F o r s t e r i t e occurs as isolated, anhedral or subhedral crystals usually bordered by

Table 3
Partial Wet-chemical Analyses of Carbonate Phases from Pietroasa Area
(% oxides)

Sample	Location	CaO	MgO	MnO	FeO	Fe_2O_3	FeO_{total}
133(1)	Sebişel Valley	29.86	19.46	0.18	0.00	0.12	0.11
153(2)	Sebişel Valley	28.94	20.40	-0.02	0.00	0.00	0.00
167(1)	Aleului Valley	43.52	5.61	0.10	0.00	0.11	0.10

(1) analyst E. Călinescu, I.P.G.G.
(2) analyst E. Colios, I.P.G.G.

Table 4
Wet-chemical Analyses of Various Monomineral Samples from Pietroasa Area (wt. per cent oxides)(1)

Sample	SiO_2	TiO_2	Al_2O_3	Fe_2O_3	FeO	MnO	MgO	CaO	K_2O	Na_2O	H_2O(3)	F(4)	O=F
139(2)	–	–	–	1.39	0.00	0.01	23.62	0.00	–	–	–	–	–
160	41.23	0.67	15.36	2.23	0.03	0.02	27.20	0.00	9.70	0.03	3.50	0.25	0.11
167	0.00	0.91	67.23	5.01	0.05	0.04	26.76	0.00	0.00	0.00	0.00	–	–
173	42.57	0.02	0.62	0.83	0.00	0.03	42.43	0.00	0.19	0.07	13.24	–	–
213	51.93	0.00	0.30	0.00	0.00	0.06	0.73	25.59	4.83	0.11	15.18	1.15	0.48

(1) analyst E. Călinescu, I.P.G.G. Samples represent: 139, forsterite; 160, phlogopite; 167, spinel; 173, lizardite; 213, apophyllite.
(2) partial analysis.
(3) water determined by the Penfield method.
(4) fluorine determined by the Grimaldi method; analyst V. Neacşu, I.P.G G.

D o l o m i t e occurs within the Pietroasa magnesian hornfels in two-textural varieties similar to those reported by Carpenter (1967) at Crestmore. Both so-called "fine-grained dolomite" (clusters of subparallel dolomite grains included in the calcite groundmass) and "coarse-grained dolomite" (equant grains of dolomite which seems to be remobilisations of the first type) have been encountered.

In magnesian marbles with calcite-dolomite intergrowths the dolomite amount within the carbonatic mass ranges between 26.62 and 91.87 per cent. It has been estimated on the basis of the partial chemical analyses presented in Table 3, after deducing the Mg contents in associated calcites by the X-ray method (Tab. 2). The stoichiometry of the dolomite formula

alpha-serpentine reaction rims. The optical features (the lack of pleochroism, +2V=85–88°, second order birefringence) indicate a term with a low content of fayalite in solid solution. The forsteritic character of the Pietroasa olivines has also been confirmed by X-ray powder study. Yoder and Sahama (1957) showed the linear dependence between the forsterite contents in olivine solid solutions and the (130) diffractometric spacing. Using their formula: forsterite (mole per cent)=4233.91–1494.59 d (130) we pointed out in the Pietroasa olivines forsterite contents ranging from 95.84 to 98.38 mole % (Tab. 5). Moreover, a partial wet-chemical analysis (sample 139 in Tab. 4) led, on the basis of the ratio $MgO:FeO_T:MnO$=23.62:1.39:0.01, to a compositional

formula of forsterite$_{97.09}$fayalite$_{2.89}$tephroite$_{0.02}$ type.

S p i n e l occurs either as disseminations throughout the carbonate mass, to which sometimes a layer texture is lent, or as inclusions in forsterite. In both situations, octahedral crystals of a blue-lavender colour and sizes ranging between 0.01 and 0.75 mm are to be found. The refractive index determinated by the Schröder's method points to an extreme magnesian term. This index is n=1,719, identical with the one indicated by Palache et al. (1961) for the magnesian end-member in spinel series. The least squares refinement of cell parameter of the same spinel sample, based on the X-ray powder data shown in Table 6, led to the value a_0=8.092 Å. This value is close to that given by Palache et al.,(1961) for synthetic $MgAl_2O_4$ (a_0=8.086±0.003 Å) but higher than that calculated by Datta and Roy (1968) for a spinel originating in some magnesian hornfels from Sweden (a_0=8,071 Å). This fact can be explained both by the magnesioferrite content (which also explains the greenish pleochroism of the Pietroasa spinel) and by a higher tetracoordinated Mg^{2+} content in the spinel formula. Such a fourfold coordinated Mg^{2+} excess characterizes the spinels generated at high temperatures (Datta, Roy, 1968).

Table 5
Forsterite Content in Olivine from Pietroasa Area, Based on Variation of (130) Spacing[1]

Sample	Location	$2\theta_{(130)}$	$d_{(130)}$(Å)	Forsterite content (mole%)
139	Aleului Valley	32.28	2.7687	95.84
167	Aleului Valley	32.30	2.7670	98.38
280	Crişul Pietros	32.30	2.7670	98.38

[1] CuKα radiation, λ=1.5418 Å, analyst C. Cristea (I.G.G.).

ence of titanium in the Pietroasa spinel indicates a $2Fe^{3+} \rightarrow Fe^{2+}(Mg^{2+})+Ti^{4+}$ type substitution, which is common in ulvöspinel. Such a substitution can also explain the increase of the cell parameter.

The infrared absorption spectra recorded for the same sample displays a trend similar to that recorded by Datta and Roy (1968) for a spinel synthesized at "low" temperatures (600° C). Similarities occur in the high intensities and the relatively tight character of the absorption band complexes between 500–800 cm^{-1} and 1000–1100 cm^{-1} (Fig. 2). The main absorption bands are those at 514 cm^{-1}, 580 cm^{-1}, 662 cm^{-1}, 680 cm^{-1}, 765 cm^{-1}, 1008 cm^{-1} and 1088 cm^{-1}.

C l i n o h u m i t e was found in many locations in the Pietroaşa zone: cu Cale Valley, Dămcoasa Hill (Rafalet, 1963), Aleului Valley (Marincea, 1992), Sebişel and Cărpineasa valleys, Borului Hill. It occurs as isolated subhedral or anhedral crystals, frequently bordered by alpha-serpentine. The diagnosis has been made based on the optical properties. The mineral has an optic axial angle (+)2V=74–77° and an extinction angle $c:n_p$=12–13°. The weak pleochroism (light yellow after n_p, colourless after n_g and n_m) and the relative low birefringence point to an extreme magnesian term (Tröger, 1959). Multiple twinning on (001) is common.

C h o n d r o d i t e occurs rarely than clinohumite in hornfels nearby the confluence of the Sebişel Valley with the Aleului Valley, where it was also reported by Rafalet (1963). The mineral was differentiated from clinohumite on the basis of the optical constants (+2V=76–81°; $c:n_p$=22–24°). It also display a weak pleochroism (golden yellow after n_p. light yellow after n_m, colourless after n_g), a relative low birefringence and is frequently twinned after (001).

D i o p s i d e scarcely occurs in the Pietroasa magnesian hornfels. Its optical properties (extinction

Table 6
The Main Diffractometric Reflections for Pietroasa Spinel[x]

d/n (Å)	4.665	2.861	2.439	2.023	1.654	1.557	1.431
I/I_o	40	45	100	45	10	35	40
(hkl)	(111)	(220)	(311)	(400)	(422)	(511)	(440)

[x] Powder method, CuKα radiation, λ=1.5418 Å; analyst C. Cristea (I.G.G.).

A wet-chemical analysis of a Pietroasa spinel (sample 167 in Table 4) led, by normalisation of the 4 (O) basis, to the following formula: $(Mg_{0.9616}Fe^{2+}_{0.0010}Mn^{2+}_{0.0008})(Al_{1.9113}Fe^{3+}_{0.0909}Ti_{0.0165})O_4$. The most probable constitutional formula would be, in this case, as follows: spinel 94.68 magnesioferrite 5.13 magnetite 0.10 jacobsite 0.09, pointing out a great amount of $MgAl_2O_4$. The pres-

$c:n_g$=38–40°; +2V=55–56°; positive elongation, lack of pleochroism, relatively low birefringence) point to a term with a low hedenbergite content, quite close to the diopside end-member.

T r e m o l i t e has, as compared with the associated minerals, a limited extent. It generally occurs in diopside+tremolite±forsterite aggregates (i.e. on Aleului Valley). The optical properties (-2V=84–85°,

extinction angle c:n_g=18–20^0, positive elongation, lack of pleochroism) also indicate a high-magnesian term, with a negligible content of ferroactinolite.

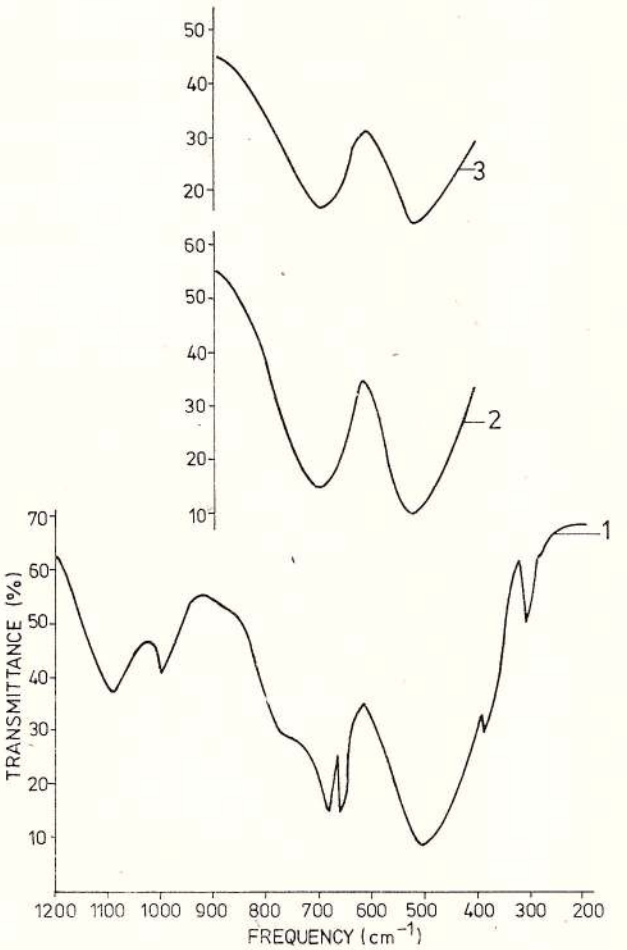

Fig. 2. Infrared absoption spectrum of a spinel from Pietroasa (1) versus similar spectra recorded by Datta and Roy (1968) for $MgAl_2O_4$ synthesized at temperatures of 600^0 C (2) and 880^0 C (3), whose transmission has been inferred from comparison with (1).

P h l o g o p i t e was first reported at Pietroasa, though this mineral is common in the magnesian hornfels area. The megascopically observed greenish colour and the quite weak pleochroism (yellowish after n_g and n_m colourles after n_p) point to a (hydroxy) phlogopite with low content of annite. The optical constants (-2V=10^0; extinction a:n_g=2^0) also indicate a magnesian term with a reduced amount of fluorphlogopite moles (-2V=0^0 for fluorphlogopite).

A wet-chemical analysis (sample 160 in Table 4) led to the following crystallochemical formula: $(K_{1.7261}Na_{0.0084})(Mg_{5.6553}Mn_{0.0025}Fe^{3+}_{0.2344}Al_{0.2770}Ti_{0.0713})(Si_{5.7518}Al_{2.2482}O_{20.6281})(OH_{3.2611}F_{0.1108})$.

The normative composition inferred from this formula points out a hydroxyphlogopite with a low content of fluorphlogopite (3.26 %) and annite-siderophyllite (4.04 %) moles.

The X-ray powder diffraction pattern recorded for the same sample (160) indicates a 2 M_1 phlogopite. This polytype is, moreover, common in the thermal contact areas (Smith, Yoder, 1956). The least squares refinement of the diffraction data rendered in Table 7 led to the following cell parameters: a_0=5.258 Å, b_0=9.252 Å, c_0=20.316 Å and β=95^{0}32′; these values are relatively close to those mentioned by Yoder and Eugster (1954) for a $2M_1$ natural phlogopite: a_0=5.347 Å, b_0=9.227 Å, c_0=20.252 Å, β=95^{0}1′.

T a l c generally occurs as isolated subhedral crystals, less commonly as bunches of crystals surrounded by the carbonate groundmass. There are noticeable some talc+tremolite aggregates which occur locally. The optical properties (-2V=0^0, positive elongation, straight extinction versus (001) perfect cleavage) are enough to identify the mineral.

C l i n o c h l o r e, first mentioned by Marincea (1992) at the confluence of the Sebişel Valley with

Table 7
X-ray Powder Data for Pietroasa Phlogopite[x]

d/n (Å)	10.07	5.052	4.608	3.810	3.540	3.371	3.285	3.157	3.024
I/I_0	100+	50	3	3	4	100	2	7	25
(hkl)	(002)	(004)	(110) (020)	(023)	(114)	(006)	(114)	(115)	(025)
d/n (Å)	2.930	2.877	2.712	2.611	2.527	2.433	2.304	2.270	2.178
I/I_0	7	15	4	6	70	4	2	3	6
(hkl)	(115)	(116)	(131)	(116)	(008)	(133)	(040) (220)	(135)	(135)
d/n (Å)	2.057	2.025	1.906		1.747	1.542			
I/I_0	4	100+	5		15	7			
(hkl)	(224)	(o.0.10)	(137)		(139)	(330) (060)			

[x] CuK_α radiation, λ=1.5418 Å; analyst C. Cristea (I.G.G.).

the Aleului Valley, has a reduced spreading within the Pietroasa contact area. Its optical properties (weak pleochroism: light green after n_p and n_m and yellowish green after n_g, low and sometimes anomalous birefringence, $+2V=20^0$, $n_p:a=0^0$) indicate an orthochlorite of pennine-clinochlore type. The diagnosis has been made based on X-ray powder diffraction data on the mineral. The high and medium-high intensities of the first five orders of the basal reflection confirm the magnesian character of this chlorite (less than 30 % Fe in octahedral coordination acc. to Brindley, 1961). Based on the values recorded for the (001) spacing (d(001)=14.24–14.27 Å) and using the formula proposed by Brindley (1961) in order to determine the diagnostic value X (d(001)=14.55–0.29X), a X variation between 0.97 and 1.07 results. Correlating this with the fairly small values of the ferromagnesian ratio $R=Fe^{2+}:(Fe^{2+}+Mg^{2+})$ inferred from the ferrous oxide deficiency in the system, the study chlorite is supposed to fall into the clinochlore field ($0\leq R\leq 0.2$ and $0.9\leq X\leq 1.2$: Hey, 1954 fide Brindley, 1961).

B r u c i t e frequently occurs in magnesian hornfels from Pietroasa. In these rocks there are two distinct, morphologically different varieties of brucite, which may be summarized as follows:

– isolated lamellas in the carbonatic mass, similar as regards their outline to those described by Carpenter (1967) as products of dolomite decomposition without periclase intermediary formation;

– small-sized lamellas as mixed radiary aggregates brucite-serpentine or brucite-szaibelyite, representing pseudomorphs after orthosilicates (forsterite, humite) or after kotoite (Marincea, 1992). "Onion-skin"-type textures have not been observed, which point to the periclase lacking in the primary paragenesis.

M i n e r a l s o f s e r p e n t i n e g r o u p are constantly found within the area of this study. Their optical properties (low birefringence, hardly visible pleochroism: colourless after n_p, fairly light greenish after n_g) are common and make impossible the discrimination of the mineral species. The prevalence of the negative optical sign, which characterizes the alpha-serpentine, suggests, however, the presence of lizardite lT (Wicks, Zussman, 1975). The occurrence of serpophite in almost all the serpentine aggregates also indicates the lizarditic nature (Wicks, Zussman, 1975 have also pointed out the equivalence serpophite=lizardite lT).

The textural aspects (alpha-serpentine mesh and hourglass textures, the former enclosing serpophite centers or relics of forsterite or clinohumite) are similar with those defining the "type 3 retrograde serpentinization" of orthosilicates (Wicks, Whittaker, 1977).

The crystallochemical formula calculated for a serpentine sample taken off from the Aleului Valley (sample 173 in Table 4) after the normalization on the basis of 18 (O, OH) of its chemical analyses, is as follows: $(Mg_{5.8430}Mn^{2+}_{0.0028}\ Fe^{3+}_{0.0578}\ Al_{0.0010}\ Ti_{0.0016}\ K_{0.0214}\ Na_{0.0116})(Si_{3.9334}Al_{0.0666}O_{9.8408})(OH)_{8.1592}$

The chemical peculiarities that can be inferred from the above formula (sum of the octahedrally coordinated cations amounts to 5.94; Mg^{2+} and Si^{4+} contents close to those from the stoichiometric serpentine; hydroxyl in excess versus the ideal formula; lack of Fe^{2+} and implicitly an infinite $Fe^{3+}:Fe^{2+}$ ratio; high Fe^{3+} content) are those pointed out by Whittaker and Wicks (1970) for lizardite.

The presence of lizardite at Pietroasa is also confirmed by the X-ray powder diffraction study. Most of the serpentine samples taken off from the study area show the characteristics considered by Whittaker and Zussman (1956) as typical of lizardite: the presence of a high intensity line at d=2.497–2.499 Å; the absence of the strong "antigoritic" line at d=1.563 Å when common lines (e.g. the high-intensity lines at d=2.524–2.530 Å and d=7.27–7.30 Å) are present; the presence of a lines doublet at d=1.503–1.507 Å and d=1.535–1.537 Å.

The thermal study points to the presence at Pietroasa of an alpha-lizardite sensu Caillère (1936) fide Todor (1972). Thus, the endothermic peak that marks the dehydration (recorded at 670^0–690^0 C on DTA curves and at 660^0–682^0 C on DTG curves) is followed by an exothermic peak recorded at 815^0–820^0 C on DTA curves, which points to a structural reorganisation (Fig. 3). The mass losses corresponding to dehydration, calculated on the basis of TGA curves, vary between 13.82 and 15.29 %, being higher than the one which corresponds to the dehydration of a stoichiometric serpentine (12.9 %). This is compatible with the H_2O^+ supracompensation mentioned by Whittaker and Wicks (1970) for lizardites.

A p a t i t e sporadically occurs in the Pietroasa magnesian hornfels. Crystals with subhedral and locally anhedral, amoeba-like contours are disseminated throughout the contact area. The characteristic features point to the "hydrothermal transport" of the mineral, within a process similar to that described by Williams and Cesbron (1977).

M a g n e t i t e scarcely occurs at Pietroasa, indicating the ferric deficit of the system. In zones affected by the boron-metasomatism, magnetite is generally pseudomorphous after ludwigite, being found in association with szaibelyite (Marincea, 1992). Otherwise, magnetite crystals are disseminated in the carbonate and silicate mass.

H e m a t i t e generally occurs in martitic pseudomorphs after magnetite. Its presence has been confirmed by X-ray diffraction. The main diffraction lines are those at 3.67 Å(I/I_0=35), 2.69 Å(100), 2.52 Å(80),

2.20 Å(25), 1.839 Å(35), 1.692 Å(40) and 1.454 Å(25).

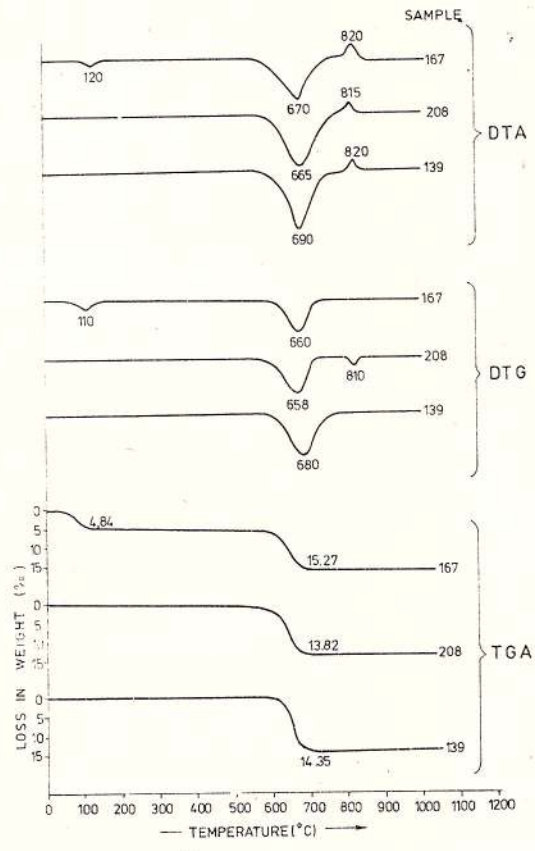

Fig. 3 Thermal curves recorded for (alpha)-lizardite samples from Pietroasa magnesian hornfels.

3.2 Calcic hornfels

Zones with calcic hornfels locally occur in the magnesian hornfels area. Generally, they are surrounded by a diopside transition zone and mainly contain assemblages of the following minerals: wollastonite, epidote, calcite, apophyllite, apatite. This mineralogy indicates an active fluorine-metasomatism and justifies our attention. The premetamorphic rock seems to be, in this case, represented by the grey limestones of Lower Anisian age (Bordea, Bordea, 1973).

A p o p h y l l i t e occurs as colourless crystals with sizes after (100) and (010) up to 6 mm, which are locally intergrown after (001). It was found on a gallery waste on the Aleului Valley, at about 500 m upstream the confluence with the Sebişel Valley. Wollastonite relics in apophyllite suggest its genesis as an alteration product of the former.

The crystal shapes are characterized by the wide development of the basal pinacoid faces (001) which determine their tabular habit. The tracht is marked by the prevalence of tetragonal prisms (100) and (010) and of tetragonal bipyramid (111) forms (Fig. 4).

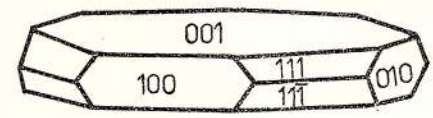

Fig. 4. – Tracht of an apophyllite crystal from the calcic hornfels in the Aleului Valley.

The mineral shows normal optical properties. It has a low birefringence with anomalous tendency (in grey-brown hues), negative elongation, straight extinction versus the (001) perfect cleavage and slightly negative relief. The relatively high refringence (a medium value for the refractive indices, obtained by the Schröder method, is n=1.539) and the uniaxial positive character indicates (acc. to Wenzel, 1917 fide Deer et al., 1962) the presence at Pietroasa of a hydroxyapophyllite (n_g=1.543 and n_p=1.542 for the end-member: Dunn et al., 1978).

The crystallochemical formula determined on the basis of the chemical analysis in Table 4 (sample 213) explains the typical optical behaviour. This formula is: $(K_{0.9488}Na_{0.0334})$ $(Ca_{4.2166}Mg_{0.1680}Mn_{0.0074})$ $(Si_{3.9924}Al_{0.0274}O_{10.1849})_2(OH_{0.5732}$ $F_{0.5570})$. $8H_2O$, pointing to the weak predominance of the hydroxyapophyllite moles (50.72 %) over the fluorapophyllite ones (49.28 %).

The X-ray powder diffraction data on the mineral (Tab. 8) also characterize an intermediary apophyllite. This fact, inferred on the basis of the displacement of the main diffractometric reflections towards 2θ values higher than those recorded for fluorapophyllite (as a result of the $OH^- \rightarrow F^-$ substitution), has been confirmed by the least squares refinement of the cell parameters. The obtained values (a_0=8.973 Å and c_0=15.769 Å) are higher than those recorded by Colville et al. (1971) for a fluorapophyllite (a_0=8.963 Å and c_0=15.768 Å), but lower than the ones recorded by Dunn et al. (1978) for hydroxyapophyllite (a_0=8.978 Å, c_0=15.830 Å).

W o l l a s t o n i t e was found as relics in apophyllite. Wollastonite needle-like crystals (with sizes of 0.10–0.25 mm after b) are arranged as sheaves which constitute bands inside apophyllite crystals, without disturbing its optical continuity. These zones seem to be due to some chemical variations in the primary wollastonite aggregates (i.e. the differentiated presence of Mg^{2+}, Mn^{2+} and Fe^{2+} as substitutes of Ca^{2+}). Because the main diffraction lines of the wollastonite are superposed over those of apophyllite, the diagnosis of the former was made on the basis of optical properties.

Table 8
X-ray Powder Data for Pietroasa Apophyllite[x]

d/n (Å)	7.83	6.32	4.535	3.939	3.880	3.573	3.350	3.165	2.975		2.812
I/I_0	30	5	50	100	15	25	15	9	95		5
(hkl)	(002) (101)	(110)	(103)	(004)	(211) (202)	(212)	(114)	(220) (213)	(105) (204)		(214)
d/n (Å)	2.666	2.490	2.481	2.426	2.185	2.107	2.103	2.004	1.770	1.763	1.721
I/I_0	5	35	50	20	3	15	15	6	10	15	4
(hkl)	(312)	(313) (320)	(215) (224)	(116)	(107)	(315)	(324)	(420)	(317)	(510)	(512)
d/n (Å)	1.671	1.619	1.605	1.578	1.546	1.470	1.453				
I/I_0	3	3	3	45	7	6	3				
(hkl)	(327)	(209)	(219) (514)	(441)	(328) (337)	(602)	612)				

[x] CuK_α, λ=1.5418 Å; analyst C. Cristea, I.G.G.

Pietroasa wollastonite has a (−)2V angle of about 40° and an extinction angle (c:n_p?) of about 30°.

E p i d o t e occurs as isolated grains in the calcic hornfels mass, pointing out, in all probability, the ferroaluminous excess in the system. The mineral has been defined as epidote s.s. considering its negative optical sign (acc. to Deer et al., 1962). The high birefringence and refringence, the extinction angle (c:n_p=9–11°) and the strong pleochroism (greenish yellow after n_m and yellow after n_p) also indicate an epidote.

4. Mineralogy of the boron-metasomatized areas

L u d w i g i t e, which has been reported by Rafalet (1963), Stoicovici and Stoici (1969) and Marincea (1992) from various zones of the Pietroasa contact area (Aleului Valley, Cărpineasa Valley, Sebişel Valley), is a certain indicator of the boron metasomatism nearby the banatitic body. Needle-like ludwigite crystals of millimetric sizes occur in nodular or fan-like aggregates which are generally disseminated in a carbonate mass.

In transmitted light the mineral shows a practically opaque behaviour, which points out the content of vonsenite (Winchell, 1959). There are, however, a few marginal translucent zones, where ludwigite is partly substituted by szaibelyite, which shows a pleochroism ranging from olive green to brown: the vibrational directions could not be specified. The ferrous content was also confirmed by the chalcographic study. The mineral has a strong bireflection in grey shades (light grey after the elongation direction – bluish grey after the other one), is anisotropic (in grey-brown tints) and displays a reflectivity lower than the one of associated magnetite. The main X-ray powder diffraction lines that are those at 5.12 Å(I/I_0=100), 2.547 Å(95), 2.163 Å(35) and 1.995 Å(30) confirm the optical diagnosis.

S z a i b e l y i t e was first mentioned by Stoicovici and Stoici (1969) at the confluence of the Sebişel Valley with the Aleului Valley and was described in detail by Marincea (1992). Its optical properties (refractive indices vary around the value n=1.65) and cell parameters (a_0=12.55 Å, b_0=10.359 Å, c_0=3.215 Å, β=95.72 Å) point out the presence at Pietroasa of a szaibelyite nearby the magnesian end-member. The chemical analysis (Marincea, 1992) confirmed the low percentage (0.37–0.42 %) of sussexite moles. The typical fibrous habit and the high birefringence (the mineral polarizes in colour belonging to the second half of the fourth order) facilitates the microscopic diagnosis. The main X-ray diffraction lines are those at 6.73 Å(I/I_0=100), 5.19 Å(50), 3.25 Å(50), 2.665 Å(55), 2.432 Å(60), 2.207 Å(75) and 2.084 Å(60).

5. Petrogenetic aspects

5. 1. Isochemical metamorphism

The acceptance of an isochemical character for the thermal metamorphism in the Pietroasa area is obviously based on the petrographic study of the premetamorphic rocks. The Anisian dolostones occurring in the study area are similar in the aspect to those described by Moore and Kerrick (1976) in the Alta aureole (Utah) as "massive dolomite" (siliceous dolomites with disseminated quartz grains). Considering that, the development of most of the reactions in the system CaO-MgO-SiO_2-H_2O-CO_2 can be presumed. The relative abundance of the alloclasts of various mineral nature (illite, sericite, chlorites, biotite, hydrobiotite, microcline, plagioclase) leads to the appearance into the system of two more important components (K_2O and Al_2O_3) as well as of some "accesories" ("indifferent") and "isomorphous" (sensu Korzinskii, 1959 fide Melson, 1966) components: TiO_2, Na_2O and FeO,

Fe_2O_3, MnO respectively. The acceptance within this framework of an ideal petrogenetic scheme based on experimental topologies, e.g. those shown in Figure 5 and Table 9, can be paragenetically proved.

under conditions of high mole fractions of carbon dioxide, as can be proved by the paragenesis forsterite + diopside + tremolite (invariant A in Figure 5), implies that water pressure differs from the total pressure and

Table 9
The Main Reactions Defining Mineral Equilibria in the System CaO-MgO-$KAlO_2$-SiO_2-CO_2-H_2O (reactions in Figure 5)[x]

Reaction No	Equilibrium	Fluid	Reference
1	dol+H_2O=cc+br+CO_2	H_2O, CO_2	Kerrick, 1970
2	dol=cc+per+CO_2	CO_2	Kerrick, 1970
3	per+H_2O=br	H_2O	Johannes, Metz, 1968 fide Kerrick, 1970
4	tr+3cc+qz=di+H_2O+CO_2	H_2O, CO_2	Melson, 1966; Skippen, 1974
5	dol+2qz=di+CO_2	CO_2	Melson, 1966; Skippen, 1974
6	5dol+8qz+H_2O=tr+3cc+7CO_2	H_2O, CO_2	Melson, 1966; Moore, Kerrick, 1976
7	di+3dol=2fo+4cc+2CO_2	CO_2	Skippen, 1974; Moore, Kerrick, 1976
8	clh+cc+CO_2=4fo+dol+H_2O	H_2O, CO_2	Moore, Kerrick, 1976
9	2clh+13dol+11CO_2=tr+15cc+H_2O	H_2O, CO_2	Moore, Kerrick, 1976
10	3dol+4qz+H_2O=tc+3cc+3CO_2	H_2O, CO_2	Moore, Kerrick, 1976
11	2tc+3cc=tr+dol+H_2O+CO_2	H_2O, CO_2	Moore, Kerrick, 1976
12	tr+3cc=4di+dol+CO_2+H_2O	H_2O, CO_2	Moore, Kerrick, 1976
13	di+H_2O+3CO_2=8fo+13cc+9CO_2+H_2O	H_2O, CO_2	Moore, Kerrick, 1976
14	5ph+6cc+24qz=3tr+5KF+2H_2O+6CO_2	H_2O, CO_2	Hoschek, 1973 (extended data)
15	2fo+3H_2O=se+br	H_2O	Johannes, 1969
16	se+2qz=tc+H_2O	H_2O	Johannes, 1969

[x] Melson's (1966) argumentation for considering K_2O as $KAlO_2$ was accepted.

The prograde isograde sequence in the Pietroasa dolomite seems to be of: talc–brucite I–phlogopite-tremolite–diopside–forsterite–spinel–chondrodite– clinohumite type. The retrograde metamorphism, whose products are essentially hydrous minerals (e.g. serpentine, brucite II), broadly coincides with the hydrometasomatism in the final evolutional stage and implies high mole fractions of water.

There are two peculiarities which differentiate the Pietroasa topologies from the "classical" ones proposed by Moore and Kerrick (1976):

1. The presence of Al_2O_3. The local abundance of magnesian chlorites, biotite or hydrobiotite can explain the thermometamorphic genesis of the spinel, which is almost always found in association with forsterite±talc. This assemblage suggests a breakdown reaction of the type: 5 clinochlore = 7 forsterite + 5 spinel + 2 talc + 18 H_2O (Segnit, 1963).

The metastability of the talc + spinel assemblage at high water pressures (Fawcett, Yoder, 1966) would make impossible such a reaction. However, the development of the reactions within this thermal range does not exclude the coexistence of two phases.

2. The presence of K_2O seems to be due both to the presence of some alloclasts of potassium minerals (i.e. potassium feldspar, illite, sericite, biotite) and to the authigenesis of the potassium feldspar in certain zones inside the Anisian dolostones mass. It is to be noted that the K_2O content of these dolostones varies between 0.02 and 0.17 per cent. Hence, there results the occurrence of phlogopite both in layered hornfels similar to those described by Melson (1966) as products of the isochemical metamorphism of some argillaceous beds interlayered with dolomite, and in isolated blasts in the magnesian marbles.

5.2. Boron-fluorine metasomatism

The presence within the Pietroasa contact area of some minerals which probably have fluorine contents (e.g. chondrodite, clinohumite, clinochlore, tremolite, talc, apatite) beside those whose contents have already been mentioned (phlogopite, apophyllite), points out the active role of the fluorine metasomatism during the mineralogenesis, as well as its continuity within a wide thermal interval.

The instability of the first-formed hydroxyl-bearing minerals (e.g. talc, tremolite), as a result of the fluorine presence in the system (Tell, 1972), originates in their low capacity to admit fluorine as a hydroxyl substitute (Tröger, 1959; Moore, Kerrick, 1976). Hence, the possibility of the talc-chondrodite and tremolite-clinohumite prograde conversion, within reactions similar to the experimental ones outlined by Tell (1972):

1 talc + 7 dolomite + 2 fluorite = 2 chondrodite + 9 calcite + 5 CO_2 + 1 H_2O

1 tremolite + 13 dolomite + 2 fluorite = 2 clinohumite + 17 calcite + 9 CO_2 + 1 H_2O

The presence of fluorite as a perfect mobile constituent of the fluid phase (Turner, Verhoogen, 1960) brings about a decrease of the OH activity in the hydroxyl-bearing phases. That certainly determines the shifting of the experimentally-determined equilibria in Figure 5, without changing the trend of the T–X curves (Moore, Kerrick, 1976).

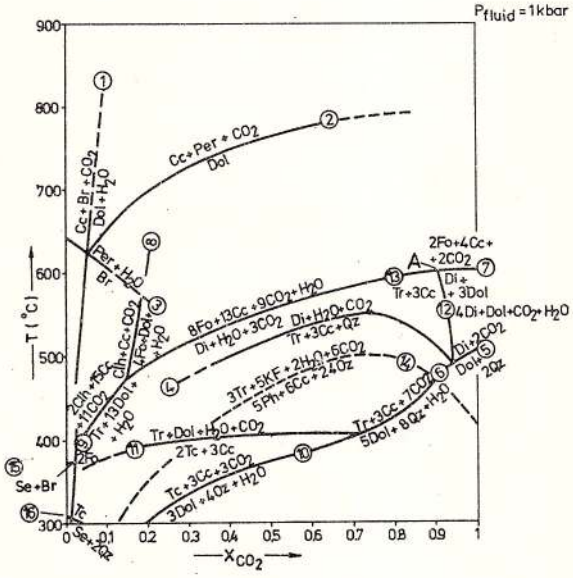

Fig. 5 – T X_{CO_2} diagram, at P_T=1kb, implying the main mineral equilibria in the system CaO-MgO-Al_2O_3-K_2O-SiO_2-H_2O-CO_2 (reactions from Table 9). Abbreviations: Br=brucite; Cc=calcite; Chl=clinohumite; Di=diopside; Dol=dolomite; Fo=forsterite; KF=potassium feldspar; Per=periclase; Ph=phlogopite; Qz=quartz; Se=serpentine; Tc=talc; Tr=tremolite.

The physico-chemical conditions for the boron metasomatism have been presented in a previous paper (Marincea, 1992). It results that the conditions considered by Barsukov and Egorov (1957) fide Marincea (1992) as essential for the crystallization of the endogene borates have been fulfilled:

1) the interaction with the mass of dolomite determines the precipitation of boron, which is probably transported by the alkaline solutions as boron-fluorine compounds;

2) iron is the primary precipitant of boron, ludwigite being the first-formed boron mineral. Its deficit in the system makes possible the synchronous crystallization of the pure magnesian borates (e.g. fluoborite, suanite, kotoite) which are later substituted by szaibelyite.

The breakdown of fluoborite because of its szaiblytization (Marincea, 1992) releases fluorine, easily to be found in the late phases of apophyllite type.

5.3. Physical conditions of thermometamorphism

5.3.1. *Temperature*

The absence of periclase among the breakdown products of dolomite indicates for the prograde metamorphism maximal temperatures below the periclase isograde (reaction 2 in Figure 5). These temperatures are, undoubtly, close to those of the granodioritic magma: 750^0 C at 1kb total pressure acc. to Turner, Verhoogen (1960). There are many mineralogical arguments which demonstrate such a maximal prograde temperature:

1) the presence of wolastonite in the calcic hornfels area;

2) the absence of minerals which commonly occur in silica-deficient associations metamorphosed in pyroxene or sanidinite hornfels facies, e.g. monticellite, melilite etc.

3) the presence throughout the contact area of $2M_1$ phlogopite and not of polytypes 3T or 1M of this mineral, more stable at higher temperatures (Yoder, Eugster, 1954);

4) the relative small lattice parameter of the spinel and the trend of its infrared absorption spectrum, which clearly differs from the one obtained by Datta and Roy (1968) after heating $MgAl_2O_4$ at 880^0 C (Fig. 2).

The occurrence in the study area of fine-grained dolomite which is clearly the result of exolution from a high-magnesian calcite after cooling (Goldsmith, 1960) indicates that $MgCO_3$ concentrations in the carbonate solid solution was initially higher. That is consistent with prograde temperatures higher than 500^0 C, at which calcite dissolves only about 5 mole per cent magnesite (Goldsmith, 1960).

The lower thermal limit for the prograde mineralogenesis in the Pietroasa contact area seems to correspond to the lower stability of talc (reaction 10 in Figure 5, acc. to Johannes, 1969).

5.3.2. *Pressure*

It is reasonable to consider that, during thermal metamorphism, the rapid recrystallization beside the devolatilization reactions can maintain the volatile pressure at a level which is sensibly equal to the lithostatic pressure. Therefore, the pressure estimation considering a system closed for the volatile phases is

reduced to the estimation of the lithostatic pressure. It is obviously higher than the minimum value of about 150 bars which was inferred based on the amount of the actual cover (Anisian-Liassic deposits with a mean density of 2.6 gms/cc). As far as considerable erosion occurred between the intrusion of the Pietroasa granodiorite and till the present and the regional tectonics was also changed, a value of about 1 kilobar was probably attained at the present level of exposure. This value was moreover considered when the equilibria in Figure 5 were established.

5.3.3. *Eh and pH evolution*

The low fugacity of O_2 between the final stage of the prograde metamorphism, due to the oxidation reactions of the organic impurities in the Anisian dolostones, obviously determines a reducing Eh. This fact is proved by the presence throughout the magnesian hornfels of the poor pleochroic varieties of chondrodite and clinohumite which crystallize under negative Eh conditions (Deer et al., 1962). During this stage the fayalite content in olivine is supposed to have been higher than the present one. The increase of the oxygen fugacity as a result of the devolatilization reactions at high temperatures probably led to the oxidation of the fayalite present in the solid solution. This transformation can be approximated by the reaction $3Fe^{2+}(SiO_4) + O_2 = 2Fe^{2+}Fe_2^{3+}O_4 + 3SiO_2$ (Nitsan, 1974) and is proved by the small inclusions of magnetite in the silicate mass.

The retrograde metamorphism led to the progressive setting of an oxidizing Eh, which determines the lizarditic nature of serpentine and the martitization of magnetite. Negative Eh is maintained only in the areas affected by the boron-fluorine metasomatism (Marincea, 1992).

The pH evolution from low alkaline to acid has been influenced, during the prograde metamorphism, by the increase of the carbon dioxide mole fraction as a result of the breakdown of carbonates. Most of the reactions which occurred in the aureole evolved a CO_2-rich fluid. Later, the hydrometasomatism induced by the normal evolution of the granitoid body, progressively led to a basic pH on the full extent of the contact aureole. It could explain why the retrograde metamorphism is mainly hydratant.

6. Conclusions

Most of the mineral assemblages in the Pietroasa contact area characterize silica-deficient magnesian associations (Turner, Verhoogen, 1960). In these associations, poorly aluminous, iron is reduced to an "isomorphous component" (Korzhinskii, 1959 fide Melson, 1966). The prograde temperatures nearby the granitoid contact correspond approximately to those estimates for the hornblende-hornfels facies (Turner, Verhoogen, 1960). Arguments in this respect are:

1) the estimation, in case of the calcic hornfels in the contact area, of a maximum temperature at the wollastonite isograde, according to this mineral occurrence in the inner contact zone. Its presence requires moderate pressures of CO_2. The lack of periclase from the Pietroasa magnesian hornfels can signify both the inversion proposed by Turner and Verhoogen (1960) of stage 5 in Bowen's series (periclase) with stage 6 (wollastonite) and higher water pressures;

2) the presence of some of the typical associations e.g. the forsterite-tremolite-diopside (which marks the invariant point A in Figure 5), forsterite-brucite-spinel-diopside and forsterite-talc-clinochlore ones.

Other associations, e.g. calcite-talc-dolomite or calcite-tremolite-dolomite, certify that in the "cold" zones of the aureole (far from the contact) the temperatures correspond to those estimated for the albite-epidote hornfels.

The temperature differences between various locations in the contact aureole facilitate the movement of the "perfectly mobile" components e.g. H_2O, CO_2, F, which explains the hydrothemal migration of apatite. The boron-fluorine supply in the metamorphic fluids locally determines an intense diffusion metasomatism, resulting in the borate crystallization in the sequence ludwigite-fluoborite (?)-suanite (?)-kotoite (Marincea, 1992). Somewhere the large extent of the boron-metasomatism is compatible only with an infiltration mechanism, tectonically controlled.

The retrograde evolution generates hydroxyl-bearing minerals e.g. brucite II, lizardite, szaibelyite, which are generally superposed over the primary associations. A thermal interval ranging between 275^0 and 350^0 C can be accepted for the crystallization of these minerals (Marincea, 1992). The subsequently-crystallized minerals (goethite, lepidocrocite) have not been described in the paper.

Acknowledgements. Thanks are expressed to Dr. G. Udubaşa and Mr. G. Sabău, Mr. Gh. Ilinca and Mr. G. Bindea for advice, criticism and interest in this work.

I am endebted also to Mrs. Elena Călinescu, Mrs. Vasilica Neacşu and Mrs. Elena Colios for chemical analyses, to Mr. T. Drăghiciu for thermal analyses, to Mrs. Gabriela Stelea for infrared spectrographic studies and to Mrs. Corina Cristea for X-ray powder diffraction data and for cell-parameters calculations.

References

Bordea S., Bordea J. (1973) Noi date stratigrafice şi structurale în nord-vestul Munţilor Bihor. *D. S. Inst. Geol. Geofiz.*, LIX/5 (1972), p. 5–12, Bucureşti.

Brindley G. W. (1961) Chlorite Minerals in "The X-ray identification and crystal structures of clay minerals". Ed. by G. Brown, Mineralogical Society, London, p. 242–296.

Brown G. (1961) Other Minerals in "The X-ray identification and crystal structures of clay minerals". Ed. by G. Brown, Mineralogical Society, London, p. 467–488.

Carpenter A. B. (1967) Mineralogy and petrology of the system CaO-MgO-CO_2-H_2O at Crestmore, California. *Amer. Min.*, 52, 9–10, p. 1341–1363, Washington.

Colville A. A., Anderson C. P., Black P. M. (1971) Refinement of the crystal structure of apophyllite (1). *Amer. Min.*, 56, 7–8, p. 1222–1234, Washington.

Datta R. K., Roy R. (1968) Order – disorder in $MgAl_2O_4$. The systems: $MgAl_2O_4$ – $LiAl_5O_8$, $MgAl_2O_4$ – $NiCr_2O_4$, $MgAl_2O_4$ - $NiAl_2O_4$ – $ZnAl_2O_4$. *Amer. Min.*, 53, 9–10, p. 1456–1475, Washington.

Deer W. A., Howie R. A., Zussman J. (1962) Rock-Forming Minerals, vol. I, Ortho- and Ring Silicates; vol III, Sheet Silicates, Longmans Ed., London.

Dunn P. J., Rouse R. C., Norberg J. A. (1978) Hydroxy-apophyllite, a new mineral, and a redefinition of the apophyllite group. I. Description, occurrences and nomenclature. *Amer. Min.*, 63, 1-2, p. 196–198, Washington.

Fawcet J.J., Yoder H. S. (1966) Phase relationships of chlorites in the system MgO-A_2O_3-SiO_2-H_2O. *Amer. Min.*, 51, 3–4, p. 353–380, Washington.

Goldsmith J. R. (1960) Exolution of dolomite from calcite. *J. Geol.*, 68, 1, p. 103–109, Chicago.

– , Graf D. L., Joensuu O. I. (1955) The occurrence of magnesian calcites in nature. *Geochim. Cosmochim. Acta*, 7, p. 212–230, London.

Hoschek G. (1973) Die Reaktion Phlogopite + Calcite + Quartz = Tremolit + Kalifeldspat + H_2O + CO_2. *Contrib. Mineral. Petrol.*, 39, p. 231–237, Berlin-Heidelberg-New York.

Johanes W. (1969) An experimental investigation of the system MgO-SiO_2-H_2O-CO_2. *Am. Jour. Sci.*, 267, 9, p. 1083–1104, New Haven.

Kerrik D. M. (1970) Contact metamorphism in some areas of the Sierra Nevada, California. *Geol. Soc. America Bull.*, 81, 10, p. 2913–2938, Boulder, Colorado.

Marincea Şt. (1992) New data concerning szaibelyite from Romania: the Gruiului Hill occurrence (Aleului Valley, Bihor Mountains). *Rom. J. Min.*, 75, p. 69–85, Bucureşti.

Melson W. G. (1966) Phase equilibria in calc-silicate hornfels, Lewis and Clark County, Montana. *Amer. Min.*, 51, 3–4, p. 402–421, Washington.

Moore J. N., Kerrik D. M. (1976) Equilibria in siliceous dolomites of the Alta aureole, Utah. *Am. Jour. Sci.*, 276, 4, p. 502–524, New Haven.

Nitsan U. (1974) Stability field of olivine with respect to oxidation and reduction. *Jour. Geophys. Research*, 79, 5, p. 706–711, Washington.

Palache Ch., Berman H., Frondel C. (1961) Dana's system of mineralogy. Vol. I, 7^{th} edition, John Wiley and Sons. New York-London.

Rafalet A. (1963) Notă asupra rocilor din aureola de contact a masivelor granodioritice de la Pietroasa şi Budureasa. *Asoc. Geol. Carp.-Balc., Congres V, II, Min-Petr.*, p. 199–204, Bucureşti.

Segnit R. E. (1963) Synthesis of clinochlore at high pressures. *Amer. Min.*, 48, 7–8, p. 1080–1089, Washington.

Skippen G. (1974) An experimental model for low pressure metamorphism of siliceous dolomitic marble. *Am. Jour. Sci.*, 274, 5, p. 487–509, New Haven.

Smith J. V., Yoder H. S. (1956) Experimental and theoretical studies of the mica polymorphs. *Miner. Mag.*, XXXI, 234, p. 209–235, London.

Stoicovici E., Stoici S. D. (1969) Contribuţii la cunoaşterea mineralizaţiei de bor din bazinul superior al Crişului Negru (Băiţa Bihor). *Studia Univ. Babeş-Bolyai, Geol.-Geogr.*, 2, p. 11–24, Cluj.

Ştefan A., Lazăr C., Berbeleac I., Udubaşa Gh. (1988) Evolution of banatitic magmatism in the Apuseni Mts and associated metallogenesis. *D. S. Inst. Geol. Geofiz.*, 72-73/2, p. 195–213, Bucureşti.

Tell I. (1972) Hydrothermal studies on fluorine and boron metamorphic reactions in dolomite. *Publ. Inst. Miner. Paleont., Quat. Geol., Univ. of Lund*, Sweden, Lund, 63 p.

Todor D. N. (1972) Analiza termică a mineralelor. Ed. Tehnică, 279 p., Bucureşti.

Tröger W. E. (1959) Optische Bestimmung der gesteinsbilden Minerale. E. Schweizerbart'sche Verlagsbuchhandlung, 147 p., Stuttgart.

Turner F. J., Verhoogen J. (1960) Igneous and metamorphic petrology. Second edition. Mc. Graw-Hill Book Company Inc., New York-Toronto-London.

Whittaker E. J. W., Wicks F. J. (1970) Chemical differences among the Serpentine "polymorphs": A discussion. *Amer. Min.*, 55, 5–6, p. 1025–1047, Washington.

– , Zussman J. (1956) The characterization of serpentine minerals by X-ray diffraction. *Miner. Mag.*, 31, p. 107–126, London.

Wicks F. J., Whittaker E. J. W. (1977) Serpentine textures and serpentinization. *Can. Miner.*, 15, 4, p. 459–488, Ottawa.

– , Zussmân J. (1975) Microbean X-ray diffraction patterns of the serpentine minerals. *Can. Miner.*, 13, 3, p. 244–258, Ottawa.

Williams S. A., Cesbron F. P. (1977) Rutile and apatite: useful prospecting guides for porphyry copper deposits. *Miner. Mag.*, 41, p. 288–292, London.

Winchell A. N. (1959) Elements of optical mineralogy. An Introduction to microscopic petrography. Fourth edition, II, Descriptions of minerals. John Wiley and Sons. Inc., 237 p., New York.

Yoder H. S., Eugster H. P. (1954) Phlogopite synthesis and stability range. *Geochim. Cosmochim. Acta*, 6, 4, p. 157–185, London.

– , Sahama Th. G. (1957) Olivine X-ray determinative curve. *Amer. Min.*, 42, 7–8, p. 475–491, Washington.

Received: May 7, 1991

Accepted: May 8, 1991

Presented at the scientific session of the Institute of Geology and Geophysics: May 21, 1991

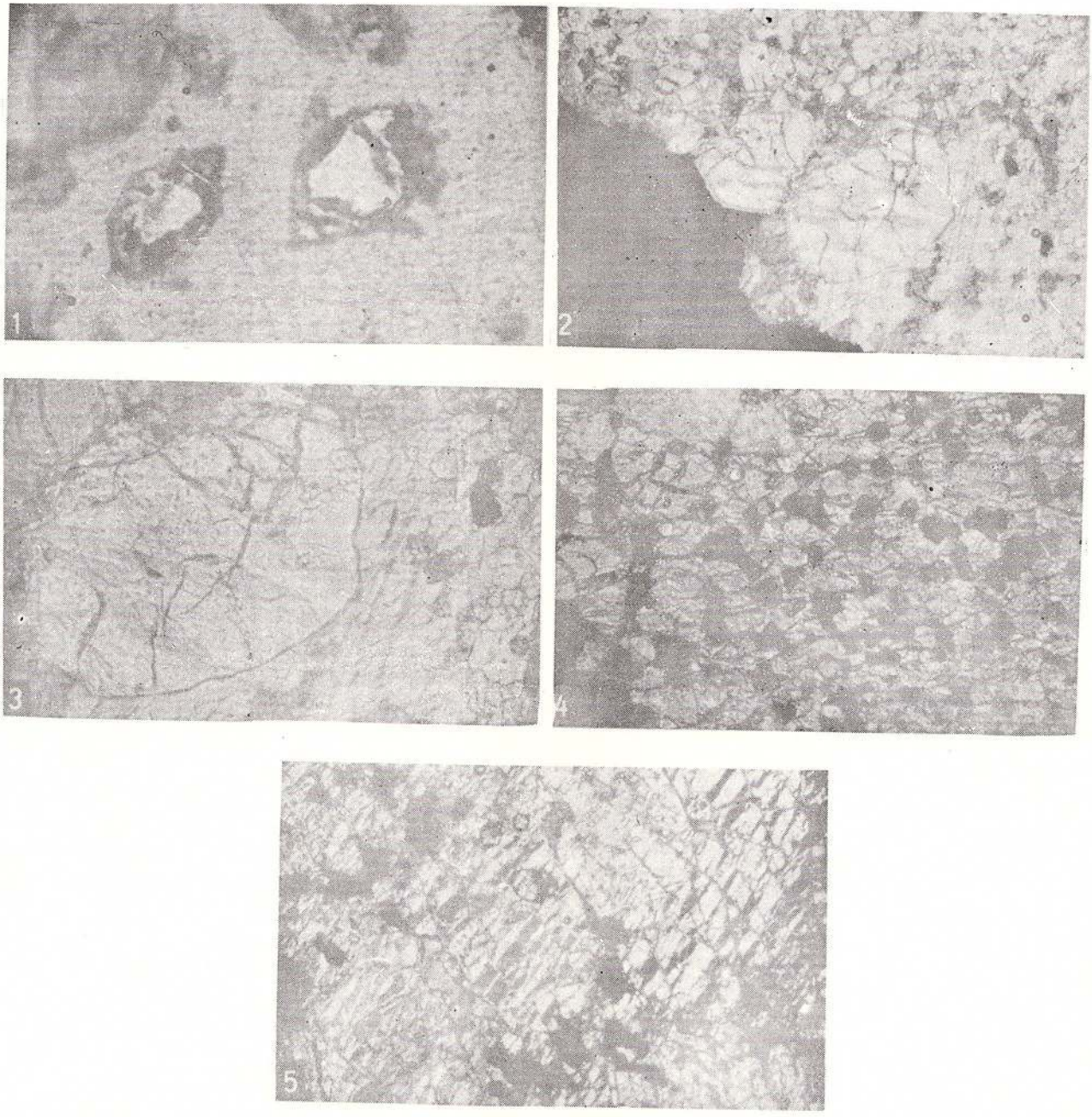

Plate I

Fig. 1 – Forsterite with alpha-serpentine rims in the carbonate mass. Crossed nicols, 20 x.
Fig. 2 – Polysynthetically twinned clinohumite beside calcite and forsterite. Crossed nicols, 10 x.
Fig. 3 – Detail of the image in Figure 2. Crossed nicols, 20 x.
Fig. 4 – Spinel crystals rimmed by forsterite. Crossed nicols, 20 x.
Fig. 5 – Incipient pseudomorphs of serpentine after forsterite (proto mesh-texture). Crossed niclos 20 x.

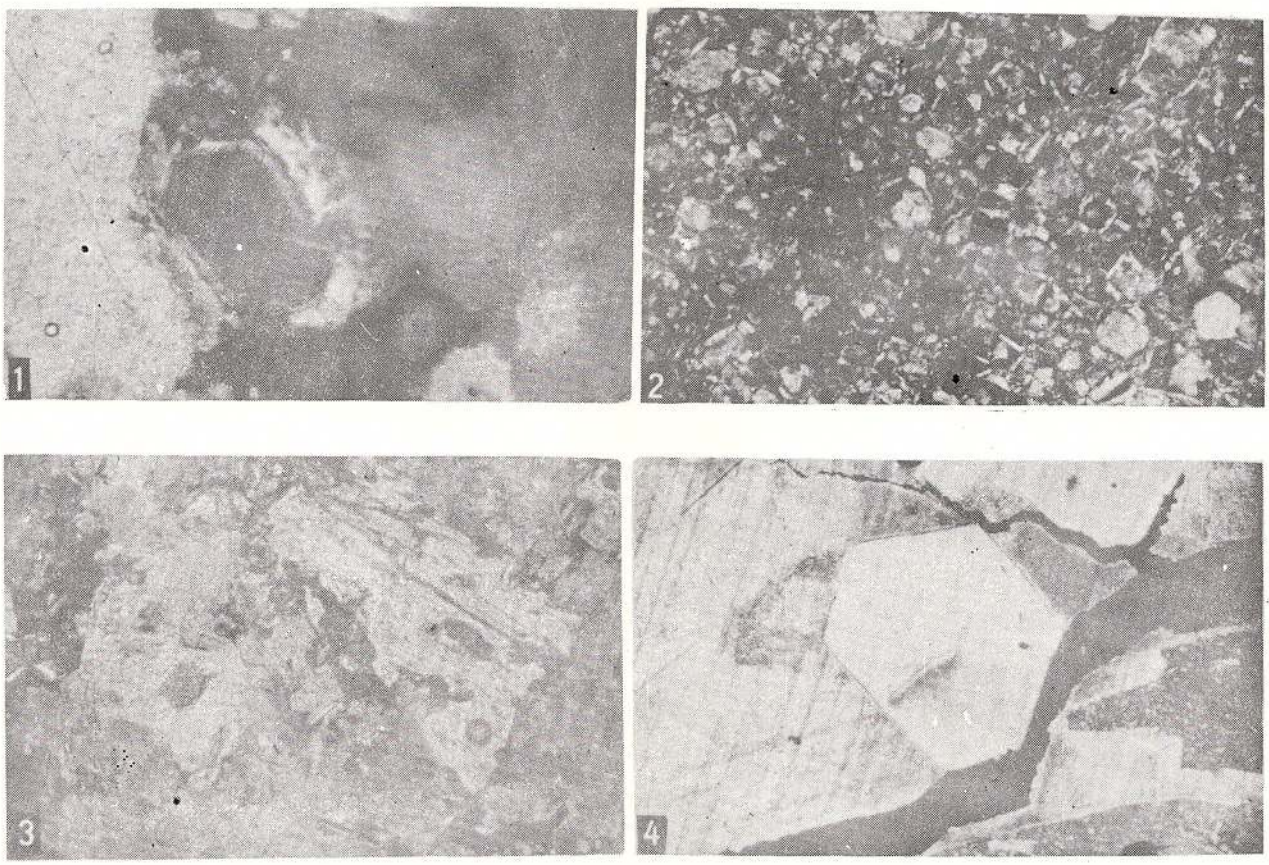

Plate II

Fig.1 – Serpophite rimmed by alpha-serpentine, pseudomorphous after forsterite. Crossed nicols, 20 x.
Fig. 2 – Serpentine mesh-texture with relict forsterite centers. Crossed nicols, 20 x.
Fig. 3 – Brucite (br) beside a szaibelyite-brucite intergrowth (sz+br). Crossed nicols, 20 x.
Fig. 4 – Phlogopite with brucite inclusions surrounded by the carbonate mass. Crossed nicols, 10 x.

Rom. J. Mineralogy, 1993, 76, 1, p. 43–46

URANIUM MINERAL OCCURRENCES IN THE CRYSTALLINE SCHIST AREA OF THE DROCEA MOUNTAINS

Haralambie SAVU

Institutul de Geologie şi Geofizică. Str. Caransebeş 1, 78344 Bucureşti 32.

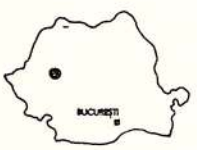

Key words: Uranium minerals. Crystalline rocks. Apuseni Mountains – Drocea Mountains.

Abstract: There are two types of uranium concentrations in the crystalline schist area (Păiuşeni Series) from the Drocea Mountains: primary and secondary. A primary concentration occurs in a feldspathic quartzite on the Păcurăreşti Brook. It is lenticular and consist of partly disintegrated pitchblende, giving rise to a black-greyish to brown-reddish earthy material. The uranium lenses contain chalcopyrite bands in the median part. The secondary concentrations occur on the unconformable plane between the Senonian sedimentary deposits or Neogene volcanics and the Paleozoic crystalline schists of the Păiuşeni Series. Uranium was carried away in aqueous solution from the Paleozoic crystalline schists and deposited in these secondary concentrations. The latter contain uranium oxides and especially autunite and torbernite, minerals present also on the fissures crossing the uranium primary concentrations.

Introduction

In 1956 I was charged by the Geological Committee with the task of mapping on scale 1:10,000 the crystalline schists zone from the Drocea Mts, where the Rare Metal Enterprise had pointed out with the help of the Geiger-Müller counters uranium mineralizations, and therefore needed a detailed geologic map. I carried out this task during the field work of that year (Savu, 1956, unpubl. data) together with a team of geologists, the componence of which changed during that period, and published subsequently a paper on the crystalline schists in the region (Savu et al., 1967).

During the field investigations I noticed a uranium mineralization on the Păcurăreşti Brook at the springs of the Prundu Valley (Păiuşeni), that occurred in a ditch made by the mentioned enterprise. This mineralization as well as some similar exposures in the region were again investigated in the next years in view of drawing up the papers that occurred subsequently (Savu, 1962; Savu et al., 1967), but owing to some unfavourable circumstances I gave up then publishing the results of my investigations, mentioning instead the presence of the feldspathic quartzites on the Păcurăreşti Brook, which were impregnated with copper minerals, iron oxides etc (Savu, 1962).

In this paper the occurrences and the physiographic aspects of some uranium minerals from the crystalline schists of the Păiuşeni Series in the region are presented (Fig. 1).

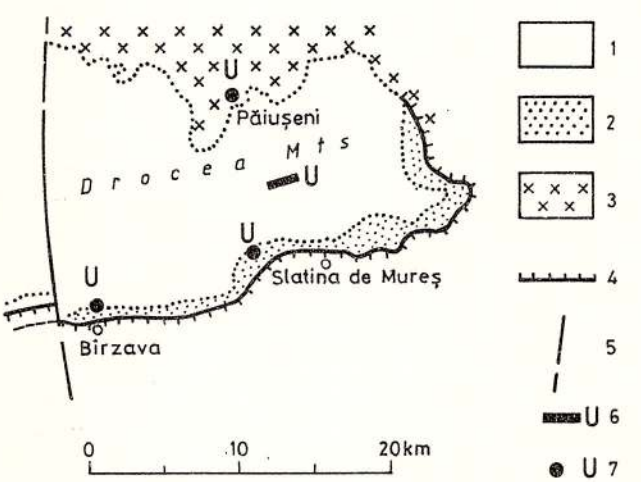

Fig. 1 – Uranium mineral occurrences in the crystalline schist zone from the Drocea Mts. 1, Păiuşeni Series; 2, Senonian deposits; 3, Neogene volcanics; 4, overthrust plane; 5, Nadaş-Laleşinţ Fault; 6, primary uranium concentration; 7, secondary uranium concentration.

Petrographic Constitution of the Păiuşeni Series and Uranium Mineral Occurrences

The Paleozoic Păiuşeni Series (Savu, 1962) lies unconformably over the Precambrian Mădrizeşti Series. In the Drocea Mts it consists of three characteristic complexes of epimetamorphic crystalline schists. Balintoni (1986) considered the three complexes of the Păiuşeni Series (sensu Savu, 1962; 1965) as three metamorphic series of various ages, in tectonic relations, so that the normal geological boundaries between complexes and some faults in the region became overthrust planes; even the stratigraphic unconformity between the Paleozoic Păiuşeni Series and its basement – the Precambrian Mădrizeşti Series – became also an overthrust plane. The lower complex developing in the northern part of the region consists of alternations of quartzites and metaconglomerates of various types, with rare interbeds of sericite-chlorite phyllites, in places also of tholeiitic metabasalts of intraplate type (Savu, Tiepac, 1982) and of crystalline limestones[1]. The median complex which is present only in the western part of the Drocea Mts and in the Highiş Mts consists of basalts and basic tuffs metamorphosed at the level of the chlorite isograde (Savu, 1965; Savu et al., 1967), as in the rest of the Păiuşeni Series. Metadolerite sills and some rocks resembling metamorphosed gabbrodolerites are rarely encountered. The upper complex is prevailingly metapelitic-phyllitic, but it frequently contains quartzite, metabasalt (metatuff) and more rarely metaconglomerate interbeds. Both in the median complex, the metavolcanic one, and in the upper complex, porphyroid rocks (metarhyolite) interbeds are encountered, pointing to the bimodal character of the intraplate type volcanism.

The Paleozoic (Silurian-Lower Carboniferous) age of the Păiuşeni Series is supported also by the spore association determined by V. Iliescu in samples collected by me throughout the crystalline schist zone from the Drocea Mts consisting of: *Veryhachium brevitrispinum, V. Trispinum, Protoleiosphaeridium parvigranulosum, P. microgramifera, P. papillatum, Protolei sphaeridium* sp., *Leiosphaeridium* sp., *Hystrichosphaeridium* sp., *Lagenvehitina* sp.

In the western part of the Drocea Mts crystalline zone the three metamorphic complexes are crossed by the intrusions of the Bîrzava alkaline masif (Savu, 1965). Round these intrusions, the metamorphism grade increases to the biotite isograde due to the influence of the synkinematic contact metamorphism, giving rise to biotite contact schists (hornfels) of a schistose texture that are often impregnated by tourmaline crystals.

The intermediate complex of the basic volcanics is lacking in the central and eastern parts of the Drocea Mts crystalline, there existing a direct passage from the lower to the upper complex. In the crystalline schists from the transition zone there occur, however, intercalations of tholeiitic metabasalts (metatuffs), chloritoid graphite schists and quartzites, among which the feldspathic quartzites of the Păcurăreşti Brook type, tributary of the Prundu Valley (Păiuşeni), are characteristic. This feldspathic quartzite level has a maximal apparent thickness of 10 m, trending approximately northeast-southwest, as in the rest of the Păiuşeni Series, slightly dipping south-eastwards. In this quartzite interbed there occurs a conformable and discontinuous level consisting of short lenses (Fig. 2) with uranium mineralizations reaching maximum 5 cm in thickness. In the median part these uranium lenses present thin chalcopyrite bands. On the fissures crossing the feldspathic quartzite intercalation perpendicularly to its direction, there formed uranium micas depositions, such as autunite and torbernite which are bright-coloured.

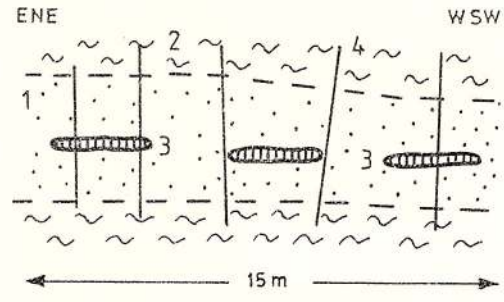

Fig. 2 Primary uranium concentration in a feldspathic quartzite on the Păcurăreşti Brook (left bank). 1, feldspathic quartzites; 2, phyllites; 3, uranium mineral and chalcopyrite lenses; 4, fissures on which uranium micas deposited.

It is worth mentioning the fact that at a certain distance from the exposure of the uranium deposition, the feldspathic quartzite intercalation is crossed by thin grey quartz veins with rare chalcopyrite and bornite nests, in places with hematite plates, as it is the case in the rest of the Păiuşeni Series (Savu, 1962).

If the above described level with uranium mineralizations is considered to represent a primary uranium concentration, at the expense of which there formed secondary minerals, in the crystalline schist area from the Drocea Mts, some other occurrences, in which secondary uranium mineral concentrations formed, are also to be found. Thus on the contact between the crystalline schists of the Păiuşeni Series and the lower (red) complex of the Senonian deposits on the south-

[1] Pană and Ricman (1988) considered the metaconglomerates from the Păiuşeni Series as laminated granites, in their opinion, the pebbles in these rocks representing quartz exudation products.

ern rim of the crystalline, there formed secondary autunites, more rarely torbernite and uranium oxide depositions on the Dupla Brook at Slatina de Mureş and north of Bîrzava. Autunite crystal depositions were also noticed in a short gallery carried out at the base of the Neogene andesite pyroclastics that overlie the Păiuşeni Series to north-west of the locality of the same name.

Mineralogical Aspects of the Uranium Concentrations

It results from the above presented data that there are primary, lenticular and secondary uranium concentrations in the Drocea Mts. The primary minerals of the first type of concentrations are represented by pitchblende associated with chalcopyrite. Pitchblende is a black, strongly radioactive amorphous UO_2–UO_3 uranium oxide. It partly weathered, becoming earthy, black-grayish, in places brown-reddish. These aspects point to what is known as nesturan or uranium black. Through alteration it grades to uranium micas in the alteration zone of the primary deposit.

Chalcopyrite forms sometimes a thin band, usually in the median zone of the lenses with uranium minerals. It appears as patches. Malachite forms at its expense. Azurite seldom occurs. During the alteration process, in the oxidation zone, where uranium lenses are to be found at present, chalcopyrite furnished the Cu ions that take part in the torbernite composition, a mineral present in the occurrence.

The secondary uranium minerals of the uranium concentrations in the Drocea Mts are represented by autunite and torbernite (uranium micas) present both in the primary uranium depositions zone and in the secondary ones in the base of the Senonian deposits and of the Neogene andesitic pyroclastics, the former mineral being the more frequent. Autunite is a hydrated uranium and calcium phosphate, some other alkaline (Na, K, Ba) and metallic (Mn, Cu, Ni, Pb) elements being possibly collected instead of these cations. It appears as scaly, micaceous masses consisting of thin, yellow lamellae with cleavage after 001. It is pleochroic Ng = Nm = golden yellow; Np = slightly yellowish.

Torbernite is a U and Cu hydrated phosphate, emerald green in colour. It appears as tabular crystals from the tetragonal system, with cleavage after 001. Its pleochroism is as follows: Ng = greenish yellow; Np = light green.

Origin of Uranium Concentrations

According to their position, the lenticular uranium concentrations appearing conformable in the feldspathic quartzite intercalation are thought to be primary and to have formed by sedimentary or volcanosedimentary processes. Their presence in the feldspathic quartzite inercalation suggests that they deposited under arid climate conditions. The primary uranium deposition took place in the miogeosyncline, in the marine environment, probably in the form of a powder of uranium oxides and iron and copper sulfides that used to impregnate the feldspathic sandstone. Due to the regional metamorphism manifested at temperatures of about 300° C (Savu, 1965), the feldspathic sandstone graded to quartzite, and the uranium oxide and sulphide powder became compact, namely recrystallized in pitchblende and chalcopyrite patches. The former mineral disintegrated in the course of time, passing partially to the black-greyish earthy mass. Subsequently the uranium micas formed at the expense of the uranium mineralizations due to the alteration processes from the oxidation zone.

The secondary uranium mineral accumulations in the base of the Senonian deposits and of the Neogene pyroclastics formed by the washing of the primary uranium depositions, such as the one on the Păcurăreşti Brook, by the meteoric waters, and its deposition on the contact plane between the mentioned geological formations. This process took place in a warm and humid atmosphere. It was pointed out by the fact that uranium is quite mobile under the supergene alteration conditions and that it occurs in reduced concentrations in several types of rocks from the crystalline schists of the Păiuşeni Series, but especially in metaconglomerates and metasandstones bearing carbonate-ankerite cement. Obvious radiometric anomalies occur on these rocks. Also, the washed uranium from the primary concentrations and transported in the supergene alteration conditions is often deposited on the fault planes, on which the meteoric waters infiltrate. These faults produce strong excitations in the detecting apparata.

The fact that the crystalline schists in the Drocea Mts, placed by me in the Păiuşeni Series, contain similar uranium concentrations, proves once more that they form a single Paleozoic metamorphic series.

References

Balintoni I. (1986) Petrologic and tectonic features of the Highiş-Drocea crystalline massif (Apuseni Mountains). *D. S. Inst. Geol. Geofiz.*, 70–71/5 (1983; 1984), p. 5–22, Bucureşti.

Pană D., Ricman C. (1988) The lower complex of the Păiuşeni series a blastomilonitic shear belt. *Rev. roum. Géol., Géophys., Géogr., (Géologie)*, 32, p. 21–36, Bucureşti.

Savu H. (1962) Cercetări petrografice în Cristalinul Masivului Drocea. *D. S. Com. Geol.*, XLIV (1956–1957), p. 11–34, Bucureşti.

– (1965) Masivul eruptiv de la Bîrzava (Munţii Drocea). *Mem. Com. Geol.*, VIII, 148 p., Bucureşti.
– , Tiepac I. (1982) Noi date asupra geochimiei masivului de roci bazice metamorfozate şi alcaline de la Bîrzava Munţii Drocea). *D. S. Inst. Geol. Geofiz.*, LXVI(1979), p. 207–224, Bucureşti.
– , Borcoş M., Hanomolo I., Hanomolo A., Trifulescu M., Ioanidu C. (1967) Date noi asupra stratigrafiei şi petrologiei şisturilor cristaline din partea centrală a Munţilor Drocea. *D. S. Inst. Geol.*, LIII/1 (1965–1966), p. 187–210, Bucureşti.

Received: March 17, 1990
Accepted: May 2, 1990
Presented at the scientific session of the Institute of Geology and Geophysics: May 21, 1991

Rom. J. Mineralogy, 1993, 76, 1, p. 47–51

L'OCCURRENCE DE CÉLESTINE D'IVĂNCĂUŢI (LA PARTIE SEPTENTRIONALE DE LA PLATE-FORME MOLDAVE)

Vasile POMÂRLEANU

Institutul de Geologie şi Geofizică. Str. Caransebeş 1, 78344 Bucureşti 32.

Iosef IMREH

Universitatea Babeş-Bolyai. Str. M. Kogălniceanu, nr. 1, 3400 Cluj-Napoca.

Key words: Carbonates. Celestite. Fluid inclusions. Limestone. Diagenesis. Major elements. Moldavian Platform.

Abstract: *Celestine Occurrence at Ivăncăuţi (North of the Moldavian Platform).* The chemistry of the celestiniferous limestones, crystallography, chemistry and certain growth particularities of celestine and the fluid inclusions of this mineral are presented. Strontium redistribution and celestine formation have taken place subsequently to the diagenetic process.

La présence de la célestine dans la partie septentrionale de la plate-forme moldave a été signalée pour la première fois par Pomârleanu et al. (1992). Elle a été identifiée dans les puits et les dérochements réalisés pour l'exploration et la prospection du gypse et emplacés au pied du versant septentrional de la colline de Grumazu d'Ivăncăuţi. La célestine décrite se présente sous forme d'agrégats de cristaux minces (submillimétriques) transparents, associés à la calcite dans de petites veines des calcaires compacts. Ceux-ci reposent sur un lit de gypse. Les deux formations sont attribuées au Badénien.

Dans cette note on présente une série de données suplémentaires concernant le chimisme des calcaires à célestine, la cristallographie de la célestine, ainsi que le chimisme de la célestine proprement-dite. On présente aussi quelques particularités de croissance, ainsi que de la genèse de la célestine.

1. Le chimisme des calcaires célestinifères

A cause du contenu très élevé en strontium (16,5 à 20,1 % SrO) le calcaire compact à célestine a été nomé par nous, antérieurement, "horizon à célestine" (Pomârleanu, in Lupu et al., 1988, données nonpubl.). Les investigations de détail effectuées ultérieurement dans le terrain ont indiqué que la minéralisation à strontium, représentée par la célestine, se trouve non seulement dans les calcaires compacts, mais aussi dans ceux poreux et à cavernes, les deux situés au-dessus de la formation gypsifère à anhydrite.

Tous ces types de calcaires se caractérisent par un chimisme semblable.

Le tableau 1 présente quelques analyses sur les calcaires compacts et poreux (à cavernes) d'Ivăncăuţi parallèlement aux analyses des certains calcaires, similaires à célestine, des environs de la ville de Hotin, cités par Lazarenko et Slivko (1958).

Les analyses effectuées sur les échantillons bruts prélevés de l'horizon à célestine d'Ivăncăuţi (qui englobe aussi les petites veines à célestine) ont signalé des teneurs entre 16, 5 et 20,1 % SrO. Pour les analyses présentées dans le tableau 1 nous avons essayé de choisir, dans la limite des possibilités, des échantillons dépourvus de veines à célestine, pour pouvoir expliquer la genèse de la célestine. Aux calcaires compacts à célestine d'Ivăncăuţi on remarque de petites variations de la silice (0,60 à 0,98 % SiO_2). On note des variations remarquables pour le strontium (3,97 à 11,90 % SrO).

Le calcaire compact de Hotin a la même composition que celui d'Ivăncăuţi, mais des teneurs plus réduites en SrO. Au contraire, la teneur en strontium des calcaires poreux de Hotin est plus élevée (5,10 % SrO échantillon 2, jusqu'à 30 % SrO) par rapport aux calcaires du même type de Grumazu (0,54 % SrO). La teneur élevée en SrO des calcaires poreux de Hotin est relevée par les analyses effectuées sur des échantillons

Tableau 1
Composition chimique des calcaires célestinifères d'Ivăncăuţi et de quelques calcaires similaires des environs de la localité de Hotin

Composants	Calcaire compacte				Calcaire poreux	
	Ivăncăuţi^{xx}			Hotin^{x}	Ivăncăuţi	Hotin^{x}
	Puits I	Puits II			Puits I	
	4548	4551	67	6^{x}	74	2^{x}
SiO_2	0,98	0,60	0,60	1,41	4,58	1,20
Al_2O_3	0,74	0,33	0,45	–	2,17	–
Fe_2O_3	0,20	0,14	0,38	–	0,42	–
MnO	0,46	0,23	0,25	–	0,31	–
MgO	1,66	1,72	2,72	0,14	0,61	0,68
CaO	52,01	47,57	41,89	52,52	46,02	48,16
BaO	n.d.	n.d.	n.d.	0,76	n.d.	–
SrO	1,57	3,97	11,90	1,62	0,54	5,10
CO_2	41,05	6,12	32,86	41,16	34,27	38,59
SO_3	1,22	3,07	9,23	1,16	1,35	4,31
Total	99,89	90,11	100,36	99,37	90,07	99,19

^{x} Vîrjikovskii (1925) – cité par Lazarenko et Slivko (1958).

^{xx} Les analyses ont été effectuées par Popescu Carmen, I.P.G.G., Bucureşti.

bruts comportant de la célestine en géode.

2. La cristallographie de la célestine

Dans le complexe de calcaires compacts à célestine à des traces fines de Miliolidés d'Ivăncăuţi, la célestine se présente sous forme d'agrégats de cristaux fins submillimétriques associés parfois à la calcite, disposés en veines et filons petits (pl. I, fig. 1). Les cristaux sous forme de colonne arrivant jusqu'à 2 cm se trouvent aussi dans les petits filons des calcaires compacts (pl. I, fig. 2). Les cristaux tabulaires et fibreux-radiaires de célestine se trouvent dans les vides des calcaires poreux et à cavernes (pl. I, fig. 3, 4).

Beaucoup de cristaux sont dépourvus de formes cristallographiques (faciès) bien développées. Ce fait s'explique par la présence de plusieurs germes de cristallisation, qui ont formé, en général, des agrégats compacts à de petits cristaux. On a rencontré 95 cristaux long prismatiques pour lesquels on a déterminé les suivantes formes:

c{001}; o{011}; r{015}; d{102}; l{104}; m{110};

Les formes susmentionées présentent:

1. des cristaux prismatiques (fig., cristal 1) selon l'axe cristallographique "a" avec le symbole (selon Chudoba, 1930)

A_a[100] (axial selon l'axe cristallographique "a" avec la zone dominante [100]

2. des cristaux prismatiques allongés selon l'axe cristallographique "b" avec le symbole A_b[010] (fig., cristal 2).

Pour les cristaux tabulaires et lamelaires du calcaire poreux on a déterminé aussi les formes r{015} et l{104} représentées dans la figure (les cristaux 6 et 7).

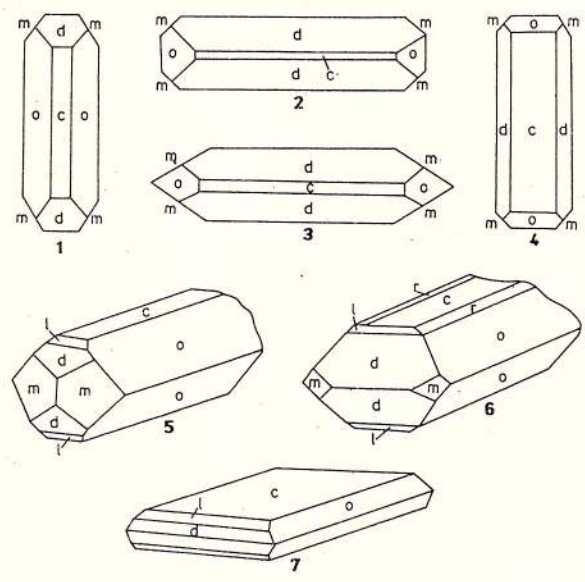

Figure – Des formes de cristaux de célestine de la colline de Grumazu (Ivăncăuţi). 1, 2, 3, 5, cristaux long prismatiques dans les petites veines et les géodes de calcaires compacts; 4, 6, 7, cristaux tabulaires et lamelaires dans les calcaires poreux et caverneux.

Les cristaux tabulaires allongés selon l'axe cristallographique "a" sont caractérisés par les suivants symboles: $P^{b}_{(100)}[010]$ [100], aplatisé selon (001), allongé selon "b" avec les zones dominantes [010] et [100].

Les formes, les symboles et les indices des faces des cristaux de la célestine sont présentés dans le tableau 2.

Tableau 2
Les principales formes des cristaux de célestine d'Ivăncăuţi

Nr. crt.	Forme	Symbole	Indice
1	Pinacoïde	c	{001}
2	Prisme ord. I	o	{011}
3	Prisme ord. II	d	{102}
4	Prisme ord. II	l	{104}
5	Prisme ord. II	r	{105}
6	Prisme ord. III	m	{110}

3. Bandes de croissance

Les cristaux tabulaires et surtout ceux fibreux-radiaires ont des bandes de croissance visibles au binoculaire ou à l'oeil nu (pl. II, fig. 1). Celle-ci compotent des bandes rectilignes, parallèles, opaques et lumineuses en alternance, à des épaisseurs variables.

La formation des bandes de croissance dans les cristaux a été expliqué par plusieurs mécanismes, analysés et critiqués par Roedder (1969). De tous les huit mécanismes, seulement la périodicité annuelle dans les conditions de croissance pourrait expliquer, de manière plausible, l'origine de ces bandes. La formation des bandes à composition (teneur en Ba) et indices de réfraction différents pourait être due à la dilution des solutions relativement chaudes où la célestine avait cristallisé (selon l'étude des inclusions fluides de ce minéral) avec les eaux superficielles qui ont varié dans la composition d'un cycle annuel à un autre. Considérant ce mécanisme on a estimé qu'un cristal long de 10 cm s'est formé pendant 10.000 ans approximativement (Roedder, 1969). Pour une telle croissance les vitesses d'écoulement sont très lentes. Tenant compte des données de la solubilité $SrSO_4$ présentées par Blount et Dickson (1968), cités par Roedder (1969), on aprécie que pour la formation d'un tel cristal a été nécessaire la circulation d'approximativement un litre de solution par an.

Si on prend en considération tant la présence de quelques cristaux perfects de célestine, aussi bien que la distribution linéaire des bandes à des différentes épaisseurs, il parait que la formation des bandes de célestine d'Ivăncăuţi (similaire à la célestine de Clay Center, Ohio, décrite par Roedder, 1969) a eu lieu sous l'influence de la périodicité annuelle du milieu de croissance. De telles bandes sont visibles aussi dans la célestine de Baciu (Transylvanie).

L'étude des bandes annuelles de croissance peut nous fournir des données quantitatives assez utiles pour l'explication des processus diagénétiques, ainsi que du régime paléohydrodynamique de précipitation, non seulement de la célestine que d'autres minéraux aussi de la série d'évaporites (sels, gypses, anhydrite etc.).

4. Inclusions fluides

Tenant compte de la transparence très accentuée, l'analyse des inclusions a été éffectuée sur des cristaux individuels. On a évidentié des inclusions fluides syngénétiques (primaires) et épigénétiques (secondaires). Les deux sont monophasiques liquides à la température du milieu d'observation.

En général les inclusions primaires ont la forme de cristal négatif ou au moins allongées (pl. II, fig. 2). Celles secondaires se trouvent le long des fissures et parfois sont étranglées. Le degré d'étranglement diffère d'un cas à l'autre; on remarque des étranglements complets quand une inclusion se sépare en deux inclusions, ou des étranglements partiaux qui conduisent à la formation d'un capilaire qui lie deux inclusions (pl. II, fig. 3). Les inclusions fluides similaires sont présentes aussi dans les cristaux de célestine de Baciu (Transylvanie)(pl. II, fig. 4).

L'absence de la phase gazeuse pour les types d'inclusions impliquent des températures d'homogénéisation (remplissage) très basse, 50^{0} C environ (Sabouraud et al., 1980).

Fréquement, dans les cristaux de célestine, à côté des inclusions primaires dispersées, apparaissent des intersections de planes d'inclusions fluides secondaires, fait qui confirme que la célestine a subi, en temps, des fissurations intermitentes pendant des périodes différentes. Le long de ces fissures ont circulé des solutions qui ont déposé des inclusions secondaires appartenant à plusieurs générations (pl. II, fig. 5).

5. Composition chimique de la célestine

On a déjà présenté quelques données sur la composition de la célestine d'Ivăncăuţi et on a discuté sur le chimisme de ce minéral par rapport à la célestine de Cheia (Pomârleanu et al., 1988). Sous le tableau 3, à côté des, deux analyses (1 et 3) on mentionne de nouveaux données sur la célestine tabulaire d'Ivăncăuţi (analyse 4) par rapport à la célestine de Darabani, près de Hotin (analyse 2) selon les données de Sidorenko (1905) – cité par Lazarenko et Slivko (1958).

La teneur élevée en CaO de la célestine qui forme des agrégats fins de cristaux sous forme de petites

veines dans les calcaires compactes à célestine (analyse 1, tableau 3) est déterminée par l'association intime entre la célestine et la calcite. La célestine tabulaire blanc-jaunâtre, trouvée dans les lacunes des calcaires poreux, se caractèrise par une teneur plus baisse en CaO (o,19 % CaO, analyse 4 du tableau 3).

Tableau 3

Composition chimique de la célestine d'Ivăncăuţi et de celle de Darabani (Hotin) et Cheia (Transylvanie)

Composants	Composition %			
	Ivăncăuţi		Darabani[2]	Cheia[3]
	Colonne[1]	Tabulaire[4]		
SrO	54,99	55,45	55,30	55,24
CaO	1,53	0,19	0,08	0,41
SiO_2	0,30	–	–	0,53
Fe_2O_3	0,27	–	–	0,12
MgO	0,10	–	–	–
BaO	0,05	n.d.	0,89	–
SO_3	42,70	43,70	43,42	43,26
H_2O	–	0,20	–	0,29
Totale	99,94	99,54	99,69	99,85

[1] Pomârleanu et al. (1988).
[2] Sidorenko (1905) – cité par Lazarenko et Slivko (1958).
[3] Imreh, Imreh (1960).
[4] Analyse effectuée par Eleonora Neagu, IAMN, Bucureşti.

6. Genèse de la célestine

En général le strontium forme un nombre assez réduit de minéraux dans l'écorce terrestre. Il est présent rarement sous forme de minéral indépendant dans des certaines conditions magmatiques et hydrothermales. Les milieux exogènes qui comportent en abondance l'anion SO_4^{-2} sont les plus favorable pour la formation de la célestine, minéral qui constitue en même temps la source pour le strontium industrial.

Dans des conditions exogènes la formation de la célestine est dépendante des roches calcaires, dolomies, calcaires bituminneux, argiles gypsifères, marnes et gisements de sel. Dans ces formations la célestine se trouve en paragenèse avec la calcite, le gypse et le soufre. L'occurrence de célestine d'Ivăncăuţi est associée avec quelques roches calcaires.

La genèse de la célestine s'explique soit par sa précipitation syngénétique, soit épigénétiquement. Imreh, Imreh (1961), après l'analyse de plus de 14 occurrences de célestine du bassin de la Transylvanie, ont adhéré à la deuxième hypothèse et sont arrives à la conclusion que le strontium provient des débris squélettiques des coquilles riches en aragonite. La célestine s'est formé ultérieurement pendant le processus de la diagenèse. Pendant ce processus les coquilles riches en $CaCO_3$ et $SrCO_3$ ont été attaquées par les eaux phréatiques à de hautes concentrations en CO_2 et H_2SO_4, qui ont facilité le passage dans les solutions de ces carbonates sous forme de $Ca(HCO_3)_2$ et $Sr(HCO_3)_2$. De la réaction des solutions aqueuses acides avec le carbonate acide de strontium et de calcium résulte le sulfate de strontium (la célestine) et le sulfate de calcium (gypse):

$$Sr(HCO_3)_2 + H_2SO_4 = SrSO_4 + 2H_2O + CO_2$$
$$Ca(HCO_3)_2 + H_2SO_4 = CaSO_4 + 2H_2O + CO_2$$

Ce mécanisme a été présenté par Imreh (1957) et réactualisé ultérieurement pour la célestine de Transylvanie (Imreh, Imreh, 1961).

Lazarenko et Slivko (1958) tentent d'expliquer la genèse de la célestine de quelques minéralisations et gisements du Nord de la Bassarabie, le long de la vallée de Dniepr. Ces auteurs ont indiqué que le strontium s'est accumulé parallèlement au complexe gypso-calcaire. Ultérieurement, pendant le processus de diagenèse des calcaires a eu lieu la redistribution du strontium et sa précipitation dans la présence de l'anion $[SO_4]^{2-}$ sous forme d'agrégats et cristaux de célestine dépôsés dans les fissures des calcaires.

Conformément aux coupes géologiques de Păltiniş (Bâgu, Mocanu, 1984) et aux colonnes lithostratigraphiques de la zone d'Ivăncăuţi-Cuzlău la source de H_2SO_4 dans eaux phréatiques qui ont facilité la formation de la célestine épigénétique d'Ivăncăuţi, provient des conglomérats et des grès à soufre, ou résulte de la dissolution des cristaux de pyrite et gypse des marnes situées au-dessus de l'horizon à célestine.

Quant à la genèse de la célestine d'Ivăncăuţi, on peut dire que le strontium s'est accumulé une fois avec la sédimentation de la roche mère. Sa redistribution et précipitation sous forme de célestine a eu lieu pendant le processus de la diagenèse.

Bibliographie

Bâgu Gh., Mocanu Al. (1984) Geologia Moldovei. Stratigrafie şi consideraţiuni economice, 296 p., Ed. Tehnică, Bucureşti.

Chudoba K. (1930) Zur morphologischen Typisierung der verschiedenen Kristalltrachten. CB1.f.Miner., Abt. A.

Imreh J. (1957) Noua ocurenţă cu celestină de la Dumbrava şi Cluj (notă preliminară). *Anal. Univ. Babeş Bolyai. Ser. Şt. Nat.*, II, 1–2, p. 211–220, Cluj.

– , Imreh G. (1959) Coelestin-Kristalle aus Cheia. *N. Jb. Miner*, Mh., 11/12, p. 248–261, Stuttgart.

– , Imreh G. (1961) Contribuţii asupra genezei celestinei sedimentare. *Stud. cerc., Geologie*, VI/2, p. 351–379, Acad. R.P.R., Bucureşti.

Lazarenko E. K., Slivko M.M. (1958) Celestinî Pridnestrov'ia. *Mineral sbornik Lvov, gheol. o-Va*, 12, p. 363–379.

Pomârleanu V., Neagu El., Cristea C. (1992) Celestina de la Ivăncăuţi (Nordul Platformei Moldoveneşti). *Rom. J. Min.*, 75, p. 107–111, Bucureşti.

Sabouraud-Rosset C., Macquar J. C., Rouvier H. (1980) Les inclusions fluides, témoins et faux-témoins des conditions de dépôt. Quelques exemples pris dans les minéralisations Pb, Zn, Ba, F du sud du Massif Central Francais. Mineral. *Deposita*, 15, p. 211–230, Berlin.

Roedder E. (1969) Varvelike banding of possible annual origin in celestite crystals from Clay Center, Ohio, and in other minerals. *Amer. Mineral.*, 54, p. 796–810, Washington.

Received: February 18, 1991
Accepted: February 18, 1991
Presented at the scientific session of the University Iaşi, October 28–29, 1989.

Rom. J. Mineralogy, 1993, 76, 1, p. 53–55

NON-SILICATE ZEOLITES (NON-SILICATE MICROPOROUS PHASES) IN MINERALOGY

Josef ZEMANN

Institute for Mineralogy and Crystallography, University of Vienna. Dr. Karl-Lueger-Ring 1, A-1010 Vienna, Austria.

Key words: Channel geometry. Phosphates. Arsenates. Pharmacosiderite. Cacoxenite. Mixite.

Abstract: The most common phases with wide channels (microporous structures) in mineralogy are the zeolites with their $[(Si_{1-x}Al_x)O_2]^{x-}$ frameworks. There exist, however, in nature also microporous structures with quite different chemical compositions. A well known example is pharmacosiderite, with a $[Fe_4(OH)_4(AsO_4)_3]^{1-}$ framework and clear zeolitic properties. According to its crystal structure cacoxenite is another possible representative, but its physicochemical properties have not been investigated yet. The microporous structure with heteroatomic walls are of special interest. A good example is mixite, $[BiCu_6(OH)_6(AsO_4)_3].\sim 3H_2O$; the recent synthesis has allowed to prove that it dehydrates reversibly.

The term "zeolite" is used in mineralogy for water containing aluminiumsilicates of (mostly) sodium, potassium and calcium for more than two centuries. The members of this group of minerals are sometimes found as beautiful crystals, e.g. from cavities in magmatic rocks; however, they occur fine-grained in much larger quantities in some sediments, e.g. in altered volcanic tuffs, where they can be main constituents. Zeolites have interesting properties: they dehydrate and rehydrate continuously, they show exchange properties for the alkali and alkaline-earth ions, etc. These properties are closely connected with their crystal structures: they are built from SiO_4 and AlO_4 tetrahedra sharing all four oxygen atoms to form a three dimensional framework. The formula of the frameworks reads $Si_{1-x}Al_xO_2]^{x-}$, usually with $0.2 \leq x \leq 0.5$. The frameworks are characterized by cavities and channels with dimensions allowing the housing and diffusion of water molecules and of the Na^+, K^+ and Ca^{2+} ions. The topologies of the frameworks vary widely.

Many of the zeolites that occur in nature can be synthesized rather easily, but also zeolites that do not occur as minerals are well known as laboratory products. Both natural and synthetic zeolites have found varied and extensive use in industry, agriculture, etc.

The literature on zeolites is enormous, and since 1981 there even appears an international journal "Zeolites", covering to a considerable extent synthetic zeolites and application-oriented investigations. Important monographs on natural zeolites are "Mineralogy and geology of natural zeolites" (Mumpton, 1977) and "Natural zeolites" (Gottardi and Galli, 1985).

As the characteristic zeolitic properties largely depend on the atomic arrangement, they are not restricted to the aluminiumsilicate framework structures of the zeolites *sensu stricto*, but also occur in chemically very diverse compounds which are, however, all characterized by having wide channels. In this context it seems appropriate to mention that such structures are often called microporous structures, quite independent of whether they have zeolitic properties or not. This is an useful expression because the degree of zeolitic properties varies with the size of the channels and grades continuously into framework structures without such properties.

Microporous structures closely related to the zeolites *sensu stricto* contain in a tetrahedral framework in addition to or instead of Si and Al the atoms Be, Zn, P and As, coordinated to four oxygen atoms. Mineralogical examples are lovdarite with a $[Be_2Si_7O_{18}]^{4-}$ framework (Merlino, 1990), or tiptopite and pahasapaite, both characterized by $[BePO_4]^{1-}$ frameworks (Peacor et al., 1987; Rouse et al., 1989). A very special and somewhat exotic position among microporous structures built from tetrahedra take Millon's base and its salts with their $[NHg_2]^{1+}$ frameworks of anti-SiO_2 structure types (Lipscomb, 1951). Mineralogical examples are mosesite, the framework of which corresponds to that of cristobalite (Switzer et al., 1953), and kleinite, where the framework has the topology of

tridymite (Heritsch, 1954). The walls of the channels are built up exclusively of mercury atoms (!), and as the N-Hg distance is larger than the Si-O distance by ca. 40 %, the widths of the channels are also considerably wider than in the corresponding SiO_2 modification.

Microporous structures are known not only built up from tetrahedra but also from octahedra. Examples with corner-sharing are only perovskite and pyrochlore, both with relatively narrow channels and, therefore, not showing clear zeolitic properties. Examples in which the octahedra share in part edges are also offered by members of the pyrolusite group.

All microporous structures dealt with so far have frameworks built up exclusively from only one geometric kind of polyhedra, – they have monopolyhedra frameworks. However, there also exist microporous structures the frameworks of which are built up from several geometric kind of polyhedra, which have heteropolyhedral frameworks. A typical mineralogical example is pharmacosiderite which has a framework built up of edge-sharing $FeO_3(OH)_3$ octahedra and of AsO_4 tetrahedra (e.g. Buerger et al., 1967). The cavities and channels house water molecules and (mostly) potassium ions. Pharmacosiderite has typical zeolitic properties (e.g. Mutter et al., 1984). Another interesting mineral in this context is cacoxenite. According to Moore and Shen (1983) it has a $[(Fe,Al)_{25}O_6(OH)_{12}(PO_4)_{17}(H_2O)_{24}]^0$ framework with (Fe,Al) in octahedral coordination. The very large channels house water molecules. Nothing seems to be known on a possible zeolitic behaviour, and the mineral seems not to have been synthesized by now.

All the compounds covered above in this paper have in common that the atoms at the walls of the cavities and channels are all of the same kind, mostly they are oxygen atoms (with, in part, attached protons), – the channels have monoatomic walls. There exist, however, also microporous structures with heteroatomic walls. They are highly interesting in basic science, but some of them might also find practical application. The mineral kingdom presents several examples; unfortunately all of them are very rare species.

A typical representative is mixite. This low-hydrothermal mineral has a framework of the formula $[BiCu_6(OH)_6(AsO_4)_3]^0$; water molecules statistically occupy the channels (Mereiter and Preisinger, 1986). The walls of the channels are formed in part of oxygen atoms and hydroxil groups, in part, of Cu atoms (!) which have in the surface of the walls four oxygen neighbours at ca. 2.0 Å. In a previous paper Schrauf (1880) reported that part of the water escapes continuously with heating, but the scarceness of the natural material prevented a more detailed investigation until recently. The successful synthesis of mixite (Miletich and Zemann, 1993) allowed a more detailed investigation of some of the properties of mixite, and has proved the zeolitic behaviour of the water content. Connelite is another example for a microporous mineral with in part Cu^{2+} in the walls (McLean and Anthony, 1972). In this case the framework is positively charged and besides water, the channels house molecules on a partly occupied position, also anions (mainly SO_4^{2-}). A possible zeolitic behaviour seems not to have been investigated.

Another mineralogical representative of microporous structures with heteroatomic walls is zemannite with its $[(Zn,Fe)_2(TeO_3)_3]^{2-}$ framework (Matzat, 1967). The walls of the channels are built up in part of the oxygen atoms and in part of the Te(IV) atoms of the TeO_3^{2-} pyramids, – or rather of their lone-electron pairs. The wide channels house cations (mainly Na^+) and water molecules on only partly occupied positions. The successful synthesis of the Zn-endmember (Miletich, 1989) allowed to investigate the dehydration-rehydration behaviour. Contrary to the expectations from the crystal structure it was found that the water content does not continuously decrease with heating (Miletich, priv. comm., 1992). This result is possibly conditioned by the low break-down temperature of the framework.

Kambaldaite can be considered to belong to this group of compounds, too. Its crystal structure is characterized by a $[Ni_4(OH)_3(CO_3)_3]^{1-}$ framework, the walls of which are formed by hydroxil and CO_3 groups (Engelhardt et al., 1985). As the CO_3 triangles form with the wall an angle of only 18^0, the C atoms are approximately located on the surface of the walls. The channels contain well ordered $[Na(H_2O)_3]^{1-}$ chains, so that the structure does not suggest zeolitic properties.

Finally, it seems appropriate to mention here also the recently discovered mineral szymanskiite. According to Szymanski and Roberts (1990) its crystal structure is characterized by a $[(Hg_2)_4(Ni,Mg)_3(OH)_6(CO_3)_3]^{2+}$ framework, the walls of which consist in part of mercury atoms and in part of hydroxil groups. The channels are reported to contain carbonate groups, H_3O^+ and water molecules, in part in a disordered arrangement.

Microporous structures with heteroatomic walls are, of course, not restricted to minerals. To mention just one example among laboratory products: $N(CH_3)_4[Sb_3S_5]$ has a microporous structure in which the walls of the $[Sb_3S_5]^{1-}$ framework are formed by S as well as by Sb atoms (Parise, 1991).

This paper is a shortened and in some parts updated English version of an earlier publication in German (Zemann, 1991).

References

Buerger M. S., Dollase W. A., Garaycochea-Wittke (1967) The structure and composition of the mineral pharmacosiderite. *Z. Kristallogr.*, 125, p. 92–108, Leipzig.

Engelhardt L. M., Hall S. R., White A. H. (1985) Crystal structure of kambaldaite, $Na_2Ni_8(CO_3)_6(OH)_6.6H_2O$. *Amer. Mineral.*, 70,p. 423–427, Washington.

Gottardi G., Galli G. (1985) Natural zeolites. Springer-Verlag, Berlin-Heidelberg-New York-Tokyo.

Heritsch H. (1954) Bemerkungen zur kristallchemischen Konstitution des Kleinits. Österr. Akad. Wiss., Nath.-naturwiss. Kl., Anzeiger Jg., 1954, p. 1–4, Wien.

Lipscomb W. N. (1951) The structure of Millon's base and its salts. *Acta Cryst.*, 4, p. 156–158, Copenhagen.

Matzat E. (1967) Die Kristallstruktur eines unbenannten, zeolithartigen Telluritminerals, $(Zn,Fe)_2[TeO_3]_3\ Na_xH_{2-x}.yH_2O$. *Tschermaks Min.Petr.Mitt.*, 12, p. 108–117, Wien.

McLean W. J., Anthony J. W. (1972) The disordered "zeolite-like" structure of connellite. *Amer. Mineral.*, 57, p. 426–438, Washington.

Mereiter K., Preisinger A. (1986) Kristallstrukturdaten der Wismutminerale Atelestit, Mixit und Pucherit. Österr. Akad. Wiss., Math.-naturwiss. Kl., Anzeiger, 123, p. 79–81, Wien.

Merlino S. (1990) Lovdarite, $K_4Na_{12}(Be_8Si_{28}O_{72}).18H_2O$, a zeolite-like mineral: structural features and OD character. *Eur. J. Mineral.*, 2, p. 809–817, Stuttgart.

Miletich R. (1989) Synthese des Zn-Endgliedes des Zemannits, $Zn_2[TeO_3]_3Na_xH_{2-x}.yH_2O$ ($x \approx 2$). Österr. Akad. Wiss., Math.-naturwiss. Kl., Anzeiger, 126, p. 77–79, Wien.

– , Zemann J. (1993) Die Synthese des Mixits. *Aufschluss*, 44, p. 17–21.

Moore P. B., Shen J. (1983) An X-ray study of cacoxenite, a mineral phosphate. *Nature*, 306, p. 356–358, Londra.

Mumpton F. A. (Ed.) (1977) Mineralogy and geology of natural zeolites. Mineral. Soc. America, Short Course Notes, vol. 4, Blacksburg, Va., U.S.A.

Mutter G., Eysel W., Greis O., Schmetzer K. (1984) Crystal chemistry of natural and ion-exchanged pharmacosiderites. *Neues Jb. Mineral., Monatsh.*, p. 183–192, Stuttgart.

Parise J. B. (1991) An antimony sulfide with a two-dimensional, intersecting system of channels. *Science*, 251, p. 293–294.

Peacor D. R., Rouse R. C., Ahn J. H. (1987) Crystal structure of tiptopite, a framework beryllophosphate isotypic with basic cancrinite. *Amer. Mineral.*, 72, p. 816–820, Washington.

Rouse R. C., Peacor D. R., Merlino S. (1989) Crystal structure of pahasapaite, a beryllophosphate mineral with a distorted zeolite rho framework. *Amer. Mineral.*, 74, p. 1195–1202, Washington.

Schrauf A.(1880) Ueber Arsenate von Joachimsthal. *Z. Krystallogr. u. Mineral.*, 4, p. 277–285, Leipzig.

Switzer G., Foshag W. F., Murata K. J., Fahey J. J. (1953) Re-examination of mosesite. *Amer. Mineral.*, 38, p. 1225–1234, Washington.

Szymanski J. T., Roberts A. C. R. (1990) The crystal structure of szymanskiite, a partly disordered $(Hg\text{-}Hg)^{2+}$, $(Ni,Mg)^{2+}$, hydronium-carbonate-hydroxide-hydrate. *Canad. Mineral.*, 28, p. 709–718, Toronto.

Zemann J. (1991) Nichtsilikatische Zeolithe. *Mitt. Österr. Mineralog. Ges.*, 136, p. 21–34, Wien.

Rom. J. Mineralogy, 1993, 76, 1, p. 57–62

CURRENT ORE PETROLOGY: PARAGENESIS, ANALYSIS AND EXPERIMENTATION (WITH PREFERENCE TO GOLD)

Günter H. MOH

Department of Mineralogy and Petrography, Heidelberg University. 6900 Heidelberg, Germany.

Key words: Sulfides. Gold. Villamaninite. Bornite. Kupferschiefer. Paragenesis. Mössbauer spectroscopy. X-ray data. Electron probe data.

Abstract: Complex sulfide ores with well analysed gold contents often cause problems during leaching processes, since the gold recovery remains incomplete unless the ores undergo prior to the recovery alteration or heating treatment. The reason for this behaviour is that gold occurs partly as sulfide, substituting, for instance, copper, silver and thallium in the crystal lattice of the respective minerals. Gold sulfide seems to be quite resistant and is not affected by aqueous cyanide solution. Results from an experimental approach show that gold sulfide is only stable in a narrow Eh–pH range, where it can be precipitated at low temperatures under hydrothermal conditions. Mössbauer spectroscopy studies on natural ores as well as on synthetic products demonstrate the presence of gold as sulfide and/or its alteration or breakdown due to subsequent heat procedures. These facts make it necessary to revise at least part of our knowledge in the geochemistry of gold.

It is an open secret that complex sulfide ores with surely proved gold contents often cause problems during cyanide leaching procedures and show incomplete extraction, unless the ores undergo prior to the recovery an alteration or heating treatment. Since these gold contents cannot be proven by microscopical investigation, it is assumed that at least parts of the gold substitute for copper, silver and even thallium in the crystal lattice of sulfide minerals.

This phenomenon was first recognized by the author in 1964, when studying Cu-Ni-S phase relations as part of the quaternary Fe-Ni-Cu-S system in connection with the Sudbury sulfide ores (Moh, Kullerud, 1963, 1964). A ternary Pa3 type phase was found equal to villamaninite $(Cu,Ni)S_2$; compare Figure 1.

This mineral was first reported by Schoeller & Powell (1920) and later examined and confirmed by Ramdhor (1937, 1960) and Hey (1962). Homogeneous members of the synthesized villamaninite solid solution series as well as synthetic bravoites were used as standards to analyse first various natural bravoites and villamaninites by microprobe and by X-ray fluorescence techniques (Moh & Ottemann, 1964). Figure 2 shows a high purity synthetic villamaninite of $CuNi_2S_6$ composition and the natural mineral which is comparably richer in copper but contains also some cobalt and iron substituting for nickel; sulfur is partly replaced by selenium. Note: the analyses were made with gold radiation, consequently the charts show the typical L-gold peak. However, when compared with the natural villamaninite of the type locality as observed under the same conditions, the gold reflex is slightly but distinctly increased. Since no native gold could be recognized under the reflecting microscope even at high magnification in oil immersion, the analysed increased gold content remained obscure.

In the course of studies on castaingite and of related experimentation some years ago the Kupferschiefer ores were also subject of investigation with material from Mansfeld (formaly GDR) and from Lubin, Silesia (Poland). There, in the lower parts of the Kupferschiefer a gold-bearing lens of approximately 1.5 cm thickness occurs horizontally, which extends for several hundred meters or more.

Among other sulfides, including castaingite, also thucholite was present, and the invisible gold content was 1 % or slightly more. Since also plenty of fossils occurred well preserved in the neighbourhood – (not only *Placoniscus freieslebeni*) – the contents of the gold can not be of hydrothermal origin. Instead, it can be assumed that gold has originated from the surrounding Devonian rocks and was transported as fine tinsels by the rivers into the Permian Ocean. Organic matter has kept the gold colloids in suspension until the final

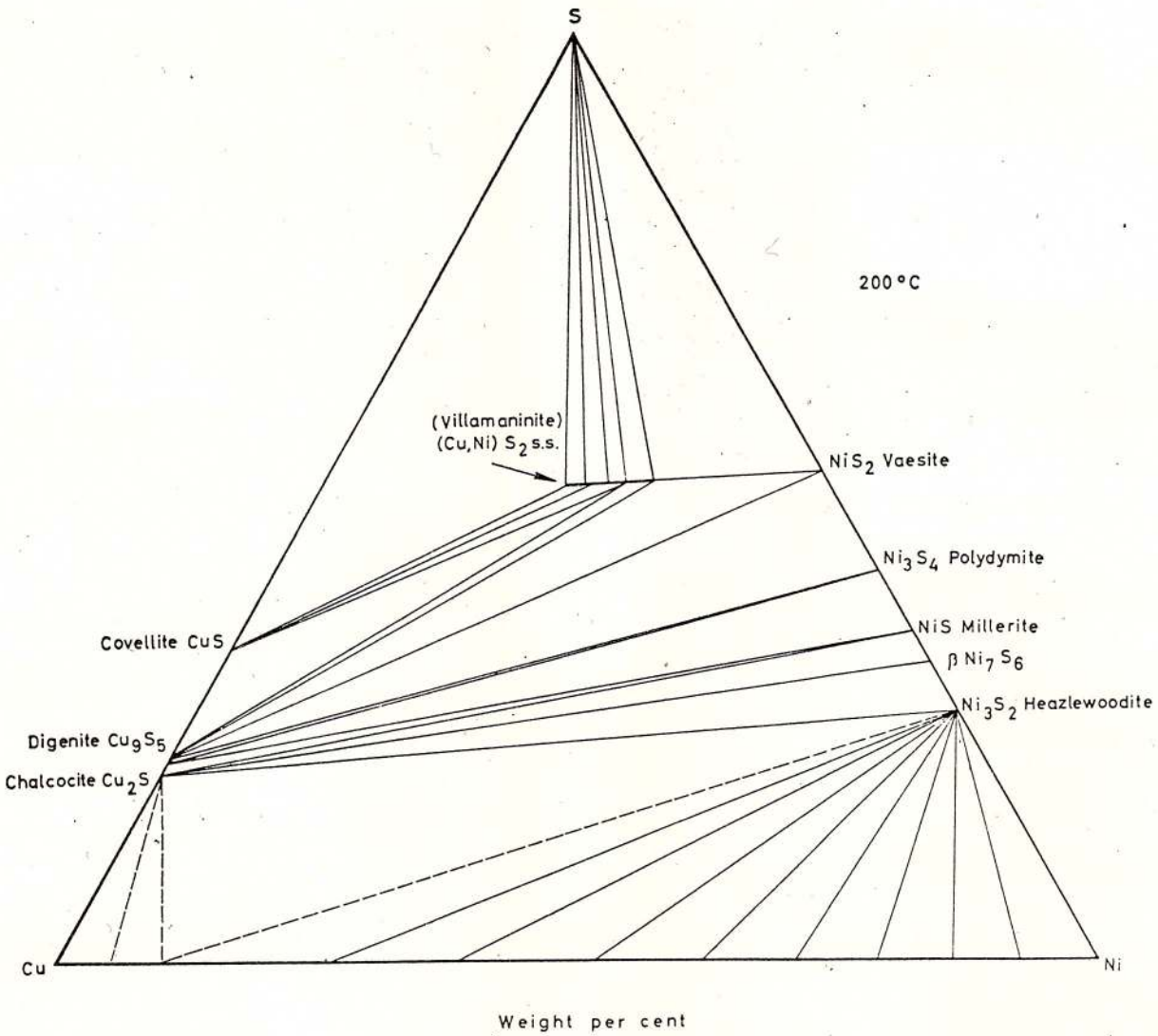

Fig. 1 – Phase relations in the dry Cu-Ni-S system at 200° C. The villamaninite phase is stable over a considerable composition range but is always stoichiometric with respect to the MS_2 formula; compare Moh, Kullerud, 1964.

sedimentation took place on the Permian sea floor. Regarding the fossils, the fauna was poisoned by small amounts of soluble copper contents in the sea water. Since copper is very toxic also to bacteria etc., the sea fauna became contaminated and well preserved. The copper contents have reacted, e.g., with the scin of *Palaeoniscus freieslebeni*, and during a period of decomposition of the organic matter, H_2S has formed naturally and reacted with both the adsorbed copper on the fish scales and their natural iron contents to chalcopyrite or more often to bornite or pure copper sulfides, preserving the original morphology.

However, the lower parts of the Kupferschiefer contain carbonaceous material, and because limestone buffers aqueous solutions to pH 8–9, a weak alkaline milieu was produced and H_2S reacted also with the precipitated gold due to its large surface area. Under these circumstances gold does not behave as a noble metal and reacts with H_2S at low temperatures quite rapidly to gold sulfides (Sobott & Moh, 1991).

In the Kupferschiefer the gold has probably substituted for copper and silver in sulfide minerals or is disseminated in the thucholite matrix but invisible. Figure 3 shows an X-ray fluorescence registogram of such gold-bearing material, obtained with rhodium radiation.

An arranged visit in 1986 to the Kupferschiefer mining area near Lubin (Poland) did not result in new findings, because the gold rich lens was already mined out.

However, the gold contents in the Kupferschiefer reveal some similarities to the villamaninite occurrence

in Spain (as mentioned above). Also in the Kupferschiefer of general sedimentary origin villamaninite was observed (Moh & Kucha, 1980), and in a recent paper high gold contents in copper sulfides were reported from these Polish deposits (Kucha & Piestrzynski, 1991).

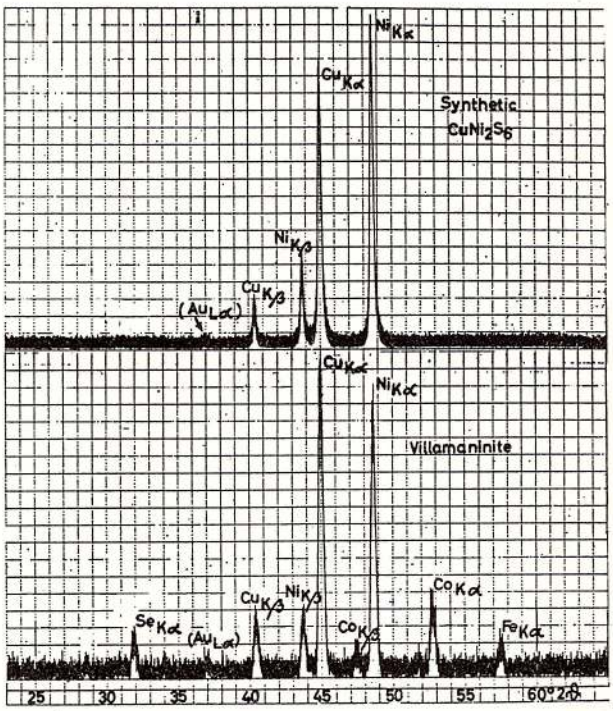

Fig. 2 – X-ray fluorescence charts, performed with rhodium radiation, of synthetic $CuNi_2S_6$ (top) and villamaninite (bottom); compare Moh, Ottemann, 1964.

Table 1 shows some villamaninite analyses from the Spanish type locality and from the Polish Kupferschiefer. While the Spanish villamaninites display a wide compositional range from almost pure CuS_2 towards vaesite NiS_2, cattierite CoS_2, and pyrite FeS_2 including Quaternary bravoites in general, or bravoites in a broader sense, the Polish occurrence is more iron rich and reminds more of cuprian bravoite or fukuchilite, respectively. Some recent villamaninite analyses are plotted on a simplified two-dimensional representation (Fig. 4) (compare Paniagua, 1991).

Since the Spanish villamaninites are found in quartz veins enclosed in dolomite, its formation must be assumed at a pH slightly higher than 7. Under these alkaline environments also CuS_2 has formed as a mineral (Paniagua, 1989). CuS_2 was known before as a high pressure phase of the Pa3 type, it has recently been synthesized at low pressure and higher pH by Schmid-Beurmann (1990).

CuS_2 and villamaninites of different compositions have been very recently synthesized hydrothermally at 85^0 C and atmospheric pressure (Elhaddad & Moh, 1993). The results under the absence of cobalt and iron confirmed earlier low temperature investigations (Moh & Kullerud, 1982): a villamaninite solid solution series extends from $CuNiS_4$ to slightly beyond $CuNi_2S_6$ composition with miscibility gaps towards vaesite NiS_2 and CuS_2, respectively. The latter phase was not known as a mineral at that time.

Table 1
Microprobe analyses of Pa3-type minerals
$(Cu,Ni,Co,Fe)S_2$
recalculated in mole fractions
a) from Villamanina, Leon/Spain
with all stages of transition from almost pure CuS_2 over villamaninite to vaesite, cattierite, pyrite and bravoite

mole fraction CuS_2	mole fraction NiS_2	mole fraction CoS_2	mole fraction FeS_2
0.9883	0.0031	0.0017	0.0069
0.7664	0.1454	0.0604	0.0278
0.6001	0.2769	0.0818	0.0412
0.5027	0.3241	0.1147	0.0585
0.2322	0.5119	0.1585	0.0974
0.0385	0.6828	0.2437	0.0350
0.0531	0.0533	0.8062	0.0874
0.0154	0.0138	0.0129	0.9579
0.0246	0.4129	0.1427	0.4198

(unpublished research from A. Paniagua, Oviedo; personal communication, Sept. 2nd, 1985)

b) from Lubin, Silesia/Poland with stages of transition from iron-rich villamaninite or cuprian bravoite to fukuchilite

mole fraction CuS_2	mole fraction NiS_2	mole fraction CoS_2	mole fraction FeS_2
0.3906	0.2544	0.0017	0.3533
0.3785	0.2133	0.0017	0.4065
0.3547	0.1636	0.0028	0.4789
0.2875	0.0217	0.0648	0.6260
0.2416	0.0018	0.0077	0.7489

(unpublished research from H. Kucha, Krakow; personal communication, May 16, 1986)

Note: Traces of selenium (Villamanin) and arsenic (Lubin) are omitted or recalculated in sulfur.

The remaining problem are the meanwhile analysed gold contents in villamaninites substituting probably for copper in the crystal lattice (Paniagua, 1991). Table 2 shows typical trace elements analyses in villamaninites of the type locality. Mössbauer spectra actually do not show any change before and after cyanidation of gold-bearing villamaninite, of which a ^{197}Au Mössbauer spectrum is shown in Figure 5 (compare Friedl et al., 1991). Thus, the gold contents can be

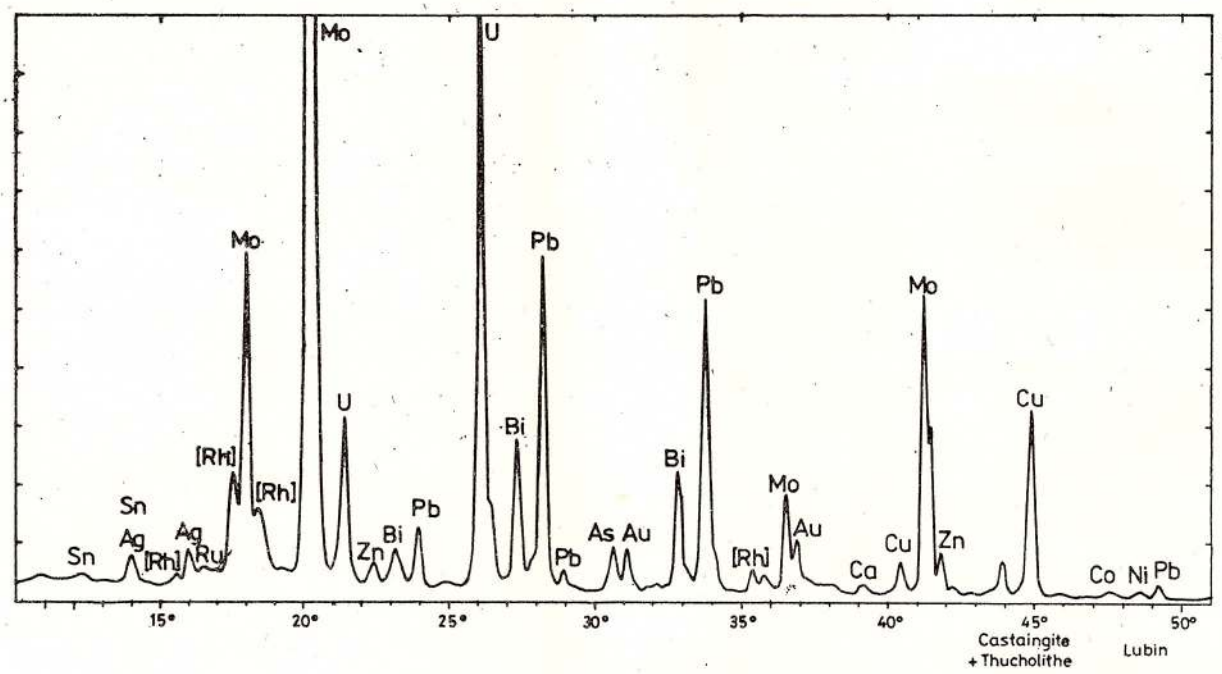

Fig. 3 – X-ray fluorescence chart, performed with rhodium radiation, of a gold-bearing castaingite-thucholite sample from Lubin (Poland).

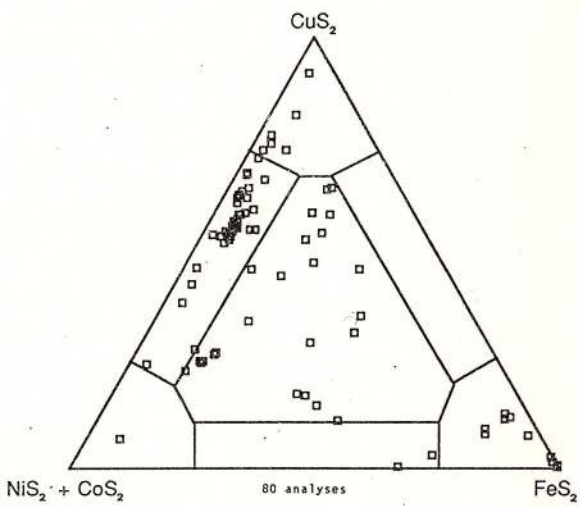

Fig. 4 – Plot of analysed points (villamaninites) in the pseudoternary system CuS_2-FeS_2-(NiS_2+CoS_2); compare Paniagua, 1991.

Table 2

Electron probe microanalyses on disulfides of the Providencia Mine, near Villamanina, Leon/Spain, showing major and trace elements: compare Paniagua, 1991.

	Max.wt.%	Min.wt.%	Med.wt.%
Major elements			
Cu	45.05	0.10	21.06
Ni	38.01	0.00	12.13
Co	8.38	0.02	3.64
Fe	45.64	1.07	11.10
S	53.56	47.35	50.37
Trace elements			
Zn	0.886	0	0.104
As	0.477	0	0.068
Se	2.865	0	0.735
Ag	0.670	0	0.087
Sb	0.191	0	0.022
Au	0.371	0	0.050
Hg	0.450	0	0.082
Tl	0.049	0	0.007
Bi	0.301	0	0.067
Total traces	1.702	0.021	0.423

considered as substitutes for copper in the crystal lattice.

It is the author's aim to synthesize gold-bearing sulfides of the Kupferschiefer type minerals and villamaninites, respectively.

At first pure gold sulfides have to be synthesized, e.g., Au_2S, of which the Mössbauer spectrum is given in Figure 6.

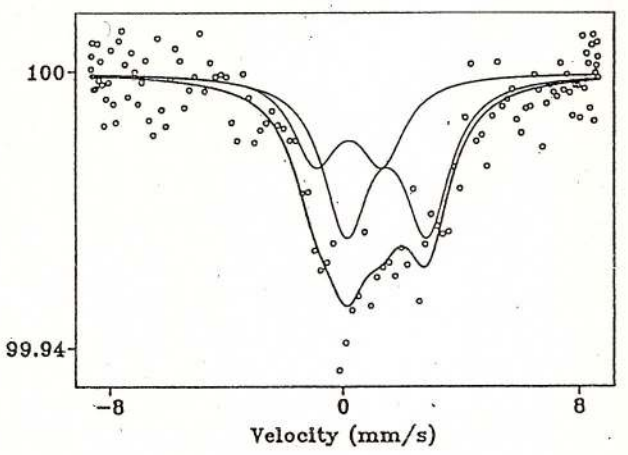

Fig. 5 ^{197}Au Mössbauer spectrum of a villamaninite concentrate taken at 4.2 K with a source of ^{197}Pt metal; compare Friedl et al., 1991.

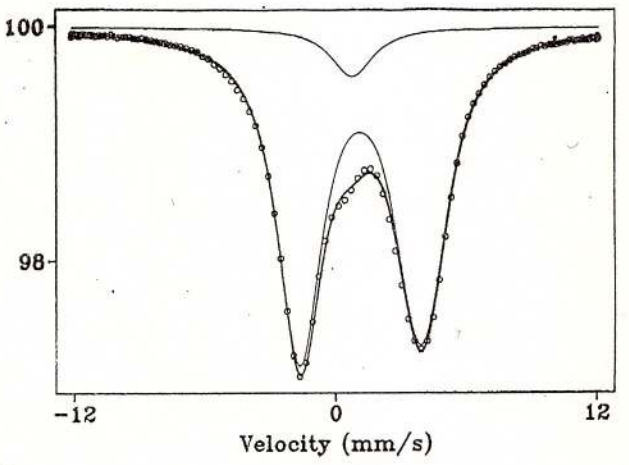

Fig. 6 – Mössbauer spectrum of a synthetic Au_2S sample in activated charcoal.

With regard to the high carbon contents in the Kupferschiefer and their possible adsorption for trace elements, activated charcoal was used for the experimentation which was saturated by aqueous gold-bearing solution before sulfidization. The reaction with diluted H_2S was performed within 2 weeks at p_H 4.5 in a light tight laboratory. Continuous experimentation showed success only in a darkened room, since light beams react with the aqueous H_2S and particularly with H_2Se solution and disturb Eh–pH-conditions considerably – as a result no gold sulfide but metallic gold forms.

At present fresh saturated clay minerals are successfully used for experimentation. For instance: this mineral group allows either absorption (e.g. substitution of Na^+, K^+, Ca^{++}, etc. in the montmorillonite structure by heavy metal ions) or adsorption (e.g., surface saturation of kaolinite by heavy metal ions). The prepared clay minerals undergo then a sulfidization procedure forming the respective sulfide minerals (compare Elhaddad & Moh, 1992).

Acknowledgements. The author thanks the German Science Foundation (DFG) for supporting parts of this study and Dr. N. Wang for reading the manuscript.

References

Elhaddad M. A., Moh G. H. (1992) The hydrothermal formation of sulphides and sulphosalts at low temperature (<100^0). *Mineralogy and Petrology*, 46, p. 185–193, Vienna.

– (1993) Villamaninite formation in aqueous-sedimentary environment (submitted to *Econ. Geol.*).

Friedl J., Paniagua A., Wagner F. E. (1991) Mössbauer study of gold-bearing villamaninite, p. 247–254. In: Moh G. H., Thallium and gold: Observations and experimental contributions to mineralogy, geochemistry and crystal chemistry. *N. Jb. Miner. Abh.*, 163, p. 197–270, Stuttgart.

Kucha H., Piestrzynski A. (1991) Gold-bearing sulfides from the Lubin copper deposit/Kupferschiefer-type, Poland, p. 236–238. In: Moh G. H., Thallium and gold: Observations and experimental contributions to mineralogy, geochemistry and crystal chemistry. *N. Jb. Miner. Abh.*, 163, p. 197–270, Stuttgart.

Moh G. H., Kucha H. (1980) Villamaninite, p. 134–136. In: Moh G. H., Ore syntheses, phase equilibria studies and applications. *N. Jb. Miner. Abh.*, 139, p. 113–154, Stuttgart.

– , Kullerud G. (1963) The Cu-Ni-System. *Carnegie Institution of Washington, Year Book*, 62, p. 189–192.

– (1964) The Cu-Ni-S system at 200^0 and 100^0 C. *Carnegie Institution of Washington, Year Book*, 63, p. 209–211.

– (1982) The Cu-Ni-S system and low temperature mineral assemblages, p. 677–688. In: Amstutz G.C., Goresy A.El., Frenzel G., Kluth C., Moh G., Wauschkuhn A., Zimmermann R.A. (eds.), Ore Genesis; the State of the Art. Springer Verlag, Berlin-Heidelberg-New York, 804 p.

– , Ottemann J (1964) X-ray fluorescence and electron-probe analyses of some pyrite-type minerals. *Carnegie Institution of Washington, Year Book*, 63, p. 214–216.

Paniagua A. (1989) The pyrite-type Cu-rich disulfides in the Providencia mine, Leon, NW Spain, p. 8–11. In: Moh G. H., Ore minerals: an experimental approach – and new observations. *N. Jb. Miner. Abh.*, 160, p. 1–69, Stuttgart.

– (1991) Trace elements in villamaninite and other pyrite-type disulfides of the Providencia mine, Leon, NW Spain, p. 241–247. In: Moh G. H., Thallium and gold: Observations and experimental contributions to mineralogy, geochemistry and crystal chemistry. *N. Jb. Miner. Abh.*, 163, p. 197–270, Stuttgart.

Ramdohr P. ´(1937) Erzmikroskopische Untersuchungen an einigen seltenen oder bisher wenig bekannten Erzmineralien. Parts 1-3. *Centralbl. Mineral.*, A, p. 193–211, p. 289–303, Leipzig.

– (1960) Die Erzmineralien und ihre Verwachsungen. Akademie-Verlag, Berlin, 3. Aufl. 1089 p.

Schmid-Beurmann P. (1960) Experimentelle Untersuchungen zur Stabilität, Kristallchemie und Kristallphysik von CuS_2-FeS_2-Mischkristallen. Dissertation Univ. Göttingen, 121 p.

Schoeller W. R., Powell A. R. (1920) Villamaninite, a new mineral. *Mineral. Mag.*, 19, p.14–18, London.

Sobott R. J. G., Moh G. H. (1991) The Ag-Au-S system, p. 228–230. In: Moh G. H., Thallium and gold: Observations and experimental contributions to mineralogy, geochemistry and crystal chemistry. *N. Jb. Miner. Abh.*, 163, p. 197–270, Stuttgart.

Rom. J. Mineralogy, 1993, 76, 1, p. 63–69

L'ALABANDITE(MnS), SES ASSOCIATIONS, SES PARAGENESES COMPLEXES: CAS DES HAUTES-PYRÉNÉES (FRANCE) ET DES MONTS MÉTALLIFÈRES (TRANSYLVANIE-ROUMANIE)

R. MAURY

Laboratoire de Minéralogie expérimentale et appliquée U.P.M.C., Place Jussieu, 75 252 Paris, France.

Elena Adriana PERSEIL

Laboratoire de Minéralogie du Muséum d'Histoire Naturelle de Paris, URA 73 661, Rue de Buffon, 75 005 France.

Ion BERBELEAC

S.C. "PROSPECŢIUNI" S.A. Str. Caransebeş 1, 78 344 Bucureşti-32, Romania.

Ion TĂNĂSESCU

MINEXFOR S.A. Str. Minerului 2, Deva, Jud. Hunedoara, Romania.

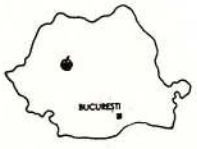

Key words: Sulfides. Alabandite. P-T conditions. Electron probe data. Hautes Pyrénées-France. Apuseni Mountains – Metaliferi Mountains. Romania.

Abstract: *Alabandite (MnS) at Hautes Pyrénées (France) and Metaliferi Mountains (Romania).* Manganese rich associations at Nabias and Adervielle (Hautes Pyrénées-France) are similar to those of Săcărîmb-Nagyag (Metaliferi Mountains-Romania). These complex associations consist in numerous sulfides (alabandite, millerite, violarite, pyrite, sphalerite, tetrahedrite, galena, etc.), manganese silicates and rhodochrosite. These complex association of sulfides and manganese minerals could be due to successive event or illustrate a single system in which all the phases are in equilibrium (same T, pH, Eh, fO_2, fS_2). Such a system must be linked to the local geological study. According to petrological study, microprobe analyses were performed for the major elements: S, Se, Te, Fe, Mn, Co, Ni, Bi, Zn, Cu, Ag, Au, Sb. Data are displayed in atome percent, resulting from 10–40 analysis. The chemical composition of Nabias and Adervielle alabandite (Hautes Pyrénées) are more scattered than Săcărîmb-Nagyag (Metaliferi Mountains) ones. Minor amounts of Fe, Cu, Co, Zn, and Ni are also found. No zonation has been evidenced for major and minor elements. In most cases, a small deficit in sulfur has been detected, the mean values ranging between 49.74 and 50.25. The other sulfides data allow to define conditions of formation: at high pH, close to 8.3 for the equilibrium temperature and finally a reducing medium with a Eh value around –0.5 in good agreement with the $fS_2(10^{-8}$–$10^{-5})$ and the $fO_2(10^{-40})$ values. Such conditions could be due to a medium metamorphism activity affecting manganese rich deposits with hydrothermal circulation of ore solutions (sulfur and likely Ni and Co). Gold is also observed in these areas (specially in Metaliferi Mountains) and is occasionally in association with tellururides. A genetic model is finally proposed: a manganese rich marine formation of shallow basin is submitted to subduction, the associated volcanic activity supplying for sulfur and other metals. Metamorphic and volcanic activities lead to the formation of manganese minerals and gold deposits.

L'alabandite (MnS-Fm3m) est caractéristique des dépôts d'origine hydrothermale ou des concentrations manganésifères ayant subi un métamorphisme de contact (Hewett & Rove, 1930; Rădulescu & Dimitrescu, 1966, Fukuoka, 1981; Lardeau, 1984; Abrecht, 1989a, 1989b). Watanabe (1970) souligne aussi le lien direct entre la présence de l'alabandite et le métamorphisme dû aux intrusions granitiques dans les concentrations de Tamagawa (Japon).

Un cortège complexe de: silicates, carbonates, sulfures, sulfoarséniures, sulfoantimoniures, sulfotellurures, tellurures, arséniures et vanadates accompagne

fréquemment l'alabandite. On observe souvent dans le cortège de sulfosels la prédominance du cuivre ou celle du nickel. Dans la plupart des concentrations où l'alabandite se manifeste, elle représente la première phase dans l'ordre de succession des phases.

Cete étude se propose d'analyser le cortège des sulfures et des autres espèces associés à l'alabandite, de tenter de comprendre s'ils appartiennent à plusieurs générations ou à un système à l'équilibre, c'est-à-dire compatible dans les même conditions de température, de Eh, de pH, fugacité d'oxygène et de soufre. Si de telles conditions existent, il convient de déterminer comment elles se situent par rapport aux histoires géologiques régionales. Deux gisements ont été choisis: l'un dans les Hautes Pyrénées, connu essentiellement pour les silicates de manganèse associés à l'alabandite, l'autre dans les Alpes de Transylvanie, les Monts Métallifères connus pour les tellurures et les sulfotellurures associés à l'alabandite. Une fois décrit le cadre géologique, nous procèderons à un examen pétrographique et analytique des sulfures.

I. Contexte Géologique

Dans les Hautes Pyrénées, des concentrations manganésifères imprègnent la lydienne carbonifère, souvent fortement plissée (Pl. I) ou les calcaires du Dévonien; il s'agit essentiellement d'oxydes (Pelissonnier, 1956; Perseil, 1968, 1969, 1971; Ragu, 1990). L'alabandite et son cortège de sulfures (pyrite, galène, millérite, sphalérite, violarite) apparaissent dans des filons et des veinules où les sulfures sont quelquefois remplacés par des carbonates et des silicates.

Dans les Monts Métallifères, l'alabandite est associées non seulement aux sulfures, mais aux tellurures et aux sulfo-tellurures d'or et d'argent (hessite, stützite, calaverite, krennerite, petzite, sylvanite, et nagyagite) qui remplissent un vaste réseau de filons. Ces concentrations épigénétiques (Berbeleac, 1985) sont liées au processus de subduction du Néogène et au magmatisme andésitique associé.

II. Contexte Pétrographique

L'alabandite des **Hautes Pyrénées** (à Adervielle, à Nabias et à Vielle Aure) est étroitement associée aux veinules de quartz, de rhodochrosite et rhodonite; ces veinules coupent aussi bien le calcaire brun que la lydienne recristallisée du Carbonifère. Tantôt la lydienne recristallisée est traversée par de fines veinules de quartz, rhodochrosite, téphröite et friedélite, accompagnées par l'alabandite, la pyrite, la millérite, la violarite, la bravoïte, la galène et la sphalérite, ainsi que des plages automorphes de hübnérite. Tantôt elle est envahie par des lamelles de friedélite associée à la pyroxmangite, la rhodonite, la téphroïte, la rhodochrosite, la spessartite, le quartz et l'alabandite dans des assemblages progrades. L'alabandite est associée à la grille pétrogénétique:

$MnO–SiO_2–H_2O–CO_2$, essentiellement par l'intermédiaire de la friedélite.

La friedélite représente la phase la plus hydratée de la famille des phyllosilicates manganésifères et la présence implique une activité importante des fluides pendant le métamorphisme. Les textures observées indique que la friedélite a pu se former, lors du métamorphisme prograde (Abrecht, 1989), suivant la réaction:

$$MnCO_3 + SiO_2 + H_2O + HCl =$$
$$Mn_8Si_6O_{15}(OH,Cl)_{10} + CO_2$$

Au microscope, on constate que l'alabandite se développe dans une masse de tephroïte largement cristallisée dont la teneur en fer ne dépasse pas 0,70 %; on peut souligner aussi l'absence en éléments en traces de cette téphroïte. Au microscope électronique à balayage, l'alabandite présente des macles répétitives très caractèristique (Pl. II, fig. 1).

En surface polie, on observe que la pyrite borde les plages d'alabandite et manifeste une nette tendance à la remplacer. La millérite, la violarite et la bravoïte apparaissent aussi bien en inclusions dans l'alabandite, que dans les plages de sphalérite et de galène associées.

La présence d'une série de minéraux rares (la helvite, la welinite, la vuorélainenite) signalée par Ragu (1990) doit être mise au compte d'une phase tardive pneumatolitique en relation avec l'intrusion des massifs granitiques voisins.

Dans les **Monts Métallifères** plus particulièrement dans le gisement de Săcărîmb, l'alabandite apparaît d'avantage comme un élément de gangue à coté du quartz, de la rhodochrosite et de la calcite que du véritable minerai. L'alabandite est cependant le premier sulfure dans la paragenèse, à côté de la pyrite, la marcasite, l'arsenopyrite, la sphalérite, la galène, la chalcopyrite, la nagyagite, l'altaïte, le cuivre gris, la boulangérite, la bournonite, la jamesonite, la stibine, l'arsenic et l'or natif (Ghiţulescu, 1934; Ghiţulescu et Socolescu, 1941; Giuşcă, 1935, 1936; Ramdhor et Udubaşa, 1973). C'est la galène, largement cristalisée dans la masse de l'alabandite, qui enferme de nombreuses inclusions de cuivre gris, de tellurures d'or (krennerite–$AuTe_2$; calaverite–$AuTe_2$), de tellurures d'argent (hessite–Ag_2Te;; stützite–Ag_3Te_2) et de tellurures d'or et d'argent (petzite–Ag_3AuTe_2; sylvanite–$AuAgTe_4$) auquel on peut ajouter aussi le tellurure de fer (la frohbergite–$FeTe_2$). Des flammèches d'antimoine sont assez fréquentes à côté de ces inclusions (Pl. II, fig. 2) est progressivement remplacées par la pyrite et les autres sulfures et tellurures (Pl. II,

fig. 3).

III. Résultats Analytiques

1. Conditions d'analyse: les analyses ponctuelles ont été réalisées sur une microsonde microbeam Camebax. Les conditions opératoires sont les suivantes: tension d'accélération 15 kV, courant image 40 nA, focalisation 1 μm, temps de comptage variant de 10 à 20 s selon l'abondance des éléments. Les étalons ont été choisis en fonction des liaisons du soufre (pyrite ou chalcopyrite) suivant une méthode décrite par Maury (1990). Après une recherche des éléments présents, l'analyse a été limitée aux seuls constituants dont la teneur soit significative, variable suivant les sulfures: S, Se, Te, Fe, Mn, Co, Ni, Bi, Zn, Cu, Ag, Au, Sb.

Les résultats correspondent à des séries de 10 à 40 mesures exprimées en atome pour cent; seules ont été retenues les analyses dont le total en poids est compris entre 99,9 et 100,1. L'écart type n'est donnée que pour les éléments majeurs;

Les résultats sont rassemblés dans les tableaux; ils appellent un certain nombre de remarques.

2. Alabandite. Les résultats concernant ce sulfure présentent une légère dispersion pour les échantillons des Hautes Pyrénées (Adervielle, Nabias, Vielle Aure), mais sont bien groupés pour les échantillons des Monts Métallifères (Săcărîmb) il ne s'agit là peut-être que d'un effet d'échantillonage; parmi les éléments mineurs, seuls le Fe, le Cu, le Zn, et le Ni présentent une valeur mesurable, qu'il convient de prendre comme seulement indicative. Aucune zonation n'a été mise en évidence, ni pour les éléments majeurs, ni pour les mineurs. On remarque dans la quasi totalité des cas un léger déficit en soufre par rapport à la somme des cations et même par rapport au Mn; la valeur moyenne est en effet pour le soufre de 49,74 et de 50,25 pour la somme des cations (Tab. 1).

3. Sulfures de nickel. Trois sulfures de nickel ont été observés: la millérite (NiS), la violarite (Ni_2FeS_4), qui présentent une substitution nickel-cobalt notable et la bravoïte $(FeNiCo)S_2$.

a) La millérite: ce sulfure est légèrement déficitaire en Ni, 47,32 %, ce qui correspond à un rapport Ni/S de 0,95, valeur qui semble très importante. Compte tenu de l'ensemble des cations, soit 49,82 %, le rapport cations/S=0,996 et l'écart type passe de 0,78 à 0,30, résultat qui semble en bon accord avec les observations de Kullerud et Yund (1962) (Tab. 1).

b) La violarite: comme Hudson et Groves (1974) nous avons affaire à un minéral de formule $(FeNiCo)_3S_4$). Toutes les analyses de violarite présentent un total en poids variant entre 97 à 100 %.

Les analyses ponctuelles indiquent quelques écarts par rapport à la formule stoechiométrique. La valeur moyenne pour le soufre est de 57,44, elle présent un faible écart type de 0,17 coerrespondant à une bonne homogénéité en soufre, en excès vis-à-vis de la valeur stoechiométrique. Hormis le manganèse, on ne trouve aucun élément en trace mesurable entrant dans la structure de la violarite. La valeur moyenne du nickel, soit 28,05 %, est inférieure à la valeur théorique de 28,57 % et l'écart type de 1,82 est considérable; on peut faire la même observation pour la somme Fe + Co qui est en moyenne de 14,03 % ± 1,61. La somme des cations, par contre, présente une valeur moyenne de 42,56 ± 0,19. On peut donc conclure à un excès de soufre de la violarite et à la substitution préférentielle du fer, et partiellement du nickel, par le cobalt. C'est par leur teneur plus élevée en cobalt (Tab. 1) que les violarites analysées diffèrent des données de Misra et Fleet (1974). La millérite ne contenant pratiquement pas de Co, la violarite ne peut en dériver par altération que par un apport conjugué de Co et de Fe, à moins, ce qui est plus probable, que la violarite soit primaire.

c) La bravoïte se manifeste en inclusions, dont le diamètre ne dépasse pas 3 μm, aussi bien dans les plages d'alabandite, que dans les plages de galène et de sphalérite. Les inclusions non zonnées, légèrement craquelées, mises en evidence à l'aide du microscope électronique à balayage, ont été analysées au détecteur par dispersion d'énergie de type Ortec.

4. Les autres sulfures:

a) La pyrite possède une composition ponctuelle (Tab. 2) qui présente une dispersion caractéristique d'une origine primaire (Laffitte et Maury, 1983); l'abondance des autres éléments, en particulier le manganèse (0,3 à 1,8 %) et le nickel (0,02 à 1,2 %), renforce cette interprétation.

b) Le sulfure de zinc, riche en manganèse et pauvre en fer (Tab. 2) possède un rapport k=S/Zn+Fe+Mn supérieur à 1, ce qui permet de le classer parmie les sphalérites. La faible teneur en fer est caractéristique des sphalérites associées à un hydrothermalisme acide. Non seulement les bordures des sphalérites de Săcărîmb (Monts Métallifères) mais aussi les bordures des sphalérites d'Adervielle et de Vielle Aure (Hautes Pyrénées) sont riches en traces d'or (0,4 à 0,8 %). Cette abondance etant plus marquée dans le premier cas.

c) La galène est très fréquente dans le gisement de Săcărîmb, où elle est directement associée aux sulfotellurures d'or et d'argent, et reste plus discrète dans les gisement des Hautes Pyrénées, où elle enferme les sulfures de nickel (Pl. III). La galène de Săcărîmb est très riche en flammèche d'antimoine. Les analy-

Tableau 1

Composition ponctuelle de l'alabandite %							
	S	Mn	Fe	Cu	Zn	Ni	Co
Formule théorique	50,00	50,00					
Htes. Pyrénées	50,02(0,12)	49,40(0,10)	0,40	0,13	0,00	0,03	
,,	49,86(0,18)	49,61(0,18)	0,31	0,14	0,00	0,03	
,,	49,62(0,19)	49,99(0,20)	0,30	0,05	0,00	0,02	
,,	49,48(0,13)	50,11(0,14)	0,31	0,05	0,00	0,02	
Moyenne	49,74(0,20)	49,77(0,20)	0,33	0,10	0,00	0,03	
Săcărîmb	49,80(0,03)	50,07(0,04)	0,72	0,04	0,02	0,00	
Composition Ponctuelle de la Millérite Atome % (Hautes Pyrénées							
Formule théorique	50,00					50,00	
	50,15(0,36)	1,01	1,10	0,00	0.02	47,32(0,78)	0,37
Composition ponctuelle de la violarite atome % (Hautes Pyrénées)							
Formule théorique	57,14		14,29			28,57	
	57,20	0,25	8,81	0,00	0,00	26,61	7,14
	57,26	1,67	13,36	0,00	0,00	24,88	2,91
	57,46	0,28	3,04	0,00	0,00	28,08	11,12
	57,43	0,45	2,05	0,00	0,00	29,08	10,97
	57,69	0,22	3,06	0,00	0,00	27,96	11,08
	57,60	0,10	3,61	0,00	0,00	29,70	8,96
	57,46	0,36	2,50	0,00	0,00	30,06	9,61

valeurs entre paranthèses = σ – écart type.

Tableau 2

Composition ponctuelle de la pyrite en atome %								
		S	Mn	Fe	Cu	Zn	Ni	Co
Formule théorique		66,66		33,33				
Htes. Pyrénées		66,21	0,97	32,48	0,04	0,00	0,49	0,00
Săcărîmb		65,66	0,01	33,87	0,20	0,00	0,02	0,00
Composition ponctuelle des blendes en atome %								
								Moyenne
Htes. Pyrénées	Zn	46,58	44,76	44,75	44,98			45,26±0,88
	Mn	5,10	4,70	4,28	4,64			4,68±0,33
	Fe	0,66	0,87	0,62	0,48			0,65±0,16
	S	47,64	49,66	50,34	49,89			49,38±1,19
Săcărîmb	Zn	42,05	42,39	43,94	43,35	43,73		43,09±0,83
	Mn	6,18	5,56	6,14	4,62	6,63		5,82±0,77
	Fe	0,19	0,25	0,14	0,20	0,03		0,16±0,08
	S	51,65	51,79	49,78	51,82	49,61		50,93±1,13

Composition ponctuelle des cuivres gris (Săcărîmb) en atome %								
	S	As	Sb	Cu	Zn	Mn	Ag	Fe
Formule théorique	44,83		13,80	41,39				
	44,18	3,92	10,74	31,67	5,21	1,72	1,58	0,15

Composition ponctuelle de la galène (Săcărîmb) en atome %										
	S	Te	Se	Pb	Fe	Zn	Bi	Mn	Au	Ag
Formule théorique	50,00			50,00						
	44,22	0,06	0,07	49,20	0,10	0,36	0,37	0.21	0,05	0,19

ses ponctuelles indiquent de nombreuses substitutions, tant à la place du soufre que du plomb (Tab. 2).

d) Les cuivres gris, très abondants et avec une composition chimique très variable dans le gisement de Săcărîmb (Tab. 2), restent plus rares dans les concentrations d'Adervielle et de Vielle Aure. Les tellurures d'or et d'argent, ainsi que les sulfotellurures, se manifestent en inclusions dans le cuivres gris, qui sont à leur tour inclus dans les plages de galène.

Nous donnons seulement la composition ponctuelle de la nagyagite, il s'agit du gisement d'origine (Tab. 3).

Tableau 3

Composition ponctuelle de la nagyagite de Săcărîmb (Nagyag)

					Moyenne (atome %)
Au	7,90	8,56	9,25	9,68	5,25
Te	13,46	14,79	15,12	15,18	13,66
S	11,18	10,92	10,62	10,78	40,43
Pb	59,03	56,96	55,10	54,20	32,37
Sb	7,19	8,12	8,29	7,64	7,62
Bi	0,31	0,30	0,31	0,43	0,01
Ag	0,03	0,20	0,12	0,19	0,00
Zn	0,00	0,00	0,33	0,13	0,01

IV. Discussion

Nous disposons de nombreuses courbes d'équilibre de ces espèces en fonction du pH, du Eh et des fugacité de soufre et d'oxygène. Nous allons examiner les domaines propres à chaque espèce et les possibilités de concordance.

a) L'alabandite. La présence systématique de ce sulfure relativement peu courant (dans les gisements classiques de manganèse), permet, compte tenu de son abondance dans les gisements analysés, de délimiter un domaine de pH, Eh où il doit jouer le rôle de tampon. Nous disposons pour cela des courbes de Gaucher publiées dans Garrels et Christ (1965); le domaine de stabilité de l'alabandite y est très limité autour d'un pH basique de 8 à 9 et un Eh réducteur de 0,5 à 0,8 Ev. Ce domaine valable à 25° C ne doit pas s'étendre beaucoup jusqu'à 300° C. De la même manière, les courbes de Barton et Skinner (1967) fixent aux environs de 300° C la fugacité du soufre à une valeur inférieure à 10^{-5} et supérieure à 10^{-8}.

b) La violarite. Il s'agit encore ici d'un sulfure dont les conditions de stabilité sont relativement réduites. En ce qui concerne la température, la violarite n'est stable qu'en dessous de 460° C (Craig, 1971), mais sa teneur en Fe limite ce domaine en dessous de 300° C (Misra et Fleet, 1974). La teneur élevée en cobalt ne doit pas changer le domaine de stabilité (Craig, 1971). Le diagramme donné par Richardson et Vaughan (1989) permet de limiter le pH entre 4 et 12 et le Eh entre -0,5 et 0. Ces même auteurs nous fournissent des limites pour la fugacité du soufre entre 0 et 10^{-10} et autour de 10^{-60} pour la fugacité de l'oxygène. L'évaluation de la fugacité de l'oxygène n'est pas très précise; elle peut varier suivant les auteurs de 10^{-40} à 10^{-60} (Crerar et al., 1982; Richardson et Vaughan, 1989). Cette ambiguïté réside sans doute dans le fait que l'on observe une série d'équilibres, dont certains correspondent à la phase primaire du métamorphisme, et les autres à la phase finale. La fugacité de l'oxygène a augmenté au cours de cette évolution et a joué un rôle important dans le mécanisme de dépôt de l'or. On notera enfin que nous n'avons pas trouvé de traces de pentlandite. L'examen au microscope électronique à balayage de la violarite riche en Co montre une surface non poreuse, qui pourrait être liée à une origine hypergène (Hudson et Groves, 1974; Patterson et Watkinson, 1984).

c) L'association millérite-violarite-pyrite peut se présenter dans un diagramme Ni-Fe-S sur une même droit de compatibilité. Cet assemblage hors équilibre peut traduire, comme cela a déjà été observé (Patterson et Watkinson, 1984), une transformation liée au métamorphisme, où le cobalt pourrait jouer un rôle stabilisateur.

d) La sphalérite se caractérise par une faible teneur en fer, 0,6 % et une teneur importante en manganèse: 4 à 7,5 % dans les deux cas. La présence de la pyrite et l'absence de la pyrrhotite sont assez caractéristiques pour permettre une évaluation de quelques paramètres. En particulier, il est possible de fixer la fugacité du soufre à 10^{-8} et la température d'équilibre au voisinage de 300° C (Barton et Skinner, 1967). Si l'on tient compte des teneurs en manganèse de la sphalérite et de la galène, on peut évaluer un coéfficient de partage $Ln(K^0)$=MnS (dans ZnS)/MnS (dans PBS)=3. Cette valeur élevée est très en dehors des diagrammes de Bethke et Barton (1971), mais correspond, dans les limites d'une simple extrapolation, à une température d'équilibre faible et compatible avec celle estimée par d'autres voies, soit T^0 C < 300° C.

V. Conclusions

Les observations microscopiques et les analyses ponctuelles réalisées permettent de donner les conditions de formation de ces paragenèse: pH élevé de l'ordre de 8, Eh réducteur de l'ordre de -0,5 en accord avec la valeur estimée de la fugacité du soufre 10^{-8} à 10^{-5}, une fugacité d'oxygène faible de l'ordre de 10^{-40} et enfin une température d'équilibre de 300°.

Pour les concentrations des Hautes Pyrénées, on peut donc imaginer un métamorphisme modéré sur des calcaires riches en manganèse, associé à des venues profondes de S et peut-être aussi des apport de nickel et de cobalt.

La violarite n'étant pas due ici à une transformation de pentlandite. L'activité hydrothermale couplée à un métamorphisme modéré peut conduire à des conditions physico-chimiques favorables aux associations des phases manganésifères avec des dépôts d'or (Sidorov et al., 1980).

La présence de l'or est très faible dans les gisements pyrénéens alors que dans les Monts Métallifères cette présence est nette et diversifiée (tellurures et sulfotellurures d'or et d'argent). Cette différence remarquable entre l'évolution des phases pour chacun des cas analysés indique une évolution tardive différente des milieux de formation. Le caractère réducteur du milieu, compatible (Seward, 1973) avec la succession des sulfo-tellurures d'or et d'argent est préservé dans le gisement de Săcărîmb (Monts Métallifères), alors que dans les Hautes Pyrénées les conditions deviennent oxydantes, comme en témoignent les remplissages tardifs en oxydes de manganèse (Perseil, 1971). Cette oxydation tardive du milieu peut-être à l'origine d'une migration tardive de l'or.

Bibliographie

Abrecht J. (1989) A hydrothermal Manganiferous Sulfide Assemblage in Carboniferous Volcanic Rocks of the Central Aar Massif (Switzerlang). *Schweiz. Mineral. Petrogr. Mitt.*, 69, p. 117–128. Zürich.

– (1989) Manganiferous Phyllosilicate Assemblages: Occurrences, Compositions and Phase Relations in Metamorphosed Mn Deposits. *Contrib. Mineral. Petrol.*, 103, p. 228–241, Berlin.

Barton P. B., Skinner B. J. (1967) Sulfide Mineral Stabilities. In Barnes H. L. (Ed.): Geochemistry of Hydrothermal Ore Deposits. Holt, Rinehart and Winston, Inc., p. 236–333, New York.

Berbeleac I. (1985) Zăcăminte de aur. Ed. tehnică, 334 p., Bucureşti.

Bethke P. M., Barton P. B. (1971) Distribution of Some Minor Elements between Coexisting Sulfide Minerals. *Econ. Geol.*, 66, p. 140–161, Lancaster.

Craig J. R. (1971) Violarite stability relations. *Am. Mineral.*, 56, p. 1303–1311, Washington.

Crerar D. A., Fischer A. G., Plaza C. L. (1980) Metallogeny and Biogenic deposition of manganese from Precambrian to Recent Time. III, p. 285–304. In: Geology and Geochemistry of manganese, edited by Varentsov I. M., Grasselly Gy., Stuttgart.

Fukuoka M. (1981) Mineralogical and genetical study on alabandite from the manganese deposits of Japan. *Mem. fac. Sci., Kyushu Univ., Ser. D. Geol.*, XXIV, 4, p. 207–251.

Garrels M. R., Christ L. Ch. (1965) Solutions, Minerals and Equilibria. 450 p., Harper & Row, New York, Evanston & London Weatherhill, Inc. Tokyo.

Ghiţulescu T. P. (1934) Distribution de la minéralisation dans les gisements d'age tertiaire de Transylvanie. *Bull. Soc. Rom. Geol.*, Ii, p. 56–97, Bucureşti.

– , Socolescu M. (1941) Étude géologique et minière des Monts Métallifères (Quadrilatère aurifère et régions environnantes). *An. Inst. Geol.*, XXI, p. 181–284, Bucureşti.

Giuşcă D. (1935) Note préliminaire sur la genèse du gisement aurifère de Săcărîmb. *Bull. Lab. Min. Gen. Univ.*, I, p. 72–82, Bucureşti.

– (1936) Nouvelles observations sur la minéralisation des filons aurifères de Săcărîmb (Nagyag). *Ac. Roum. Bull. Sect. Sc.*, XVIII, p. 3–5, 1936, Bucureşti.

Hewett D. F., Rove O. N. (1930) Occurrence and relations of alabandite. *Econ. Geol.*, 25, p. 36–56, Lancaster.

Hudson D. R., Groves D. I. (1974) The composition of violarite coexisting with vaesite, pyrite, and millerite. *Econ. Geol.*, 69, p. 1335–1340, Lancaster.

Kullerud G., Yund R. A. (1962) The Ni-S System and Related Minerals. *J. Petrol.*, 3, p. 126–175, Oxford.

Lafitte M., Maury R. (1983) The Stoechiometry of Sulfides and Its Evolution, a Chemical Study of Pyrites, Chalcopyrites and Sphalerites from Terrestrial and Oceanic Environment. *Earth Planet. Sci. Lett.*, 64, p. 145–152, Amsterdam.

Lardeau M. (1984) Alabandite: Gisements et paragenèses; Rôle du fer dans l'évolution de son paramètre cristallin. D. E. A. Université d'Orleans.

Maury R. (1990) A propòs de l'analyse de sulfures à la microsonde électronique. *C. R. Acad. Paris*, 310, Série II, p. 193–198, Paris.

Misra K. C., Fleet M. E. (1973) The Chemical Composition of Synthetic and Natural Pentlandite Assemblages. *Econ. Geol.*, 68, p. 518–539, Lancaster.

– , Fleet M. E. (1974) Chemical Composition and Stability of Violarite. *Econ. Geol.*, 69, p. 391–403, Lancaster.

Patterson G. C., Watkinson D. H. (1984) Metamorphism and Supergene Alteration of Cu–Ni Sulfides, Thierry Mine, Northwestern Ontario. *Canad. Mineral.*, 22, p. 13–20, Toronto.

Pelissonnier H. (1956) Caractère syngénétique du manganèse des Hautes Pyrénées. XX^{e} Congrès géologique Int.T.v., p. 173–195, México.

Perseil E. A. (1968) Contribution à la métallogénie du manganèse dans la France méridionale. Thèse de Doctorat-es-Sciences, 208 p., Toulouse.

– (1969) Caractères minéralogiques de quelques types de gisements manganésifères de la France méridionale. *Bul. Soc. géol. France*, 7^{e} série, X, p. 408–412, Paris.

– (1971) Les minéralisations manganésifères des Hautes Pyrénées. Minéralogie et Métallogénie. *Bull. Soc. Hist. Nat. Toulouse*, p. 503–533, Toulouse.

Ramdhor P., Udubaşa G. (1973) Frohbergit–Vorkommen in den Golderzlagerstätten von Săcărîmb und Faţa Băii (Rumänien). *Mineral. Deposita (Berlin)*, 8, p. 179–182.

Ragu A. (1990) Pétrologie et minéralogie des minéralisations manganésées métamorphiques dans la Paléozoïque des Pyrénées Centrales. Thèse de Doctorat de l'Université, 328 p., Paris VI, Paris.

Rădulescu D., Dimitrescu R. (1966) Mineralogia topografică a României. Ed. Acad. 376 p., Bucureşti.

Richardson S., Vaughan D. J. (1989) Surface Alteration of of Pentlandite and Spectroscopic Evidence for Secondary Violarite Formation. *Mineral. Mag.*, 53, p. 213–222, London.

Seward T. M. (1973) Thio Complexes of Gold and the Transport of Gold in Hydrothermal Ore Solutions. *Geochim. Cosmochim. Acta*, 37, p. 379–399, London.

Sidorov A. A., Naiborodin V. I., Savva N. E. (1980) Manganese Mineral Associations in Gold-Silver Deposits. In: Geology and Geochemistry of Manganese, p. 285–289, Stuttgart.

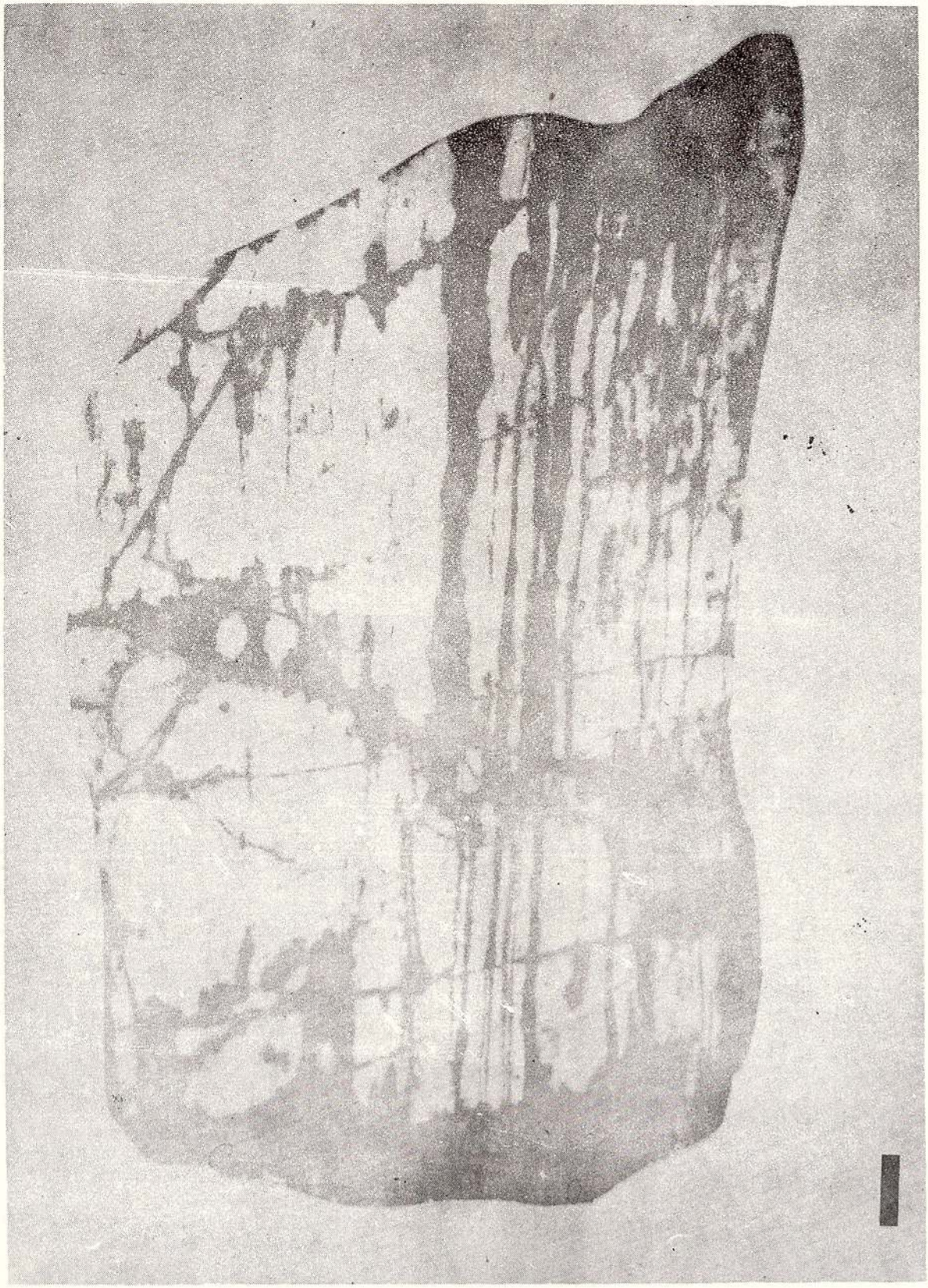

Planche I

Les oxydes de manganèse imprègnent la lydienne carbonifère dans les Hautes Pyrénées. Le trait = 1cm.

Planche II

Fig. 1 — En cassure, au MEB, la présence des macles polysynthétiques est très caractéristique pour l'alabandite.

Fig. 2 — La galène, largement cristallisée dans la masse de l'alabandite, enferme de nombreuses inclusions (cuivre gris, tellurures d'or et d'argent et aussi des flammèches d'antimoine (Sb). Le tiret = (50μm). Lumière naturelle réfléchie.

Fig. 3 — Le remplacement progressif de l'alabandite par la pyrite et les autres sulfures et tellurures; Săcărîmb (monts Métallifères.).

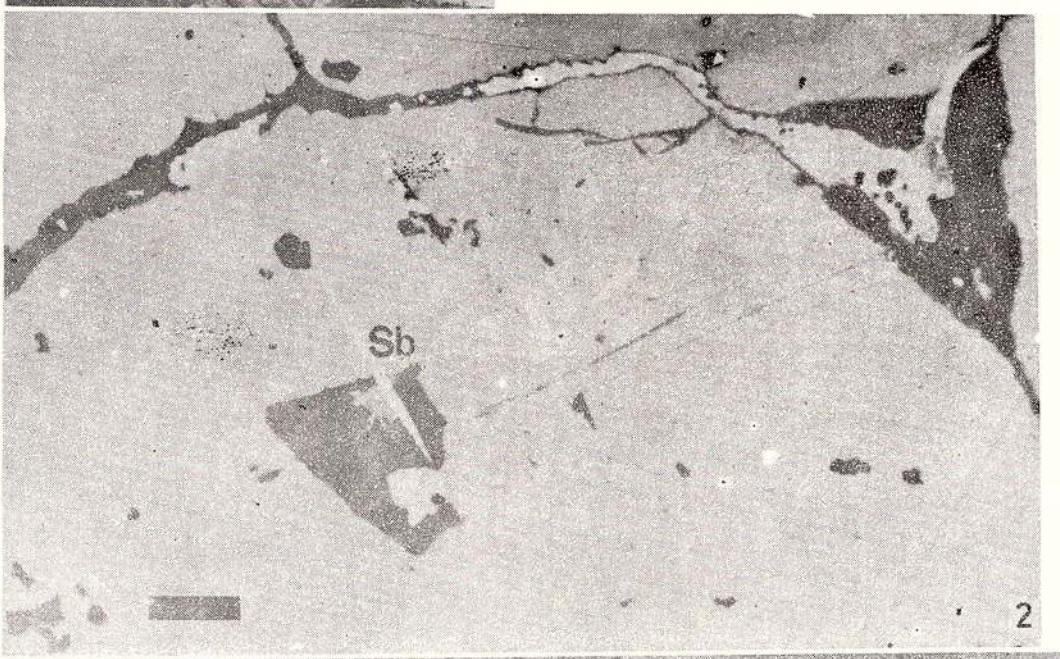

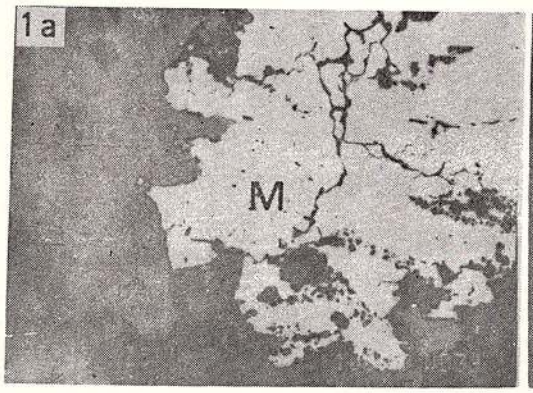

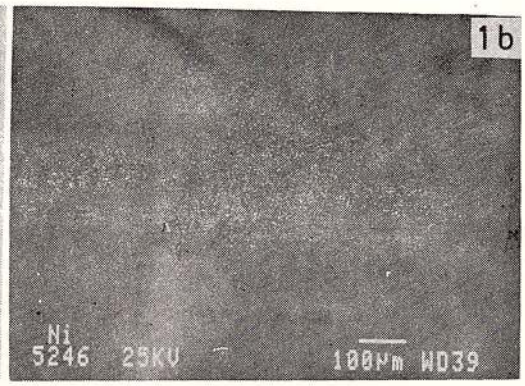

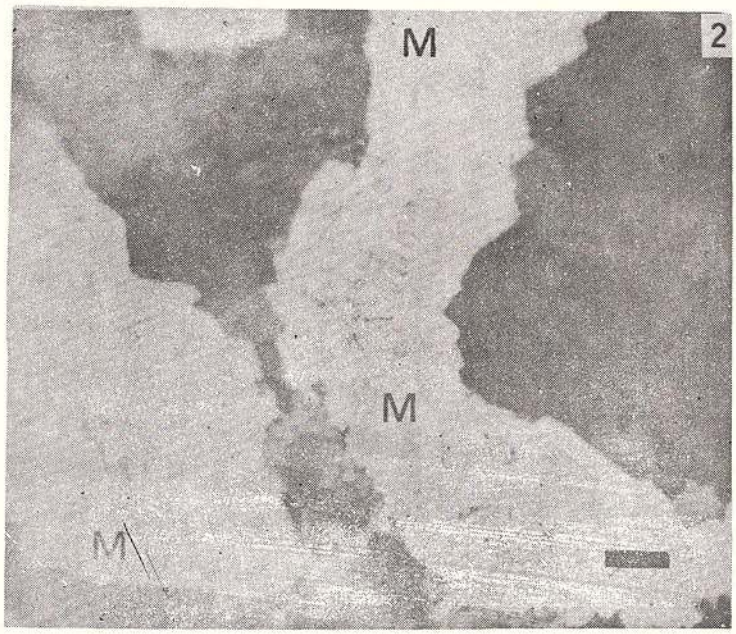

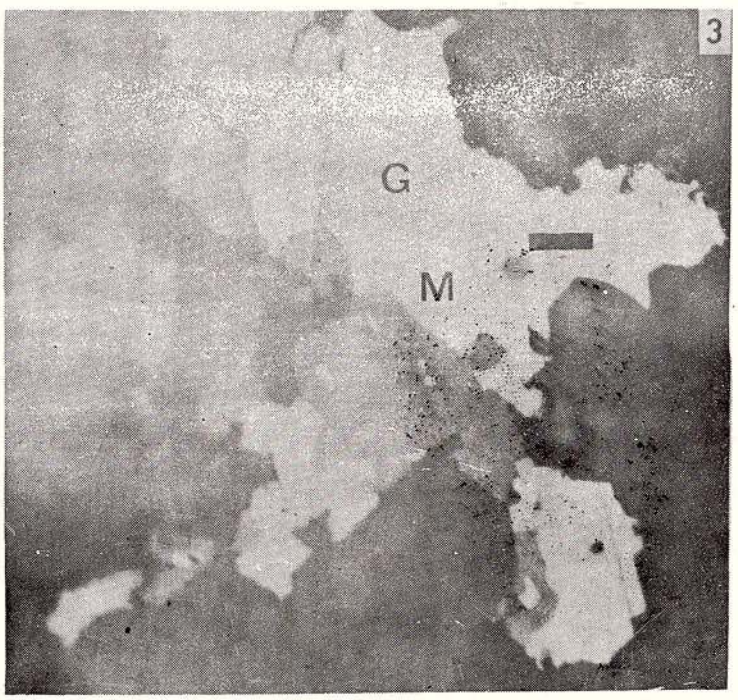

Planche III

Millérite (M) en inclusion: 1. dans l'alabandite; microscope électronique à balyage; 2. dans la sphalérite; lumière naturelle réfléchie, le tiret=50μm; 3. dans la galène; lumière naturelle réfléchie, le tiret=50μm.

Rom. J. Mineralogy, 1993, 76, 1, p. 71–78

L'ALABANDITE DANS LES GISEMENTS DE ROUMANIE

Ioan MÂRZA, Dana POP

Université "Babeş-Bolyai", Département de Minéralogie-Pétrométallogénie. 1, rue M. Kogălniceanu, 3400 Cluj-Napoca.

Liviu DĂRĂBAN

Université "Babeş-Bolyai" Cluj-Napoca, Département de physique. 1, rue M. Kogălniceanu, 3400 Cluj-Napoca.

Key words: Sulfides. Alabandite. Paragenesis. Mineral assemblages. Hydrothermal process. X-ray data.

Abstract: *Alabandite in the Deposits of Romania.* Romania is well-known for its classical alabandite mineralizations; furthermore, the Săcărîmb occurrence is unofficially considered to be the first locality of the "black manganese mineral" considered a sulphide by Reichenstein (1784) and accordingly called "schwarze Blende". The ore deposits containing alabandite are hydrothermal either of gold/silver type, with tellurides (Săcărîmb) or without (Căraci, Roşia Montană, Breaza) or of the polymetallic type (Baia de Arieş, Cavnic). There is only one exception – the alabandite at Argestruţ (Vatra Dornei) associated with the metamorphosed manganese deposit. As for the hydrothermal occurrences, the prevailing nonmetallic minerals accompanying the alabandite are carbonates (rhodochrosite, Mn-calcite) and manganese silicates (Mn-pectolite, rhodonite).

La présence de l'alabandite dans certains gisements de Transylvanie, plus précisément à Săcărîmb, a été signalée sous la dénomination générique de "schwarze Blende" ou "Schwarzerz" longtemps avant qu'elle soit reconnue comme une nouvelle espèce minérale; cela en raison de la fréquence du minéral, de son apparition sous forme cristallisée (octaèdres) et de son association aux tellurures, plus particulièrement au nagyagite (Săcărîmb), minéral qui a fait sensation lors de sa découverte et a attiré de nombreux chercheurs de renom aux XVIII^{e} – XIX^{e} siècles (Fig. 1).

Trois modes génétiques d'alabandite sont reconnus sur le territoire de la Roumanie: le type hydrothermal-filonien (Săcărîmb, Roşia Montană, Căraci, Cavnic, Baia de Arieş – partiellement), hydrothermal-métasomatique (Baia de Arieş – prépondérant) et l'alabandite associée aux minerais carbonatiques de manganèse (Argestruţ, Vatra Dornei). Comme position génétique, l'alabandite suggère des conditions épithermales (solutions riches en manganèse et hydrogène sulfuré) et métamorphiques (sans doute hydrothermales-métamorphiques, comparables au domaine épithermal). La présence de la rhodochrosite (± rhodonite, parfois Mn-pectolite), en quantité appréciable, dans les gisements de sulfures, constitue un élément symptomatique de l'apparition possible de l'alabandite en association.

L'alabandite de Săcărîmb. De par l'occurrence de Săcărîmb, la Transylvanie détient, de façon non officielle, la primauté mondiale quant à la découverte du "minerai noir de manganèse" (Hintze, 1904). Reichenstein (1784; d'après Hintze, 1904) remarque le premier la nature sulfidique du minerai noir de Săcărîmb, qu'il appelle "schwarze Blende", en le distinguant des oxydes et hydroxydes de manganèse auxquels il avait été assimilé jusque-là. Les analyses chimiques de ce minerai, effectuées par Bindheim en 1784, Klaproth en 1802, Vauquelin en 1805, Gehlen en 1806 (d'après Hintze, 1904), dépistent de manière erronée dans sa composition, à côté du manganèse (exprimé sous forme de pyrolusite), du soufre, ainsi que la présence de SiO_2 et CO_2. D'autres analystes (Proust, 1802; Gehlen, 1811; d'après Hintze, 1904) considèrent le nouveau minerai, dénommé par Karsten (1808; d'après Hintze, 1904) "Manganglanz", comme étant un sulfure de manganèse. La première détermination chimique quantitative correcte (Mn=62,10 %, S=37, 90%), effectuée sur un matériel provenant de Săcărîmb, appartient à Arfvedson (1822; d'après Hintze, 1904). La composition chimique obtenue de la sorte est définitoire aussi pour la formule chimique du nouveau

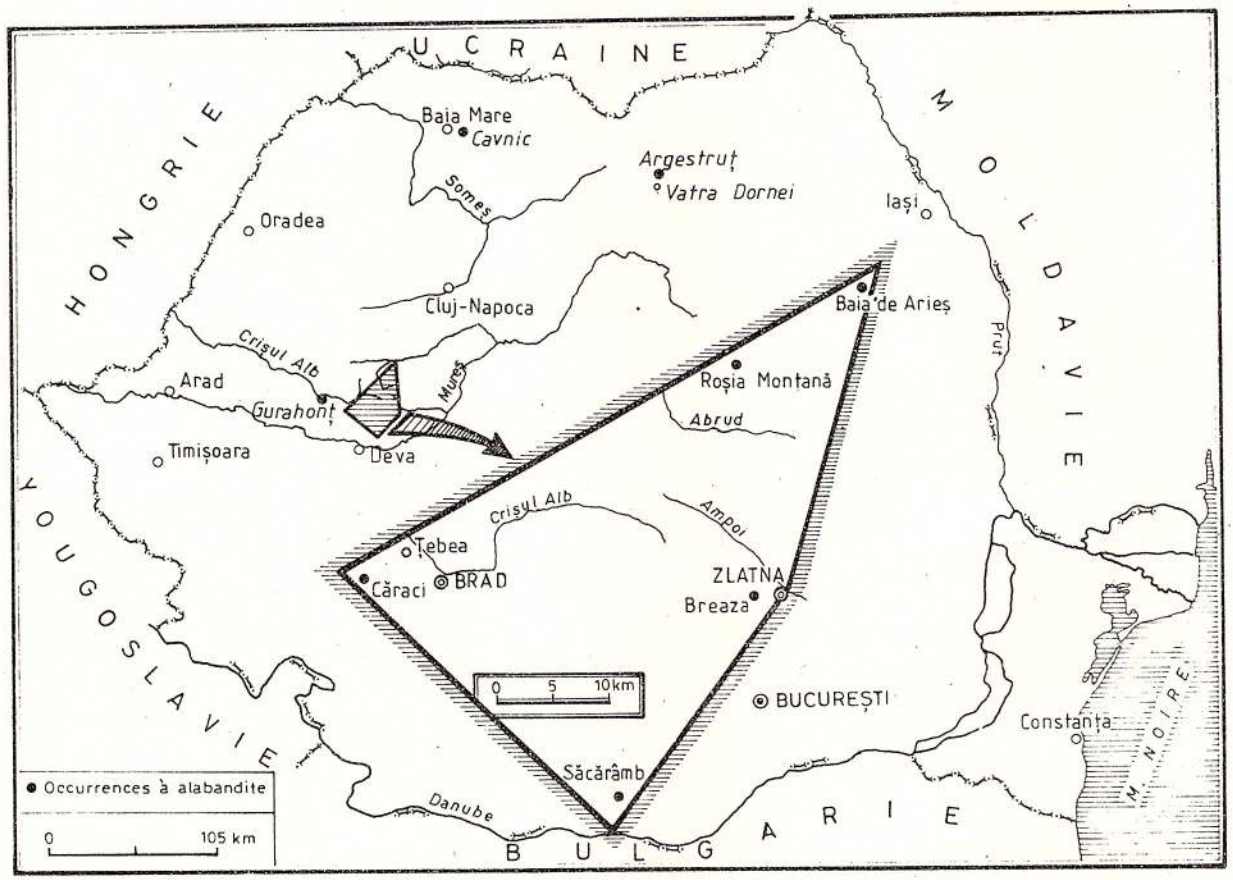

Fig. 1 – Répartition des occurrences à alabandite en Roumanie et dans le quadrilatère aurifère des Carpates Occidentales.

minéral, dont la paternité a été attribuée à Beudant (1832; d'après Strunz, 1982).

La dénomination d'"alabandite" donnée par Beudant (1832) au minéral "Manganblende" – par laquelle Breithaupt (1818; d'après Hintze, 1904) nominalisait l'ancien "Manganglanz", décrit de Săcărîmb et inclus dans "la famille des blendes" définie par Hausmann (1813; d'après Hintze, 1904) – reprend la filière mexicaine, soit l'appellation de "alabandina sulfurea", sous laquelle Del Rio (1804; d'après Hintze, 1904) avait décrit le même minéral, provenant du Mexique, et écarte malheureusement la primauté des occurrences de Transylvanie.

Les premières mentions quant aux occurrences de Săcărîmb, après l'attestation de l'alabandite comme une nouvelle espèce minérale, appartiennent à Breithaupt (1849; d'après Zepharovich, 1859) reprises par Acker (1855). Hingenau (1857), reprenant des données du manuscrit de Debreczényi[1] sur Săcărîmb – tel qu'il le mentionne lui-même – ébauche la paragenèse avec des tellurures et du quartz rose et fait mention de cristaux maclés d'alabandite. Des données de grande valeur quant à la paragenèse de l'alabandite de Săcărîmb – association à des tellurures, de la pyrite, tétraédrite, sphalérite, du quartz et de la rhodochrosite –et concernant la cristallographie de ce minéral nous sont offertes par Zepharovich (1859, 1873, 1893), dont les considérations ont en vue les observations faites quant au macles de forme tétraédrique reconnues par Peters (1861) et aux concrétions de macle circulaire (composée de cinq octaèdres), remarquées par Schrauf (1866; d'après Zepharovich, 1873). Cotta et Fellenberg (1862) signalent la présence de la dolomite en association avec l'alabandite et indiquent la succession de cristallisation. Hauer et Stache (1863) délimitent la répartition spatiale de l'alabandite de Săcărîmb (le périmètre Frăsinata), sa superposition aux zones à tellurures. Des informations ultérieures sur l'alabandite de Transylvanie sont fournies par Tóth (1882), Koch (1884) et Bielz (1889).

Dans le premier ouvrage monographique roumain

[1]Debreczényi F. (1844 ?) "Bergmännisch geognostische Notizen über Nagyag und dessen nächste Umgebung" (manuscrit).

consacré au patrimoine minéralogique du pays, Cădere (1925), faisant suite à l'oeuvre de Poni, complète l'association de l'alabandite de Săcărîmb avec de nouveaux composants minéraux (miargirite) et décrit des cristaux qui présentent les faces (100), (111), (212). Helke(1934) donne des interprétations sur la structure et la texture en bandes alternantes de l'alabandite et de la rhodochrosite, ainsi que sur les relations génétiques existant entre l'alabandite, la pyrite et les carbonates, constatant que l'alabandite est recouverte de pyrite et englobée dans la rhodochrosite. Dans le cas du gisement Săcărîmb, l'alabandite est caractéristique des corps Carolina et Longhin. La relation d'englobement et de substitution de l'alabandite par la rhodochrosite est mentionnée aussi par Petrulian (1934). Giuşcă (1935) mentionne la succession de début suivante de la minéralisation dans les filons de type Magdalena: sphalérite, alabandite, galénite. Dans un ouvrage de synthèse sur les Monts Métallifères, Ghiţulescu et Socolescu (1941) signalent l'alabandite dans le champ minier Magdalena. Koch et Donáth (1950) analysent l'alabandite de Săcărîmb – à base d'échantillons des musées de Budapest – en la comparant à la hauerite de Kalinka (Monts Javorite, Slovaquie) et déduisent les rapports génétiques avec les minéraux de l'association. Rădulescu et Dimitrescu (1966) ainsi que Ianovici et al. (1969, 1976) rappellent cette importante occurrence.

Nos observations sur l'alabandite de Săcărîmb reposent sur les échantillons du Musée de Minéralogie de l'Université de Cluj, où l'on remarque de l'alabandite massive déposée en filons, associée à la rhodochrosite, la calcite, la pyrite et le quartz (cristaux de la taille de 1 cm environ) qu'elle inclut. Dans les géodes (1 x 3 cm) apparaissent des cristaux octaédriques d'alabandite (en dessous de 1,5 cm), souvent recouverts totalement ou partiellement d'un croûte de quartz (1 mm environ en épaisseur) (Pl. I, fig. 1,2); on remarque accidentellement des cristaux de soufre, superposés à l'alabandite des géodes. C'est de Săcărîmb que proviennent les plus beaux cristaux d'alabandite de Roumanie.

En sections minces elle est semi-transparente (brûnatre, tachetée), présente un clivage parfait (100) est isotrope et est traversée de petits filons de rhodochrosite qui provoquent sur les bords la corrosion de l'alabandite et son inclusion sous forme de microfragments (Pl. I, fig. 3). Au calcographe on distingue la couleur de réflexion gris clair, les réflexes internes verdâtres et la présence des microinclusions de chalcopyrite, pyrite et marcasite (Pl. II, fig. 1). Les valeurs diffractométriques, caractéristiques de l'alabandite, sont consignées au tableau 1.

L'alabandite de Baia de Arieş. La source bibliographique la plus ancienne dont on dispose, relative à l'alabandite de Baia de Arieş coïncide avec la monographie minéralogique de Ackner (1855), élaborée, comme de bien entendu, sur la base de sources bibliographiques qui ne sont pas mentionnées. Ackner indique la paragenèse de l'alabandite, de la sphalérite, de la galénite et de la rhodonite. Zepharovich (1859, 1873) décrit des occurrences d'alabandite massive et sous forme de bandes ou aux contours irréguliers, dans les zones minéralisées des calcaires cristallins. Par la suite, les informations sont reprises par Tóth (1882) et Bielz (1889). Cădere caractérise sommairement l'alabandite de Baia de Arieş, tel que le font aussi Ghiţulescu et Socolescu (1941), Superceanu et al. (1954, non publ.), Cochet (1957). D'autres mentions, plus récentes, appartiennent à Rădulescu et Dimitrescu (1966), Lazăr (1966) qui confirment la substitution sélective de l'alabandite par la rhodochrosite (conservée dans la masse de celle-ci) et remarquent la succession de cristallisation: pyrite-sphalérite-galénite-chalcopyrite-tétraédrite-alabandite; Ianovici et al. (1969, 1976) reprennent en partie les observations précédentes.

L'alabandite semble s'être déposée plus abondamment dans des zones plus écartées des voies d'accès des solutions hydrothermales, en association avec des silicates et des carbonates de manganèse, avec des sulfures (Fe, Pb, Zn, Cu).

L'alabandite du gisement polymétallique (Valea Lacului) de type hydrothermal – métasomatique (engendrée par des corps sous-volcaniques d'andésites néogènes) s'associe au minerai plombo-zincifère et se caractérise par des masses compactes et des bandes métasomatiques (texture Liesegang), constituées d'agrégats granulaires de couleur noire, où apparaissent très rarement des cristaux (1–2 mm) partiellement bordés de faces (cube, cube avec octaèdre); minéralogiquement, elle s'associe à la calcite (I, II), à la rhodochrosite (I, II); la seconde génération de rhodochrosite – calcite traverse, sur les fissures, l'alabandite (Pl. II, fig. 2, 3). La minéralisation avec la pyrite, la galénite et la sphalérite se produit par voie métasomatique et imprégnante dans les calcaires cristallins mésométamorphiques paléosomatisés (Unité de Baia de Arieş), les sulfures étant contenus dans tous les minerais de gangue de première génération, y compris dans l'alabandite (Pl. III, fig. 1, 2, 3).

En sections minces, l'alabandite est faiblement transparente, présente des macles, une teinte noire-verdâtre et de l'isotropisme; elle s'associe à la rhodochrosite et à la calcite qu'elle contient fréquemment comme inclusions, mais aussi à la Mn-pectolite (parfois partiellement calcitisée), sporadiquement à la trémolite et au quartz. La Mn-pectolite, la trémolite et la calcite-rhodochrosite de première génération ont préexisté à l'alabandite (Pl. IV, fig. 1); le quartz hydrothermal est disposé aussi le long

Tableau 1
Le spectre de diffraction Rx des échantillons analysés

ALABANDITE									
Săcărîmb[x]		Baia de Arieş[xx]		Căraci[xx] (Ţebea)		Argestruţ (Vatra Dornei) (Bălan, 1976)		ASTM	
d/n(A)	I	d/n(A)	I	d/n(A)	I	d/n(A)	I	d/n(A)	I
3,0153	3,9	3,0173	3,5	3,0153	4,8	–	–	3,045	14
2,6047	100,0	2,6047	100,0	2,6077	100,0	2,60	100,0	2,612	100
1,8433	23,8	1,8433	27,5	1,8433	35,7	1,84	31,0	1,847	50
–	–	1,7911[xxx]	3,7	–	–	–	–	–	–
1,6310	3,0	–	–	1,5724	4,0	–	–	1,575	6
1,5042	5,5	1,5060	5,9	1,5051	7,8	1,50	10,0	1,509	20
1,3034	4,0	1,3052	3,0	1,3006	2,0	1,30	13,0	1,306	8

Par diffractométrie il a été mis en évidence aussi des réflexes spécifiques pour la rhodochrosite[x] et le quartz[xx] (non inclus dans le tableau), minéraux associés à l'alabandite.
[xxx] Valeur attribuée par Miheev (1957) à l'alabandite.

des clivages des silicates ainsi que dans les vides résultés par intersection de ces cristaux prismatiques.

L'alabandite se substitue métasomatiquement au calcaire cristallin et, plus rarement, aux silicates raison pour laquelle elle dessine des contours irréguliers et contient comme inclusions des minéraux antérieurement formés. Par conséquent, l'alabandite est le résultat de la métasomatose hydrothermale, sous l'effet d'une récurrence avec des solutions riches en manganèse sur le calcaire cristallin et la minéralisation préexistante (la séquence avec des silicates, des carbonates et des sulfures). La succession de cristallisation est: Mn-pectolite, trémolite, calcite I, rhodochrosite I, quartz, sulfures (pyrite, chalcopyrite, sphalérite, galénite), alabandite, calcite II, rhodochrosite II. Par une légère altération supergène de l'alabandite résultent des hydroxydes de manganèse.

L'étude calcographique de l'alabandite révèle une structure hétérogranulaire, conservant fréquemment le contour quasi polygonal des granuloblastes de calcite du calcaire cristallin métasomatisé (Pl. IV, Fig. 2). La couleur de réflexion est grise, plus brillante que celle de la sphalérite de l'association, et le relief plus bas; au microscope on distingue quelquefois des faces de cube; les réflexes internes verdâtre foncé constituent une note distincte du minéral. L'alabandite contient des inclusions de pyrite, marcassite, sphalérite, galénite, carbonates (rhodochrosite, calcite) et de quartz; dans la gangue carbonatée on distingue accidentellement des lamelles d'or. A son tour, la minéralisation à l'alabandite est traversée de petits filons de rhodochrosite-calcite, de dernière génération.

Dans l'alabandite surviennent parfois des taches au relief sensiblement plus élevé et à la couleur aux reflets gris, plus foncée comparativement à l'alabandite, sans doute de la hauérite. Le tableau 1 présente l'analyse roentgénographique de l'alabandite.

L'alabandite de Căraci. La première mention faite de l'alabandite de Căraci, près de Ţebea (Brad) appartient à Benkö (1886, 1887), qui mentionne des agrégats granulaires, sur la rhodochrosite et dans les géodes de la rhodochrosite, en l'absence de toutes formes cristallographiques. Par la suite, les même informations sont reprises successivement par Bielz (1889), Zepharovich (1893), Cădere (1925), Rădulescu et Dimitrescu (1966).

Les échantillons que nous avons analysés[2] révèlent de l'alabandite granulaire incluse dans la rhodochrosite – à laquelle elle s'associe et se subordonne –, du quartz et, fréquemment, des microcristaux de pyrite, – y compris des cristaux octaédriques disposés en géodes (1 x 2 cm), couvertes d'une pellicule crustiforme de carbonate (0,10 mm en épaisseur), de couleur brun-verdâtre empruntée par transparence au minéral support. La paragenèse à l'alabandite, rhodochrosite et au quartz cristallisé représente une minéralisation superposée à une autre plus ancienne, représentée par du quartz vacuolaire, enclavé dans la masse du minéral contenant de l'alabandite, et parcouru sur les fissures par l'alabandite. La roche support de la minéralisation est un andésite à hornblende et biotite, intensément hydrothermalisé (adularisé, sériciţisé, silicifié).

En sections fines l'alabandite est légèrement transparente, a une couleur brunâtre à faible teinte verdâtre, un bon clivage et renferme des inclusions de rhodochrosite; les minéraux hôte où se trouvent les nids d'alabandite sont la rhodochrosite et, de façon subordonnée, la Mn-pectolite (incolore) à structure fibroradiale (Pl. IV, fig. 3). Le quartz de

[2] Echantillons du Musée de Minéralogie de l'Université "Babeş-Bolyai" de Cluj-Napoca.

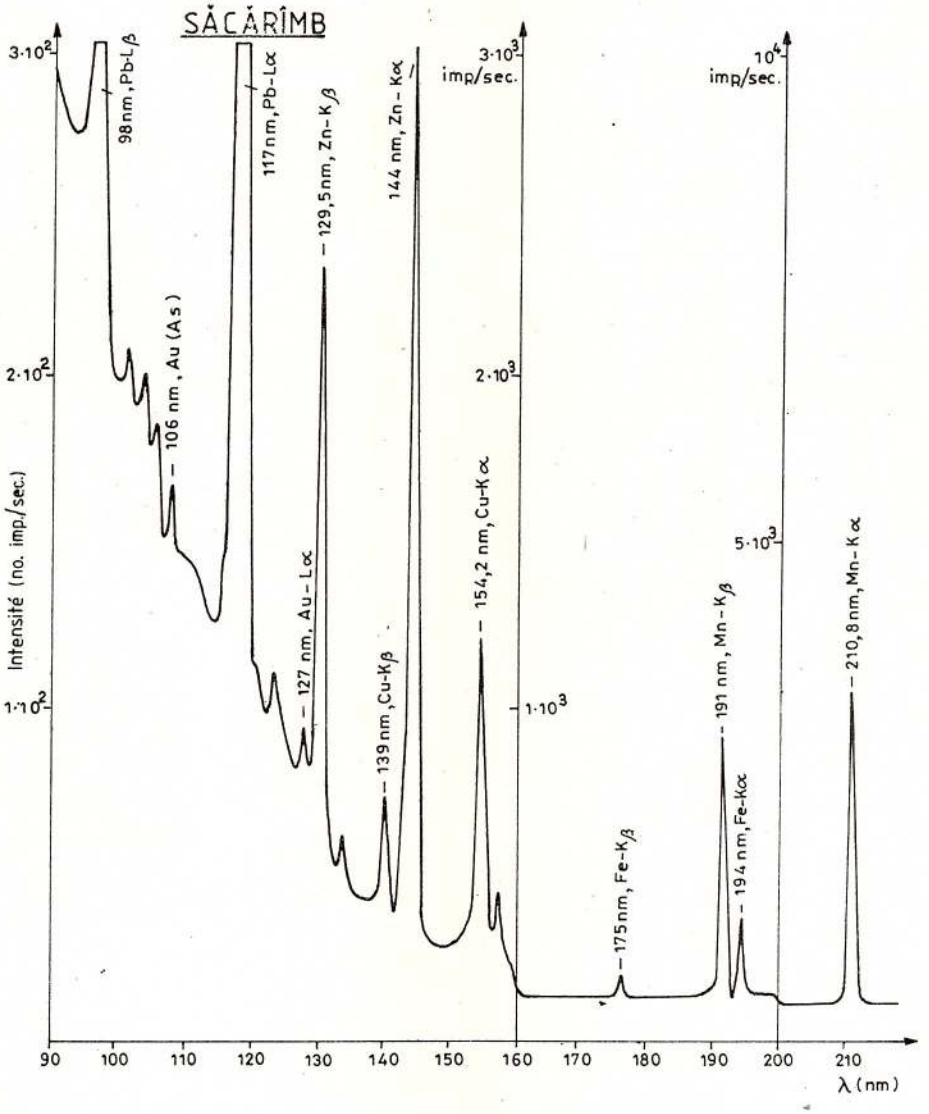

Fig. 2 — Le spectre de fluorescence de rayons X, pour l'alabandite de Săcărîmb

l'association, terme final, corrode les deux autres minéraux non métalliques.

Au calcographe, l'alabandite se distingue par une couleur de réflexion caractéristique et renferme des inclusions de pyrite et de chalcopyrite, comme la rhodochrosite et la Mn-pectolite. La succession de cristallisation est la suivante: Mn-pectolite, rhodochrosite, pyrite, chalcopyrite, sphalérite, alabandite, quartz. Au tableau 1 sont présentés les résultats de l'analyse diffractométrique de l'alabandite.

L'alabandite de Cavnic. Ackner (1855), sans faire d'envois bibliographiques aux auteurs précédents, mentionne le gisement de Cavnic parmi les occurrences contenant de l'alabandite en Transylvanie, minéral associé à la paragenèse avec des sulfures et des sulfosels. Cotta et Fellenberg (1862) soulignent l'intéret purement minéralogique de l'alabandite de Cavnic et des minéraux en association (quartz, rhodochrosite, galénite, pyrite, tétraédrite, marmatite, baryte, calcite, etc.). Certains aspects cristallographiques de l'alabandite sont consignés dans l'ouvrage de Vivenot (1869), qui identifie la forme d'octaèdre. Des remarques intéressantes d'ordre minéralogique sont dues à Reuss (1870) sur un échantillon du Musée de l'Université de Vienne, représenté par une pseudomorphose de rhodochrosite après alabandite et par l'alabandite compacte de couleur noir-verdâtre.

Les informations fournies par Reuss ont été reprises par Tóth (1882) et Zepharovich (1873, 1893), ce dernier revenant avec des précisions cristallographiques supplémentaires, provenant de l'ouvrage de Groth (1878; d'après Zepharovich, 1893), où sont

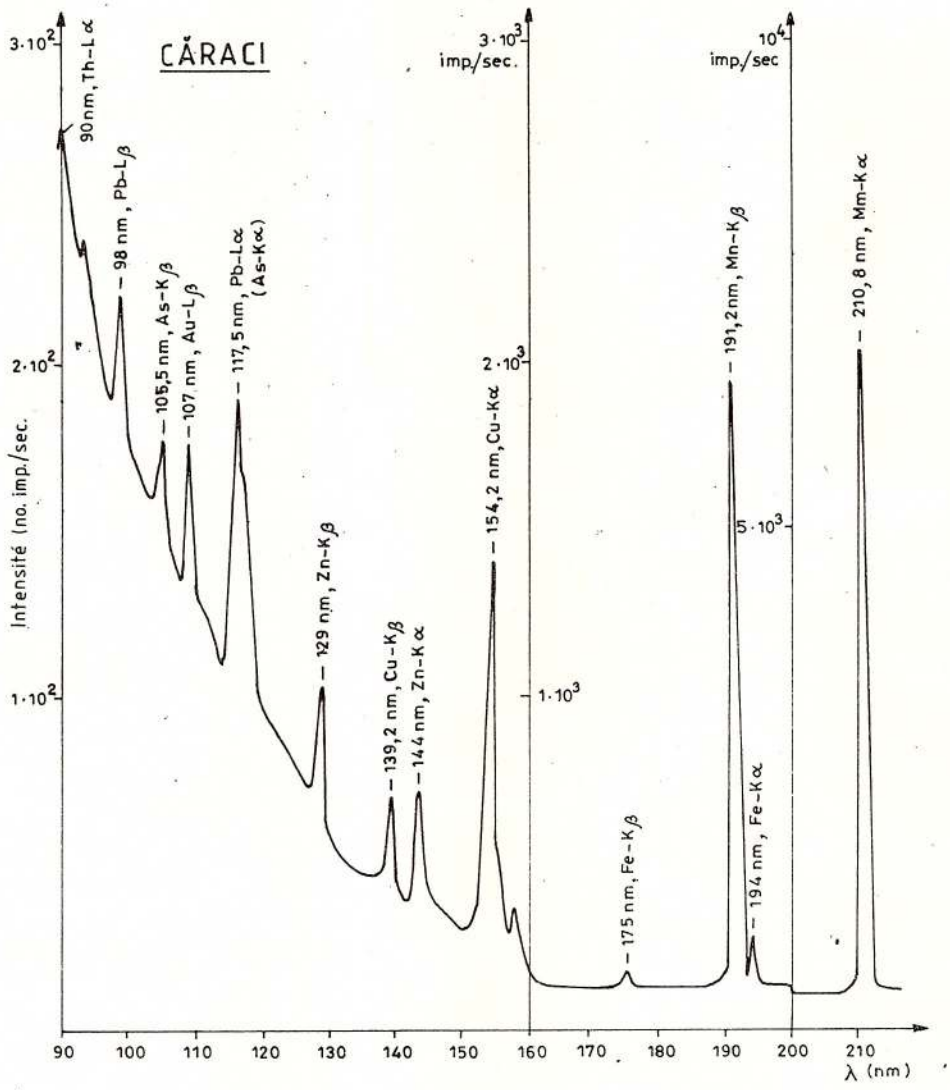

Fig. 3 – Le spectre de fluorescence de rayons X, pour l'alabandite de Căraci

décrits des cristaux individuels et des macles ayant comme plan de macle la face de tétraèdre (111): Des informations générales existent aussi dans les travaux de Cădere (1925) et Rădulescu et Dimitrescu (1966). Ces derniers temps l'alabandite n'a pas été signalée à Cavnic, sur la base des observations directe dans le gisement; sont apparition est sans doute rattachée à certains niveaux des filons à rhodochrosite.

Breaza (Alamaşu Mare). Une première mention bibliographique concernant l'alabandite du massif Breaza est fournie par Ramdohr (1975), reprise par la suite par Rădulescu et Dimitrescu (1966), Ianovici et al. (1969); la minéralisation avec de l'alabandite dans certains filons du massif Breaza est reconfirmée.

L'alabandite de Argestruţ (Vatra Dornei). C'est un minéral métallique de couleur noire (équigranulaire), associé à des carbonates et à la téphroïte, existant dans des minerais volcanogènes-sédimentaires de manganèse, épimétamorphosés (Bălan, 1976). Au microscope, on reconnaît sa couleur vert-olive, vert-brun et brune, variation due à sa teneur en fer.

Il est évident que, dans les mêmes conditions génétiques, l'alabandite est présente aussi dans d'autres gisements (occurrences) de Roumanie, mais la couleur noire des hydroxydes supergènes de manganèse la masque.

Les investigations bibliographiques relatives à l'alabandite de Roumanie ont attiré notre attention sur les confusions portant sur les aspects historiques de la primauté de la description de ce minéral dans différentes occurrences et, quelquefois même, sur la véridicité des occurrences citées. A part les occur-

Tableau 2
Analyse quantitative de l'alabandite par fluorescence de Rx

L'élément déterminé et la longueur d'onde du pic de fluorescence Rx	Concentration des éléments déterminés dans les échantillons d'alabandite (%)x		
	Săcărîmb	Baia de Arieş	Căraci
Mn, K_α – 210,9 nm	51,8	57,5	–
Mn, K_β – 191,3 nm	53,0	54,2	–
Fe, K_α – 194 nm	0,6	0,7	0,3
Fe, K_β – 175,7 nm	0,9	0,5	0,45
Cu, K_α – 154, 4 nm	0,6	0,3	0,3
Cu, K_β – 139, 5 nm	0,7	0,4	0,4
Zn, K_α – 144 nm	0,7	0,35	0,3
Zn, K_β – 129, 7 nm	1,0	0,6	0,5
Pb, L_α – 117,3 nm	0,2	0,8	0,1
Pb, L_β – 96,5 nm	0,3	0,2	0,2

x Echantillons sélectionnés sous la loupe binoculaire.

rences décrites, la littérature de spécialité mentionne aussi d'autres points recelant des sulfures de manganèse (alabandite, hauérite), en Roumanie, lesquels sont contestés aujourd'hui ou prêtent à suspicion; nous reviendrons là-dessus dans ce qui suit.

Zărneşti (Braşov). Ackner (1855, p. 336) cite l'alabandite au lieu dit "Fontina Roncs" (probablement "Fîntîna Roncii"). La même occurrence est reprise dans des écrits ultérieurs (Zepharovich, 1859; Tóth, 1882 et Koch, 1884), où est placée sous le signe du doute la valabilité des affirmations concernant l'occurrence d'alabandite de Zărneşti, contestée ultérieurement par Zepharovich (1893) aussi.

Hauérite (MnS_2). La présence de la hauérite à Moneasa est citée par Cădere (1925) et par Rădulescu et Dimitrescu (1966), mais elle n'a pas été confirmée par des études récentes.

Tableau 3
Détermination de la teneur en manganèse, au moyen de l'activation par les neutrons

Occurrence de l'échantillon d'alabandite	Concentration en Mn (%)
Săcărîmb	48,3
Baia de Arieş	63,1
Căraci (Ţebea)	54,4

Analyse par fluorescence de rayons X[3]. Elle a mis en évidence dans les échantillons analysés (tab. 2): Mn, Fe, Cu, Zn et Pb, les quatre derniers éléments étant liés, dans l'ordre, à la pyrite, la chalcopyrite, la sphalérite et la galénite, sulfures présents dans l'association. En vue de prévenir d'éventuelles erreurs, il a été vérifié pour le Mn la teneur au moyen de la méthode de l'activation par des neutrons (tab. 3). Evidemment que la teneur en Mn dépend de la pureté des échantillons; pour ce qui est de l'échantillon de Baia de Arieş, la teneur est très proche de la teneur théorique.

En conclusion, sur le territoire de la Roumanie sont présentes des occurrences à alabandite hydrothermale, déposée en filons (Săcărîmb, Roşia Montană, Căraci, Cavnic, partiellement Baia de Arieş) et hydrothermale-métasomatique (Baia de Arieş). Il est mentionné une seule occurrence à alabandite associée aux minerais silicatiques-carbonatés, métamorphosés (Argestruţ, Vatra Dornei).

L'alabandite hydrothermale s'est déposée de façon mono- ou polyascendante de solutions épithermales à Eh réducteur, riches en manganèse et H_2S, en association avec la rhodochrosite, la Mn-pectolite, le quartz et les sulfures communs (Cavnic, Baia de Arieş) ou avec des minéralisations d'or et de tellure (Săcărîmb, Căraci, Roşia Montană). Les analyses microscopiques, les spectres de rayons X révèlent les minéraux de l'association et les spectres de fluorescence de rayons X illustrent les associations géochimiques.

[3]Les analyses ont été réalisées au moyen d'un spectromètre de fluorescence X, du type SPARK-1, de fabrication soviétique. L'appareil ne peut pas détecter des éléments au Z plus bas que celui du titane et a une zone "blanche" autour de l'étaine (de Cd à Cs).

Bibliographie

Ackner M. J. (1855) Mineralogie Siebenbürgens, mit geognostischer Andeutung. 391 p., Hermannstadt (Sibiu).

Bălan M. (1976) Mineralogia zăcămintelor manganifere de la Iacobeni. Ed. Acad., 123 p., Bucureşti.

Benkö G. (1886) Bericht über die Resultate des Mineraliensammelns im vergangenen Sommer im Hunyader Comitat. *O. t. t. Ert.*, 11, p. 15–20, Kolozsvár (Cluj).

– (1887) Mineralogische Mittheilungen aus Siebenbürgen. *O.t.t. Ert*, 12, p. 236–238, Kolozsvár (Cluj).

Bielz E. A. (1889) Die Gesteine Siebenbürgens. Eine systematische Aufzählung der in diesem Lande vorkommenden Mineralien und Felsarten mit ihren Fundorten und ihrem Vorkommen. 2 Auflage. Separatbuch, 82 p., Hermannstadt (Sibiu).

Cădere D. M. (1925) Fapte pentru a servi la descrierea mineralogică a României. *Mem. Acad. Rom.*, III, 3, p. 5, Bucureşti.

Cochet Y. R. (1957) Contribuţii geologice asupra zăcămintelor aurifere de la Baia de Arieş. *Rev. Min.*, VIII, 10, p. 467–475, Bucureşti.

Cotta E. v., Fellenberg E. v. (1862) Die Erzlagerstätten Ungarns und Siebenbürgens, Freiberg.

Ghiţulescu T. P., Socolescu M. (1941) Étude géologique et miniére des Monts Métallifères (quadrilatère aurifère et régions environnantes). *An. Com. Geol.*, XXI, p. 181–464, Bucureşti.

Giuşcă D. (1935) Note préliminaire sur la genèse du gisement aurifère de Săcărîmb. *Bul. Lab. Min. Univ. Buc.*, 1, p. 72–82, Bucureşti.

Hauer Fr. v., Stache (1863) Geologie Siebenbürgens. 636p., Wien.

Helke A. (1934) Die Goldtellurerz lagerstätten von Săcărîmb (Nagyag) in Rumänien. *N. Jb. Min.*, 68, A., p. 19–85, Stuttgart.

Hintze C. (1904) Handbuch der Mineralogie. Leipzig/Berlin.

Hingenau O. F. v. (1857) Geologisch-bergmänische Skizze des Bergamtes Nagyag in Siebenbürgen und seiner nächsten Umgegend. *Jb. R. A.*, VIII, p. 82–143, Wien.

Ianovici V., Giuşcă D., Ghiţulescu T. P., Borcoş M., Bleahu M., Savu H. (1969) Evoluţia geologică a Munţilor Metaliferi. Ed. Acad., 741 p., Bucureşti.

– , Borcoş M., Bleahu M., Patrulius D., Lupu M., Dimitrescu R., Savu H. (1976) Geologia Munţilor Apuseni. Ed. Acad., 631 p., Bucureşti.

Koch A. (1884) Erdèly Ásványainak kritikai átnézete. *O. t. t. Ert.*, VI, 1, p. 1–52, Kolozsvár (Cluj).

Koch S., Donath E. (1950) Data relating to the alabandine deposits in Săcărîmb (Nagyag, Romania) and to those hauerite in Kalinka (Czechoslovakia). *Acta Szeged*, 4, p. 42–46, Szeged.

Lazăr C. (1966) Contribuţii la cunoaşterea zăcămîntului polimetalic de la Baia de Arieş (Munţii Apuseni. *Stud. cerc., ser. geol.*, 11, 2, p. 403–415, Bucureşti.

Mihneev V. I. (1957) Rontgenometriceskii opredelitel mineralov, *Gosgeoltechizdat*, 870 p., Moskva.

Peters C. (1861) Geologische Studien im südöstlichen Ungarn. *Sitzungsber d. K. Akad. im Wien*, 43, p. 415, 434, Wien.

Petrulian N. (1934) Étude chalcographique du gisement aurifère de Roşia Montană (Transylvanie, Roumanie). *An. Com. Geol.*, XVI, p. 499–538, Bucureşti.

Ramdohr P. (1975) Die Erzmineralien und ihre Verwachsungen. Akad. Verlag, 4 Auflage, 1277 p., Berlin.

Rammelsberg C. F. (1875) Handbuch der Mineralchemie. 2 Auflage, Theil I, Wilhelm Engelmann Verlag, 744 p., Leipzig.

Rădulescu D., Dimitrescu R. (1966) Mineralogia topografică a României. Ed. Acad., 377 p., Bucureşti.

Reuss A. E. (1870) Zwei neue Pseudomorphosen. *Jb. R. A.*, 20, p. 521–525, Wien.

Strunz H. (1982) Mineralogische Tabellen. 621 p., Leipzig.

Toth M. (1882) Magyarország ásványai, Különös tekintettel termöhelyeik megállapitására. 565 p., Budapest.

Vivenot F. v. (1869) Beiträge zur Mineralogischen Topographie von Oesterreich und Ungarn. *Jb. R. A.*, XIX, p. 595–612, Wien.

Zepharovich V. v. (1859, 1873, 1893) Mineralogisches Lexicon des Kaiserthums Österreich. I Band, 627 p., II Band, 436 p., III Band, 478 p., Wien.

*** (1962) X-ray powder data file, ASTH., Philadelphia.

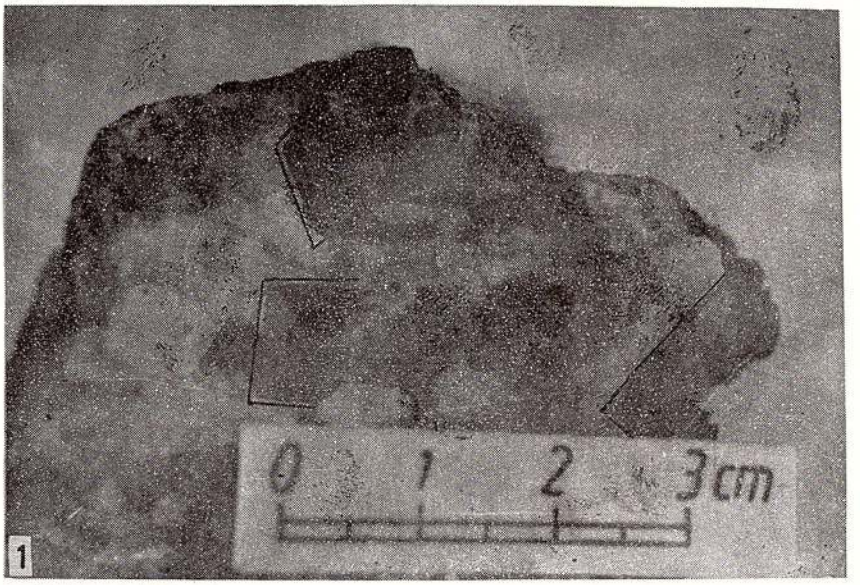

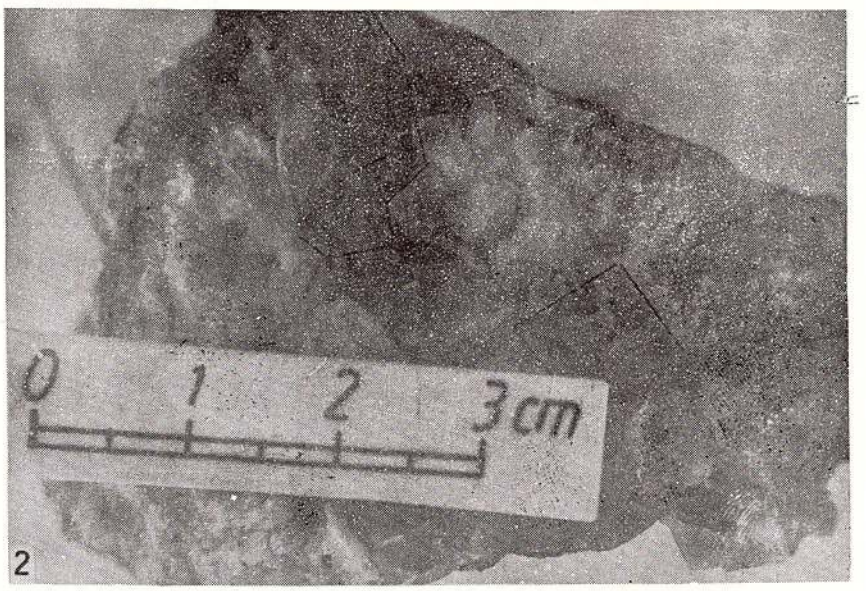

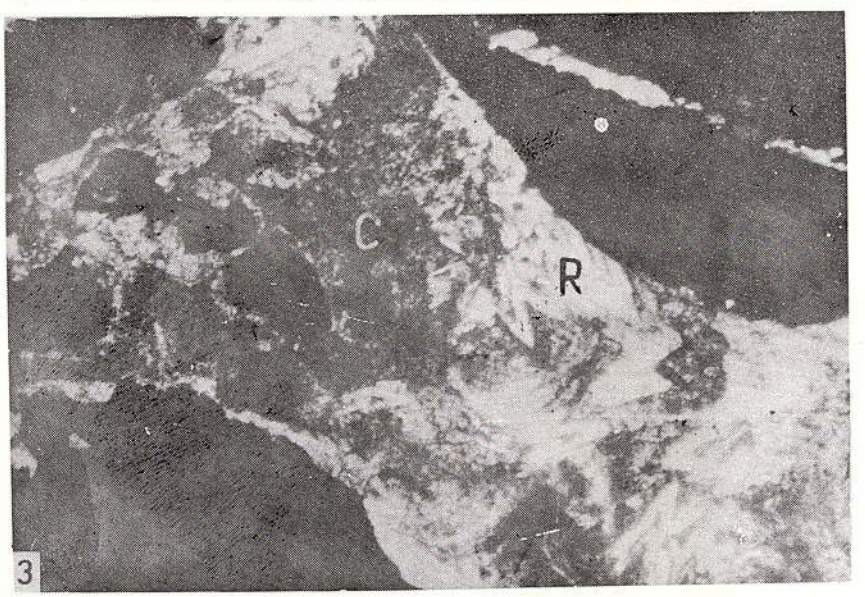

Planche I

Figs. 1-2 – Cristaux octaédriques d'alabandite (Săcărîmb).

Fig. 3 – Alabandite (noire) traversée et incluse (fragments) de petits filons à rhodochrosite (R) calcite (C). 1N; 45 x (Săcărîmb).

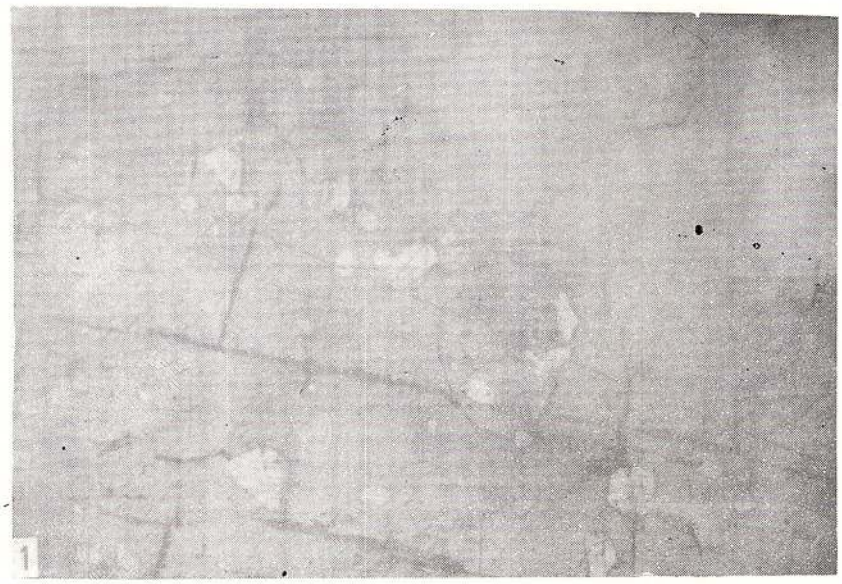

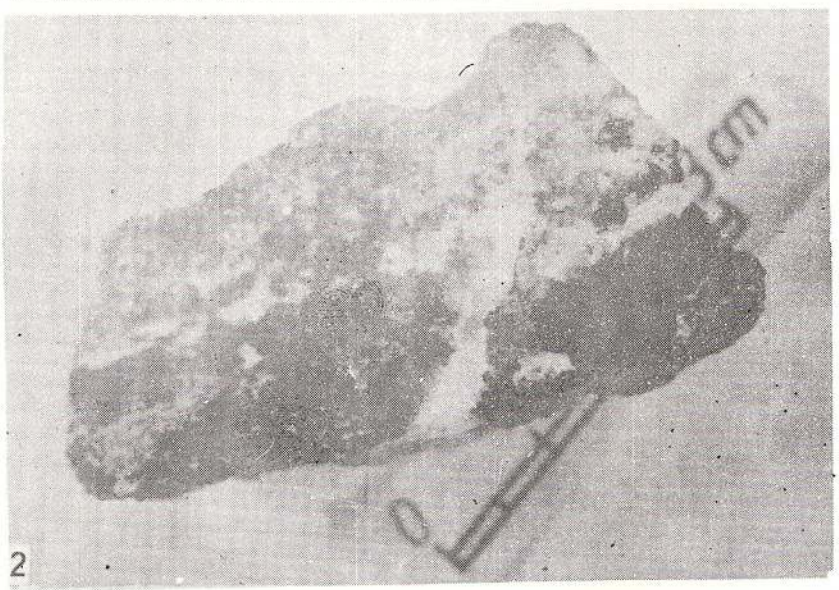

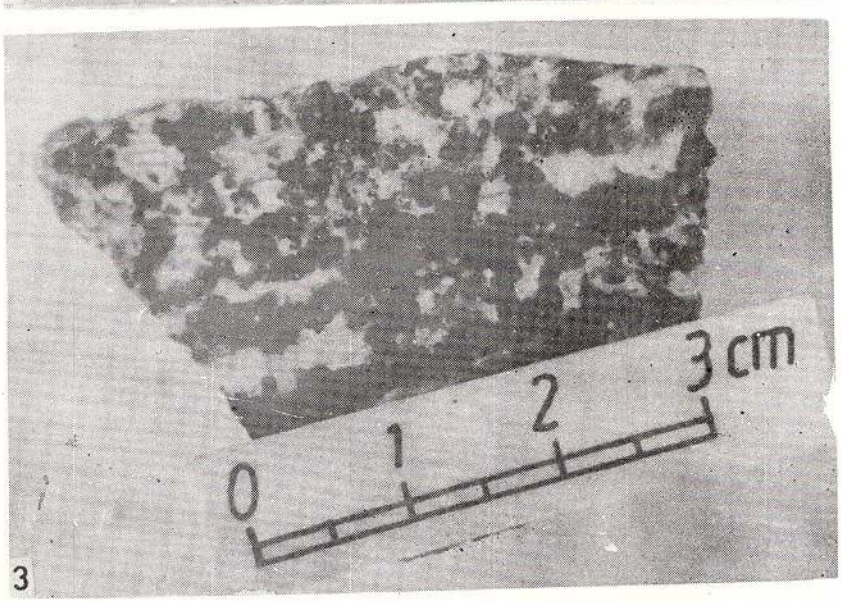

Planche II

Fig.1 – Alabandite à inclusions de pyrite; section polie. 1N; 45 x (Săcărîmb).

Fig. 2 – Alabandite (noire) hydrothermale - métasomatique dans du calcaire cristallin, traversée par un petit filon à rhodochrosite échantillon, Baia de Arieş).

Fig. 3 – Alabandite (noire), hydrothermale - métasomatique dans des calcaires cristallins (échantillon, Baia de Arieş).

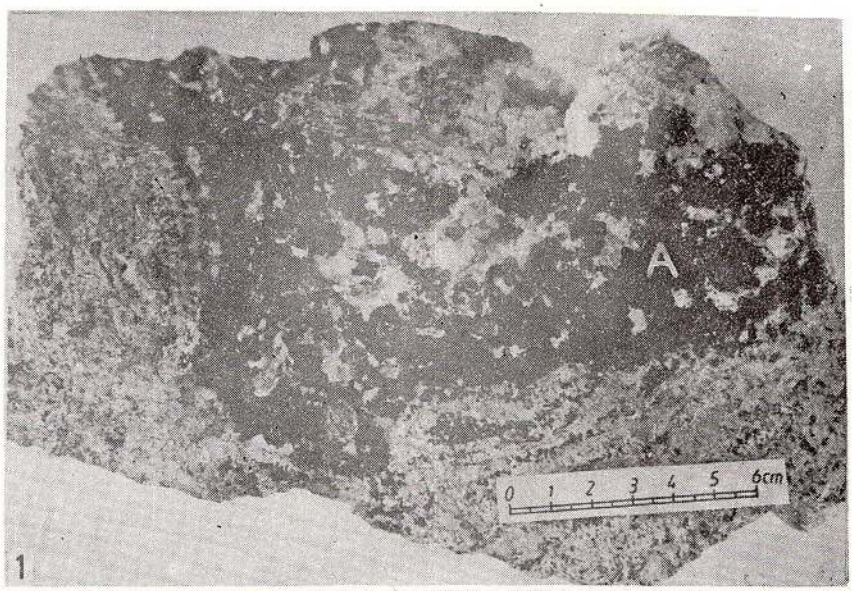

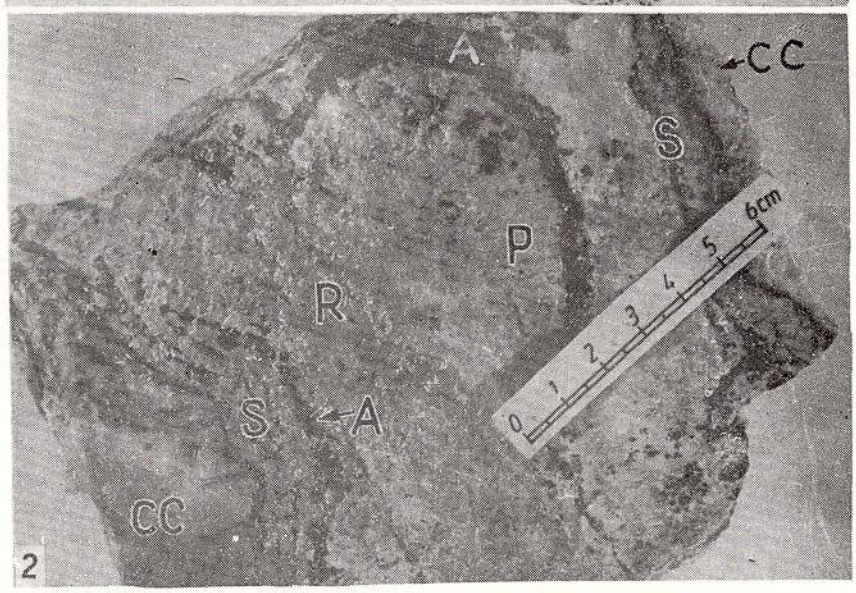

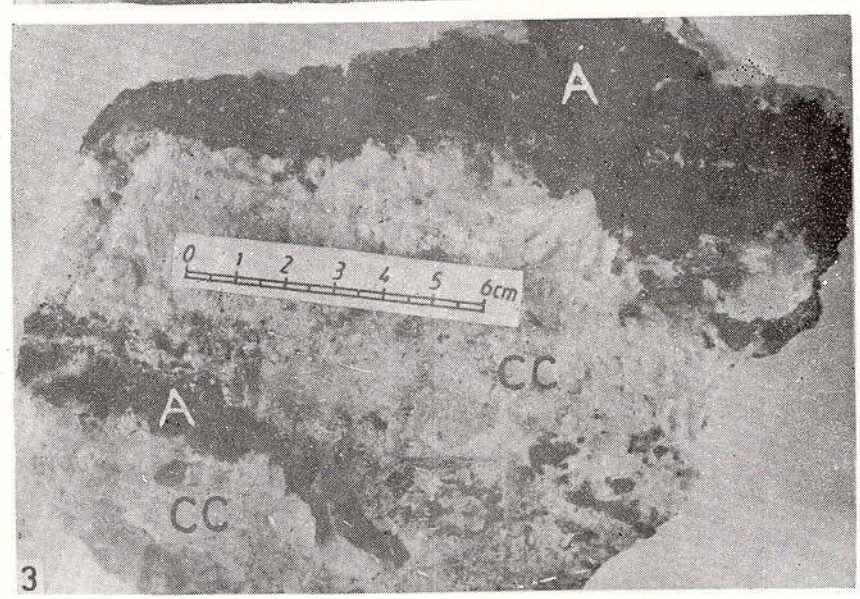

Planche III

Figs. 1, 2, 3 – Mineralisation hydrothermale-métasomatique dans des calcaires cristallins (CC): association avec alabandite (A), rhodochrosite (R), Mn-pectolite (P) et bandes des sulfures (sphalérite, galénite, pyrite) (S) (Baia de Arieș.

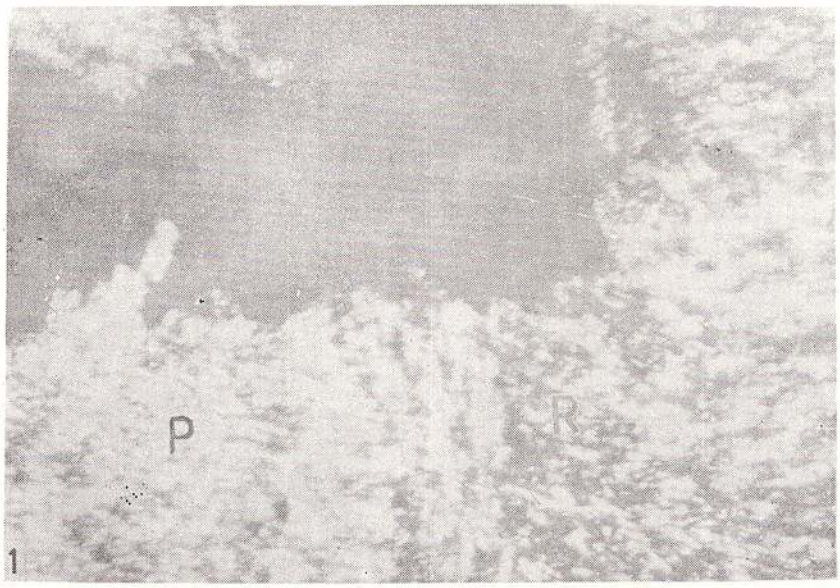

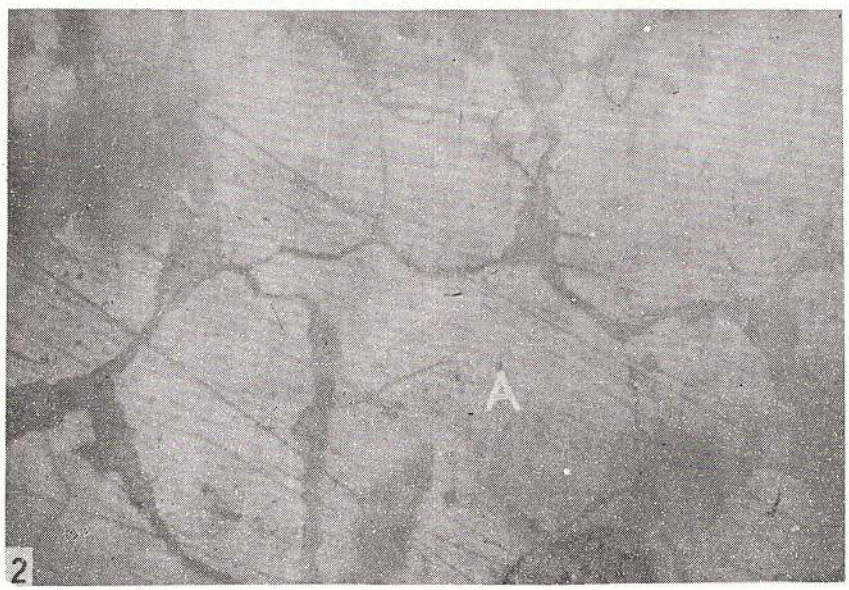

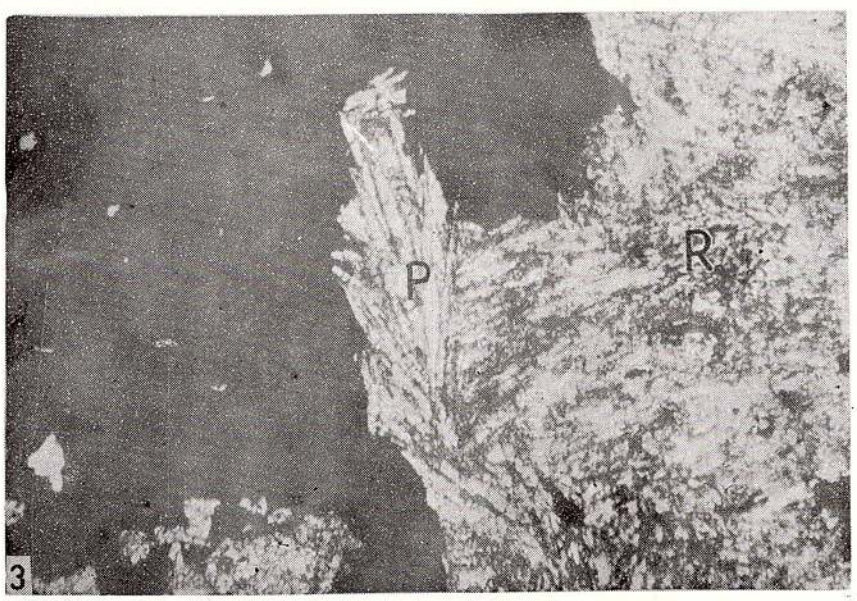

Planche IV

Fig. 1 – Alabandite (noire), rhodochrosite microgranulaire (R) et Mn-pectolite (fibroradiale; P). 1N; 75 x (Căraci).

Fig. 2 - Alabandite (A) à structure granulaire (résultée par la métasomatose du calcaire cristallin granoblastique), prise dans une gangue carbonatée; section polie. 1N; 45 x (Baia de Arieş).

Fig 3 – Association d'alabandite (noire), de rhodochrosite (microgranulaire) (R) et de Mn-pectolite (fibres) (P). 1N; 45 x (Baia de Arieş).

Rom. J. Mineralogy, 1993, 76, 1, p. 79–86

NEW DATA REGARDING THE SIGNIFICANCE OF THE PYRITE MORPHOLOGY AND OF THE FLUID INCLUSIONS IN QUARTZ CRYSTALS AT BAIA SPRIE

Liviu NEDELCU, Ioan PINTEA

Institutul de Geologie şi Geofizică. Str. Caransebeş 1, 78344 Bucureşti 32.

Key words: Sulfides. Pyrite. Habit. Fluid inclusions. Crystallization. Temperature. Solution. Saturation. Hydrothermal processes. East Carpathians.

Abstract: Pyrite of Main Vein at Baia Sprie displays two principal morphologic trends also defining two distinct domains in the plane of vein. One domain, situated at the upper part, is represented by cube-pentagonal dodecahedron (C-P) trend which corresponds to low supersaturation-high temperature (S_L-T_H) conditions. The other one, at lower part (under level XIII), is characterized by cube-octahedron-pentagonal dodecahedron±{hkl}(C-O-P±{hkl}) trend and corresponds to high supersaturation-low temperature (S_H-T_L) conditions. The paragenetic quartz crystals contain many types of fluid inclusions which are in a positive relationship with crystal growth zones. The Tmi/Th diagram indicates that with decreasing of temperature there is an obvious evolution of the initial fluid, poor in gases and of low concentration, to a more concentrated final liquid phase. The relationship between homogenisation temperature and quartz crystal zonality would suggest that the hydrothermal process at Baia Sprie is monoascendent. Fluid inclusions data render also evident a superposition on the pyrite morphology domains.

1. Introduction

The present study aims to continue our previous researches (Nedelcu et al., 1992) both on the pyrite morphology and on fluid inclusions in quartz from the Baia Sprie Main Vein with a view to reconstructing the mechanism and evolution of the hydrothermal process. Our researches took into consideration the works of Sunagawa (1957), Amstutz (1963), Endo (1978), Endo and Sunagawa (1973), Murowchick and Barnes (1987) on the pyrite morphology and its dependence on the physico-chemical conditions of the hydrothermal system as well as the fundamental studies of Crawford (1981), Roedder (1984), Hedenqvist and Henley (1985) on the fluid quartz inclusions.

The study was carried out on 297 pyrite and quartz samples collected from nine active horizons (gallery +516 and horizons IX-XVI), from the quarry (Minei Hill), and from six boreholes situated in the eastern half of the deposit (507, 508, 511, 511A, 529, 536). The sampling had in view a good representation of the crystalline forms of pyrite within the deposit mineral parageneses as well as the achievement of a high statistic homogeneity.

2. Pyrite morphology

Pyrite from the Main Vein at Baia Sprie shows eight characteristic crystallographic forms: cube a {100}, octahedron o {111}, pentagonal dodecahedron e {210}, {321}, {421}, {311}, {211}, {110} combined in seven habits: cubic (C), cubic-octahedral (CO), cubic-pentagonal (CP), pentagonal (P), pentagonal-cubic (PC), pentagonal-octahedral (PO), octahedral (O), and the eighth one, resulting from the combination of the dominant forms (a, o, e) with undeterminable forms {hkl}. There have also been determined (Nedelcu et al., 1992) forms with negative striae as well as forms with negative and positive striae superposed on the same crystal.

The frequency of these habits on horizons is presented in Table 1 which shows the following facts:

– the frequency of the cube forms (C) increases with depth but especially under horizon XIII;

– the frequency of the combinations of cube with octahedron (CO), though of reduced percentage as compared to that of the cube, also shows a rise tendency under horizon XIII;

Table 1
Average frequency of pyrite habits on the mining levels (%)

Mining level	C	CO	CP	P	PC	PO	O	{hkl} forms
+516	2.3	–	24.4	12.8	54.1	–	–	5.7
IX	35.9	3.1	53.3	3.6	1.9	–	–	0.1
X	36.7	0.9	47.1	2.1	17.3	1.3	0.2	0.6
XI	40.3	0.3	40.8	3.1	15.2	0.1	–	0.2
XII	48.7	0.3	36.4	6.2	3.0	–	–	0.3
XIII	21.5	0.8	67.9	4.0	1.6	0.1	0.2	1.0
XIV	55.6	11.4	17.0	8.3	5.6	0.1	0.6	0.01
XV	54.3	11.7	20.5	2.7	15.3	0.01	–	2.1
XVI	67.3	17.1	7.6	4.5	1.4	0.05	0.8	1.5

– the high frequency domain for the combinations of cube with pyritohedron (CP) lies also at the upper part of the Main Vein, between horizons IX and XIII;

– the pyritohedron forms (P) show insignificant variations of the frequencies, which are low, and the combinations of pyritohedron with cube (PC) have a very high frequency at the horizon of gallery +516 in the structure top;

– the combinations of pyritohedron with octahedron (PO) as well as the forms of octahedron (O) and {hkl}, although showing the lowest frequencies, suggest by their occurrence and association with the other forms, certain variations of the crystallization conditions.

On the whole the frequency of the pyrite habits from the Main Vein reveals the following distribution: the CP forms situated at the upper part of the vein (up to horizon XIII) and the forms C and CO at its lower part (under horizon XIII).

The recent experimental researches carried out by Murowchick and Barnes (1987) concerning the effects of temperature and degree of supersaturation on the habit of hydrothermally grown pyrite prove the indicator role which the pyrite morphology (habit, face microtopography) may play in the estimation of the crystallization conditions.

A comparison of the pyrite morphology at Baia Sprie with that resulted from these researches shows their good correlation on three concentration-temperature domains, as follows (Tab. 2):

a) high supersaturation-low temperature (S_H-T_L) suggested by perfectly smooth cubes;

b) low supersaturation-high temperature (S_L-T_H) revealed by weakly striated cubes with small octahedral faces;

c) high supersaturation-high temperature (S_H-T_H) marked by rough cubes (strongly striated), by the development of the octahedral forms as well as of those of pyritohedron and trapezohedron (in the case of the quench crystals).

It can be inferred, according to Murowchick and Barnes's determinations (1987) that the general sequence indicating the increasing degree of the supersaturation is from cube to octahedron to pyritohedron, and is in accordance with the series of morphological variations determined by Sunagawa (1957). Less common forms such as {311}, {110} as well as the {hkl} forms would be probably situated in this sequence between the octahedral and pyritohedral forms.

Table 2
The frequency of supersaturation and temperature parameters (%)

Mining level	S_L-T_H	S_H-T_H	S_H-T_L
Quarry + Gallery 516			100.0
IX	25.0		75.0
X	33.3		66.7
XII	16.7	33.3	50.0
XIII	5.6	27.8	66.6
XIV	38.5	19.2	42.3
XV	33.3	7.4	59.3
XVI	11.1	50.0	38.9
Under level XVI	33.3		66.7

Starting from the fact that the pyrite morphology may define various concentration-temperature domains of the hydrothermal fluids, its mapping in the straight plane of vein has been attempted. The image resulted (Fig. 1) reveals the separation of two main concentration-temperature domains: an upper one of low supersaturation and high temperature (S_L-T_H) and a lower one, of high supersaturation and low temperature (S_H-T_L). At the boundary between the two domains, which varies in width, apexes of high supersaturation and temperature (S_H-T_H) of the hydrothermal solutions appear, which are in turn bordered by cooling zones.

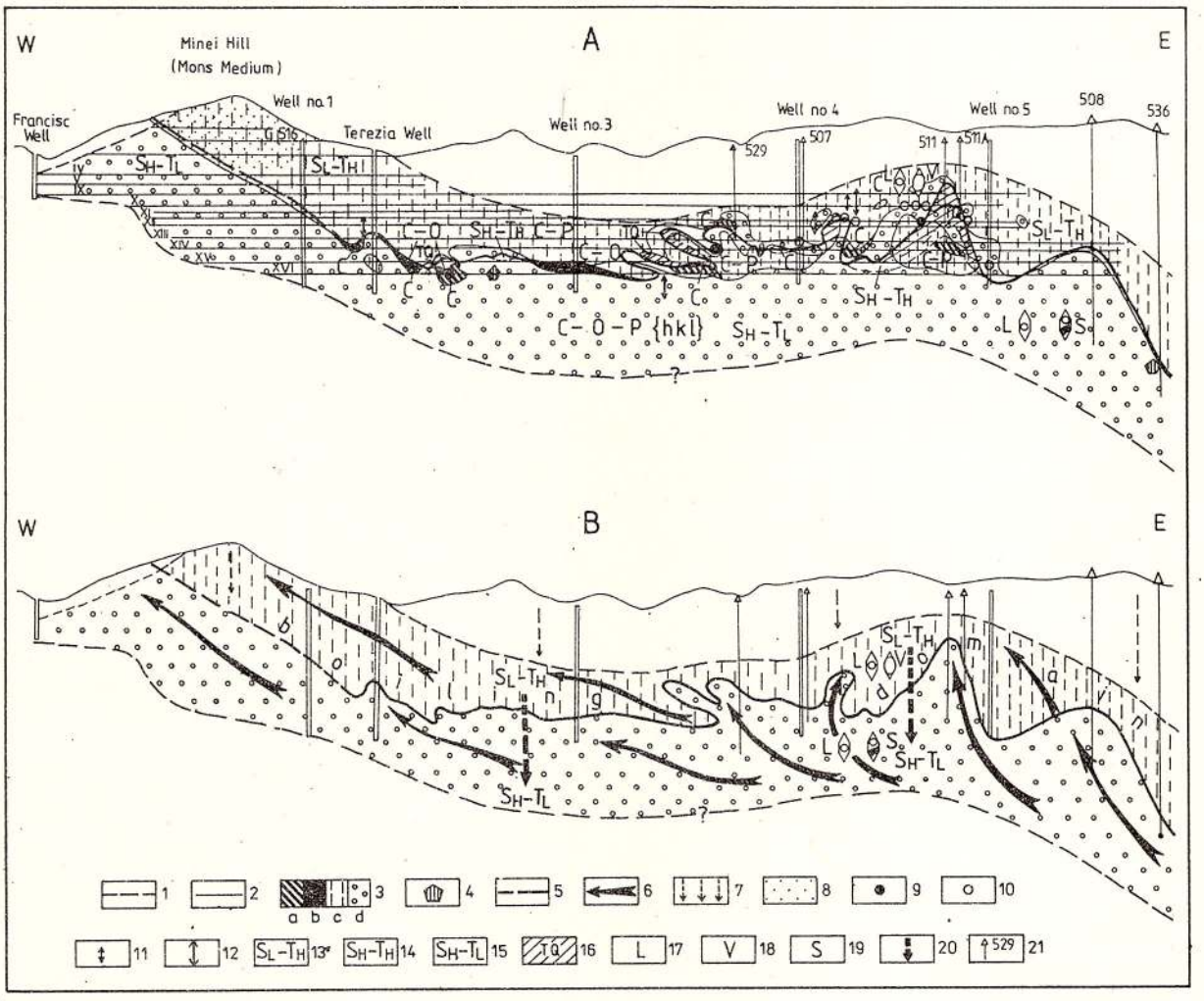

Fig. 1 – Model of the hydrothermal process in the straight plane of the Main Vein – Baia Sprie. 1, boundary of the mineralized zone; 2, boundary between the domains of the morphological trends of pyrite; 3, zones with trends: cube C(a), cube-octahedron C–O(b), cube-pentagonal dodecahedron C–P(c), cube-octahedron-pentagonal dodecahedron ± {hkl} forms C–O–P ± {hkl} (d); 4, pyritohedron with negative striae; 5, base of the boiling domain; 6, flow direction of the endogenous fluids; 7, flow direction of the meteoric water; 8, gold zone; 9, isotopic equilibrium; 10, isotopic inequilibrium; 11, pyrite dissolution process; 12, quartz dissolution process; 13, low supersaturation – high temperature; 14, high supersaturation – high temeperature; 15, high supersaturation – low temperature; 16, quench temperature; 17, liquid inclusions; 18, gas (vapour) inclusions; 19, heterogeneous fluid inclusions with solid phases; 20, descendant deposition of the mineralization; 21, borehole.

The modification of the habit and topography of the pyrite faces in this zone can be thus explained by the modification of the crystallization conditions (i.e. concentration and temperature of the hydrothermal fluid).

3. Pyrite morphology trends

As it is already known, there is a general tendency of combination of the crystal forms given by cube-octahedron-pyritohedron sequence (Sunagawa, 1957; Murowchick, Barnes, 1987). A statistics of the pyrite habit trend from the Main Vein for each horizon is presented in Table 3. It shows that the habits are grouped in four main trends:

a) cube trend = C

b) cube-octahedron trend = C-O

c) cube-pentagonal dodecahedron trend = C-P

d) cube-octahedron-pentagonal dodecahedron± faces {hkl} trend = C-O-P±{hkl}

The plotting of these trends in the vein plane (Fig. 1) leads to the separation of two domains with different morphological trends:

a) one with C-P trend, situated at the upper part of the deposit, superposed on the S_L-T_H concentration-temperature domain;

b) the other with C-O-P±{hkl} trend situated at its lower part, corresponding to the S_H-T_L domain.

The zones of reduced dimensions with C and C-O trends are located at the boundary between the two main domains and correlate both with the high supersaturation and temperature zones (S_H-T_H) and with the cooling zones.

Table 3
The frequency of pyrite habit trend (%)

Mining level	C	C-O	C-P	C-O-P ± {hkl}
Quarry + Gallery 516			85.7	14.3
IX			69.2	30.8
X	6.2		62.5	31.3
XI			80.0	20.0
XII	18.7		56.3	25.0
XIII			74.2	25.8
XIV	23.1	2.6	35.9	38.4
XV	6.8	4.5	56.8	31.8
XVI	17.2	17.2	27.6	37.9
under level XVI		33.3	33.3	33.3

4. Fluid inclusions

The quartz crystals associated with the various parageneses from the Baia Sprie deposit contain three types of fluid inclusions separated according to the nature and number of phases presented in Table 4 as follows:

a) L type inclusions consist of a dominant liquid phase and a vapour bubble representing 10–15 % of the volume of the cavities (Plate, Fig. 4). In the course of the microthermometric experiments Te, Tmi and Th have been determined (Tab. 4).

b) V type inclusions are almost entirely represented by vapours associated with a thin liquid film (Plate, Fig. 6). On the whole they accompany L type, the homogenization temperatures being generally similar, a fact indicating that they were simultaneously trapped in the course of a boiling process.

c) S type inclusions in which, beside liquid and vapours, one or several solid phases are present, being irregularly distributed from one inclusion to another, even if these belong to the same generation (Plate, Figs. 5, 7). With a few exceptions (Plate, Fig. 3) where the solid phases appear as characteristic agglomerations suggesting the presence of dawsonite, in most cases these are not real daughter phases. They generally represent carbonate grains dispersed within fluids before trapping. In many cases they are the very cause of the formation of the fluid inclusions. They do not usually dissolve when heated, which makes impossible the determination of the fluid homogenization temperature. The temperature at which the vapour bubble disappears does not as a rule exceed 300° C (Fig. 2).

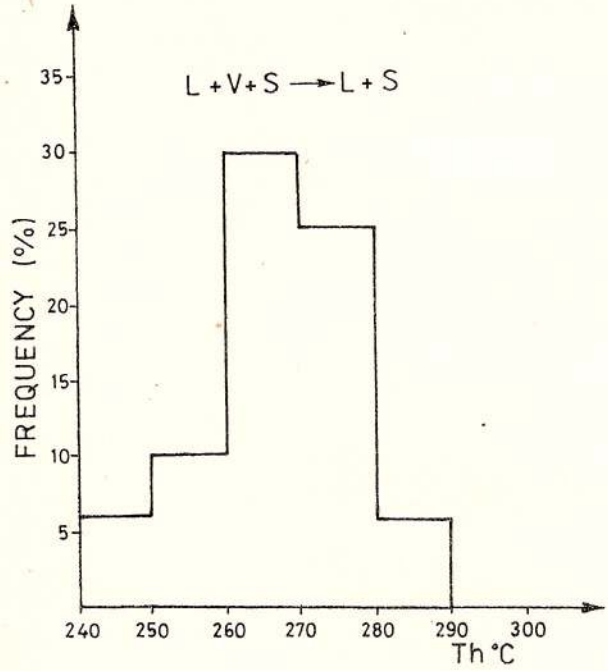

Fig. 2 Histogram of the temperatures of disappearance of the vapour phase in the S type fluid inclusions in which the solid phases remain undissolved. Symbols: L=liquid; V=vapours; S=solid.

Thus the values of the dissolving temperatures obtained by Pomârleanu in 1978 (Pomârleanu et al., 1985) cannot represent the real homogenization temperatures as the vapour bubble disappears much before some of the solid phases melt. As it has already been mentioned, the latter do not represent real daughter phases (Roedder, 1984). A main characteristic of the quartz crystals at Baia Sprie is the obvious zonality (Savul and Pomârleanu, 1961). An interesting relationship can be noticed between the latter and the distribution of the fluid inclusions in the sense that the L and V types associate with the generally clearer internal zones (Plate, Figs. 1, 2), while those with solid phases are as a rule distributed in the external zones (Fig. 3, Plate, Fig. 7). In the vertical plane of the Main Vein complete crystals (with the zone I and II) prevail within the interval between horizons X–XIII, where the co-existence of the L and V inclusions is much more obvious. As the depth increases, the quartz crystals are less zoned, while the clear internal zones lack altoghether. The homogenization temperatures decrease from the centre towards the external zones of the crystals and in the vertical plane of the vein the temperature variations are sometimes insignificant between horizons X–XVI. These facts lead to the idea

Table 4
Microthermometric Parameters of the L Type Fluid Inclusions from the Quartz Crystals of the Baia Sprie Deposit

Sample/ level	Te	Tmi	Salinity % NaCl weight	T_h °C
B9/X	−28	−4.6	7.20	342
	−28	−4.6	7.20	286
B12/X	−23.6	−3.9	6.10	325
	−27.0	−4.6	7.20	273
B8/X	−29.8	−7	10.50	305
	−28.0	−3.9	6.10	289
	−24.6	−2.2	3.60	249–308
B22/X	–	−3 to −1	4.9–1.7	–
	–	−3.8	6.10	–
B29/XI	– 26.4	−12	15.90	221–235
B121/XI	−24.6	−6.4	8.40	−302
	−32.0	−6.4	10.20	−310
B116/XI	−32	−7	10.00	−280
	−23	−7	10.50	−298
	−35.2	−6.4	10.20	−308
B33/XI	−45.4	−13.8	17.50	222–231
B32/XI	−22.2	−9.6	13.50	182
	−28.6	−9.6	13.50	258–259
B114/XII	−38.4	−16.4	19.95	164
B238/XIII	−24.5	−11.1	15.10	273
	−31.3	−12.8	16.75	286–303
	−30.8	−13.8	16.52	327
	−29.7	−13.8	16.52	328
	−26.8	−14.5	18.26	342
B232/XII	−32.9	−14.5	18.26	329
	−32.4	−15	18.69	278
	−30.7	−13.4	17.30	–
	–	−14.5	18.26	329
B235/XIII	−31.3	−15	18.69	327
	−41.4	−7.6	11.21	327–347
BS50/XIV	−24.6	−12.0	16.10	147
BS54/XIV	−32.5	−14.6	18.44	284
	−32.5	−11.4	15.45	300
	−32.5	−11.8	15.84	300
	−32.5	−12.1	16.14	261
BS58/XV	−48.2	−15.4	19.12	261
BS59/XV	−30.4	−14.6	18.44	203–253
B120/XV	−41.2	−16.4	19.95	282.5
BS69/XV	−12.8	−12.8	16.68	209
	−31.4	−11.4	15.45	229
	−31.4	−12.8	16.68	352
	−31.4	−12.0	16.10	359
BS63/XV	−33.0	−4.6	7.30	295
BS66/XV	−36.4	−9.8	13.76	335
	−37.2	−12.0	16.10	264
BS67/XVI	−24.6	−8.8	12.65	200–217
	−23.0	−5.6	10.00	228–240
BS68/XVI	−28.0	−8.8	12.65	277
	−24.3	−6.2	9.47	294

that the hydrothermal process at Baia Sprie is on the whole monoascendent, the various parageneses deposited being the result of the physico-chemical variations undergone by fluids, mainly due to boiling. According to the distribution mode of the fluid inclusions and of the metallic mineral parageneses (the presence of wolframite and scheelite), the paroxysmal moments of boiling are superposed on the zone between horizons X–XIII.

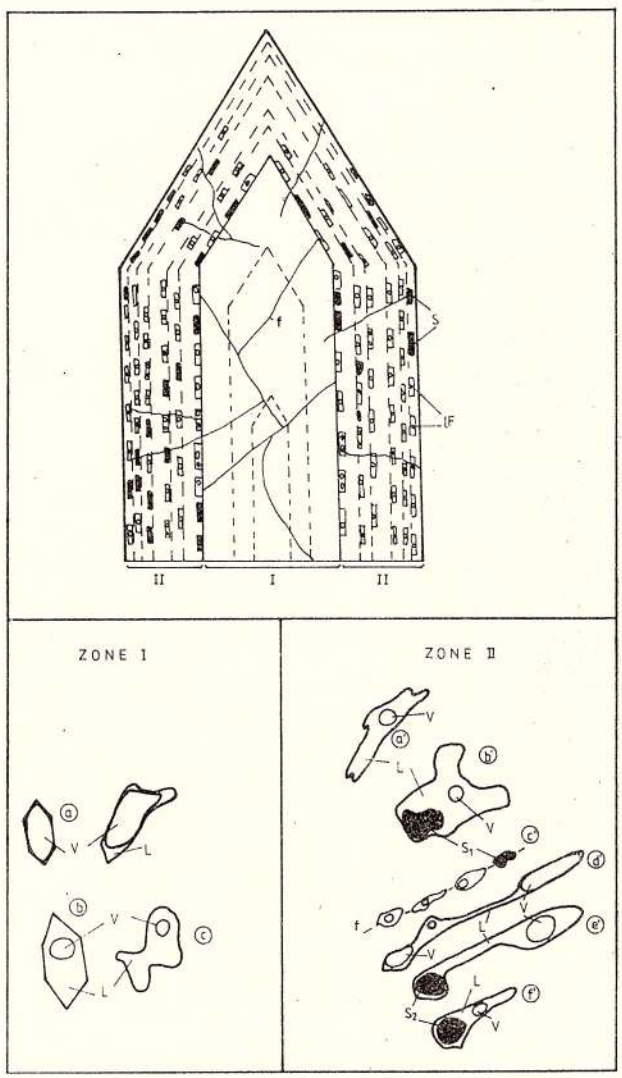

Fig. 3 – Relationship between the quartz crystal zonality and the types of fluid inclusions in the Baia Sprie mineralization. a, b, c, – L and V type fluid inclusions from the internal zones (I); a'–f' – L and S type fluid inclusions characteristic of the external zones (II) of the same quartz crystals; L – liquid phase; V-vapours; S_1 – carbonate grains dispersed in the fluid inclusions and in the crystal mass; S_2 – solid phases which, according to the distribution mode and habit, might represent dawsonite microcrystals.

The general trend of the Th and Tmi values for the fluid inclusions at Baia Sprie on Hedenqvist and Henley's diagram (1985) (Fig. 4) suggests the evolution of some fluids poor in vapours in the sense of the increase of their salinity as the temperature generally decreases rather slowly. It is also worth noting that both the presence of the solid carbonatic phases and the very different Te values from those of the H_2O-NaCl system (Tab. 4) indicate that the salinity of the fluids is mainly given by the presence of Ca and Mg (Crawford, 1981).

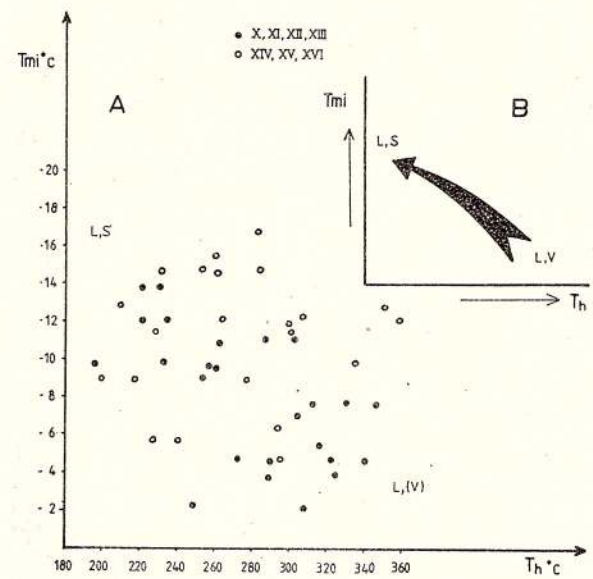

Fig. 4 – Th/Tmi diagram for the L, V and S fluid inclusions from the quartz crystals at Baia Sprie (A). As the homogenization temperature decreases, the fluid becomes even more concentrated and the gaseous phases leave the system (B). X – XVI accessible horizons in the Baia Sprie mine.

In conclusion the fluid inclusions at Baia Sprie represent heterogeneous aqueous fluids of relatively low salinity that evolved in a general monoascendent process and whose physico-chemical variations determined mainly the formation of the various parageneses.

5. Conclusions

The researches on the morphology of the pyrite crystals as well as the study of the inclusions from the quartz at Baia Sprie led to a reconstruction of the evolution of the hydrothermal process within this structure that differs substantially from the previous one (Nedelcu et al., 1992).

Based on the pyrite morphology trend two distinct domains have been separated in the Main Vein plane as follows: an upper one, with C – P trend and a lower one, with C–O–P ± {hkl} trend. The two domains correspond to the concentration and temperature conditions inferred from the topographic analysis of the faces and habit of the pyrite crystals, characterized

by: low supersaturation – high temperature (S_L–T_H) for the upper domain (C–P) and high supersaturation – low temperature (S_H–T_L) for the lower domain (C–O–P ± {hkl}).

Of the previous data (Nedelcu et al., 1992) the fractionation of the sulfur ^{34}S isotope in the sphalerite-galena pairs indicates inequilibrium in most of the studied cases situated at the boundary (transition zone) between the two mentioned domains. Also in the transition zone, aspects connected with the dissolving of pyrite and quartz are noticed.

The study of the fluid inclusions from the quartz crystals reveals a few important elements suggesting both the conditions and the course of the hydrothermal process:

a) First the co-existence of the L and V type inclusions as well as the Th corresponding values suggest that boiling was the main process undergone by the hydrothermal fluid.

b) The fluid type-depth relationship makes possible the separation of two domains:

– at the lower part (under horizon XIII) the S type fluid inclusions and a not too high homogenization temperature (Th) prevail;

– at the upper part (between horizons XIII and X), the co-existence of the L and V type inclusions indicates the maximal boiling zone (important decompression determined by the opening of the fissure ± obvious mixture with meteoric water).

c) The quartz crystals are zoned. An evident and significant relationship between the crystal zonality and the type of fluid inclusions is presented in Figure 3, which shows the existence of:

– a central zone (I) in which the L + V type inclusions prevail;

– external zones (II) in which the S type inclusions prevail.

In this case the decrease of the homogenization temperature (Th) from (I) to (II) indicates a monoascendent hydrothermal process, the parageneses deposited being the result of the physico-chemical variations undergone by fluids, mainly due to boiling.

In accordance with the distribution mode of the fluid inclusions and of the metallic mineral parageneses (the presence of wolframite and sheelite), the boiling paroxysmal moments superpose on the zone between horizons X and XIII.

d) The Tmi and Th diagram suggests that in the case of the Main Vein the fluids evolved towards a continual unmixing, from initial fluids (probably of magmatic origin) poor in vapours, with low salinity and high temperature, to fluid phases of high salinity (liquid part) and water vapours which leave the system concomitantly with the temperature decrease.

It follows that the fluid inclusions at Baia Sprie represent heterogeneous aqueous fluids of relatively low salinity that evolved within a generally monoascendent process, whose physico-chemical variations determined the formation of the main parageneses.

The comparison between the results of the morphologic study of pyrite and those of the study of the fluid inclusions in quartz reveals the superposition of the morphological trends on the domains of the fluid inclusions as follows:

– upper domain: the L + V type inclusions correspond to the C-P trend and to the S_L–T_H concentration-temperature domain;

– lower domain: the S type inclusions correspond to the C–O–P ± {hkl} trend and to S_H–T_L domain as well as to the appearance of the negative striated pyritohedron which would underline the subsequent Cu deposition (Endo, Sunagawa, 1973).

All these suggest that the deposition of the metallic charge took place descendantly from the upper part towards the lower part of the vein (Fig. 1). Also, the present geometry of the mineralization in the straight plane of the Main Vein, with its inflexions and eastern sinking permits the outlining of a model of the hydrothermal process with a great approximation degree, based on the flowing trends of the fluids, the boiling process and the metal deposition (Fig. 1 B). This model indicates that:

a) The fluids evolved along the fracture, from the lower eastern part of the structure towards its upper, western part in the Minei Hill.

b) The opening of the fracture led to an important decompression of the fluids resulting in the starting of the boiling process and the sulfide precipitation.

c) The deposition of the metals took place descendantly, beginning with Pb and Zn at the upper part and ending with Cu at the lower part of the hydrothermal "pipe". The mixture of the meteoric water in this process seems evident, especially in the "discharge" zone of this "pipe" in the Minei Hill, a zone characterized by the gold precipitation.

References

Amstutz G. C. (1963) Accessories on pyrite, pyrite zoning, and zoned pyrite. *Schweiz. Miner. Petrogr. Mitteilungen*, 33, p. 111–122, Zürich.

Crawford M. L. (1981) Phase equilibria in aqueous fluid inclusions. In L. S. Hollister and M. L. Crawford (eds). Short course in fluid inclusions: applications to petrology, 6, p. 75–100, *Min. Assoc. Canada*, Ottawa.

Endo Y. (1978) Surface microtopographical study of pyrite crystals. *Geol. Soc. Japan Bull.*, 29, p. 701–745, Tokyo.

– , Sunagawa J. (1973) Positive and negative striations in pyrite. *Am. Mineral.*, 58, p. 930–935, Washington.

Hedenqvist J. W., Henley R. W. (1985) The importance of CO_2 on freezing point measurements of fluid inclusions: evidence from active geothermal systems and implications for epithermal ore deposition. *Econ. Geol.*, 80, p. 1379–1406.

Murowchick J. B., Barnes H. L. (1987) Effects of temperature and degree of supersaturation on pyrite morphology. *Am. Mincr.*, 72, p. 1241–1250, Washington.

Nedelcu L., Voicu G., Voicu C., Roşu E., Zămîrcă A., Gaftoi F. (1992) Morphology of the pyrite crystals from the Main Vein at Baia Sprie. Genetical significances. *Rom. J. Mineralogy*, 75, p. 53–64, Bucureşti.

Pomârleanu V., Răduţ M., Neagu E. (1985) Studiul incluziunilor fluide din zona Baia Sprie-Şuior; implicaţii privind regimul termodinamic al soluţiilor hidrotermale. *Stud. cerc. geol., geogr., ser. geol.*, 30, p. 102–110, Bucureşti.

Roedder E. (1984) Fluid Inclusions. *Min. Soc. America. Rev. in Mineralogy*, 12, 644 p., Blacksburg, Virginia.

Savul M., Pomârleanu V. (1961) Cercetări paleogeotermometrice asupra zăcămîntului hidrotermal filonian de la Baia Sprie. *Stud. cerc. geol., geogr., geofiz. (geol.)*, VI, 2, p. 287–298, Bucureşti.

Sunagawa J. (1957) Variation in crystal habit of pyrite. *Geol. Survey of Japan Report*, 175, p. 1–47, Tokyo.

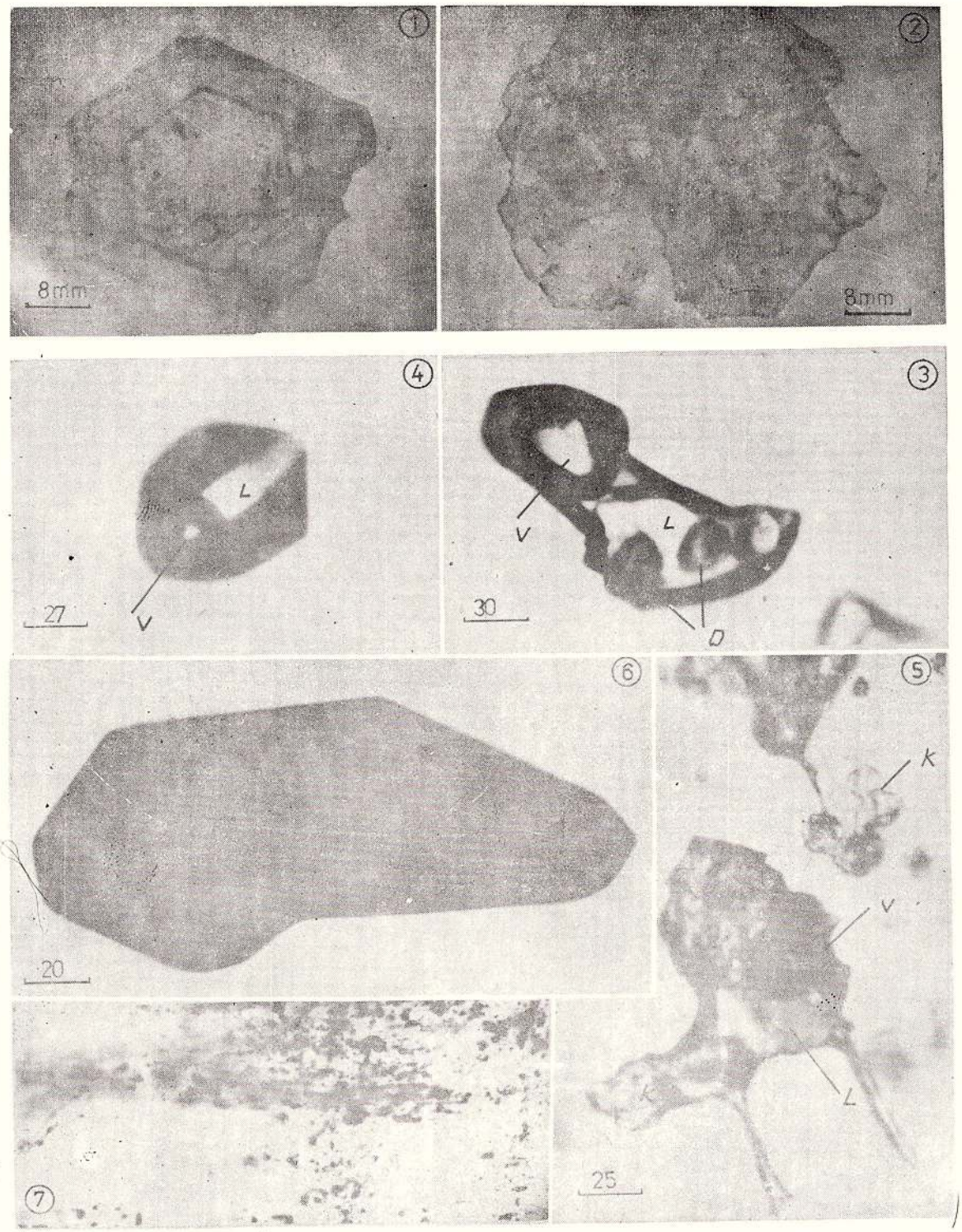

Plate

Figs. 1, 2 – Zonality characteristic of the quartz crystals from the Main Vein at Baia Sprie.
Fig. 3 – Polyphase fluid inclusion with solid phases as sheafs that might represent dawsonite (D) crystals. In the course of the microthermometric experiments it has a metastabile behaviour.
Fig. 4 – Biphase fluid inclusion with dominant liquid L type from an internal zone within the quartz at Baia Sprie.
Fig. 5 – Polyphase inclusions with carbonate grains (K), in suspension before trapping. The dispersion of the same grain type is also noticed in the crystal mass.
Fig. 6 – Fluid inclusion rich in vapours (V type) from an internal zone of a quartz crystal at Baia Sprie.
Fig. 7 – Fluid inclusions (mainly of S type) with oriented disposition in the external zones of a quartz crystal at Baia Sprie.

Rom. J. Mineralogy, 1993, 76, 1, p. 87–96

CRYSTALLOGENESIS OF CALCITE FROM PIATRA ALTARULUI CAVE (BIHOR MTS, ROMANIA)

Lucreţia GHERGARI, Robert-Octavian STRUSIEVICZ, Gheorghe FRĂŢILĂ, Ana SÎNTĂMĂRIAN

Universitatea "Babeş-Bolyai", Catedra de Mineralogie-Petrometalogenie. Str. Kogălniceanu nr. 1, 3400 Cluj-Napoca.

Key words: Carbonates. Calcite. Crystals. Crystal form. Frequency. Caves. Apuseni Mountains – Bihor Mountains.

Abstract: The Piatra Altarului Cave situated in the Bihor Mountains (NW of Romania) is characterised, besides very interesting speleothems, by the presence of several sectors completely covered with perfectly shaped calcite crystals. Three sites in the cave, i.e. the two walls of the Lake Room and "Geode" were chosen for a statistical crystallographical study. A total of 21 crystallographical forms were identified: the hexagonal prism, the hexagonal bipyramid (8.8.$\bar{1}$6.1), 13 rhombohedrons and 6 scalenohedrons. The general persistency diagram for the 460 measured crystals shows values over 10 % only for the hexagonal prism and for 8 rhombohedrons. In each site the crystals were grouped in three vertically superposed zones. Frequency diagrams for the number of forms on one crystal showed a clear zoning of populations with one generation of crystals and of populations with 2 generations of crystals.

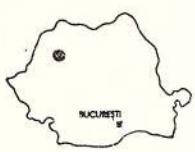

The recently discovered Piatra Altarului Cave is decorated by beautiful and very diverse speleothems. The cave was discovered and mapped by its discoverer, together with members of the Speological Club of the Cluj-Napoca Polytechnics (Gligan et al., 1986).

1. Localisation

The cave is situated in the NE part of the Bihor Mountains, in the area of Ic Ponor, on the right side of the Ponor Valley, a left tributary of the Someşul Cald River, 1 km upstream from the confluence, at an altitude of 1112 m, and at about 25 m above the valley level. It has been carved in Jurassic limestones of the so-called Someşul Cald Graben, which is separated from the intense retromorphosed schists of the Someş Group (Ghergari et al., 1991) by the E-W directed Someşul Cald Fault. The cave itself seems to be developed along a secondary fault oriented parallel with the main fault (Fig. 1).

2. Crystallographical data

Crystallographical studies were performed on perfectly shaped calcite crystals that carpet the walls, the stalactites, stalagmites and draperies of the Lake Room and of "The Geode" (Figs. 2, 3).

The first approach in this study consisted in the identification of the crystallographical forms that build the crystals shape – the tracht, as well as in the establishment of their dominance, which gives the crystal habit. This work was accomplished through "in situ" measurements of the angles between the crystal faces, and also by measurements made in the laboratory, on fallen fragments.

The second step consisted in statistical studies performed on a total of 460 crystals. This studies registered the persistency of the crystallographical forms, the different types of combinations of forms, as well as their frequencies.

The morphological and statistical studies comprised crystals from three distinct sites (Fig. 3 a, b), i.e. the Western wall, the Eastern wall of the Lake Room and "The Geode". In each of these sites the crystals that occur in a 5–7 cm wide vertical stripe were analysed.

2.1. Western wall of Lake Room

From this site 168 crystals were studied, which showed 11 different crystallographical forms. Only four of them have a persistency over 80 %, three have a persistency between 6–15 %, whereas 4 have a persistency of 2–3 % (Fig. 4B-a; Tab.1). The major parts of the crystals are well developed, having a short prismatic habit, terminated with the (10$\bar{1}$1) rhombohedron. The prismatic shape is given by the steeply inclined rhombohedrons (50$\bar{5}$1) and (05$\bar{5}$1), which are dominant and with high persistency, as well as by the paired rhombohedrons (40$\bar{4}$1) – (0$\bar{4}$41) and (80$\bar{8}$1) –

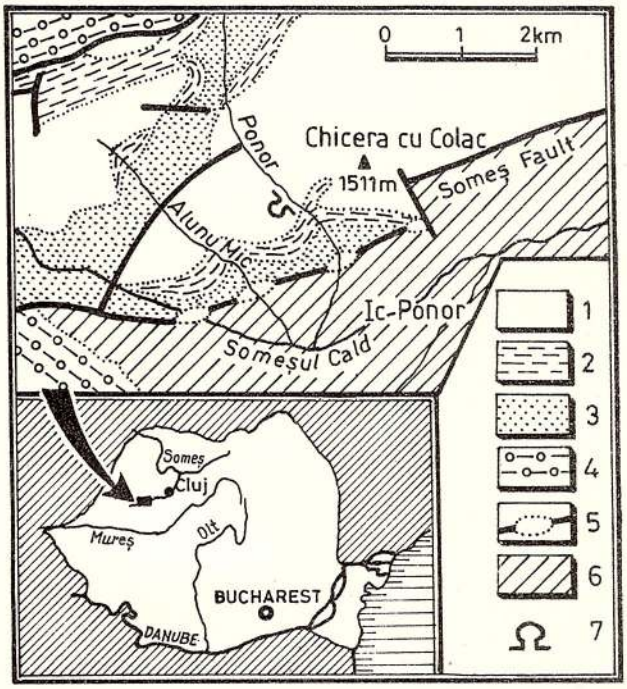

Fig. 1 – Location of the Piatra Altarului Cave. 1, Tithonian (limestones); 2, Middle and Upper Liassic – Dogger (marly slates); 3, Lower Liassic (sandstones); 4, Lower Triassic (quartzites and conglomerates); 5, Permian (rhyolites); 6, Precambrian (retromorphosed schists of the Someş Group); 7, Piatra Altarului Cave.

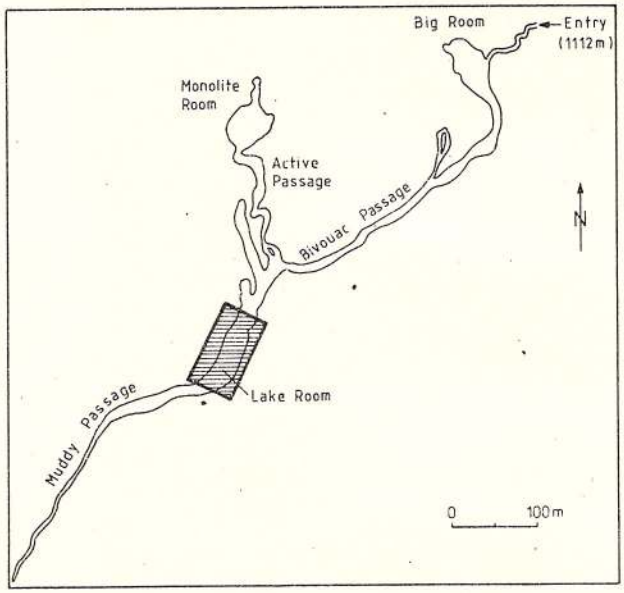

Fig. 2 – Simplified map of the Piatra Altarului Cave, with location of the Lake Room area (striped – detail in Fig. 3).

Table 1

Dominancy, persistency and combinations of forms – Lake Room, western wall

Number of crystallographical forms in one combination	Crystallographical forms											Frequency of the combinations of forms			Zones
	$10\bar{1}0$	$10\bar{1}1$	$01\bar{1}2$	$02\bar{2}1$	$40\bar{4}1$	$04\bar{4}1$	$50\bar{5}1$	$05\bar{5}1$	$80\bar{8}1$	$08\bar{8}1$	$35\bar{8}4$	Number of crystals	Type of combination %	Total %	
1					D							7	4	4	I
2	I								D			3	2		I
	D	I										1	0.5	2.5	I
3		I					D	D				11	6.5		I+II
		I			D	D						3	2		II
		I			I					D		3	2	13	II
	D	I				I						3	2		I
	I				I					D		1	0.5		I
4	I	I		S	I		D	D				120	71		I+II+III
		I			D	D				D		5	3		II
		I	S				D	D				3	2	77	I
							D	D			S	1	0.5		I
												1	0.5		I
5	I	I	S				D	D			S	3	2		I+II
	I	I	S				D	D			S	2	1	3.5	I
	S		S		S					D	S	1	0.5		I
Persistency No	137	156	5	5	23	9	138	138	3	10	4	168			
Persistency %	81	93	3	3	14	5	82	82	2	6	2	100			

I - upper zone (20 cm); II - median zone (40 cm); III - lower zone (60 cm).

D - dominant form; I - intermediary form; S - subordinate form.

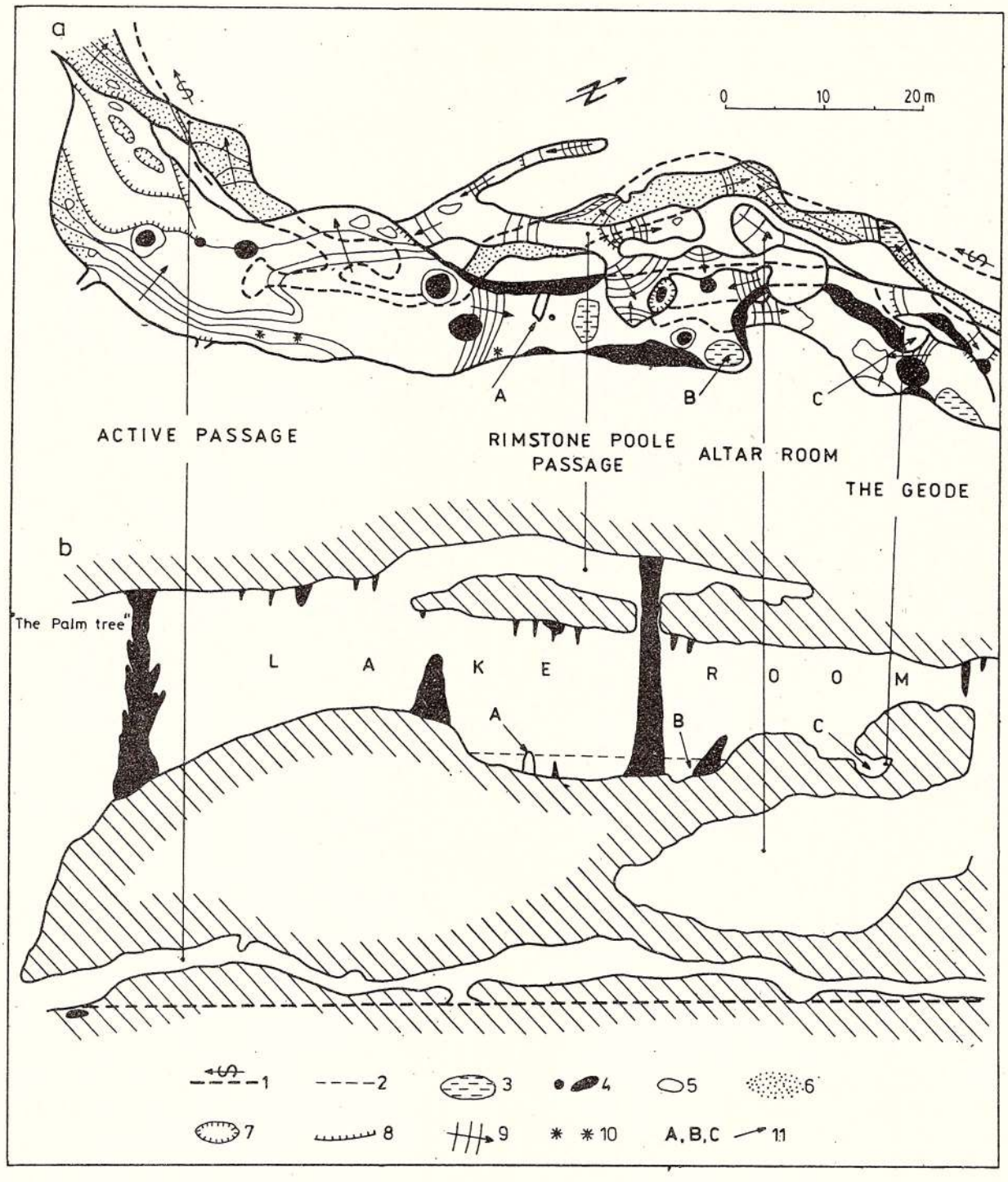

Fig. 3 – Sketch (a) and profile (b) in the Lake Room area of the Piatra Altarului Cave. 1, active flow direction; 2, ancient water level; 3, lake; 4, flowstones; 5, blocks; 5, alluvia; 7, pit; 8, pitch (teeths downwards); 9, level curves (1 m equidistance); 10, helictites; 11, location of the studied areas (A– transverse block on the western wall of the Lake Room; B– "Big Maces" on the eastern wall of Lake Room; C– "The Geode"):

$(08\bar{8}1)$, which are also dominant, but with low persistency, whereas the hexagonal prism $(10\bar{1}0)$ is only intermediary, but with high persistency (Fig. 5b, 6a and c). Other rhombohedrons or the scalenohedrons have no influence on the crystal shape as they are subordinated and with low persistency (Fig. 5c, 6b). The habit and the tracht of the crystals is constant on the vertical, but their size increases towards the bottom

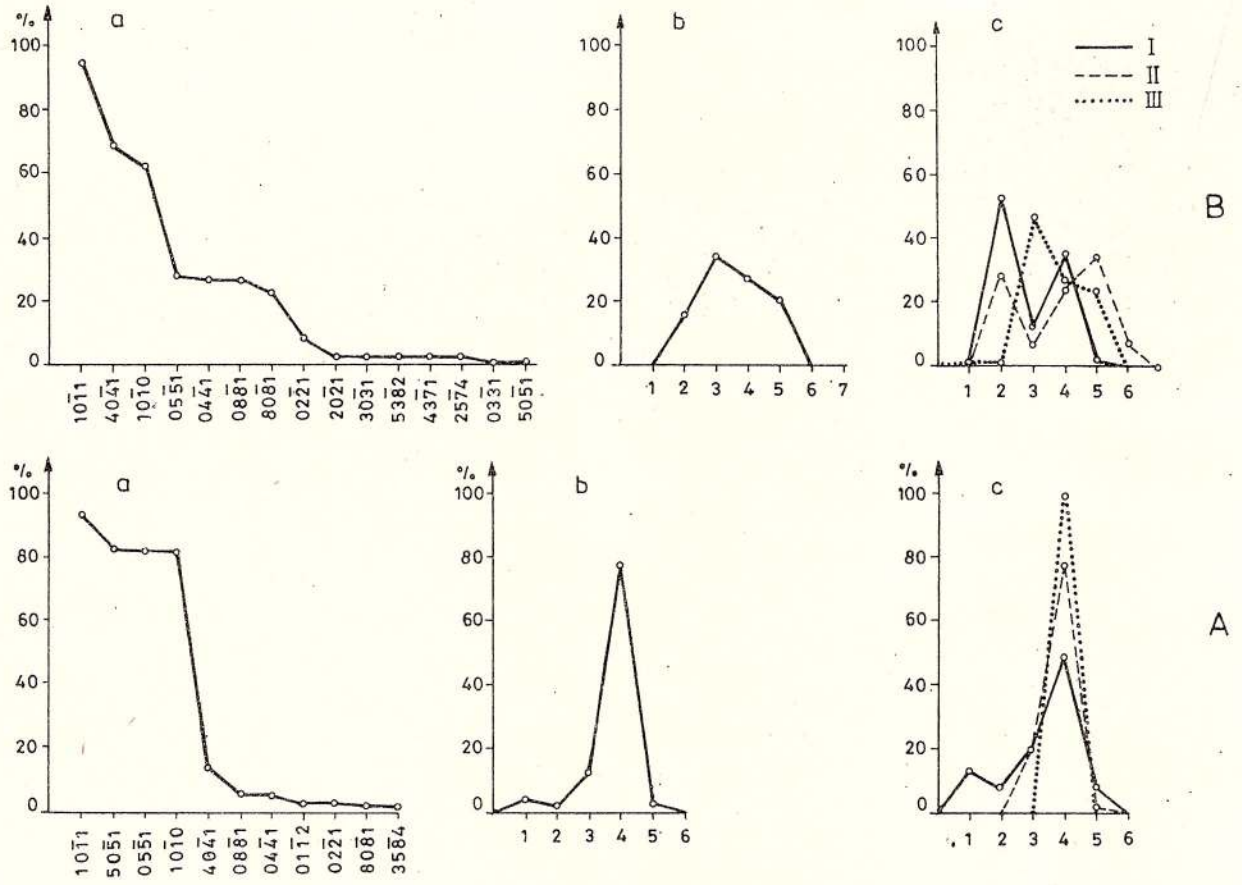

Fig. 4 Persistency (a) and frequency (b and c) diagrams for calcites from the western wall of the Lake Room (A) and the "Geode" (B); I – upper level; II – median level; III – lower level.

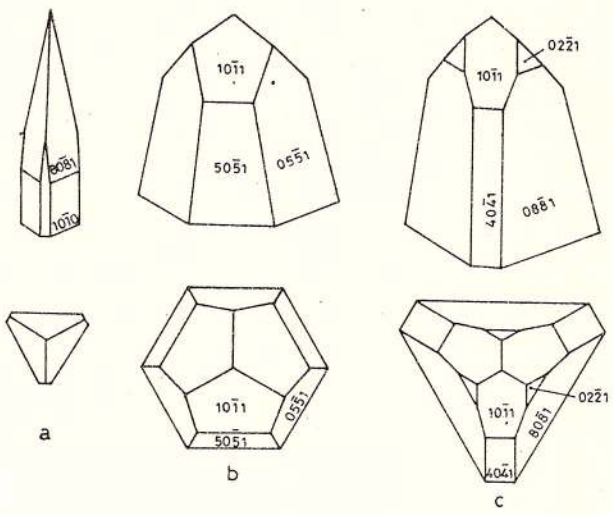

Fig. 5 Calcite crystals from the western wall of the Lake Room.

of the wall. Many crystals on this wall are polyterminated, and this feature is very common in the lower part of the wall, where single-terminated crystals represent the rarity. This parallel intergrowths have no connection to with twinning, but are due to internal dislocations that affect the inner structure of the crystals, leading to change of low-angle limits in high-angle limits, and so to a parallel growth of subindividuals on the same basis (Fig. 6d). At the upper part of the block spear-shaped crystals of a younger generation can be seen between the already mentioned crystals. These crystals are very poor in forms, being build up of only one (40$\bar{4}$1) or two forms – (80$\bar{8}$1)D and (10$\bar{1}$0)I (Fig. 5a; Pl. I, Fig. 3).

The frequency diagram of combinations of forms is bimodal, with a very acute maximum for crystals built of 4 forms (77 %), and with another maximum for crystals build up of only one form (Fig. 4B-b), pleading for the existence of two generations. By dividing the whole population into 3 superposed zones (i.e. an upper (I) zone of 20 cm, a median (II) zone of 40 cm, and a lower (III) zone of 60 cm), it becomes obvious that

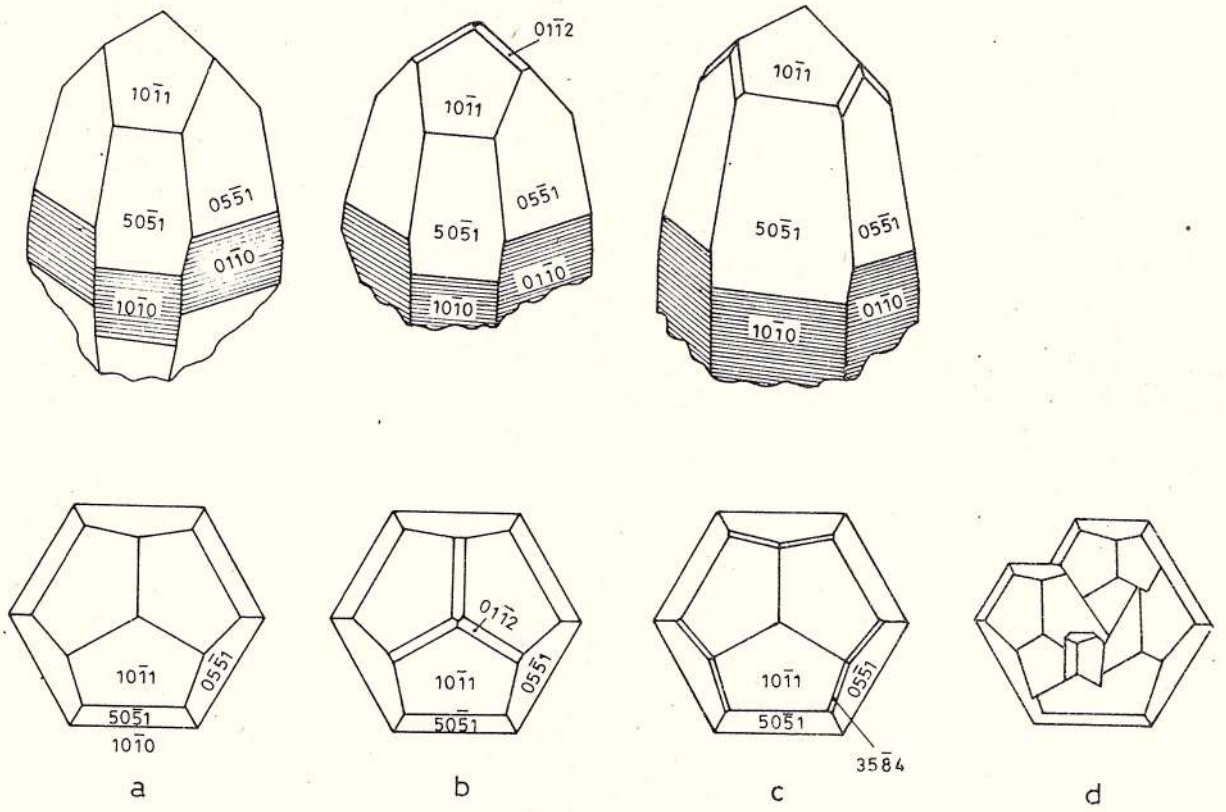

Fig. 6 — Calcite crystals from the western wall of the Lake Room.

the second generation of crystals appears only in the upper zone, where the concentration of the water increased through intense evaporation, and where concentration currents prevailed over the diffusive ones (Fig. 4B-c).

2.2. Eastern wall of the Lake Room – "The Big Maces"

The calcite crystals that carpet the walls of the ancient lake, and which also grew around the big stalactites on the eastern side of the Lake Room, giving them a mace-shape (Pl. II, Figs. 1, 2), reveal a greater diversity of forms, pleading for more dramatic changes of the crystallisation conditions. From this site 95 crystals were studied which revealed the presence of 16 forms. Considering the whole population a persistency diagram with a maximum situated under 50 % and a trimodal frequency diagram were obtained (Fig. 7D-a and b; Tab. 2).

In order to identify groups of crystals with a more uniform morphology this population was also divided into 3 superposed zones.

The upper zone (I) consists of 33 crystals grown at the upper part of the stalactites, all of one generation, and which display a total of only 3 crystallographical forms (Fig. 7A-a, b), i.e. the negative rhombohedron ($02\bar{2}1$), the hexagonal (8.8.$\bar{1}$6.1) and the scalenohedron (7.6.$\bar{1}$3.1) (Fig. 8).

The median zone (II) consists of 30 crystals formed at the tip of the stalactites (Pl. 2, Fig. 4). They display a total of 10 crystallographical forms, and comprise 2 generations (Fig. 7B-a, b), the combination of forms being intermediary, between the zones (I) and (III):

The lower zone (III) is represented by the crystals on the pool bottom; 32 analysed crystals showed a total of 12 forms, with maximal frequencies for crystals with 4–5 and 7 forms, respectively (Fig. 7C-a and b). Their habit has a great resemblance with that of the crystals on the western wall of the Lake Room (Fig. 9). A rare form found here is the (9.3.$\bar{1}$2.5) scalenohedron (Fig. 10 a).

3.3. "The Geode"

The so-called "Geode" is an irregular cavity situated northwards of the Lake Room, decorated with many stalactites and draperies, these and the walls being completely covered with calcite crystals (Pl. 1, Figs. 1, 2). The 197 analysed crystals have a total of 15 forms, of which 15 are positive and negative rhombo-

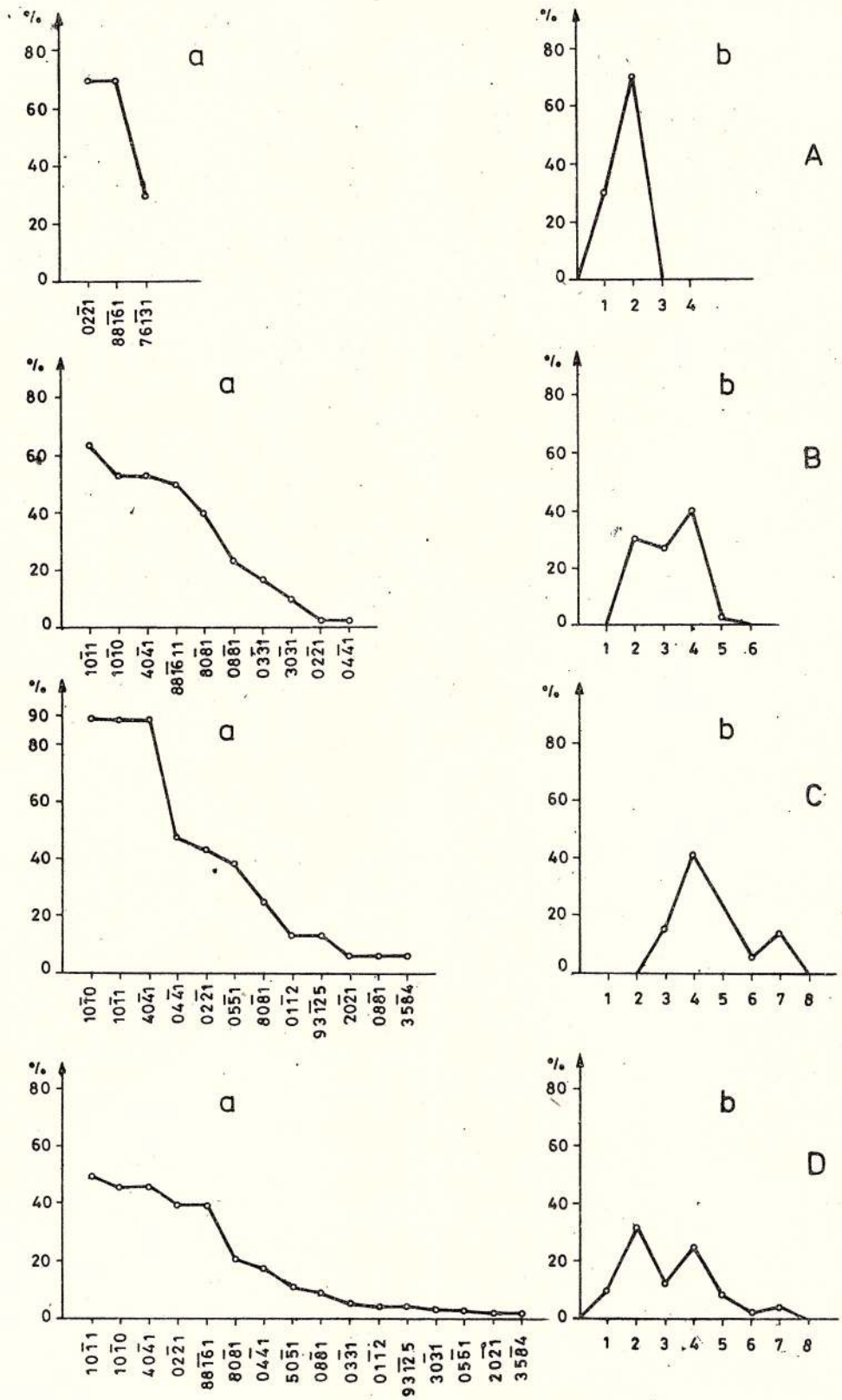

Fig. 7 – Persistency (a) and frequency (b) diagram for calcites from the eastern wall of the Lake Room: A–upper zone; B– median zone; C–lower zone; D–whole population.

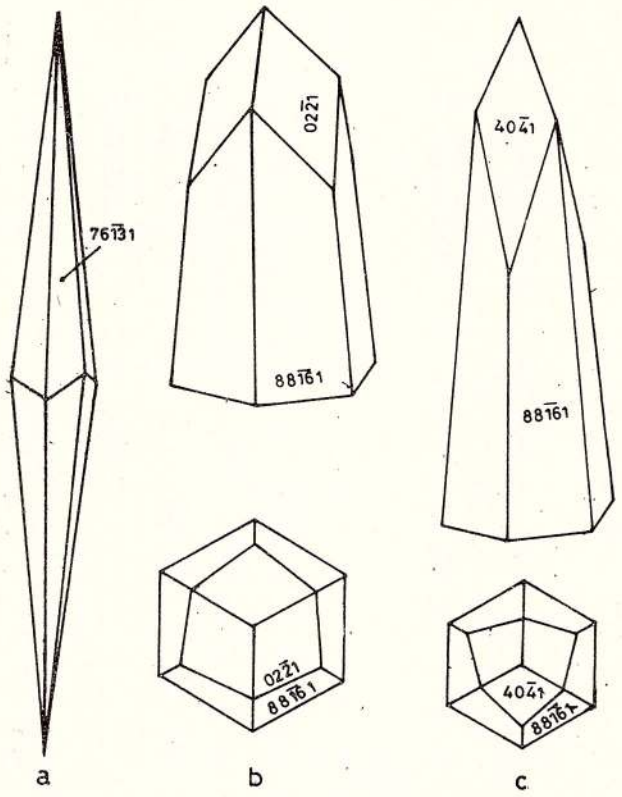

Fig. 8 – Calcite crystals from the upper zone of the eastern wall in the Lake Room.

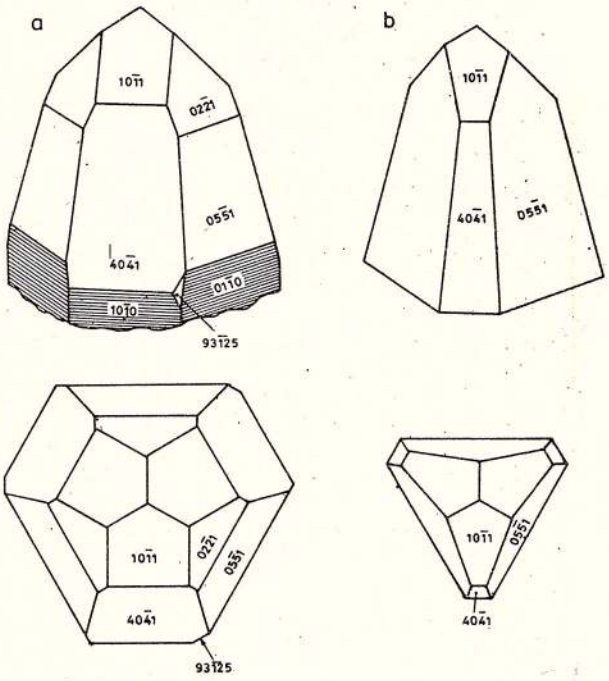

Fig. 10 – Calcite crystal with the rare (9.3.$\bar{1}$2.5) scalenohedron from the eastern wall of the Lake Room (a) and calcite with dominant (0551) rhombohedron from the "Geode" (b).

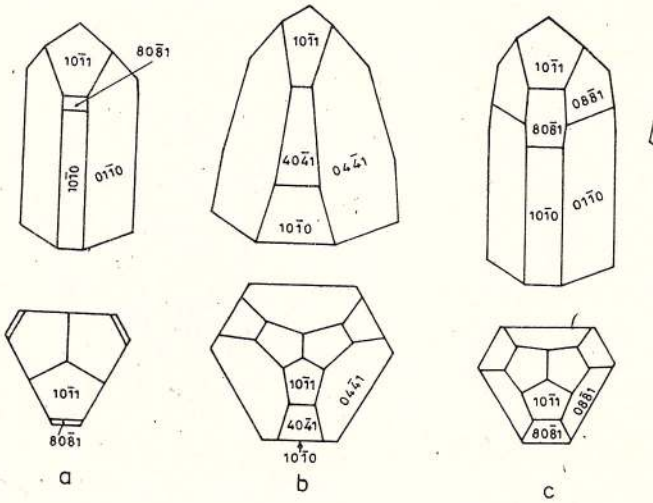

Fig. 9 – Calcite crystals from the lower zone of the eastern wall in the Lake Room.

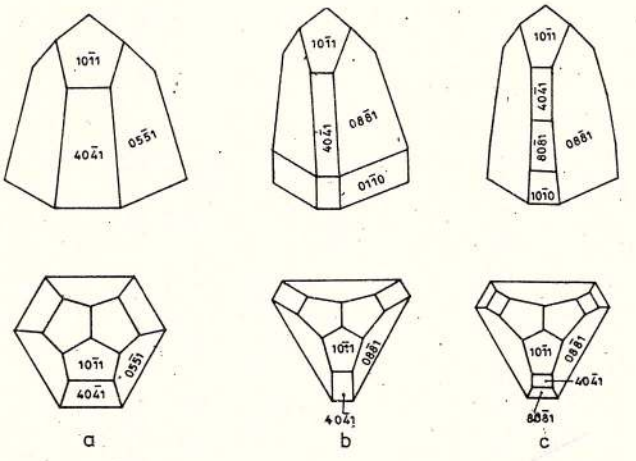

Fig. 11 – Calcite crystals with dominant negative rhombohedrons from the "Geode".

Table 2

Dominancy, persistency and combinations of forms – Lake Room, eastern wall

Number of crystallographical forms in one combination	Crystallographical forms																Frequency of the combinations of forms			Zones
	$10\bar{1}0$	$10\bar{1}1$	$01\bar{1}2$	$20\bar{2}1$	$02\bar{2}1$	$30\bar{3}1$	$03\bar{3}1$	$40\bar{4}1$	$04\bar{4}1$	$05\bar{5}1$	$80\bar{8}1$	$08\bar{8}1$	$8.8.\bar{16}.1$	$35\bar{8}4$	$7.6.\bar{13}.1$	$9.3.\bar{12}.1$	Number of crystals	Type of combination %	Total %	
1															D		10	10.5	10.5	III
2					S			D					D				23	24.5		III
	D	S											D				7	7.5	34	II
																	2	2		II
3	D	I				I		D			S		D				4	4.5		II
							S	D					D				2	2		II
	S							D				I					2	2	13.5	II
	S								D		I						2	2		I
	D	I						S									2	2		I
																	1	1		I
4	I	I						I	D								9	9.5		I
	D	S									II	I					7	7.5		II
	I	I			S			I									3	3	26	I+II
		S					S	D					D				3	3		II
		I							D					S			2	2		I
	D	S							D				D				1	1		II
5	S	I			I			D		D							8	8.5	9.5	I
	D	I				S		S			S						1	1		II
6	D	S		I				I	I		I						2	2	2	I
7		I	S		I			D		D	S					S	4	4.5	4.5	I
Persistency No	44	47	4	2	38	3	5	44	16	12	20	9	38	2	10	4	95		-	
Persistency %	46	19	4	2	40	3	5	46	17	13	21	9	40	2	11	4	100			

I - lower zone; II - median zone (fragments); III - upper zone of the big maces (fragments).

D - dominant form; I - intermediary form; S - subordinate form.

hedrons, and 3 are scalenohedrons with low persistency and dominance (Fig. 4B-a; Tab. 3). As the frequency curve showed a bride peak (Fig. 4B-b), this population was also divided in 3 superposed zones.

The upper zone (I) covers the first 15 cm below the ancient level of the lake. The 44 analysed crystals contain several oblique truncated "horse-teeth" crystals, developed immediately below the water level. The dominant forms are the $(25\bar{7}4)$ scalenohedron and the $(80\bar{8}1)$ steep rhombohedron. The frequency of the combinations has 2 maximus, one for crystals with 2 forms, and one for crystals with 4 forms (Fig. 4B–c–1).

The medium zone (II), consisting of 29 crystals on a 40 cm wide stripe, below the upper zone, is characterised by the presence of spear-shaped crystals, build up merely of 2 or 5 forms (Fig. 4B-c-2). The dominant form is the positive rhombohedron $(40\bar{4}1)$, sometimes truncated by negative rhombohedrons like $(04\bar{4}1)$, $(08\bar{8}1)$, and others (Fig. 4B–b, c; Fig. 10 b).

The lower zone (III), consisting of 124 crystals on a 1 m wide stripe, comprises 2 generations of crystals. The first generation crystals are greater in size and very similar to those of the medium zone, while the overgrown second generation crystals are very little in size and poor in forms (Fig. 11 a; Pl. I, Fig. 3, 4). The frequency curve shows maximums for crystals with 3 and 5 forms, respectively (Fig. 4B-c-3).

3. Discussion

The crystals that cover the walls, the stalactites and draperies of the Lake Room and of the "Geode", up to a height of 1.5–2 m, are the result of slow crystallization from water of long lasting subterranean lakes and pools. A total of 21 crystallographical forms were identified on these crystals, i.e. the hexagonal prism, 13 rhombohedrons, the hexagonal bipyramid $(8.8.\bar{16}.1)$, and 6 scalenohedrons (Tab. 4).

Table 3

Dominancy, persistency and combinations of forms "The Geode"

Number of crystallographical forms in one combination	Crystallographical forms																Frequency of the combinations of forms			Zones
	$10\bar{1}0$	$10\bar{1}1$	$20\bar{2}1$	$02\bar{2}1$	$30\bar{3}1$	$03\bar{3}1$	$40\bar{4}1$	$04\bar{4}1$	$50\bar{5}1$	$05\bar{5}1$	$60\bar{6}1$	$80\bar{8}1$	$08\bar{8}1$	$53\bar{8}1$	$43\bar{7}1$	$25\bar{7}4$	Number of crystals	Type of combination %	Total %	
1		D															1	0.5	0.5	II
2	D	I						S				D					26	13		II
	S						D										3	1.5		I
		S															1	0.5	16	II
				I									D			D	1	0.5		I
																	1	0.5		III
3		I		S			I	D		D							35	18		III
		S					S	D									13	7		III
		I															9	5		III
	D	I						S								D	2	1		I
		I					S	S				D					2	1	34.5	I
		I											D				2	1		III
	D	S						S	D	D							1	0.5		II
		S		D												D	1	0.5		II
																	1	0.5		I
4	S	I					S	i					D				27	13		II + III
	I	I					I			S		D					9	5		I + II + III
	S	S	I					D									6	3		I
	I	I					I			D		D					4	2		III
	S	I		S			S	S									3	1 5	27.5	III
	I	S					S					D					2	1		I
	S	D		I		D											1	0.5		II
		I					S									D	1	0.5		I
					S		D	S					D	S			1	0.5		III
																	1	0.5		I
5	S	I					S					S	D				20	10		III
	S	I					S			D		S					10	5		III
	I	I					S	D							S		4	2	20.5	II
	S				D		S	D						S			4	2		II
	I	I					I						D		S		2	1		II
	S	I					I				S		I				1	0.5		I
6	I	S	S				S	D				I					2	1	1	II
Persistency No.	124	187	6	17	5	1	135	53	1	55	1	46	53	5	6	5	197			
Persistency %	63	95	3	9	3	0.5	69	27	0.5	28	0.5	23	27	3	3	3	100			

I - upper zone (15 cm); II - median zone (40 cm); III - lower zone (100 cm).

D - dominant form; I - intermediary form; S - subordinate form.

The persistency curve drawn for the 460 analysed crystals has 4 distinct steps (Fig. 12 a), while the frequency curve of the combinations of forms shows a pregnant maximum for crystals with 4 forms, with a slight inflection for crystals with 2 forms (Fig. 12b).

The nearby isometric habit of the crystals pleads for a slow crystallisation rate in pools with quiet waters, highly concentrated in calcium bicarbonate. The long lasting ideal concentration of the water is the result of an equilibrium between evaporation and fresh water supply, while uniform concentration in the pools was favoured by concentration currents. These currents are also responsible for the growth of larger crystals in the lower levels. Subordinate diffusive currents led to the development of some spear-shaped crystals in the spaces between the larger crystals.

Crystallization conditions changed in time, due to variations of the water supply, which induced changes of the concentration and of the level of the waters in the lake and in the pools. Repeated inrushes of muddy waters caused the zonation of some calcites (alternance of pure, colourless zones with reddish zoned impurified with clay and iron hydroxides). Such zoned crystals (Pl. II, Fig. 4) are more frequent in the "Geode", showing that an active flow existed in this area. In fact, a fossil colmated passage was discovered in the eastern wall between the "Geode" and the "Big Maces", in the eastern wall of the Lake Room. We assume that this water source is also responsible for the greater diversity in habit and tracht of the crystals in the area of the

"Big Maces".

On the other hand, a level difference of 20 cm between the upper limit of the crystal carpet in the Lake Room and the "Geode" pleads for a drainage of waters from the former zone to the latter.

Table 4
Crystallographical forms observed on calcite from Piatra Altarului Cave

No	hkīl	Symbol	Crystallographical form	Persistency %
1	$10\bar{1}0$	a	Hexagonal prism	67
2	$10\bar{1}1$	π		85
3	$01\bar{1}2$	δ		2
4	$20\bar{2}1$	λ		2
5	$02\bar{2}1$			12
6	$30\bar{3}1$			3
7	$03\bar{3}1$		Rombohedrons	1
8	$40\bar{4}1$	α		40
9	$04\bar{4}1$			17
10	$50\bar{5}1$	n		33
11	$05\bar{5}1$			44
12	$60\bar{6}1$	ζ		0.25
13	$80\bar{8}1$	γ		13
14	$08\bar{8}1$			16
15	$88\bar{1}61$	τ	Bipyramid	9
16	$53\bar{8}2$	N		1
17	$43\bar{7}1$	T		1
18	$25\bar{7}4$			1
19	$35\bar{8}4$	b	Scalenohedrons	1
20	$76\bar{1}31$	X		2
21	$93\bar{1}25$			0.75

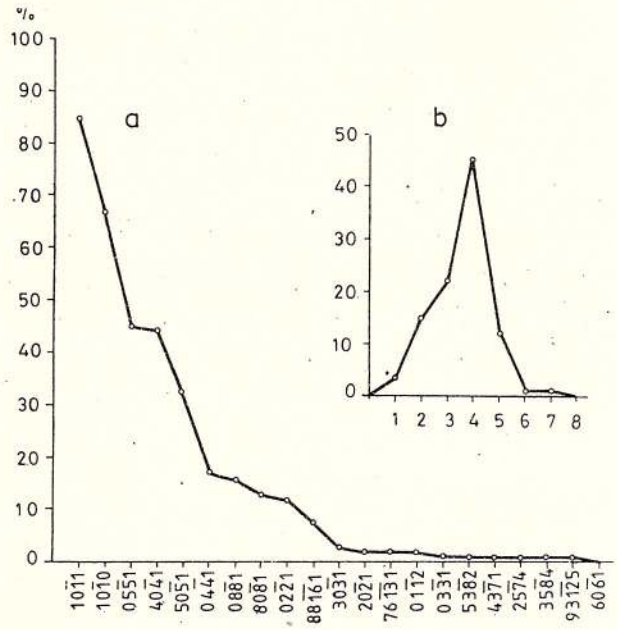

Fig. 12 — Persistency (a) and frequency (b) diagram for the 460 analysed calcites of the Piatra Altarului Cave.

References

Ghergari L., Strutinski C., Nicolescu Şt. (1991) Petrometallogenetical data on the crystalline formations from the Ic Ponor area (Apuseni Mts). I. The Petrogenesis of metamorphic rocks. *Studia Univ. "Babeş-Bolyai", Geol. Geogr.*, XXXVI/1, Cluj.

Gligan M., Pătraş S., Arba S. (1986) Consideraţii morfogenetice asupra peşterii din Piatra Ponorului. *Bul. Inf. al Com. Centr. de Speologie*, 8, Bucureşti.

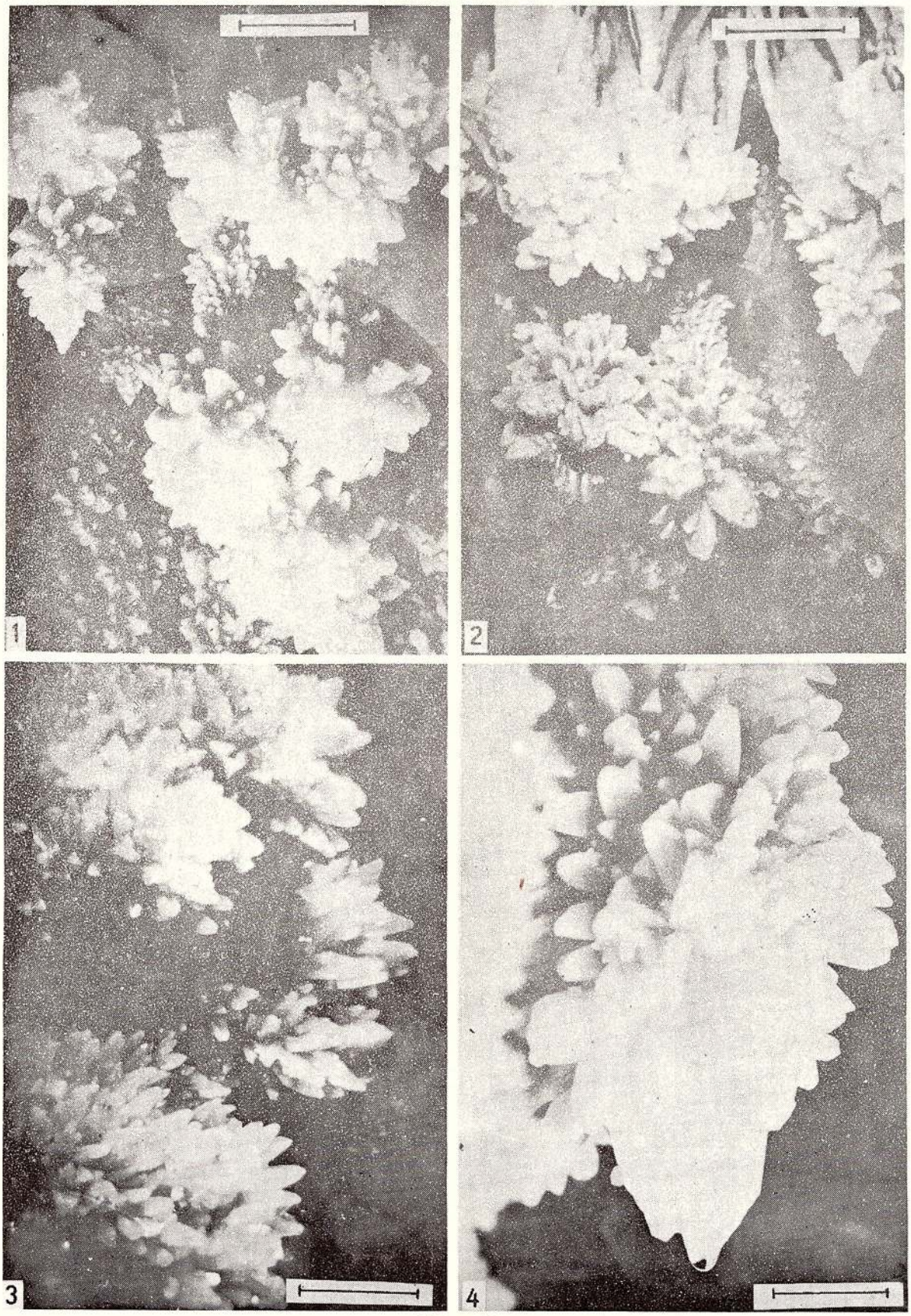

Plate I

Calcite crystals from the Lake Room in the Piatra Altarului Cave (photographs by Bogdan Dan)

Figs. 1, 2 — "The Big Maces" — stalactites and draperies terminated with diverging aggregates of calcite (scale bar 20 cm).

Fig. 3 — Spear-shaped calcite crystals (dominant steeply inclined rhombohedrons) from the western wall of the Lake Room (scale bar 4 cm).

Fig. 4 — Calcite crystals on the top of a stalactite (scale bar 2 cm).

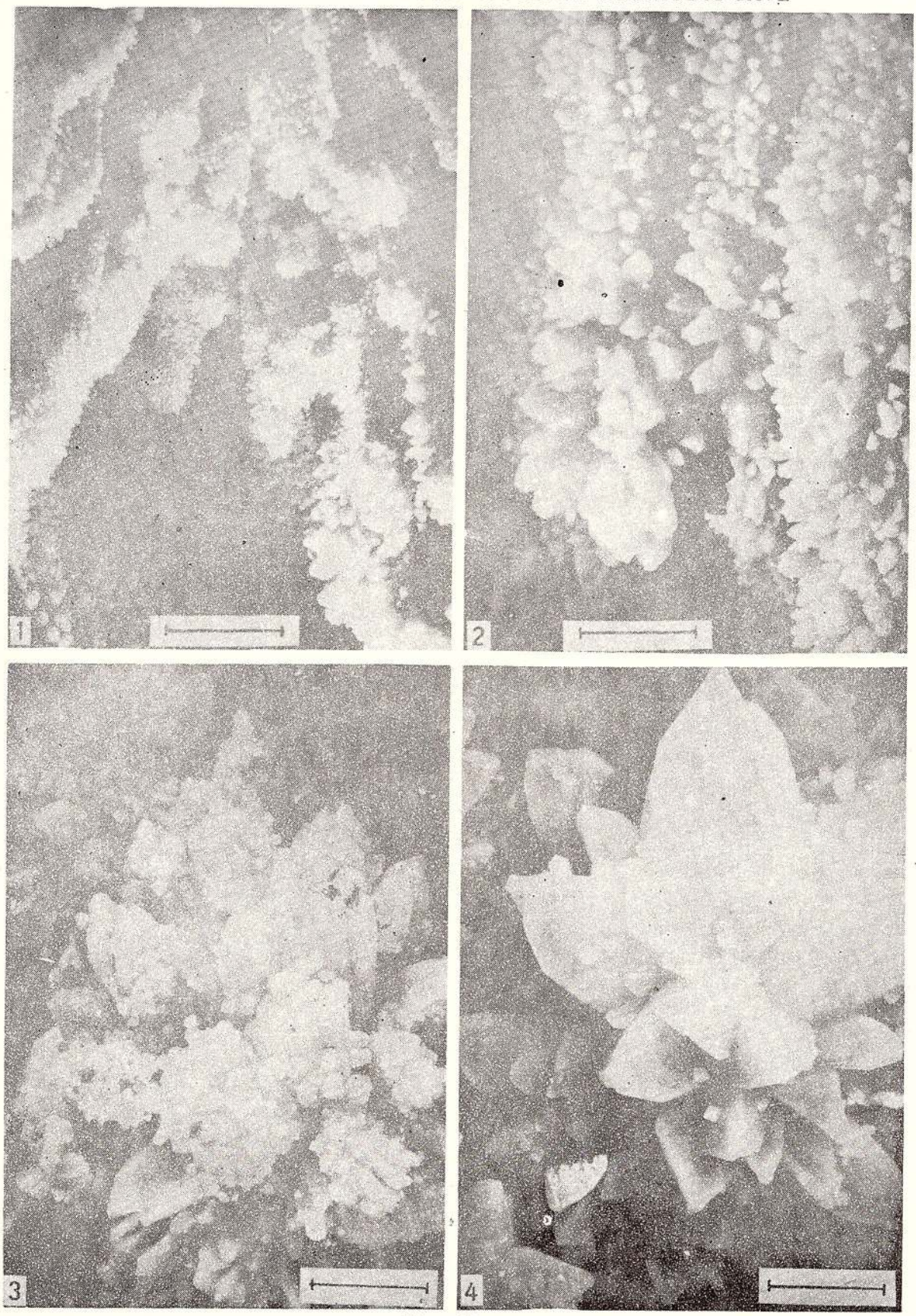

Plate II

Calcite crystals from "The Geode" in the Piatra Altarului Cave

Fig. 1 Draperies and stalactites covered with calcite crystals (scale bar 50 cm).
Fig. 2 Calcite crystals on the walls of the "Geode" (scale bar 10 cm).
Fig. 3 Little size calcites of a younger generation overgrown on large size calcite crystals (scale bar 1 cm).
Fig. 4 Zoned calcite crystals, showing a white rim of pure calcite (scale 2 cm).

Rom. J. Mineralogy, 1993, 76, 1, p. 97–98

WHAT IS MONSMEDITE?

Josef ZEMANN

Institute for Mineralogy and Crystallography, University of Vienna. Dr.-Karl-Lueger-Ring 1, A-1010 Vienna, Austria.

Key words: Sulfates. Monsmedite. Voltaite. X-ray data. Major elements. East Carpathians.

Abstract: Samples labelled "Monsmedite from Transylvania" from two mineral collections were shown to be voltaite with at most minor contents of thallium, although the macroscopic properties and the X-ray powder pattern agree well with the original description of this mineral. This result is not compatible with the formula $K_2O.Tl_2O_3.8SO_3.15H_2O$ given for monsmedite and makes a reinvestigation of the type material highly desirable.

Monsmedite seems to have been dealt with in two publications only, i.e. in the monograph on the Baia Sprie ore deposit (Manilici et al., 1965) and in a special paper presenting the full mineralogical description (Götz et al., 1968).

The mineral occurs in the oxidation zone of the Baia Sprie deposit, Romania, grown on quartz or marcasite, but also as loose crystals in a matrix of fibrous sulphates. Morphologically, monsmedite is cubic, with the cube as the dominant form. The size of the crystals may reach 1 cm, but usually they measure 0.25 to 0.50 cm. The colour is very deep green. Under the polarizing microscope the mineral shows zoning. Monsmedite is described as optically negative, with variable 2V, a birefringence of 0.011 and an average index of refraction of 1.608. A wet chemical analysis led to the chemical formula $K_2O.Tl_2O_3.8SO_3.15H_2O$. X-ray powder data and information on the thermogravimetric behaviour are given.

According to this description, monsmedite is a highly remarkable mineral, because it is (1) the most acid sulphate in mineralogy[1], (2) the only sulphate of thallium in mineralogy known by now, and (3) apparently the only dark coloured sulphate of Tl^{3+} in inorganic chemistry. Therefore, a further investigation seemed to be worthwhile. Samples labelled monsmedite and macroscopically corresponding to this mineral were obtained from collections in Hungary and Romania.

Single-crystal investigation resulted in a cubic cell with a = 25.29(2) Å and space group Fd3c – O_h^8. This result agrees well with the data of Mereiter (1972) for a synthetic voltaite with formula $K_2Fe_5^{2+}Fe_3^{3+}Al(SO_4)_{12}.18H_2O$, namely a = 27.254(8) Å and the same space group. Our "monsmedite" material undoubtedly belongs to the voltaite group.

In this context it seems important to note that part of the properties given for monsmedite in Götz et al. (1968) agree fairly well with those of voltaite: The morphology and the colour are the same, the mean index of refraction is very near to that of natural voltaite, and the density, D = 3.00 g.cm^{-3}, is only slightly higher than that of usual voltaite. In addition the X-ray powder data published for monsmedite in the region correspond fairly well to those of voltaite (Tab. 1). One is, therefore, tempted to consider also the original monsmedite to be identical with or closely related to voltaite.

However, the chemical analysis of monsmedite given by Götz et al. (1968) cannot be reconciled with such an interpretation (Tab. 2). It is true that among the many synthetic representatives of the voltaite type several members with Tl^{1+} instead of K^+ are known (e.g. Mereiter, 1970 a and b, 1972, with references to the older literature). But the high K_2O content found in monsmedite precludes such an interpretation, even if one assumes that the determination of the oxidation state of thallium as Tl^{3+} was in error. Although voltaites with Tl^{3+} for Fe^{3+} seem not to have described in the literature, one cannot exclude that they can exist. Unfortunately, such an assumption for monsmedite does not help much. In such a case, the mineral had to contain more than 10 weight-% FeO

[1]The chemical formula given as oxides allows the interpretations $K_2Tl_2[SO_3(OH)]_8.11H_2O$, $K_2Tl_2(SO_4)_8.8H_3O.3H_2O$, $K_2Tl_2(SO_4)_8.3H_5O_2.5H_3O$, or anything in between. For the constitution of the only other hydrated acid sulphate in mineralogy, i.e. rhomboclase, $(H_5O_2)Fe^{3+}(SO_4)_2.2H_2O$, see Mereiter (1974).

(and/or MnO+ZnO+MgO), contrary to the analytical result.

Table 1

Comparison of X-ray powder data of monsmedite (Götz et al., 1968) and of voltaite (ASTM 20-1388). In both cases only reflexions with 6.00 Å> d_{hkl} > 2.50 Åare being considered

Monsmedite		Voltaite	
$I_{estimated}$	d(Å)	d(Å)	I_{rel}
weak	5.485	5.55	60
		4.81	2
		4.59	2
		4.30	2
		4.10	8
		3.92	6
		3.63	18
strong	3.560	3.54	80
very strong	3.403	3.40	100
very weak	3.181	3.20	16
		3.14	25
weak	3.063	3.03	45
		2.98	8
		2.90	4
strong	2.860	2.85	35
		2.78	4
weak	2.647	2.62	18
very weak	2.526	2.53	20

Table 2

Comparison of the chemical analysis of monsmedite (Götz et al., 1968) with the theoretical compositions of $K_2O.Tl_2O_3.8SO_3.15H_2O$ and of $K_2O.5FeO.2Fe_2O_3.12SO_3.18H_2O$

	Monsmedite	$K_2O.Tl_2O_3.8SO_3.15H_2O$	$K_2O.5FeO.2Fe_2O_3.12SO_3.18H_2O$	
	weight-%	weight-%	weight-%	
K_2O	5.45	6.44	4.58	K_2O
Fe_2O_3	1.16			
Tl_2O_3	28.70	31.25	32.97	FeO+ Fe_2O_3
other oxides[1]	0.50			
SO_3	47.54	43.82	46.69	SO_3
H_2O	16.17	18.49	15.76	H_2O
Total	99.52	100.00	100.00	

1 - MnO+ZnO+CaO+BaO+Al_2O_3

The results presented here show that at least part of the material kept in collections as monsmedite from Romania is as a matter of fact (possibly Tl-bearing) voltaite. Because, with the exception of the chemical composition, the data published for original monsmedite are rather close to those of normal voltaite, a new chemical analysis of type material seems to be badly needed to establish this mineral as a valid species.

Acknowledgements. I heartly thank Dr. V. Gorduza, Baia Mare, and Prof. J. Kiss, Budapest, for working material, and Prof. F. Pertlik, Vienna, for the X-ray investigations.

References

Götz A., Mihalka Şt., Ioniţă I., Toth Z. (1968) Monsmeditul – un nou mineral de taliu de la Baia Sprie. *Rev. Minelor*, 19, 4, p. 154–159, Bucureşti.

Manilici V., Giuşcă D., Stiopol V. (1965) Studiul zăcămîntului de la Baia Sprie (reg. Baia Mare). *Mem. Com. Geol.*, 7, p. 1–113, Bucureşti.

Mereiter K. (1970 a) Der Strukturtyp der Voltaite. *Naturwissenschaften*, 57, p. 670–671.

– (1970 b) Synthese und Gitterkonstanten einiger Selenvoltaite. *Österr. Akad. Wiss., Math.-naturwiss. Klasse, Anzeiger*, 107, p. 239–240, Wien.

– (1972) Die Kristallstruktur des Voltaits, $K_2Fe_5^{2+}Fe_3^{3+}Al[SO_4]_{12}.18H_2O$. *Tschermaks Min. Petr. Mitt.*, 18, p. 185–202, Wien.

– (1974) Die Kristallstruktur von Rhomboklas, $H_5O_2^+\{Fe[SO_4]_2.2H_2O\}^-$. *Tschermaks Min. Petr. Mitt.*, 21, p. 216–232, Wien.

Rom. J. Mineralogy, 1993, 76, 1, p. 99–101

FIRST OCCURRENCE OF ARTINITE AND COALINGITE IN SERPENTINITES OF ROMANIA

Robert-Octavian STRUSIEVICZ

Universitatea "Babeş-Bolyai", Catedra de Mineralogie. Str. Kogălniceanu 1, 3400 Cluj-Napoca.

Key words: Carbonates. Artinite. Coalingite. Serpentinite. Weathering crust. X-ray data. East Carpathians. South Carpathians.

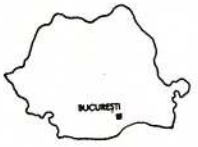

Abstract: Artinite, $Mg_2[(OH)_2/CO_3].4H_2O$, was found in a brecciated-laminated serpentinitic body of the Latoriţa Formation in the Parîng Mountains (South Carpathians). It occurs as very fine needle-like crystals, 1 to 3 mm long, white, translucent, with glassy luster. The X-ray powder diffraction pattern showed 20 peaks that are in perfect agreement with those quoted in JCPDS card No. 6-0484. The strongest lines are 8.20 (30), 5.36 (65), 3.66 (100), 2.736 (20) and 1.920 (24). Coalingite, $Mg_{10}Fe_2(OH)_{24}CO_3.2H_2O$, was found in serpentinites of the Transylvanian Nappe in the northern part of the East Carpathians, at Breaza. It occurs as pseudomorphs after 4 to 5 mm long chrysotile slip-fibers. They very fine (0.02 x 0.005 mm) lamellar aggregates that substitute the chrysotile are pale brown, with resinous luster. Determined refraction indices are $\omega = 1.596$ and $\varepsilon = 1.580$. The strongest lines in the X-ray diffraction pattern are 7.75 (12), 6.00 (35), 4.29 (100), 2.345 (3), in good agreement with JCPDS card No. 22-708. Both artinite and coalingite apear mixed with lizardite, with which they are intimately intergrown. This is the first mention of coalingite in Romania, while artinite was already identified by means of IR spectra in calcitic concretions of the loesses from Dobrogea.

The aim of this paper is to present the discovery of two new minerals for the Romanian serpentinites, i.e. artinite and coalingite. They are typical representants of the surface weathering zone minerals in serpentinites, from which only hydromagnesite is mentioned so far in the literature. Artinite and coalingite are both magnesium compounds with CO_3 and OH radicals, but, depending on their ratio classified to the hydroxides and to the carbonates respectively.

Artinite was found in a sole occurrence (Fig. 1), in the Parîng Mountains, (Central South Carpathians), in a brecciated-laminated serpentinitic body hosted by the Paleozoic Latoriţa Formation (Schuster, 1980). This formation represents a metamorphosed ophiolitic melange which contains lenses of serpentinites and metagabbroic rocks in a matrix of calcschists and prasinites (basic tuffs metamorphosed in the greenschist facies). The serpentinitic body in which artinite was found crops out at the sources of the Ştefanu Brook, a right tributary of the Lotru River, immediately below the thrusting plane of the Getic Nappe. This fact explains the advanced cataclasys of the rock, which is transformed in a tectonic breccia penetrated by a multitude of fissures and crevices. Artinite was found in this little crevices (sometimes 2 cm wide), forming crusts on their walls.

The crystals appear as massive or divergent aggregats, no more than 5 mm thick, while the crystals themselves are very fine, acicular, 1 to 3 mm long. Due to their extreme small size it is practically impossible to discriminate by simple observation between artinite and aragonite which is also to be found in these crevices (sometimes as crystals of 10–15 mm long). The crystals are acicular, white, translucent, with glassy luster, extremely friable. The identification of artinite was made by X-ray diffraction, which gave 20 reflexions similar to those of the JCPDS card No. 6-0484 (Tab. 1).

Comparing the two data an inversion of intensities between the reflexes 3.66 and 2.736 can be noticed, the latter being the strongest in the JCPDS card, while 3.66 is the strongest in our data. This thing may be well explained by the fact that 3.66 is the strongest line of lizardite which appears as impurity in our sample. Due to the very small quantity of material we could prelevate, no other analyses could be performed on artinite from Ştefanu. This is second mention of artinite in Romania, the first one being that of Gâţă et al.

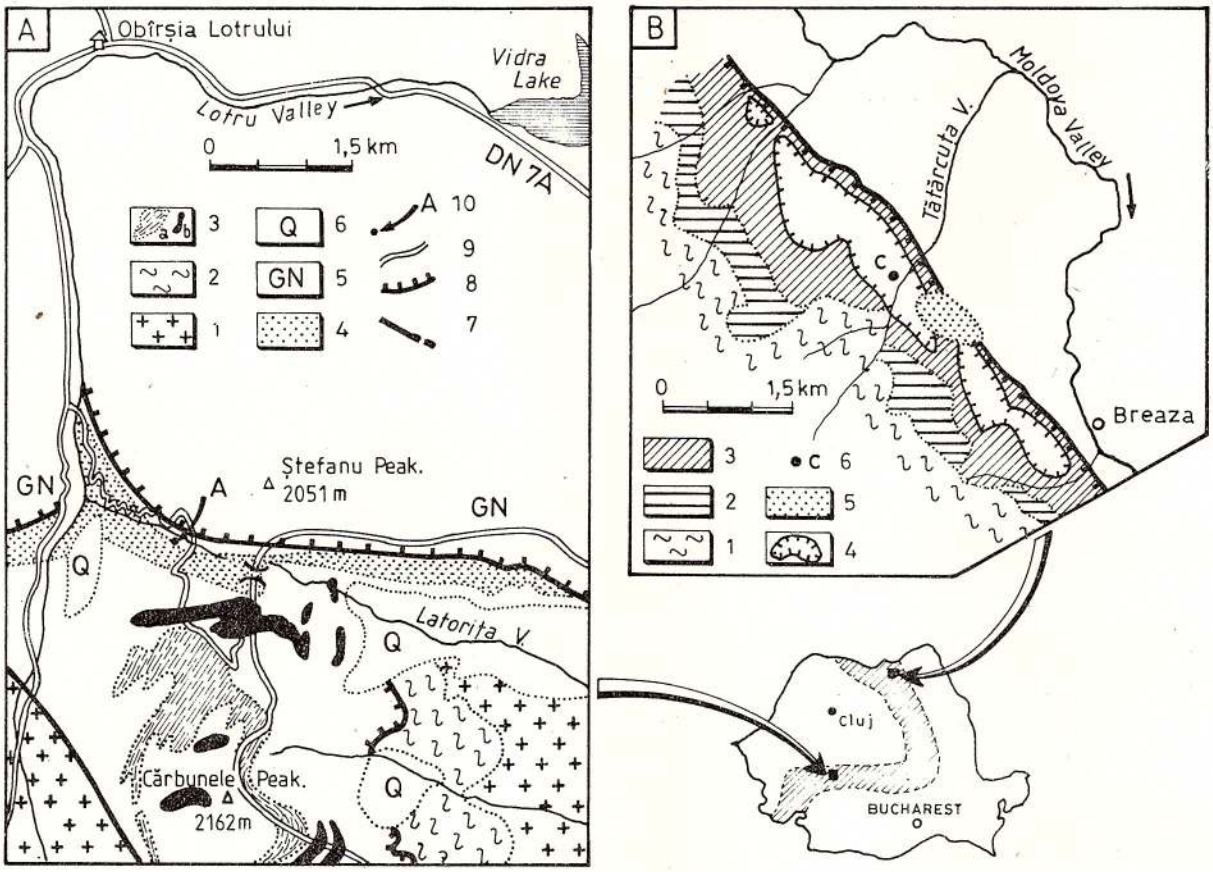

Fig. 1 –Location of artinite and coalingite occurrences.
A. Artinite occurrence in the Parîng Mountains (South Carpathians): 1, Parîng granite; 2, Drăgşan Group (amphibolites); 3, Latorița Formation (prasinites: a) calcschists; b) serpentinites); 4, Schela Formation (black slates); 5, Getic Nappe; 6, Quaternary; 7, fault; 8, overthrust; 9, road; 10, artinite occurrence.
B. Coalingite occurrence in Obcina Mestecăniș (East Carpathians): 1, Crystalline formations; 2, Pre-Barremian sedimentary; 3, wildflysch; 4, lherzolites (nappe outlier); 5, post-tectonic cover; 6, coalingite occurrence.

(1968), who found artinite in paragenesis with calcite in carbonatic concretions from loesses in Dobrogea.

Coalingite was found at Breaza (Obcina Mestecăniș) in the northern part of the East Carpathians (Fig. 1), in fissures of a serpentinised lherzolitic body cut by the Tătărcuța Valley. This Mesozoic ultramafic body is in fact an outlier of the Transylvanian Nappe preserved in the Wildflysch of the so-called Rarău-Hăghimaș Marginal Sincline (Russo-Săndulescu et al., 1982).

Coalingite occurs as pseudomorphs after 4 to 5 mm long chrysotile slip-fibers, which can be very easily taken as limonite coated crysotile. The colour of this fiber is pale brown, with a silky luster on the surface and a resinous one when broken. Only under microscope one can see the 0.02 x 0.005 mm coalingite platelets, arranged like coin columns, oblique to

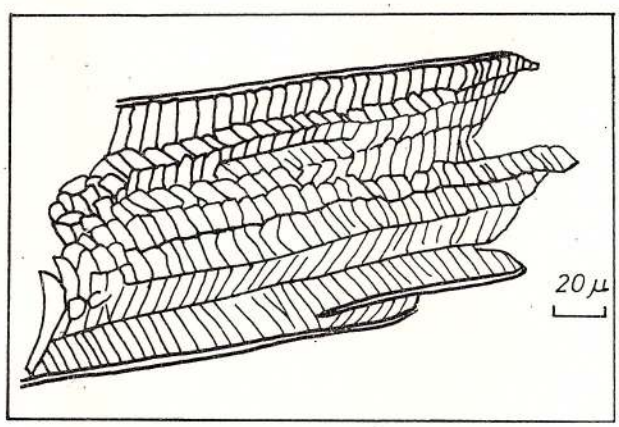

Fig. 2 – Coalingite platelets arranged oblique to the length of the chrysotile fibers.

Table 1
X-ray diffraction pattern of artinite

No.	Artinite, Ştefanu, Parîng Mts		Artinite JCPDS card No. 6-484	
	d	I	d	I
1	8.200	35	8.100	30
2	6.200	11	6.150	16
3	5.360	55	5.340	65
4	4.580	13	4.580	4
5	4.060	8	4.090	6
6	3.660	100	3.690	50
7	3.175	4	3.180	10
8	3.050	10	3.040	16
9	2.820	6	2.800	16
10	2.736	20	2.736	100
11	2.675	15	2.672	20
12			2.428	2
13	2.350	4	2.360	8
14	2.295	10	2.290	12
15			2.271	20
16			2.225	2
17	2.205	7	2.218	4
18	2.056	4	2.058	6
19	2.049	5	2.051	10
20	1.920	24	1.918	20
21			1.897	2
22	1.859	4	1.865	20
23			1.844	4
24	1.732	4	1.737	16
25	1.702	3	1.707	12

the former direction of the chrysotile fibers (Fig. 2). They exhibit a weak pleochroism from pale brown to reddish brown, very weak birefringence and $\omega = 1.596$, $\varepsilon = 1.580$. X-ray diffraction pattern is very similar with that of coalingite from Muscox, quoted in JCPDS card No. 22-708 (Tab. 2). As one can see, the only marked difference between the two data is the presence of the bride peak cited in the literature at values of 13.2 – 13.4, at values of 14.40 – 14.45 in our sample.

As quoted from the literature, coalingite, firstly discovered in the New Idria serpentinite, near Coalinga, California (Mumpton et al., 1965), is a very common product of alteration in serpentinites, formed mainly at the expense of the pre-existing brucite. Laboratory studies showed that coalingite is formed by the oxidation and carbonation of iron-rich brucite, after exposing the latter to the atmosphere for several months. The same authors mention that artinite and hydromagnesite, that are also found in the weathering zone, are later products, precipitated directly from magnesium-rich ground waters. Although we didn't find artinite and coalingite in the same occurrence, we also assume that coalingite, formed directly on the expense of chrysotile, or by oxidation of brucite, and which we found only in very narrow fissures in the serpentinite, must be a younger phase than artinite which is found in larger fissures and crevices.

Table 2
X-ray diffraction data for coalingite

Breaza (East Carpathians)		Muscox JCPDS card No. 22-708	
d	I	d	I
14.400	10	13.20	10
7.750	12	7.83	5
6.000	35	6.05	30
4.740	2	4.75	10
		4.62	5
4.290	100	4.26	100
2.345	3	2.34	20
1.770	1	1.76	5

The discovery of artinite and coalingite in the two occurrences enlarges the number of surface weathering zone minerals found in the Romanian serpentinites. It is to be noticed that these occurrences can not be the only ones, the two minerals being probably overlooked in many other weathering zones of serpentinites, where they were assimilated with hydromagnesite (artinite) or limonite coatings (coalingite).

References

Gâţă Gh., Gâţă E., Băjescu I., Chiriac A., Kiss Şt. (1968) Mineralogic Nature of Carbonates from some Loesses of Dobrogea. *Ştiinţa solului*, 6/2-3, p. 40–44, Bucureşti.

Mumpton F. A., Jaffe H. W., Thompson C. S. (1965) Coalingite, a new mineral from the New Idria serpentinite, Fresno and San Benito Counties, California. *Am. Min.*, 50, 11-12, p. 1893–1913, Washington.

Russo-Sădulescu D., Udrescu C., Medeşan A. (1982) Petrochemical Characteristics of the Mesozoic Ophiolites of the Rarău-Hăghimaş Marginal Syncline. *D. S. Inst. Geol. Geofiz.*, LXVI/1 (1979), p. 153–185, Bucureşti.

Schuster A. K. (1980) Geologische und petrographische Untersuchungen im Danubikum der Südkarpaten, Parîng-Gebirge, Rumänien. (Diss. Th.), 178 p., Clausthal.

Rom. J. Mineralogy, 1993, 76, 1, p. 103–108

ZIRCON TYPOLOGY IN PORPHYROIDS OF THE EAST CARPATHIANS

Hans G. KRÄUTNER, Lucia ROBU, Nicolae I. ROBU, Gabriel BINDEA

Institutul de Geologie şi Geofizică. Str. Caransebeş 1, 78344 Bucureşti 32.

Key words: Nesosilicates. Zircon. Habit. Metarhyolite. Metadacite. Crystallization. Temperature. East Carpathians.

Abstract: The two main porphyroid types of the East Carpathian Mîndra Porphyroids (Cambrian alkali-feldspar metarhyolites) and Pietrosul Porphyroids (metadacites) differ by the contrasting zircon crystal morphology. Zircons from the Mîndra Porphyroids belong to two distinct populations. The most important (88 %) suggests (according to Pupin's typological evolutionary trend diagram) crystallization temperatures of 750–850^0 C in an alkali rich environment of calc-alkaline magmatic series, typical of rhyolites. The second, low populated collectivity (12 %), is consistent with an Al rich environment of crustal (SiAl) type and probably represents zircon crystals included during magma ascension from the gneissic envelope. From the Pietrosul Porphyroids a single homogeneous zircon population was recorded. Its typological evolutionary trend suggests crystallization temperature of 700–800^0 C in an Al rich crustal environment, pointing to an anatectic origin. The mentioned differences cannot be explained only by the chemical differences due to the rhyolitic and dacitic constitution of the rocks. Therefore it seems that the Mîndra and Pietrosul Porphyroids evolved in different geotectonic environments.

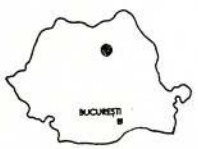

In the crystalline zone of the East Carpathians two types of porphyroids are known, described by Savul, Mastacan (1952) as Mîndra Porphyroids and Pietrosul Porphyroids. These rocks are considered to derive from subvolcanic bodies, intruded in sedimentary educts and subjected together with them to a low grade regional metamorphism.

Mîndra Porphyroids occur only in the southern part of the East Carpathian metamorphics (Borsec-Tulgheş-Pîngăraţi area). They are included in the upper part of the Tulgheş Group, assigned to the Cambrian (Iliescu et al., 1983), and subject to an Early Caledonian regional metamorphism as well as to local Variscan and Alpine overprints. The Mîndra Porphyroids are considered late products of the important Cambrian prevailing rhyolitic bimodal volcanism. They are intruded in the sedimentary sequence of the waning stage developed subsequent to the main volcanic stage, marked by a thick volcano-sedimentary formation (Formation Tg3) with at least five periods of rhyolitic extrusions (Fig. 1).

The Mîndra Porphyroids are represented by metarhyolitic rocks with well preserved relict porphyric structure, marked by magmatic corroded quartz phenocrysts and albite-orthoclase aggregates in idiomorphic forms, preserved from the initial high-temperature alkali feldspars. According to the normative mineral composition, the rocks derive from alkali feldspar rhyolites (Fig. 2). The metamorphic overprint produced a partial recrystallization, destruction and mobilization of the quartz phenocrysts; decomposition of the high temperature anorthoclase in albite+orthoclase as stable low temperature forms in the greenschist facies; chloritisation of biotite; total recrystallization of the groundmass following the general metamorphic schistosity. Polymetamorphic overprints may be recognized locally, either by a late growth of stilpnomelane in static condition or by dynamic retrogressive alteration due to Variscan and/or Alpine shearing.

The Zr content of the rocks ranges between 100–280 ppm (mean value of 15 spectral analyses $\bar{x}$ = 211 ppm). Two distinct populations of zircon crystals with unequal quantitative distribution may be distinguished: a) various coloured (colourless, light- and dark-pink, light- and dark-brown) crystals are predominant. They show evident overgrowth zones, various thin needle-like or globular inclusions and a morphology dominated by prisma faces, with prevailing (100) on (110), subordinate pyramid faces with preferential development of (101) and only accidental presence of (211) faces; b) limpid, light-pink, unzoned and nuclei-

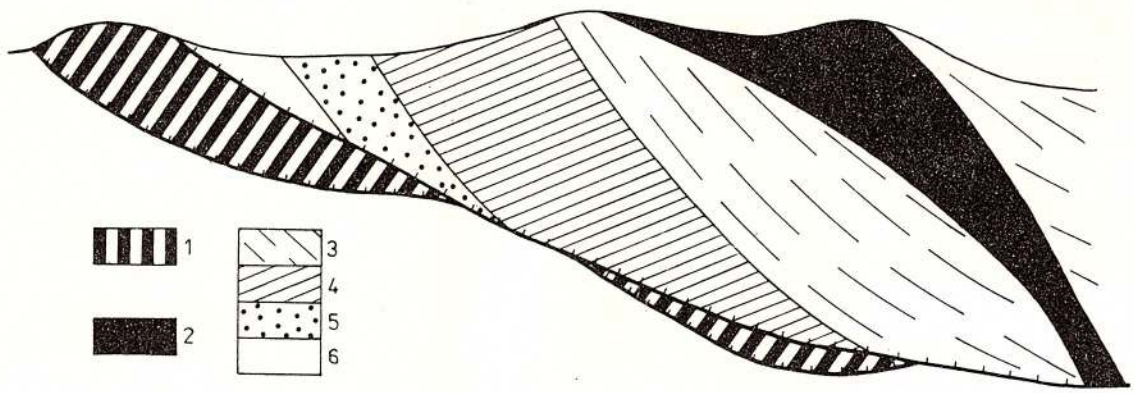

Fig. 1 – Pietrosul Porphyroids and Mîndra Porphyroids in their geological setting (model representation).
1, Pietrosul Porphyroids; Tulgheş Group (Cambrian): 2, Mîndra Porphyroids; 3, Formation Tg_4; 4, Formation Tg_3; 5, Formation Tg_2; 6, Formation Tg_1.

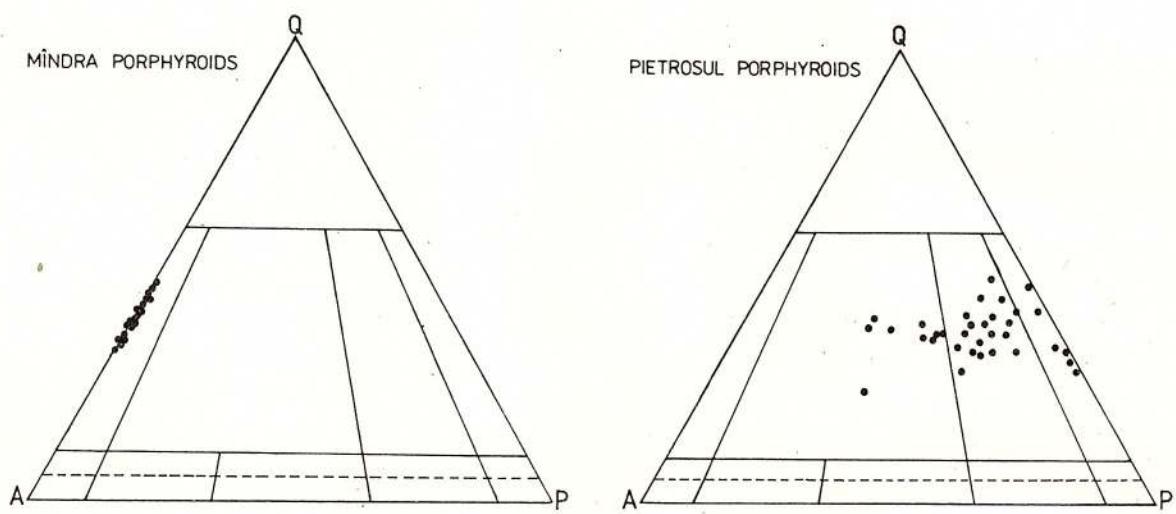

Fig. 2 – QAP (Streckeisen) diagram for volcanic rocks.

less crystals with few, mainly needle-like inclusions and simple morphology – predominance of (100) on (110) prisma faces and of (211) on (101) among the pyramidal faces.

Pietrosul Porphyroids are widespread over the whole area of the East Carpathian crystalline. Unlike the Mîndra Porphyroids they occur only in tectonic slides, depleted of their envelope derived from sedimentary educts (Fig. 1). Thus no primary relationships with other metamorphics of the East Carpathians may be implied for age estimation. Balintoni, Gheuca (1977) advocated a normal lithostratigraphic position, above the Negrişoara Formation (of unknown age), suggesting a subaerial emplacement (predominantly lava flows) (Balintoni, Neacşu, 1980). K-Ar ages ranging between 311–70 Ma have been recorded on biotite and whole rock samples (Kräutner et al., 1976). Tentative interpretations based on a K-Ar isochron for biotite suggest 500 Ma for the main metamorphic event. Isolated zircon lead ages of 473±42; 414±42 Ma were

recorded by Sherbak (unpubl. data). It was presumed that the Pietrosul Porphyroids could be an equivalent of the upper part of the Precambrian Rebra Group (Balintoni, Gheuca, 1977) or of an unknown metamorphic sequence, but an equivalence to an early part of the Tulgheş Group cannot be excluded.

Tectonic slides of Pietrosul Porphyroids, in some places of remarkable rock volumes (e.g. Pietrosul-Budacu lineament; Svaiţeria slide), over the whole area of the East Carpathians and in several pre-Alpine and Alpine tectonic units (mainly nappes), suggest an extended source area. Thus a rather homogeneous lithological body or a dyke swarm, extended over a length of over 150 km, may be suspected as source for the mentioned tectonic slides.

The Pietrosul Porphyroids are represented by metadacite-metarhyolite (or metagranite-granodiorite porphyric rocks) with well preserved porphyric structure. Relict phenocrysts of magmatic corroded quartz and of reorganised plagioclase (albite) are frequent. The normative mineralogical constitution suggests the mentioned dacite-rhyolitic composition of the primary rocks (Fig. 2). A partial depletion of CaO by metamorphic mobilisation due to albitisation of plagioclase in P_{CO_2} conditions was assumed by Balintoni, Neacşu (1980).

Compared to the Mîndra Porphyroids a higher intensity of the main metamorphism is suggested by a larger recrystallization of the groundmass, a more penetrative schistosity, and the constant and abundant development of biotite on the mentioned schistosity. Polymetamorphic features may be locally recognized by partial or total chloritisation of biotite and by structural reorganisation due to dynamic overprint (mainly shearing).

The Zr content of the Pietrosul Porphyroids is sensibly higher than in the Mîndra Porphyroids. It ranges between 200–470 ppm. A mean value of 11 spectral analyses is $\bar{x} = 299$ ppm. Zircon crystals form a single homogeneous population, suggesting a sole evolution stage. They are limpid, with only low colour variation, unzoned and nucleiless. The morphology is dominated by prism faces of variable extent; (100) faces prevail over (110) faces. The less developed pyramidal faces are preferential (211) and only subordinate (101).

Statistical Evaluation of the Zircon Morphology. From a sample of Pietrosul Porphyroids (Bistriţa Valley at Zugreni) and a sample of Mîndra Porphyroids (Baratu Mare Valley at Tulgheş), 100 zircon crystals have been recorded according to the models given by Pupin, Turco (1972), Pupin (1980). Data are represented in the typologic morphologic classification proposed by Pupin, Turco (1972) (Fig. 3) and in the typologic evolution diagram (IT-AT) (Pupin, 1980) (Fig. 4). The mentioned homogeneous population, especially in the Pietrosul Porphyroids, confirm the previous statements (Pupin, Turco, 1981) that during low grade metamorphism zircon crystals are preserved without significant morphological modifications. Only rarely edges and slightly rounded tips have been observed. Therefore some information on the primary volcanic rocks may be obtained.

Most of the data on zircon typology refer to granitoids. Unfortunately only few data are available for acid volcanic rocks. Differences between zircon in plutonic and volcanic rocks were mentioned by Pupin, Turco (1981). They are mainly due to the fast cooling of volcanic rocks and the comparatively longer evolution of zircon crystallization in plutonic rocks, both in time and temperature range, as well as in the increasing fluid pressure (Pupin et al., 1978).

The typology method of zircon populations is based on the observed relationships between development of some crystallographic faces of zircon and the chemical and physical properties of the crystallization medium (Pupin, 1980). Alkalies and Al content control the relative development of pyramids (high alkalies = 101 and 301 pyramids; high Al = 211 pyramid) and the crystallization temperature controls the development of prisms (high $T^0 = 100$ prism; low $T^0 = 110$ prism) (Pupin, Turco, 1975). On the typologic evolution diagram, the zircon population plots into fields along differentiation trends, allowing a petrogenetic classification (Pupin, 1980).

Interpretation of the zircon typology. As it is shown in Figures 3 and 4, the zircon populations of the two investigated types of porphyroidic rocks differ by quite contrasting crystal morphology.

Zircon crystals from *Mîndra Porphyroids* belong to two distinct populations. The most important one (88 %) is marked by a clear dominance of (100) pyramid faces and the total (101) predominance of the prisma ones. According to the typologic diagram (Fig. 4), this suggests an alkali rich environment and crystallization temperatures of about 750–850^0 C. This is a common feature of rhyolitic rocks. In spite of the fact that the Mîndra Porphyroids belong to a calc-alkaline magma type (Fig. 5, 6), the maximal frequency plots between the fields of calc-alkaline and alkaline rhyolites (Fig. 4). This probably reflects the relative high alkali content, as it is shown by the Streckeisen diagram (Fig. 2), where the rocks plot in the field of alkali-feldspar rhyolites. The "typological evolutionary trend" indicated in Figure 4 by the arrow is parallel with trends mentioned by Pupin (1981) for both calk-alkaline magmatic series and alkaline series of mantle origin. The second population, quantitatively unrelevant (12 %), suggests by the predominance of (211) pyramids an Al rich environment of crustal (Si-Al) type. Therefore it could represent zircon crystals from gneiss fragments of

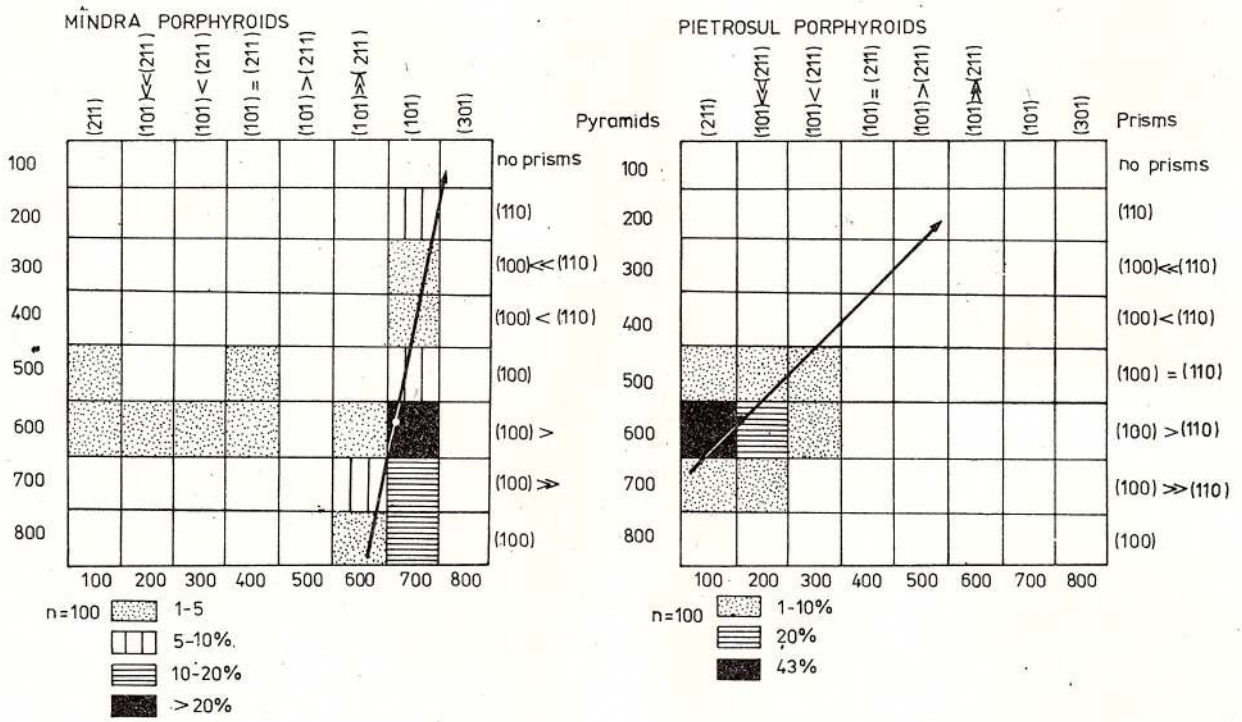

Fig. 3 - Typologic morphologic classification of zircon populations (according to Pupin, Turco, 1972).

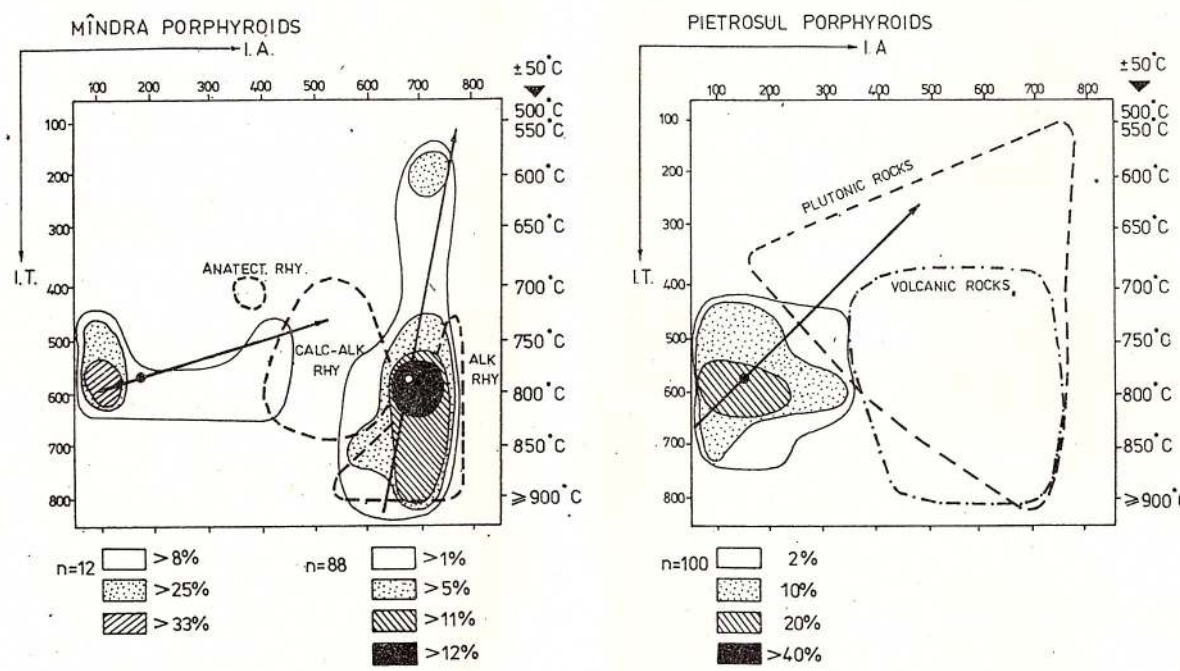

Fig. 4 – Typologic evolution diagram (IT-AT) for zircon populations (according to Pupin, 1980).

the metamorphic envelope, included during the magma ascension. This assumption is supported also by the quite different "typological evolutionary trend" (arrow in Fig. 4), suggesting a change from an Al rich to an alkali rich environment. Therefore it could be assumed that the magma of the Mîndra Porphyroids evolved in an early stage in an alkaline environment (of mantle origin according to Pupin, 1980) and turned later, due to sialic assimilation, to a calc-alkaline trend.

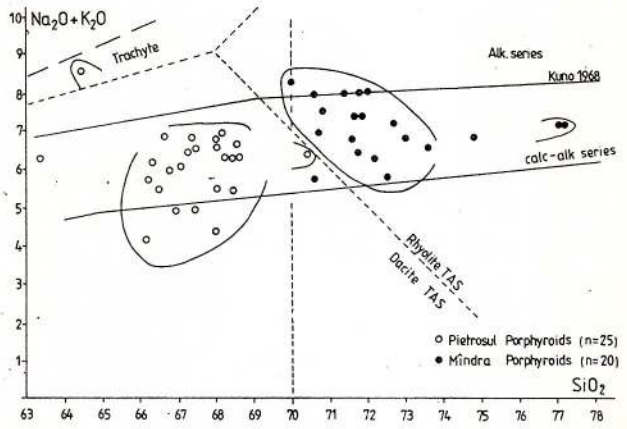

Fig. 5 Na_2O+K_2O/SiO_2 (TAS).
(According to Le Maitre, 1984). Fields for calc-alkaline and alkaline series according to Kuno (1968).

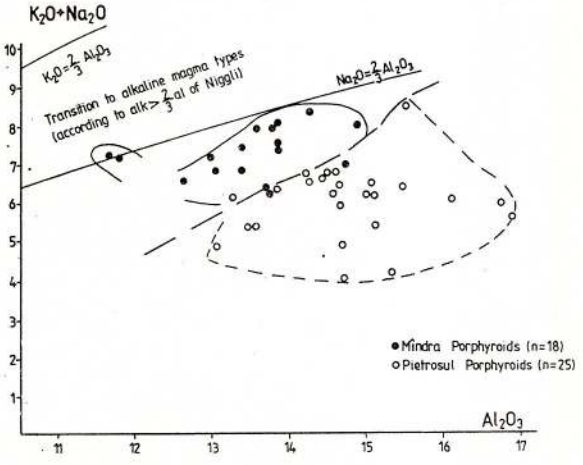

Fig. 6 – Na_2O+K_2O/Al_2O_3 diagram.

Zircon crystals from the *Pietrosul Porphyroids* form a single homogeneous population, characterized mainly by the predominance of (211) pyramid faces. It contrasts strongly with the main population of the Mîndra Porphyroids, but it overlaps with the second, low populated collectivity of the Mîndra Porphyroids. The Pietrosul zircon plots outside the field of volcanic and plutonic rocks (Pupin, Turco, 1981) in the typologic evolutionary diagram. Their position suggests an Al dominated environment and a temperature range between 700–800° C. Its "typological evolutionary trend" is similar to those of aluminous granodiorite-granite associations and is directed towards the field of anatectic melts. According to the mentioned large extension of the primary body (over 150 km) and the zircon typology, it may be assumed that the Pietrosul Porphyroids could be of anatectic origin.

Concluding Remarks. The mentioned differences in zircon typology between the two types of investigated porphyroids can not be explained only by the chemical differences due to the dacitic and rhyolitic constitution of the investigated rocks. It suggests a high discrepancy of the Al:Alkali ratio in the sources as well as a higher thermic regime at the beginning of the zircon crystallization in the Mîndra Porphyroids. Therefore probably different genetic aspects are involved in the contrasting zircon morphology and it seems that the Mîndra and Pietrosul Porphyroids evolved in different geotectonic environments.

The differences between the zircon typology in the Pietrosul Porphyroids and in the products of the Cambrian rhyolitic magmatism related to the Tulgheş Group (Mîndra Porphyroids) support the assumption that the tectonic slides with Pietrosul Porphyroids originated in a different crustal segment, probably with Variscan accretion relationships to the Tulgheş type crust. Later this tectonic framework was reworked in the alpine event.

References

Balintoni I., Gheuca I. (1977) Metamorfism progresiv, metamorfism regresiv şi tectonica în regiunea Zugreni-Barnar (Carpaţii Orientali). *D. S. Inst. Geol. Geofiz.*, LXIII, p. 11–38, Bucureşti.

– , Neacşu V. (1980) Studiul petrografic al unor gnaise porfiroide de Pietrosul Bistriţei. *D. S. Inst. Geol. Geofiz.*, LXV/1, p. 79–100, Bucureşti.

Iliescu V., Kräutner H. G., Kräutner Fl., Hann H. P. (1983) New palynological proofs on the Cambrian age of the Tulgheş Group (East Carpathians). *An. Inst. Geol. Geofiz.*, LIX, p. 7–17, Bucureşti.

Kräutner H. G., Kräutner Fl., Tănăsescu A., Neacşu V. (1976) Interprétation des âges radiometriques K/Ar pour les roches métamorphiques régénérées. Un exemple – les Carpathes Orientales. *An. Inst. Geol. Geofiz.*, L, p. 167–229, Bucureşti.

Le Maitre R. W. (1984) A proposal by IUGS Subcommission on the systematics of igneous rocks for a chemical classification of volcanic rocks, based on the total alkali-silica (TAS) diagram. *Australian Journ. Earth Sci.*, 31, p. 243–255.

Pupin J. P., Turco G. (1972) Une typologie originale du zircon accessoire. *Bull. Soc. Fr. Minéral. Cristallogr.*, 95, p.348–359, Paris.

– , Turco G. (1975) Typologie du zircon accessoire dans les roches plutoniques, dioritiques, granitiques et sienitiques. *Pétrologie*, 1/2, p. 139–159.
– , Bonin B., Tessier M., Turco G. (1978) Role de l'eau, les caractères morphologiques et la cristallisation du zircon dans granites. *Bull. Soc. Géol. Fr.*, 20/5, p. 721–725, Paris.
– (1980) Zircon and granite petrology. *Contrib. Mineral. Petrol.*, 73, p. 207–220, Berlin.
– , Turco G. (1981) Le zircon, minéral commun significatif des roches endogènes et exegènes. *Bull. Minéral.*, 104, p. 724–731, Paris.
Savul M., Mastacan Gh. (1952) Contribuţii la cunoaşterea gnaiselor porfiroide din Carpaţii Orientali. *Acad. RPR, Bull. Şt. (Secţia Bio-Agr.-Geol.-Geogr.)*, IV/2, p. 427–439, Bucureşti.

Rom. J. Mineralogy, 1993, 76, 1, p. 109–119

A CRITICAL STUDY ON CRYSTALLINITY MEASUREMENTS OF KAOLINITES

Mária FÖLDVÁRI, Péter KOVÁCS-PÁLFFY
Hungarian Geological Survey. H-1143 Budapest, Stefánia 14.

Key words: Sheet silicates, clay minerals. Kaolinite. Crystallinity. X-ray data. DTA data. Infrared spectra.

Abstract: Different genetic types of kaolinite were investigated in point of view of crystallinity. The measurements were carried out by different methods of thermal analysis, infrared spectroscopy and X–ray diffraction. The different parameters of degree of crystallinity based on a series of samples were critically studied. The estimated parameters of different methods shows relatively bad correlation. The reason of the difference in the data come from the fact that the methods give informations about the different part and/or features of the mineral structure. The result is better if several parameters are simultaneously used. Different localities of kaolinite were first of all investigated by computer controlled thermal methods. Observation of fine changes in certain parameters such as corrected temperature of thermal decomposition or activation energy for dehydroxylation etc. can be useful for genetic interpretation. One of the model areas was the kaolinite occurrence at Stejera (Romania).

1. Introduction

The occurrence of each mineral in the nature generally indicates different genetical conditions such as temperature, pressure, or concentration of the elements etc. The same mineral may be frequently encountered in environments of different genetics. Conclusions on the genesis and antecendents of a mineral (for instance the temperature during its genesis, the bauxitization, the diagenezis etc.) can be drawn by studying the form of appearance of the minerals. The degree of crystallinity can be a possible genetic feature of clay minerals, in case way of kaolinites.

Various instrumental analytical methods have been known for use in the determination of the polytype modifications, crystallinity and the stage of order of kaolinite (Fig. 1).

When using an X-ray diffraction method, the crystallinity of kaolinites is indicated by the intensity conditions of certain reflections, the shape and "d" value of basal reflections, and the measure of splitting up of reflections that are close to each other (Brindley, Kurtossy, 1961; Hinckley, 1963; Nemecz, 1973).

In the relevant Hungarian specialized literature a new complex figure for use in the X-ray diffraction determination of the degree of cristallinity of kaolinite has been introduced by Tóth (1975). The reflection shifts obtained in various thermal and chemical (K-acetate, hydrazine) treatment procedures are also suitable for the determination of the degree of crystallinity (Wada, 1961; Range et al., 1969). The classification of kaolinite-type minerals based on X-ray diffraction after different authors is presented in following:

	Hinckley-index	
	1	2
Soft type	0.7–1,2	0–1.6 increasing with
Hard type	0.2–0.7	the crystallinity

1. According Hinckley (1963)
2. According Kocsárdy, Heidemann (1980)

On the thermoanalytical methods, mainly the temperature and geometrical parameters of thermal effects appearing on the DTA curve (peak temperature, peak symmetry, peak width, intensity ratios of thermal reactions etc.) can be used to draw conclusions on the stage of order. (Norton, 1939; Caillère, Henin, 1947; Bramao et al., 1952; Murray, 1954; Robertson et al., 1954; Carthew, 1955; Murray, Lyons, 1960; Smykatz-Kloss, 1974 a-b). Murray, White (1949) could distinguish minerals corresponding to different kaolin groups on the basis of the activation energy of the decomposition reactions. Information is also supplied by the mass ratio of the interlayer and lattice waters mea-

thermal analysis

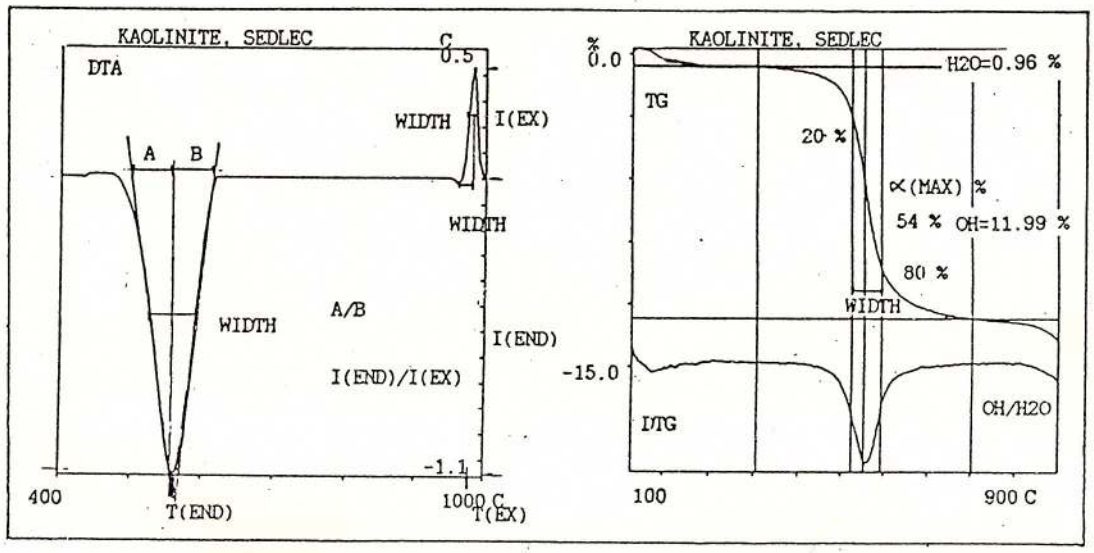

'X- ray diffraction technique

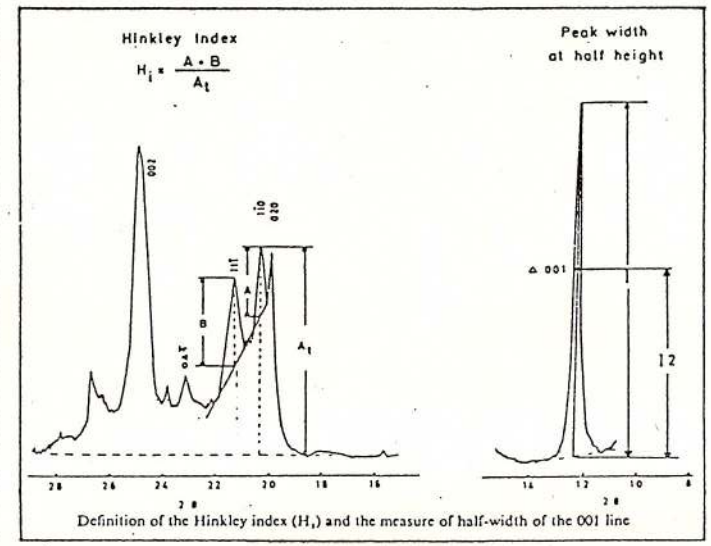

IR spectroscopy

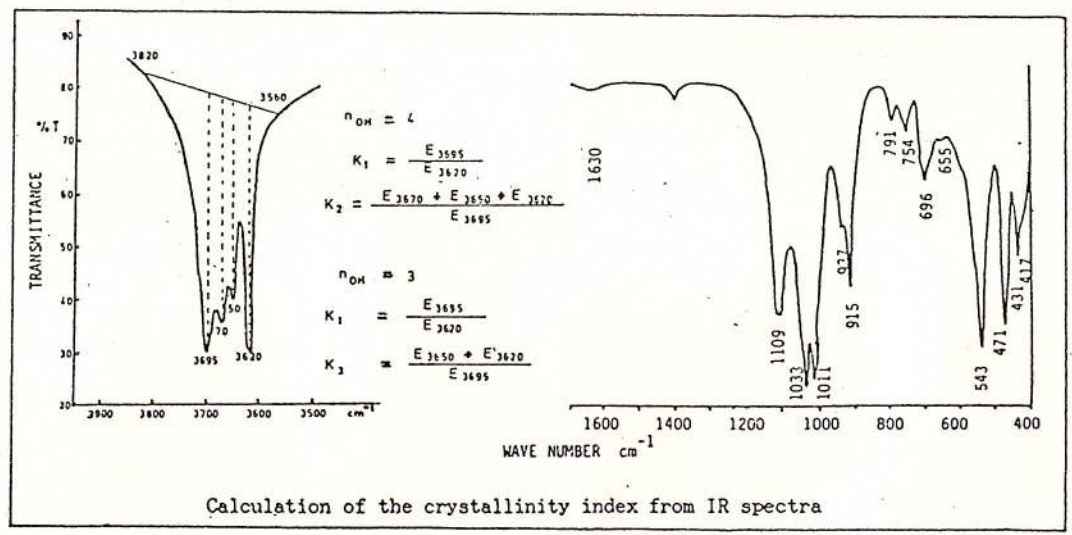

Fig. 6 – Main parameters used in the determination of the cristalinity of the kaolinite from Stejera (Romania).

sured on the thermogravimetric curve. The classification of kaolinite-type minerals based on different kinds of thermal parameters is presented below:

	1	2	3	4	5
	C^0		A/B		C^0
Dickite	680				
Nackrite	660				
Kaolinite	580	> 575	0.78–1.5	0.8–1	980–1005
Fireclay		< 575	1.5–2.4	1.2–1.4	940
Halloysite	560		2.5–3.8	1.8	

1. Peak temperature of thermal decomposition after Mackenzie (1957)
2. Peak temperature of thermal decomposition after Smykatz-Kloss (1974)
3. Slope ratio of the mean endothermic peak after Bramao et al. (1952)
4. Slope ratio of the mean endothermic peak after Robertson et al. (1954)
5. Peak temperature of the exothermic reaction after Smykatz-Kloss (1974)

Kinetic data for the thermal decomposition			
	1	2	3
	Kcal/g-mol (kjoule/mol)		
Dickite	48	(200)	
Kaolinite	38–40	(158–168)	1.06
Fireclay	22–30	(90–125)	
Halloysite	34–37	(142–155)	0.5–0.7

1.-2. Activation energy (isothermal weight loss) after Murray, White (1949)

3. Reaction order (DTA) after Kissinger (1957)

When using IR-spectrometric analysis, the politype modification of kaolinites, as well as the various degrees of crystallinity within the kaolinite are most frequently determined on the basis of the intensity ratios of the OH valence stretching (Lyon, Tuddenham, 1960; Parker, 1969; Reh, 1970; White et al., 1970; Giese, Datta, 1973; Rouxhet et al., 1977; Kocsárdy, Heydemann, 1980; Földvári, Kocsárdy, 1984). Kaolinites can also be featured by the intensity ratios of the OH deformational vibrations (Beutelspacher, van der Marel, 1961), the width of OH valence vibrations, as well as the dimensions of the water deformation band of 1630 cm^{-1} and the valence stretching of 3440 cm^{-1} (de Keyser et al., 1963). According to Gribina et al. (1972) extinction ratio of the lattice vibrations is used to characterize the degree of crystallinity. Classification of kaolinite according to infrared parameters as follows:

	E_{3690}/E_{3620}		
	1	2	3
Dickite	0.6–0.8	0.5–1.1	0.35–0.9
Kaolinite	1.2–1.5	1.0–1.7	1.1–1.8 (in 4 subranges)
Fireclay		1.1–1.5	0.9–1.1
Halloysite	0.8–1		0.8–1.1

1. According to Lyon, Tuddenham (1960)
2. According to Kocsárdy, Heidemann (1980)
3. After Földvari (unpublished data)

When using any of the methods listed above, actually in practice, it is frequently experienced that measurements show a bad correlation. The reason of the difference in the data come from the fact that the methods give pieces of informations about the different parts or features of the mineral structure. A great number of problems arise, when other monomineralic sample is used for the determination of the crystallinity degree of kaolinite. For instance, the application of Hinckley's index is disturbed if the sample has a high goethite or quartz content. In addition, the water content OH ratio cannot be measured, unless the sample contains either clay minerals of 2:1 structure or any other water-bearing mineral. Any interference of accessorial minerals (clay minerals, bauxite minerals, siderite, pyrite etc.) can also disturb the determination carrried out by thermoanalytical or IR-spectroscopic methods.

Our study is first of all based on computer controlled thermal analysis and gives a description of the critical investigation of each method, including the conclusions to be drawn therefrom.

2. Applied methods

For thermal analysis the equipment used is a derivatograph-c: a microcomputer automated apparatus, which is suitable for the simultaneous recording of thermogravimetric (TG), derivative thermogravimetric (DTG), thermogastitrimetric (TGT) and either differential thermoanalytical (DTA) curves. If necessary, the device can also graphically display the DDTG, DDTA, DTGT curves, i.e. curves to be obtained by deriving the primary curves (Paulik et al., 1987).

The mass of the sample measured by the semimicroelectronic and automatic balance of the equipment (sample weight at this study about 100mg).

The temperature of the furnace was regulated by a linear heating program with a 10 C^0 min^{-1} heating rate.

The measured parameters of thermoanalytical curves are the following:

– Corrected peak temperature of thermal decomposition (measured on DTG). This parameter was introduced for the measuring of the crystallinity of kaolinite by the authors of this study, because the temperature of decomposition depends not only on the stage of order or the possible substitution in the lattice (for instance iron), but also on the concentration at the same conditions of the investigation. The so-called "Proben Abhängigkeit" curves show the temperature versus logarithmic concentration in the case

a well-ordered kaolinite and a fireclay after Smykatz-Klos (Fig. 2). The difference in decomposition temperature between the two minerals – in the case of the same concentration – is 28 C^0. A curve with a similar slope has been obtained from our data for a kaolinite sample with bauxite genesis (in the middle).

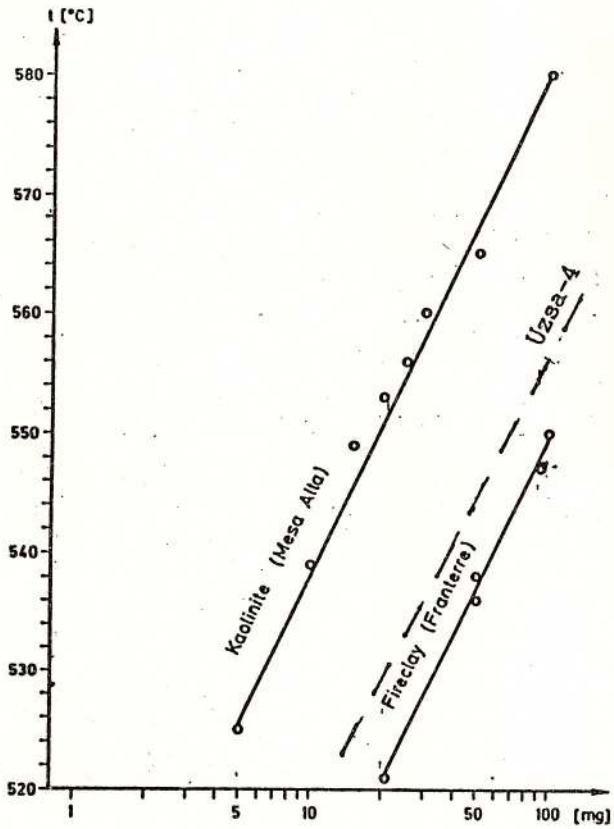

Fig. 2 – PA-curves of different kaolinites – slope of decomposition temperature versus logarithmic concentration (after W. Smykatz-Kloss, 1974). Increasing the concentration by order of magnitude: 42.3^0 C (Mesa Alta); 41^0 C (Franterre); 41.3^0 C (Uzsa-4).

– Width of the endothermic peak: T(0.8–0.2) (Pokol et al., 1985)

– Sharpness of the endothermic peak: $\frac{T(0.8-0.2)}{1/(d\alpha/dt)}$ (Pokol et al., 1985)

– Symmetry of the endothermic peak: A/B or αmax/m

where α = the percentage of decomposed part at the maximum rate of the reaction

The relation between symmetry parameters:

A/B	α_{max}
0.8	45 %
1.0	50 %
1.2	55 %
1.4	58 %
1.8	64 %

– Kinetic parameters for thermal decomposition (calculated from dynamic TG). For data processing and data handling a rich software program is designed in derivatograph-c with the help of which, the calculus of the formal kinetic parameters becomes possible:

– virtual reaction order:

– $n = 1.26 \cdot (a/b)^{1/2}$ (Kissinger, 1957),

– activation energy:

– $E = \frac{n.[ln(1-\alpha_1)-ln(1-\alpha_2)]}{(1/T_1-1/T_2)}$ (Arnold et al., 1987)

– Temperature of the exothermic peak.

– Intensity of the exothermic peak: dT (DTA_{max}–DTA_{min}). Values were obtained after enlargement, base line correction and converted into the same amount of kaolinite. (This value corresponds to the endothermal peak intensity/exothermal peak intensity parameter used earlier by others.).

– Width of the exothermic peak: T (DTA_{max}–DTA_{min})

– Proportion of OH/H_2O

Later, sharpness and reaction order were left out from our analysis, because sharpness greatly depends on the concentration, and order of reaction has – obviously – a rather good correlation with the symmetry.

– Hinckley index and E_{3690}/E_{3620} were parameters used in a recent study for determination of crystallinity of kaolinite by X-ray diffraction and IR spectroscopy.

3. Results

The next step of the critical study was the evaluation of the measurement parameters of a series of kaolinite standards. A major part of the sample studied were from Hungary or a neighbouring country (Tab. 1), having a different genetics, such as post-volcanic hydrothermal (genetic type 1), low temperature weathering (genetic type 2), terrestrial sandstone (genetic type 4), bauxite (genetic type 4), products of thermal spring activities (genetic type 5) etc.

The following statements can be made on the basis of all parameters: in the case of near monomineralic standard samples the OH/H_2O ratio, temperature and activation energy of decomposition reaction, the temperature and intensity of exothermic reaction – not always in the same manner – reflects well the dickite-kaolinite-fireclay-halloysite series, and within this, the specific genetical features of kaolinite, although the iron-oxid contamination on the surface of particles has a great influence on the size and the shape of the exothermic peak. The possible characterization based on thermal data:

- OH/H_2O (see data of table above):

hydrothermal:	> 15
sandstone:	6.3–15
bauxite and weathering:	1.4–8.2
thermal spring:	< 1.2

Table 1
The measured samples in order of OH/H_2O proportion

Locality	OH/H_2O	Genetic type
Dickite, Beregovo (Ukraine)	*	1
Kaolin, Beregovo (1st-class)	*	1
Euroclay (international standard)	69.7	1
China-clay (China)	48.3	1
Sárospatak (Hungary)	47.8	1
"Dickite" Mád-Bomboly (Hungary)	43.5	1
Baia Mare (Romania)	37.3	1
Asztagkő, Mátra (Hungary)	32.6	1
Kaolin, Beregovo (2nd-class)	23.1	1
Kaolin, Mád-Királyhegy (Hungary)	16.9	1
Stejera-Nord: (Romania) (<2μ)	14.8	2
Felsőpetény (201) (Hungary)	13.9	3
Sedlec (Czech Republic)	12.5	2
Felsőpetény (202) (Hungary)	12.3	3
Felsőpetény (205): (<2μ)	12.0	3
Felsőpetény (206): (<2μ)	10.85	3
Stejera: technological sample	10.4	2
Stejera: sandstone (average)	10.0	3
Sárisáp (Hungary)	9.1	3
Alsóőrs (Hungary)	8.1	4
Răzoare (Romania)	7.7	2
Kaolin, Beregovo (3th-class)	7.1	1
Felsőpetény (23)	6.3	3
Stejera: (average)	5.7	2–3
Kolodusszállás (Hungary)	5.7	4
Mesterberek (Hungary)	4.6	4
Uzsa (Hungary): (average)	4.6	4
Tahanovce (Slovak Republic)	4.3	4
Kaolin, Cserszegtomaj (Hungary)	4.2	4
Stejera, gneiss	4.0	2
Stejera: schist	3.5	2
Fireclay, Sofia (Bulgaria)	2.7	?
Bauxite (international standard)	1.4	4
Halloysite, Budapest (Hungary)	1.15	5
Halloysite, Cserszegtomaj	0.7	4–5
Allophane, Venezuela	**	?

* without H2O
** without OH

– Corrected temperature of the thermal decomposition:

dickite:	+ 30 – + 100° C
well ordered kaolinite:	+ 10 – – 10° C
halloysite and little disordered kaolinite:	– 10 – – 20° C
strongly disordered kaolinite, fireclay:	– 20 – – 35° C

related to kaolinite Mesa Alta (Smykatz-Kloss, 1974).
– Reaction order or symmetry of thermal decomposition is not characteristic (confront with literary data)

Activation energy (E):	kjoule/mol
well ordered kaolinite:	120–165
dickite:	105–130
contrary to literary data published by Murray, White (1949)	
little and strongly disordered kaolinite:	105–120
extremly disordered kaolinite (fireclay):	< 100

As clearly shown by the data, the measured activation energy values are lower for dickites than for the well-cristalline kaolinites. This is especially striking when we deal with samples taken from the same locality (for example Beregovo or Mád).

Kaolinite (Beregovo) (1st class)	161.5 kjoule/mol
Kaolinite (Beregovo) (2nd class)	154.0 kjoule/mol
Kaolinite (Beregovo) (3th class)	143.9 kjoule/mol
Dickite (Beregovo)	130.3 kjoule/mol
Kaolinite (Mád)	124.8 kjoule/mol
Dickite (Mád)	105.5 kjoule/mol

These data are contrary to those published by Murray, White (1949). As experienced by Stoch, Waclawska (1981) for dickites, the dehydroxilation process can be devided into two stages having a difference of approx. 20 % in activation energy. The introduction part that relates to the exit of one-third of the OH groups has an activation energy corresponding to that of poor-crystalline kaolinites, whereas the second part has indicated values corresponding to the well-crystalline kaolinites. The value of activation energy we have measured obviously corresponds to the average of them.

– Temperature of exothermic peak:

dickite and well ordered kaolinite:	> 985° C
halloysite and little disordered kaolinite:	970–990° C
strongly disordered kaolinite and fireclay:	< 970° C

Intensity of exothermic peak:

halloysite:	> 1.2
dickite and well ordered kaolinite:	0.5–1.3
little and strongly disordered kaolinite:	0.2–0.55
extremly disordered kaolinite (fireclay):	< 0.2

– According to the width of the exothermic peak only a few conclusions can be drawn, however, it is clear that the exothermal peak of fireclay and halloysite covers the greatest temperature range.

As far as data obtained through an IR-spectroscopy (Tab. 2), for a first approximation, they do not reflect the sequences obtained by using thermoanalytical measurement. The major problem is the well-crystalline kaolinite, which has low crystallinity index. An explanation of this contradiction, that kaolinite and dickite have the two extreme intensity ratio because dickite according its structure, has more OH in internal position than kaolinite. The intensity values of the band at 3620 cm^{-1} compensate each other in the well-

crystalline kaoline samples, which always contain more or less dickite and the measurement value will shift into a range for poorly-crystallized kaolinites.

Table 2
The measured samples in order of Infrared K and X-ray Hinckley index

	(K = E_{3690}/E_{3620})	Hinckley
1 Dickite Beregovo		1.32
1 China-clay		1.13
1 Beregovo 1st		1.00
2 Stejera Nord (gneiss)		0.90
1 Euroclay		0.85
2 Georgia (USA)	1.74	
2 Sedlec	1.71	0.83
2 Stejera (schist)		0.81
4 Alsóörs	1.52	
3 Felsôpetény 205 (<2μ)	1.44	0.83
3 Felsôpetény 206 (<2μ)	1.43	
3 Sárisáp	1.39	
3 Felsôpetény 204	1.34	
4 Koldusszállás	1.34	
4 Cserszegtomaj	1.30	
1 Mád-Bomboly (dickite)	1.28	0.79
1 Beregovo 2nd		0.73
1 Beregovo 3th		0.67
2 Stejera (sandstone)		0.59
2 Stejera (gneiss)		0.45
4 Mesterberek	1.28	
3 Felsôpetény 202	1.28	
2 Stejera (techn.)	1.20	
3 Felsôpetény 23	1.16	
1 Mád-Királyhegy	1.14	0.78
? Fireclay Sofia	0.89	
1 Asztagkô (dickite)	0.63	

Based on those discussed above, it can be stated that a combined application of several measuring parameters would characterize the samples of different genetic.

Further on, a combined analysis of parameters within different occurrences was applied to obtain more detailed information on the development of the deposit.

At the Uzsa Kaolinite Deposit in Hungary Upper Triassic dolomite chimneys and sink-holes contain the kaolin clay which, owing to its elevated position, was not involved in a bauxitization, that took place at other sites at that time. In the area a total of 34 samples from the filling of 2 sink-holes, were subject of a detailed study. For these, only the data from thermal measurements are presented here, since the X-ray measurement of Hinckley's index was greatly disturbed by an interference caused by the high goethite content.

On the basis of the data it can be observed that the tendencies of the two profiles are remarkably different.

For profile Uzsa-4, the data (Tab. 3) concerning the crystallinity of kaolinite show a scattered pattern, only the decomposition temperature indicates a minor increasing tendency towards the depth. However, on the basis of two parameters (OH/H_2O and the temperature of exothermic peak) there are two samples at 18.5 and 19.5 m considerably different from the other samples of the profile and reflecting a higher degree of crystallinity.

Table 3
Measured thermal parameters for the samples of borehole Uzsa-4

m	OH/H_2O	T_d (C^0)	T_{20}–T_{80} (C^0)	α (%)	E (kjoule/mol)	T_{ex} (C^0)
1.5	4.1	–26.1	63.6	carb.	136.1	960.3
2.5	4.0	–25.2	62.1	carb.	141.1	956.1
3.5	4.5	–30.4	64.5	carb.	140.4	953.8
4.5	5.0	–24.6	66.4	57	151.3	974.0
5.5	5.3	–22.0	66.3	57	129.2	968.9
6.5	4.6	–20.4	67.7	56	129.2	968.9
7.5	4.6	–23.8	71.0	54	128.7	966.8
8.0	5.0	–20.6	70.0	57	121.2	966.5
8.5	4.4	–27.3	67.2	56	126.2	954.1
9.5	4.5	–25.1	66.6	55	129.9	964.0
10.5	5.3	–22.7	67.5	58	124.4	961.3
11.5	5.1	–22.1	66.4	56	127.1	961.9
12.5	4.9	–19.3	70.0	52	130.1	966.5
13.5	5.3	–16.7	71.6	55	122.2	974.2
14.5	4.6	–20.6	67.8	56	131.4	965.2
15.5	4.3	–19.6	66.4	58	129.3	962.0
16.5	4.9	–24.1	71.1	53	125.9	960.1
17.5	3.8	–23.4	72.6	52	126.8	966.2
18.5	7.7	–19.8	66.5	54	134.5	989.2
19.5	8.4	–21.1	68.7	56	128.8	980.8
20.5	4.8	–26.6	68.2	50	144.6	962.0
21.5	4.2	–23.3	61.9	carb.	150.3	958.3
22.5	5.2	–18.2	69.0	55	123.7	968.2

These two samples have a goethite content of 5 to 6 %, which is lower than the average of others, and a considerable high hematite content from 20 to 22 %, as compared to an average of 4 % of the other samples (Fig. 3):

	Goethite	Hematite
18.5–19.5 m	5–6 %	20–22 %
average of the others	14 %	4 %

The higher degree of crystallinity of kaolinite, as well as the alteration of goethite into hematite, indicates that these two samples underwent a stronger diagenesis. These data have led to the conclusion that the profiles consist of samples which are transported from different sites and were subject of different processes.

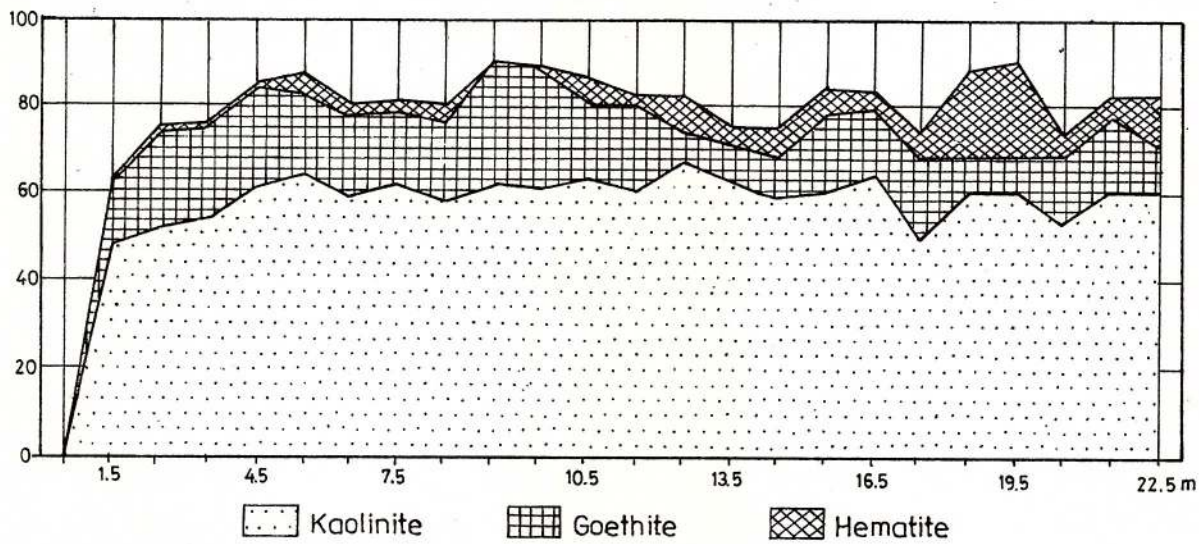

Fig. 3 - Selected mineralogical composition of Uzsa-4 boreholes (Hungary).

For profile Usza-6, which from the point of view of mineral composition is similar to Uzsa-4, the measured parameters usually show a good correlation, showing a gradual change towards the depth (Tab. 4). Samples found at the top in the sink-hole seem to have the highest degree of crystallinity, according to the OH/H_2O ratio, the activation energy, the width and the symmetry of the decomposition reaction as well as the intensity of the exothermic peak are not listed in the table. In this profile the transported samples underwent a further kaolinization in the sink-hole.

Table 4

Measured thermal parameters for the samples of borehole Uzsa-6

m	OH/H_2O	T_d (C^0)	$T_{20}-T_{80}$ (C^0)	α (%)	E (kjoule/mol)	T_{ex} (C^0)
1.5	6.2	-26.9	61.0	61	150.2	959.9
2.5	5.7	-24.1	62.0	61	150.7	969.5
3.5	5.6	-20.0	61.0	62	140.9	963.8
4.5	4.2	-22.3	68.8	56	127.1	959.3
5.5	4.5	-23.8	66.3	55	126.8	959.9
6.5	4.0	-22.6	70.0	57	126.1	959.5
7.5	5.3	-26.6	68.0	58	130.1	973.5
8.5	2.7	-22.4	71.0	58	125.3	979.4
9.5	2.9	-27.4	70.0	57	124.9	966.7
10.5	2.1	-25.5	76.5	50	117.1	978.6
11.5	2.4	-26.9	76.5	54	113.5	963.5

The Stejera kaolin deposit is found on the northern slope of the Ticau crystalline block mountains in the NW part of Romania. In this area, the hypergenic weathering of crystalline schists (mainly gneisses) caused kaolinized rocks to develop. As a result of the reworking of these kaolinized rocks, secondary deposits (kaolinite bearing sandstones) were formed at the lower level of the Paleogene.

In the area a total of 55 samples (36 gneiss, 16 sandstone and 3 schist samples) and 15 samples ($<2\mu$ fraction) were studied along 8 profiles. The aim of our study was to determine whether pieces of information are obtained about the mechanism of development by the detailed examination of kaolinites and whether there are differences between the kaolinite mineral of different rocks.

Based on the mineralogical composition the gneiss and sandstone samples were clearly distinguished:

- Gneiss has a comparatively high feldspar content, however, its quartz content is lower than that of sandstones (less than 20 %).
- Sandstone has a feldspar content of 1 to 2 %, and quartz content higher than 20 %.
- Gneisses contain muscovite mica, whereas sandstones contain illite clay-mica.
- The iron content of gneiss is usually less than that of sandstones.
- The micaschist composition is hardly different from that of gneiss. It can be distinguished on the basis of its higher mica content using a macroscopic observation.

In regard to kaolinite minerals, samples have been analized from 4 different aspects which are as follows:

1. Within the gneiss profile:

- the samples, taken at levels that are either subsurface or close to a bed boundary, have the highest kaolinite content, towards the fresh rock the degree of

kaolinization becomes lower (Fig. 4), verifying that weathering took place due to external influences, resulting in an alteration bed different thickness.

width and activation energy of decomposition show that the degree of crystallinity of kaolinite is higher than for the gneiss samples.

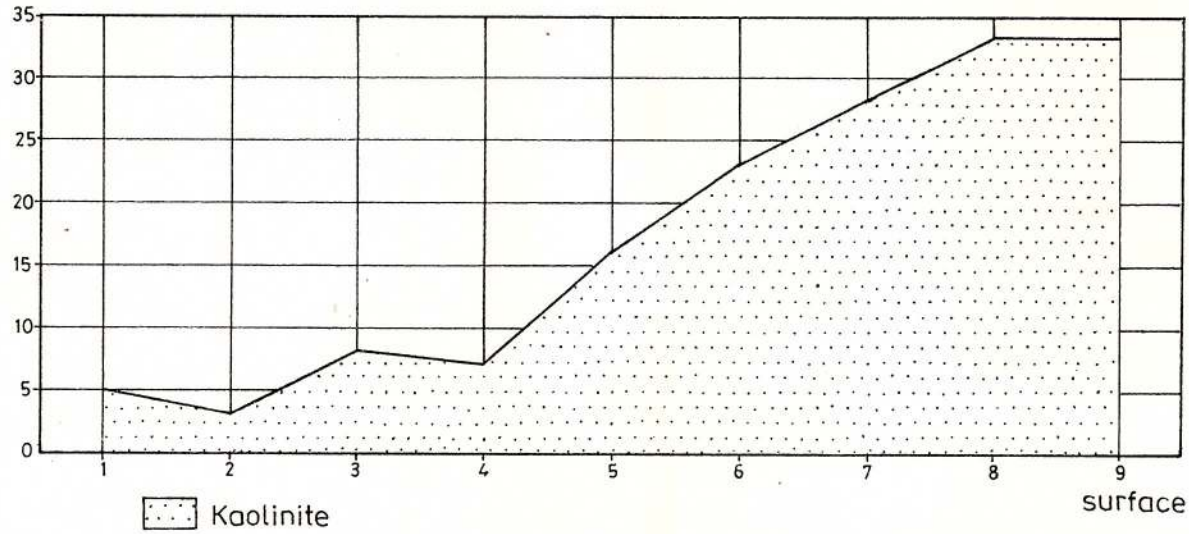

Fig. 4 – Variation of the kaolinite content in the section S. 110 in depend on depth.

– with regard to the stage of order, the value of certain parameters show increasing tendency, simultaneously with the increasing kaolinite content. However in the case of subsurface samples, kaolinites with a lower degree of crystallinity are encountered.

2. Changes within the whole profile:

– The kaolinite content is higher for sandstone than for gneiss rock.

– based on three parameters (width, symmetry and activation energy decomposition reaction) within each profile, the kaolinite has a higher degree of crystallinity in sandstone than in the gneiss rocks of the profile.

– Other parameters show a different behaviour from one profile to another.

– In case of samples macroscopically classified as schist, or found in the close vicinity thereof, the Hinckley's index is striking, whereas the temperature and symmetry of the decomposition reaction numerically indicate that kaolinite has a higher order here than in the gneiss.

3. Average value of various rocks: similar to those which are mentioned before at the profiles.

the crystallinity parameters for kaolinite in sandstone are usually less scattered than those of the gneiss samples.

according to the character of kaolinite there is a significant difference between the width and the symmetry value of the decomposition reaction, in favour of the sandstone.

in the schists, in addition to the above mentioned striking value of Hickley's index, the temperature,

4. Areal separation: in a comparison of all profiles it has been found, that the parameters concerning the degree of crystallinity also show considerable differences according to the areal position of each profile (Fig. 5).

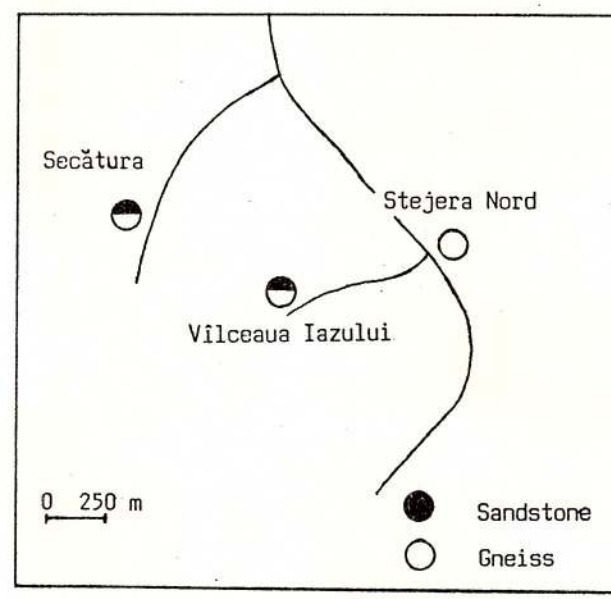

Fig. 5 – Areal localization of kaolin deposit from Stejera (Romania).

For samples from the Stejera Nord profile, the degree of crystallinity of kaolinite is high, according to almost every parameter (Fig. 6).

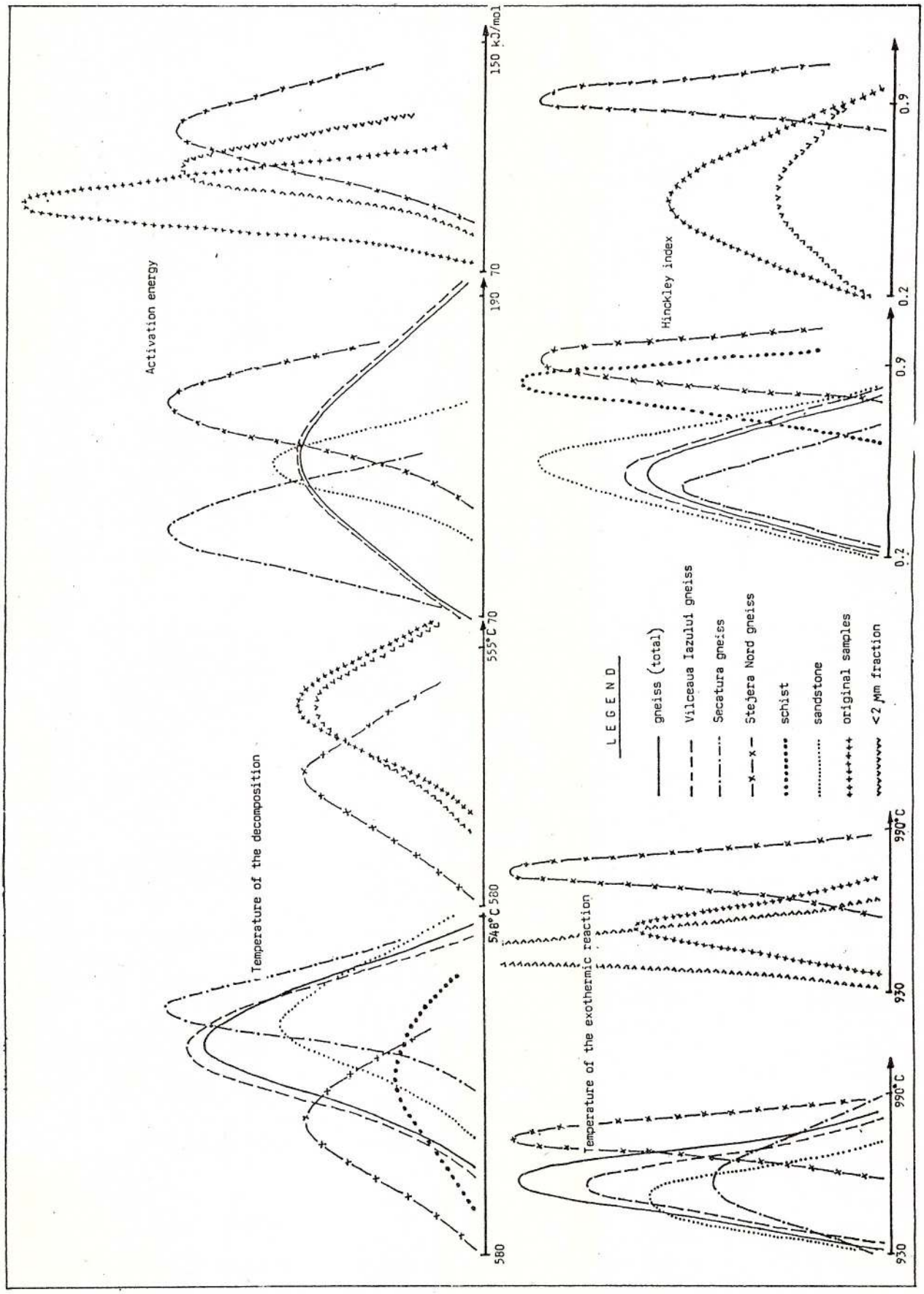

Fig. 1 – Methods of the determination of the kaolinite crystallinity.

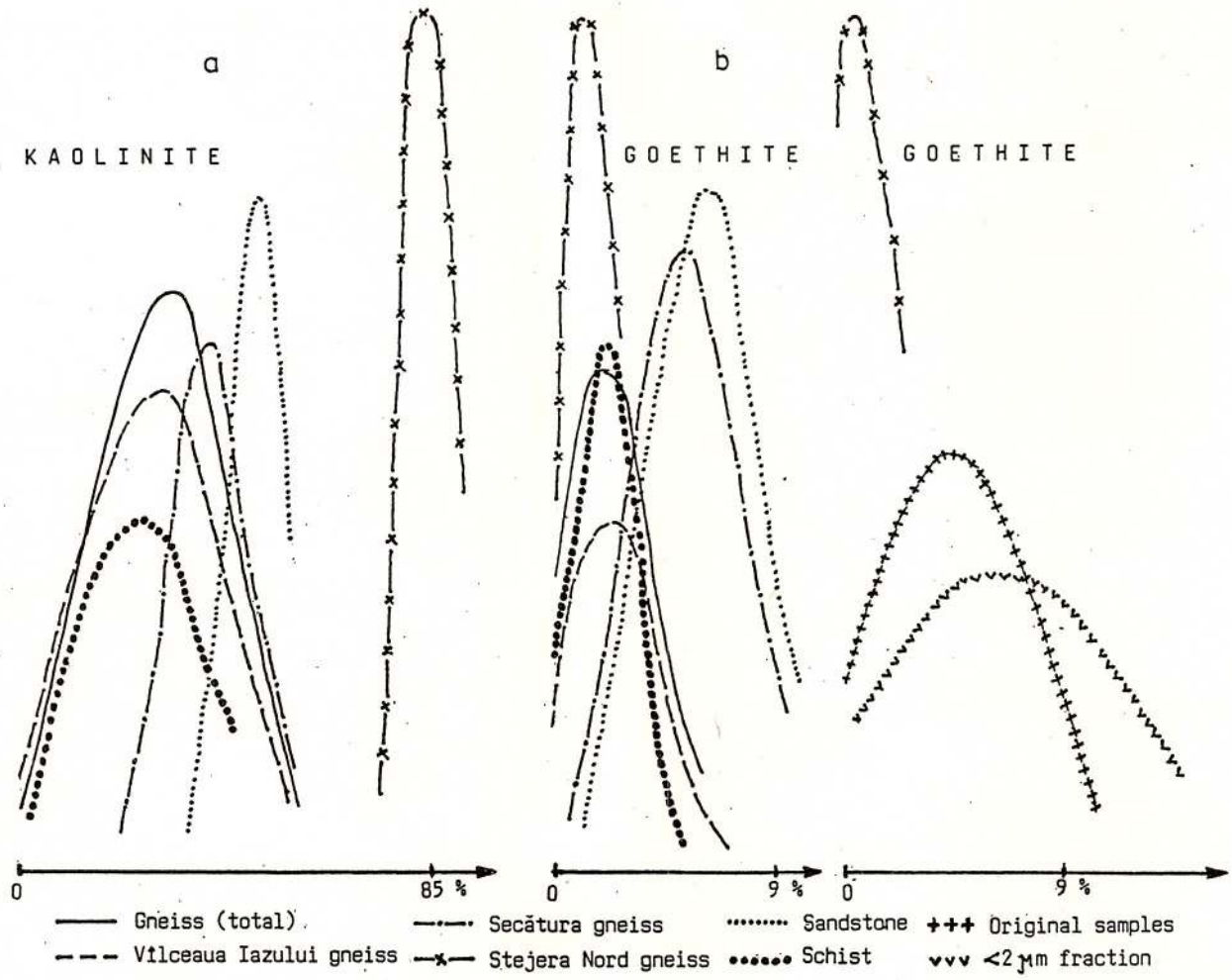

Fig. 7 – Histograms of quantity of kaolinite and goethite for different rocks and part of Stejera kaolin-deposit (Romania).

Though, this is true, that only samples of $<2\mu$ taken from this profile were examined and their parameters generally show a better value, as compared to the data relating to the original samples. However, the difference is less than the areal difference, as shown in the enclosed histograms (Fig. 6) giving a comparison of data on a total of 9 original and separated samples.

Differences are smaller between the same data of Vîlceaua Iazului and Secătura deposit parts Vîlceaua Iazului and Secătura deposits parts to the detriment of the latter.

The areal layout of changes in crystallinity parameters of kaolinite is not directly linked with the kaolinite content, since samples from Secătura have higher kaolinite content, than those taken from Vîlceaua Iazului (Fig. 7/a).

The iron content for Vîlceaua Iazului, especially represented by goethite, is considerable lower than that of Secătura samples. In samples from Stejera Nord, where the wheatered gneiss is not overlain by a Paleogene sandstone bed, the iron content is very low (Fig. 7/b).

Based on this, in the Stejera Nord area the kaolinization dragged on and, as a result, – both quantitatively and qualitatively – a more intensive kaolinitization took place.

The difference between the other two parts of the deposit – as far as the degree of crystallinity of kaolinite is concerned – can be due to the a difference in the degree of a later ironization. Kocsárdy, Heydemann (1980) referred to a similar phenomenon in the examination of samples from the Szegilong kaolin deposit in Hungary.

4. Conclusion

Based on the above mentioned examples it can be stated that in the detailed analysis of each locality,

some parameters that were not significant in the case of kaolinites of the series of standards, can be also very useful. The application of more than one parameter at a time also offers a possibility to observe fine phenomena.

References

Arnold M., Somogyvári P., Paulik J., Paulic F. (1987) The Derivatograph-c. A microcomputer-controlled simultaneous TG, DTG, DTA, TD and EGA apparatus. II. A simple method of estimating kinetic parameters. *J. Thermal Anal.*, 32, p. 679–683.

Beutelspacher H., van der Marel H. W. (1961) Kennzeichen zur Identifizierung von Kaolinit, "Fireclay"-Mineral und Halloysit, ihrer Verbreitung und Bildung. *Tonindustrie-Zeitung und Keramische Rundschau*, 85, p. 517–570

Bramao L., Cady J. G., Hendricks S. B., Swerdlow M. (1952) Characterization of kaolin minerals. *Soil Sci.*, 73, p. 273–287.

Brindley G. W., Kurtossy S. S. (1961) Quantitative determination of kaolinite by X-ray diffraction. *Amer. Mineral.*, 46, 11-12, p. 1205–1215, Washington.

Caillère S., Henin S. (1947) Thermal study of clay minerals. *Ann. agron.*, 17, p. 23–72.

Carthew A. R. (1955) The quantitative estimation of kaolinite by differential thermal analysis. *Amer. Mineral.*, 40, p. 107–117, Washington.

Földvari M., Kocsárdy É. (1984) Factors influencing the IR spectrometric determination of the crystallinity state of kaolinite. *Anual report of the Hungarian Geological Institute of 1982*, p. 417–422, Budapest.

Giese R. F. Jr., Datta P. (1973) Hydroxyl orientation in kaolinite, dickite and nackrite. *Amer. Mineral.*, 58, p. 471–479, Washington.

Gribina I. A., Tarasevich I. I., Pliusnina I. I., Belov N. V. (1972) O spektroskopicheskih proiavleniah neuporiadochennosti structuri kaolinita. *Vestn. Mosk. Univ.*, 27, p. 32–39, Moscova.

Hinckley D. N. (1963) Variability in "crystallinity" values among the kaolin deposits of the coastal plain of Georgia and South Carolina. *Clays and Clay Minerals.*, 11th Conf., p. 229–235.

Keyser W. L. de, Wollast R., Lact L. de (1963) Contribution to the study of OH groups in kaolin materials. *Proc. Int. Clay Conf.*, Stockholm, 2, p. 75–86.

Kissinger H. E. (1957) Reaction Kinetics in Differential Thermal Analysis. *Anal. Chem.*, 29, p. 1702–1706.

Kocsárdy É., Heydemann A. (1980) Characterisation of kaolin minerals of different origin. *Acta Mineralogica Petrogr. Univ. Szeged.*, XXIV, p. 91–99, Budapest.

Lyon R. J. R., Tuddenham W. M. (1960) Infra-Red determination of the Kaolin Group Minerals. *Nature*, 47 616, p. 835.

Mackenzie C. R. (1957) The Differential thermal investigation of clays. Min. Soc. (Clay Min. Group), London.

Murray H. H. (1954) Structural variations of some kaolinites in relation to dehydrated halloysite. *Amer. Mineral.*, 39, p. 97–108, Washington.

– , Lyons S. C. (1960) Further correlations of kaolinite cristallinity with chemical and physical properties. *Clays and Clay Minerals*, 8th National Conference on clays and clay minerals, p. 11–17.

– , White J. (1949) Kinetics of clay decomposition. *Clay Min. Bull.*, 1, p. 84–87.

Nemecz E. (1973) Agyagásványok. Akadémiai Kiadó, Budapest.

Norton F. H. (1939) Identification of clay minerals by d.t.a. *J. Amer. ceram. Soc.*, 22, p. 54–63.

Parker T. W. (1969) A classification of kaolinites by infrared spectroscopy. *Clay Miner.*, 8, p. 135–141.

Paulik J., Paulik F., Arnold M. (1987) The Derivatograph-c. A microcomputer-controlled simultaneous TG, DTG, DTA, TD and EGA apparatus. I. *J. Thermal. Anal.*, 32, p. 301–309.

Pokol Gy., Gál S., Pungor E. (1985) The application of empirical quantities describing the shape of thermoanalytical curves. Proc. 8th ICTA, *Thermochimica Acta*, p. 89–92.

Range K. J., Range A., Weiss A. (1969) Fire-clay type kaolinite or fire-clay mineral? Experimental classification of kaolinite-halloysite minerals. *Proc. Internat. Clay Conf.* Tokyo, 1, p. 197–206.

Reh H. (1970) Ein Beitrag zur Ermittlung des Ordnungsgrades von Kaolinit durch Infrarot-Untersuchung. *Ber. Deutsch. Ges. Wissensch.* B–15, p. 345–361, Berlin.

Robertson R. H. S., Brindley G. W., Mackenzie R. C. (1954) Mineralogy of kaolin clays from Pugu, Tanganyika. *Amer. Mineral.*, 39, p. 118–139, Washington.

Rouxhet F.G., Ngo Samudacheta, Jacobs H., Anton O. (1977) Attribution of the OH streching bands of kaolinite. *Clay Miner.*, 12, p. 171–179.

Smykatz-Kloss W. (1974a) Differential Thermal Analysis – Application and Results in Mineralogy. Springer Verlag, Berlin-Heidelberg-New York.

– (1974b) The determination of the degree of (dis)-order of kaolinite by mean DTA. *Chemie der Erde*, 33, p. 358–364, Jena.

Stoch L., Waclawska I. (1981) Dehydroxylation of kaolinite group minerals II. Kinetics of dickite dehydroxylation. *J. Thermal Anal.*, 20, p. 305–310.

Tóth M. (1975) A new index to characterize the cristallinity degree of kaolinite. *Acta Geologica Academiae Scientiarium Hungaricae*, 19, 1-2, p. 197–213, Budapest.

Wada K. (1961) Lattice expansion of kaolin minerals by treatment with potassium acetate. *Amer. Mineral.*, 46, p. 78–91, Washington.

White J. L., Laycock A., Cruz M. (1970) Infrared studies of proton delocalization in kaolinite. *Bull. Groupe fr. Argiles*, 22, p. 157–165, Paris.

Rom. J. Mineralogy, 1993, 76, 1, p. 121–125

SMECTITE TO ILLITE REACTION IN THE HARGHITA BĂI HYDROTHERMAL SYSTEM (EAST CARPATHIANS)

Iuliu BOBOŞ

Universitatea Tehnică. Str. Stadion 1a, 1900 Timişoara.

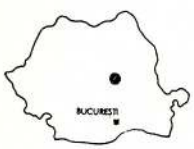

Key words: Sheet silicates, clay minerals. Smectite. Illite. Mineral interlayers. Order-disorder. Hydrothermal conditions. Major elements. X-ray data. East Carpathians – Harghita Mountains.

Abstract: Mineralogical analysis with XRD and bulk chemical analysis of the mixed layer clay mineral assamblages of pervasive argillic alteration from Harghita Băi hydrothermal area (Harghita Mountains) indicate the presence of illite/smectite multiphase with randomly mixed layer (R=0) and ordered (R=1 or R=3) mixed layer. Fluctuating temperatures of hydrothermal convective system were thermodynamically controlled and produced a multiple reaction series by which mixed layer might form. The random layer (R=0) contains more expandable layers and if they are less expandable, layers become ordered. During the smectite-illite reaction random and ordered mixed layers coexist when the expandability is between 40–60 %. Estimation of contents of expandable layers (smectite) was made with method proposed by Watanabe (1981) and the measured peak position differs from those which characterize pure illite/smectite mixed layers. Assemblages containing illite/smectite mixed layers cannot belong to the chemical solution.

1. Introduction

The transformation of smectite into illite is an important mineralogical reaction which includes information about thermic history of argillization rocks in hydrothermal areas. The mineralogical reaction explained by the transformation of smectite into illite has been very controversal in the last decade. The genetic mechanism of the conversion of smectite into illite has been described covering two aspects: a mechanical transformation into solid phase and a neoformation process. Hower et al. (1976) have shown the transformatio mechanism into solid state and considered that transformation of smectite into illite took place by substituting the exchangeable cation interlayer of smectite structure. Nadeau et al. (1985) and Inoue et al. (1980, 1983) advocated the mechanism of neoformation processes which appear through dissolution and recrystallization.

Based on X ray diffraction and bulk chemical analysis on two microns fractions the paper explains the presence of multiphase with random and ordered illite/smectite mixed layers in the Harghita Băi hydrothermal area (Harghita Mountains). Mineralogical reaction of transforming dioctahedric smectite into illite/smectite mixed layers with different ordering degree occurred together with temperature rise (over 70^0 C) and continued due to temperature fluctuations generated under different hydrothermal conditions.

2. Geological Setting

Harghita Băi hydrothermal area represents the most important field of andesite and/or microdiorite rocks of Neogene volcanism in the East Carpathians. The argillic alteration of this area represents the effect of the action of the meteoric convective system which has been controlled in the first phase by the evolution of deep geothermal systems (porphyry copper ?) and also in a late phase by post-intrusive north-southwards oriented fracture system, which permitted the circulation of hydrothermal solutions and amplified the intensity of the argillisation process. The eruptive structure Harghita Băi consists of a deep andesite-dacite formation succeeding important andesitic rocks formation developed to the surface. The investigated area is situated in an extracraterial zone and joins the upper volcanic compartment (Rădulescu, 1964; Peltz et al., 1986) (Fig. 1).

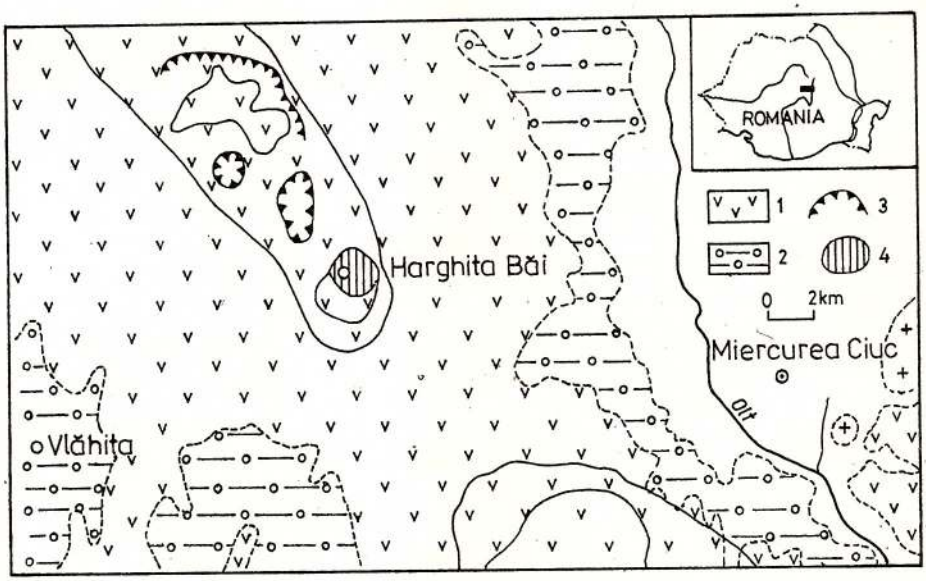

Fig. 1 – The geological sketch with central area of Harghita Mts.
1, upper structural compartment; 2, lower structural compartment; 3, crater;
4, argillization area.

The geological age of the rocks belonging to the upper volcanic compartment has been radiometrically dated (Peltz et al., 1986); the petrographic-volcanologic correlations suggest a Pontian-Dacian age (Al. Szakacs, pers. comm.).

3. Materials and Methods

Clay fractions less than two micrometers have been obtained by sedimentation method and the suspensions have been oriented on glass lamellae (10 mg/cm^2). The fraction separation has been achieved without chemical treatment, excepting some clay fractions achieved by using the NH_4 buffer in the solution. The fractions have been investigated by X-ray diffraction with DRON 2M and PHILIPS PW-1730 (CuK_α anticathode of CuK_α and Ni filter) diffractometer. Recording has been made at speed $1^0=2\theta$. XRD analysis has been carried out using air dried samples and saturated samples with ethylene glycol (T=60^0 C, 8 h.).

The Reichweit values (R) as well as percentage of expandability mixed layers structures have been determined by using the Watanabe diagram (1980, 1981). The percentage of expandability layers below 15 percent of illite/smectite mixed layers has been estimated using the Eberl et al. (1987) diagram plot. The obtained diffraction patterns have been compared with calculated computer patterns and the 2θ values have been correlated with theoretical values for illite/smectite mixed layers with different random and order stage (Reynolds, 1985).

Chemical analyses have been performed by atomic adsorption and flame emission spectroscopy; only illite/smectite mixed layers samples without other impurities have been investigated.

4. Mineralogical Results

The most common mixed layers structure which appears in the Harghita Băi central hydrothermal area is of illite/smectite type. The differences between illite and "illitic material" have been considered according to Srodon, Eberl (1984).

Illitic materials of the Harghita Mountains have been defined from a structural mineralogic views point by Neacşu, Urcan (1978) as representing a hydromica with d_{001}=10.50 Å.

In this paper the X-ray diffraction analysis pointed out the smectite to illite reaction by mineralogical sequence : smectite – smectite/illite mixed layers (R=0) – illite/smectite layers (R=0/R=1) – illite/smectite mixed layers (R=3) – illite.

4.1 Measuring the Expandability

The expandability of the illite/smectite mixed layers has been determined by XRD patterns achieved on ethylene glycol saturated samples. The methods used for measuring the expandability are those published by Watanabe (1980, 1981) and Eberl et al. (1987).

The Watanabe diagram (Fig. 2) used the area between 10.1 Å and 16.9 Å for the illite/smectite components and there are considered in calculus the most sensitive reflexes to the variation degree of ordering. The most sensitive reflexes are at 2θ of 5.1 – 7.6 Å; 8.9–10.2 Å; and 16.1–17.2 Å. The accuracy of determination of the percentage of expandability layers is ±5 percent.

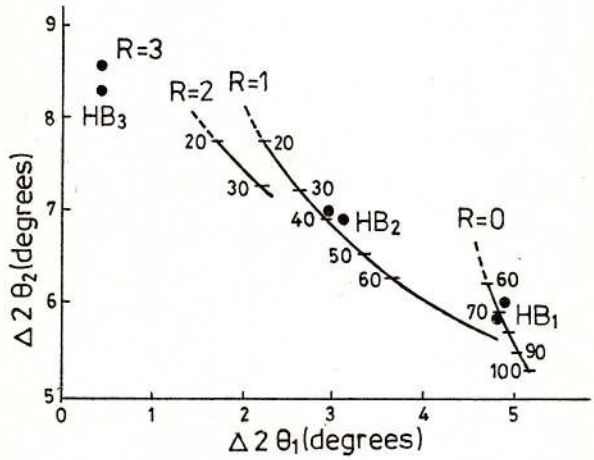

Fig. 2 - The diagram proposed by Watanabe and used for mixed layers illite/smectite. A, B, C correspond with samples HB_1, HB_2 and HB_3.

The structures with over 50 percent expandable layers are due to random (R=0) and below 50 percent to transition into ordered mixed layering (R=1, R=2, R=3). For determination of ordered illite/smectite mixed layers (R=3) where the expandable structures are below 15 % the Eberl et al. (1987) diagram has been used, as shown in Figure 3.

The X-ray diffraction patterns achieved on different illite/smectite mixed layers are shown in Figure 4. The mineralogy by XRD for interstratified illite/smectite minerals of Harghita Băi hydrothermal alteration area is listed in Table 1.

Table 1
Percentage of smectite layers of I/S

Sample	Depth (m)	Mineralogy % smectite
HB-1	-110	80 ± 5, R=0
HB-15	-80	60 ± 5, R=0
HB-18	-64	60 ± 5, R=0
HB-26	-68	45 ± 5, R=1
HB-2	-76	40 ± 5, R=1
HB-30	-55	10 ± 5, R=3
HB-3	-52	6 ± 5, R=3

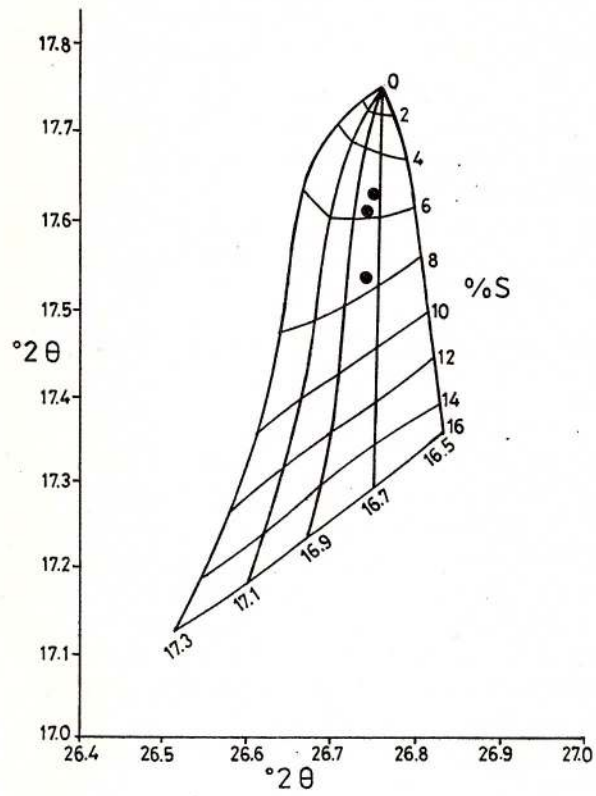

Fig. 3 - The diagram for determination of the smectite layers in illite/smectite (R=3) (after the computer model Eberl et al., 1987). The solid circles correspond to samples HB_3.

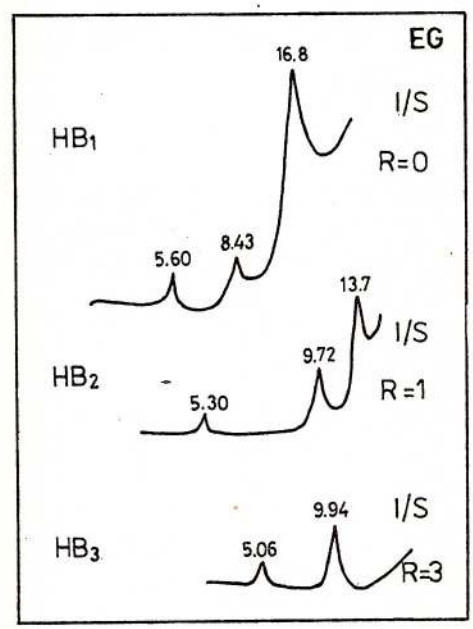

Fig. 4 – X-ray powder diffraction patterns representative for I/S with R=0, R=1 and R=3 of Harghita Băi hydrothermal area.

The expandability varies between 80 % and 6 % smectite layers. Illite/smectite minerals mixed layers with degree R=2 have not been outlined.

4.2 Polytype Transformation of Illite

Polytypes were identified on the XRD patterns of randomly oriented samples and were clearly observed in samples of illite/smectite mixed layers with R=3 (below 15 percent smectite layers); the peaks are typical of 1 M polytype. The 2 M_1 polytype has not been identified.

5. Chemical Analysis of Illite/Smectite Mixed Layers

The bulk chemical composition of illite/smectite mixed layers with different Reichweite values (R=0, R=1 and R=3) are shown in Table 2. Structural formulae were calculated by normalizing cation analysis to a theoretical structure containing $O_{10}(OH)_2$ and are shown in Table 3. Iron has been calculated as trivalent. The main difference is to be observed at the exchangeable interlayer Na^+, Ca^{2+}, fixed K^+ cations and tetrahedric sheet too. Octahedric sheet presents a nearly constant chemical structure.

Table 2
Chemical analysis of illite/smectite from Harghita Băi

Samples	SiO_2	Al_2O_3	Fe_2O_3	MgO	CaO	Na_2O	K_2O
HB_1	54.2	21.14	3.61	2.48	3.14	0.86	0.92
HB_2	56.2	28.60	2.72	0.86	0.24	1.27	5.11
HB_3	47.8	26.40	4.30	1.42	0.61	0.49	6.84

Analyst: Dr. A. Köhler

Table 3
Structural formulae of illite/smectite

Samples	HB_1	HB_2	HB_3
Tetrahedral			
Si^{4+}	3.760	3.41	3.49
Al^{IV}	0.234	0.59	0.51
Sum	4.000	4.00	4.00
Octahedral			
Al^{VI}	1.497	1.66	1.76
Fe^{3+}	0.189	0.19	0.05
Mg^{2+}	0.257	0.08	0.15
Sum	1.943	1.93	1.96
Ca^{2+}	0.234	0.16	0.04
Na^+	0.116	0.16	0.07
Fixed-K^+	0.082	0.44	0.64
Type ordering	R=0	R=0/R=1	R=3

In the randomly illite/smectite mixed layers (R=0) the content of K is very low compared to ordered illite/smectite mixed layers (R=1, R=3). Between the content K of interlayer cation and the content of expandable layers of illite/smectite structures there is an inverse proportionality correlation shown in diagram of Figure 5.

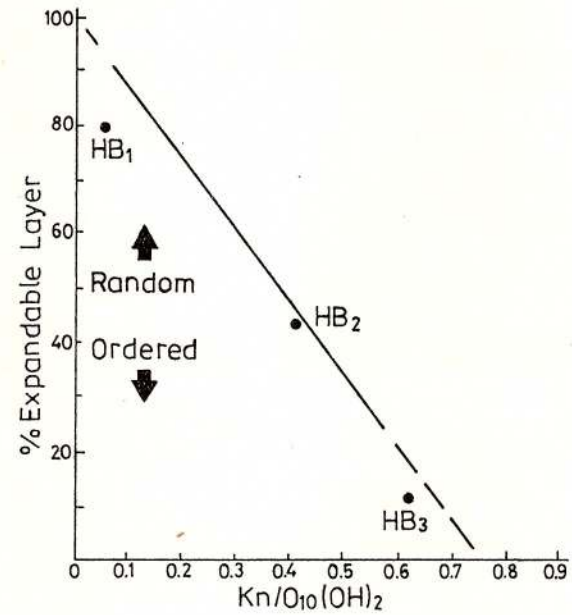

Fig. 5 Relation of percentage expandability layers and fixed interlayer $K/O_{10}(OH)_2$. The solid circles correspond to samples HB_1, HB_2 and HB_3.

Between the content of Si^{4+} and K^+ in illite/smectite mixed layers there is a linear correlation too, explained by three ideal series expressed in the celadonite-pyrophylite-muscovite ternary diagram (Garrels, 1984). These ideal series are shown in Figure 6 by the beidellite-muscovite, montmorillonite-muscovite and montmorillonite-celadonite lines. All our values are plotted in the area between the beidellite-muscovite and montmorillonite-muscovite lines.

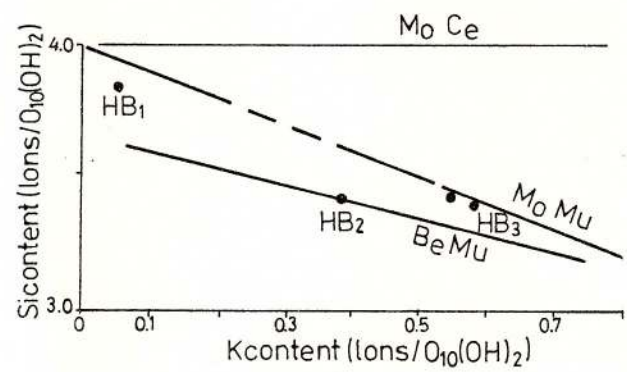

Fig. 6 - The diagram of correlation between K and Si contents.

The HB_3 sample has a high content of Ca^{2+} in exchangeable interlayer cation, a fact that proves the presence of a calcic montmorillonite.

6. Discussions and Conclusions

The mineralogical reaction of conversion of smectite into illite has been demonstrated from the structural mineralogical and chemical points of view. This reaction was recognized for the first time in the Harghita Băi hydrothermal area. The progress of this mineralogical reaction was controlled by the cations composition and the temperature of the hydrothermal solutions. During the reaction, the Na and Ca exchangeable interlayer cations from smectite were changed with K after the following reaction: $M^z + zK = K$ smectite $+ M^z$, where M = Na, Ca and z is ion valence (Inoue, 1983).

The fixing of K under exchangeable interlayer cation in the smectite structure is real and possible at the same time with increasing layer charge (Inoue, 1980). This increasing of the layer charge could be responsible for the K enrichment and fixed in the layer cations of the smectite structure. The illitization of smectite took place through intermediate illite/smectite mixed layers with different degrees of ordering which were recognized in the Harghita Băi hydrothermal area.

A special situation is the lack of illite/smectite mixed layers which are ordered R=2 and $2M_1$ polytype. We explain this by the possibility of producing disturbing in the equilibrium of the chemical and thermodynamic system which produced a stopping of mineralogical reaction to a certain expandability and its replay afterwhile. The illitization reaction stops when K becomes depleted even if the temperature is still sufficient to drive the reaction (Whitney, Northrop, 1988). The rate and nature of the reaction were influenced by the starting material and by K availability.

Three important stages are connected to this mineralogical reaction: the first, in which the expandability is great, and the illite/smectite mixed layers are random, the second, of transition, in which the ordering begins, and the last one, in which the ordering is almost maximal.

Acknowledgements. The author expresses thanks to Iulian Vanghelie for introduction into technical analysis of XRD and Prof. Vladimir Sucha for critical reading of manuscript.

References

Eberl D. D., Srodon J., Lee M., Nadeau P. H., Northrop R. (1987) Sericite from the Silverton Caldera, Colorado: correlation among structure, composition, origin and particle thickness. *Amer. Mineral.*, 74, pt. 9-10, p. 914–934, Washington.

Garrels M. R. (1984) Montmorillonite stability diagram. *Clays and Clay Minerals*, 32, p. 161–166.

Hower J., Esliger E. V., Hower M. W., Perry E. A. (1976) Mechanism of burial metamorphism of argillaceous sediments. 1. Mineralogical and chemical evidence. *Geol. Soc. Amer. Bull.*, 87, p. 725–737.

Inoue A. (1980) The transformation from montmorillonite into illite through their interstratified minerals (unpubl. data).

– (1983) Further investigations of a conversion series of dioctahedral mica/smectite in the Shinzan hydrothermal alteration area. *Clays and Clay Minerals*, 31, p. 401–412.

Nadeau P. H., Wilson M. J., McHardy W. J., Tait J. M. (1985) The conversion of smectite to illite during the diagenesis: Evidence from some illitic clays from bentonites and sandstones. *Mineralogical Mag.*, 49, p. 393–400, London.

Neacşu G., Urcan T. (1978) 10.50 Å, Hydromica, a principal component of Kaolin from Harghita. *St. tehn. econ.*, I-14, p. 107–117, Bucureşti.

Peltz S., Vâjdea E., Balogh K., Pecskay Z. (1986) Contributions to the chronological study of the volcanic processes in the Călimani and Harghita Mountains (East Carpathians). *D. S. Inst. Geol. Geofiz.*, 72-73/1, p. 323–338, Bucureşti.

Rădulescu D. (1964) Contribuţii la cunoaşterea structurii geologice a părţii centrale a Munţilor Harghita. *D. S. Com. Geol.*, L/2, p. 151–160, Bucureşti.

Reynolds R. C. (1985) Program for the calculation of one dimensional diffraction patterns of mixed layered clays. 8 Brook Road, Hanover, NH (published by author).

Srodon J., Eberl D. D. (1984) Illite. *Rev. in Mineralogy, Miner. Soc. of America*, p. 495–544, Blacksburg, Virginia, USA.

Watanabe T. (1980) On the component layer of interstratified illite/smectite. *Sci. Repts., Dept. Geol. Kyushu Univ.*, 13, p. 225–231.

– (1981) Identification of illite/montmorillonite interstratification by XRD. *J. Miner. Soc. Japan Spec. Issue*, 15, p. 32–41 (in Japanese).

Whitney G., Northrop H. R. (1987) Diagenesis and fluid flow in the San Juan Basin. *Am. Journ. Sci.*, 287, p. 353–382, New Haven.

– , Northrop H. R. (1988) Experimental investigation of the smectite to illite reaction: dual reaction mechanism and oxygen-isotope systematics. *Am. Mineralogist*, 73, p. 77–90, Washington.

Rom. J. Mineralogy, 1993, 76, 1, p. 127–128

A NEW OCCURRENCE OF HELVITE IN ROMANIA – OIŢA, BISTRIŢEI MOUNTAINS

Marian MUNTEANU

Institutul de Geologie şi Geofizică. Str. Caransebeş 1, 78344 Bucureşti 32.

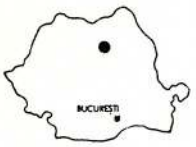

Key words: Framework silicates. Helvite. New occurrence. X-ray data. Infrared spectra. East Carpathians – Bistriţei Mountains.

Abstract: IR and X-ray tests revealed the presence of helvite in the Mn deposit from Oiţa, in greenschist facies metamorphic rocks, considered to have a sedimentary origin. It is associated with rhodonite, rhodochrosite and an anisotropic spessartine. The unit-cell size of a = 8.279 indicates a danalite+genthelvite content of about 10 %. The helvite from Oiţa is the first Be mineral to be recorded in the metamorphic formations of the East Carpathians.

Helvite, $Mn(BeSiO_4)_3S$, has been known in Romania in two localities: Cavnic (Szabo, 1882; Zepharovich, 1893; Cădere, 1927; Helke, 1938) and Roşia Montană (Helke, 1938), both of them in veins of Tertiary volcanics. Unlike them, the new occurrence was discovered in a low grade metamorphic formation from the East Carpathians.

The metamorphic rocks of the East Carpathians were attributed to several thrust nappes. The pile resulted from pre-alpine thrusts has been cut by alpine thrusts, giving rise to four major alpine thrust nappes, each of them comprising the more or less completed suite of pre-alpine nappes, as follows:

– on top, Rarău Nappe which consists of medium-grade Bretila Group;

– beneath, Putna Nappe comprising low-grade Tulgheş Group;

– Pietrosu Bistriţei Nappe including medium-grade Negrişoara Formation and Pietrosu Bistriţei porphyroid;

– at the bottom, Rodna Nappe comprising medium-grade Rebra Group.

Among the above-mentioned formations Tulgheş Group is, by far, the richest one in ore deposits, being divided in four members: the oldest one is quartzose, detrital and barren; the second one is graphitic with Mn deposits; the third one is metarhyolitic with polymetallic deposits; the fourth one is detrital with a bimodal volcanism and barren.

Oiţa is known as a Mn deposit in the northern parts of the East Carpathians mined and quarried in the black quartzites of the second member of Tulgheş Group. It consists of carbonate-silicate Mn ore which turns into oxidic ore in the upper part. Towards its bed, the vicinity of the adjacent schists has been materialized by a greater mineralogical diversity. It is here where helvite occurs, as light green, up to a half centimeter irregular aggregates, with an opaque appearance, a resinous lustre and an uneven fracture. A poor cleavage can be easily noticed. The neighbouring rhodonite, rhodochrosite and spessartine are largely crystallized unlike the mass of the rock which is mylonitic, fine grained. A few crystals of pyrite and galena are scattered around. In thin section the helvite from Oiţa has a high relief, an uneven surface and a greenish shade. It is isotropic and shows no crystallographic shape of its own; it just fills the space left by the other crystals as if it had been the last to form (Pl., Fig. 1). It is usually invaded by an interlacement of acicular crystals (Pl., Figs. 2, 3). The associated spessartine is strongly anisotropic and has a zoned structure (Pl., Fig. 3).

Helvite from Oiţa has been identified by IR analyses (Tab. 1), using a German SPECORD M-80 spectrophotometer, and by X-ray spectrum obtained with a Soviet DRON-3 diffractometer using a Cu-K radiation (Tab. 2). The resulting refined unit-cell size of a = 8.279 was determined with CAPA program (using the least squares method for refinement). According to Clark, Fejer (1976) this unit-cell size would correspond to a relatively pure mineral with a cumulated content of danalite, $Fe_4(BeSiO_4)_3S$, and genthelvite, $Zn_4(BeSiO_4)_3S$, slightly above 10 %. Qualitative electron microprobe investigations have permitted to average a danalite content of about 10 % and a genthelvite one below 1 %.

Table 1
IR data for helvite from Oiţa

Measured values (cm^{-1})	Moenke catalog (cm^{-1})
420	424
536	535
712	706
744	742
770	770
926	930
950	955

Table 2
X-ray powder data for helvite from Oiţa

d_{obs}	$d_{calc.}$ (after Dunn)	h k l
4.152	4.147	2 0 0
3.700	3.709	2 1 0
3.386	3.386	2 1 1
2.616	2.622	3 1 0
2.389	2.394	2 2 2
2.214	2.216	3 2 1
2.070	2.073	4 0 0
1.951	1.955	3 3 0
1.850	1.854	4 2 0
1.806	1.809	4 2 1
1.691	1.693	4 2 2
1.512	1.514	5 2 1

Helvite is not the proper mineral for a deposit like Oiţa. The Mn ore is considered to have a sedimentary origin and the confining rocks are former sediments too. Metamorphism has not exceeded greenschist facies P, T conditions. No igneous or hydrothermal activity is known for miles around. The assumption that helvite would be inherited from a pre-metamorphic material is to be descredited from the very start. It looks more sensible to associate the presence of helvite with fluid circulation from the surrounding silicate rocks into the initial rhodochrosite body. This process is proved by the numerous diaclases filled with rhodonite, dannemorite or quartz and by the skarn-like selvadge from around ore body. In such a hybrid border helvite would be the result of reactions between silica-bearing fluids and silica-poor country rock. Still, the question of beryllium source arises since the helvite from Oiţa is the first beryllium mineral to be registered in the metamorphic core of the East Carpathians.

Acknowledgements. The author is indebted to Mrs. Corina Cristea for X-ray data and Mrs. Gabriela Stelea for IR tests; thanks are due to Mr. C. Vieru who made possible electron microprobe tests and to Mr. Gh. Ilinca and Mr. Şt. Marincea for their usefull advice. The critical reviewing of the manuscript by Dr. G. Udubaşa is especially acknowledged.

References

Burt D. M. (1980) The stability of danalite, $Fe_4Be_3(SiO_4)_3S$. *Am. Mineral.*, 65, p. 355–360, Washington.

Cădere D. M. (1927) Fapte pentru a servi la descrierea mineralogică a României. *Mem. Acad. Rom.*, III, 4, p.151–176, Bucureşti.

Clark A. M., Fejer E. E. (1976) Zoned genthelvite from the Cairngorn Mountains, Scotland. *Mineral. Mag.*, 40, p. 637–639, Londra.

Dunn P. J. (1976) Genthelvite and the helvite group. *Mineral. Mag.*, 40, p. 627–636, Londra.

Hassan I., Grundy H. D. (1985) The crystal structures of helvite group minerals, $(Mn,Fe,Zn)_8(Be_6Si_6O_{24})S_2$. *Amer. Mineral.*, 70, p. 186–192, Washington.

Helke A. (1938) Die jungvulkanischen Gold-und-Silber-Erzlagerstätten des Karpathenbogens. *Archiv. Lagerstättenforsch.*, 66.

Knorring O: v., Dyson P. (1959) Occurrence of genthelvite in Nigeria. *Am. Mineral.*, 44, p. 1294–1298, Washington.

Scott G. R. (1957) Genthelvite from Cookstova Mountain, El Paso County, Colorado. *Am. Mineral.*, 42, p. 425–428, Washington.

Szabo J. (1882) Helvin von Kapnik, ein für Ungarn neues Mineral. *Mag. Tud. Akad. Term. Ert.*, 16, Budapest.

Zepharovich V. v. (1893) Mineralogisches Lexikon des Kaiserthums Österreich. Wien.

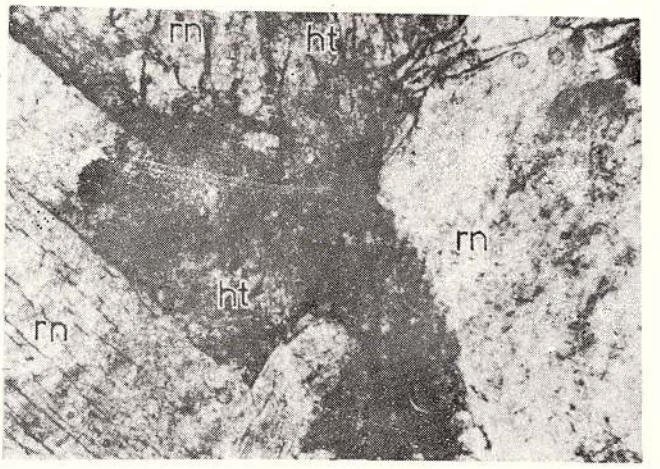

1

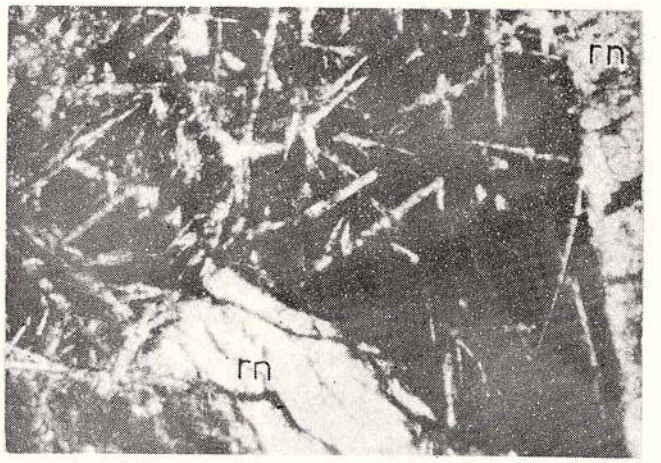

2

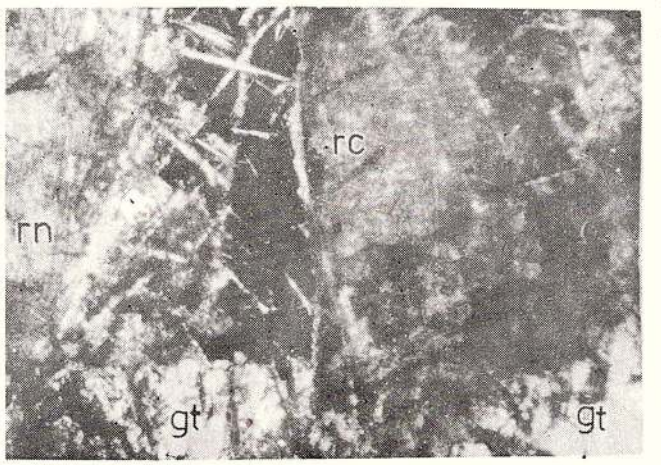

3

Plate

Fig. 1 – Helvite(ht)-center-among rhodonite crystals(rn).
Paraleled nichols. The base of microphoto is 4.15 mm.

Fig. 2 – Helvite(black) with included acicular crystals.
Crossed nichols. The base of microphoto is 1.30 mm.

Fig. 3 – Helvite(black), rhodonite(rn), rhodochrosite(rc) and garnet(gt).
Crossed nichols. The base microphoto is 1.30 mm.

Rom. J. Mineralogy, 1993, 76, 1, p. 129–131

THE PROCESS OF OBTAINING SOME PYROXENIC ROCKS BY PETRURGIC METHODS

Ioan BEDELEAN, Voicu DUCA

Universitatea Babeş-Bolyai, Catedra de Mineralogie. Str. Kogălniceanu 1,.3400 Cluj-Napoca.

Mihaela DUCA

Institutul de Cercetare pentru Sticlă şi Ceramică Fină, "CERO". Str. Treboniu Laurian 1, 3400 Cluj-Napoca.

Horea BEDELEAN

Universitatea Babeş-Bolyai, Catedra de Mineralogie. Str. Kogălniceanu 1, 3400 Cluj-Napoca.

Key words: Chain silicates. Diopside. Synthetic materials. Glass materials. X-ray data. Infrared spectra.

Abstract: This paper presents the results of some experiments in which pyroxenic masses belonging to the CaO-MgO-SiO_2-Al_2O_3 system have been crystallized. The main component synthetized was diopside showing a limited range of jadeite mole percentage. The crystalline phase shows a quite high Vickers hardness (720) and a high chemical resistance (R=0.35 % after boiling for 3 hours in an 1N HCl solution).

Introduction

The performances obtained by melting and recrystallizing basalts are limited as a consequence of chemical instability of iron oxides and of the simultaneous presence of several mineral species whose crystal size is frequently greater than 10 μm.

For the above-mentioned reasons, modern petrurgy was oriented towards obtaining microstructures including a single mineral species with crystals as small as possible. The reduced iron content represents a very important condition imposed to materials of this type.

In the present paper experiments of obtaining pyroxenic rocks with a low iron content are described; the crystalline phase of such rocks is a phase of diopside composition and structure.

Methods and Analyses

The samples used in experiments belong to the Quaternary system CaO-MgO-Al_2O_3-SiO_2, their oxide composition ranging within the limits indicated in Table.

Most of them have an Al_2O_3 content of about 10 %, which enabled us to represent them in a 10 % Al_2O_3 section of the system.

The raw materials used in this experiment were the following: volcanic tuff from Bocşa and Mirşid (Sălaj district), sand from Surduc (Sălaj district), limestone from Baciu (Cluj district), dolomite from Voşlobeni (Harghita district). After weighing, the mixture was melted at 1450^0 C and the resulting glass was subsequently crystallized.

Table

Variation limits in the oxide composition of the synthetical pyroxene rocks

SiO_2	Al_2O_3	TiO_2	Fe_2O_3	CaO	MgO	Na_2O	K_2O
50–65	9.5–10.2	0.1–0.12	0.72–1.21	15–24	10–17	0.47–1.80	1.60–2.20

Among the main elements of the system, Ca^{2+} has the role of stabilizing the $[SiO_2O_6]^{4-}_{\infty}$ anion groups, providing the control of the crystallizing mechanism and the formation of the pyroxenes (Lipovski, Dorofeev, 1972).

The R^{2+} ions association generates conditions for the development of monocline pyroxenes (Han, 1963) and the presence of MgO in masses with low iron content leads to the formation of diopside (Kalinina, 1963).

While calculating the composition of oxides, the existence of the above-mentioned criteria was thoroughly supervised, so that a microcrystalline material consisting of about 90 percent diopside crystals and glassy phase making up less than 10 percent has been obtained.

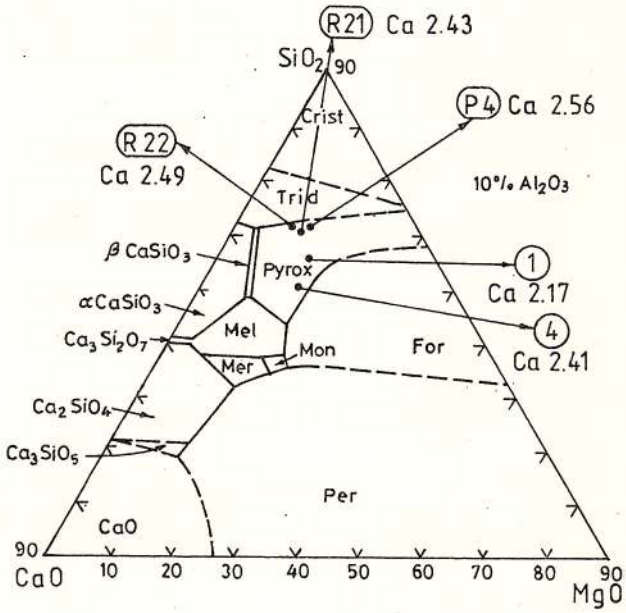

Fig. 1 — The CaO-MgO-Al_2O_3-SiO_2 Quaternary system (10 % Al_2O_3 section of the system) (Phase Diagrams for Ceramists, 1968); The Ca acid coefficient values are specified for the projection of each composition.

The small quantities of Na_2O enable jadeite to form by replacing the (Ca^{2+}-Mg^{2+}) groups with the (Na^{+}-Al^{3+}) groups (Rankama, Sahama, 1970). Pyroxenes are characterized by an extensive isomorphism, so that the jadeite moles can be included in the diopside composition. It is known that diopside may contain up to 30 % mole jadeite (Kalinina, 1963).

The fine-grained aggregate obtained is practically monomineral, a very important condition for generating materials with certain physical and chemical properties. A uniform dilatation of the crystals will prevent the appearance of fissures and tensions in the material.

The nucleator employed was fluorine and chrome-spinel on which diopside crystals up to 3–4 μm in size have formed. The marked tabular habit is a consequence of the ratio [Ca/(Fe+Mg)]>1 (Hietannen, 1971). The diopside crystal aggregate exhibits a nearly continuous developed pellicular vitreous phase (Fig. 2).

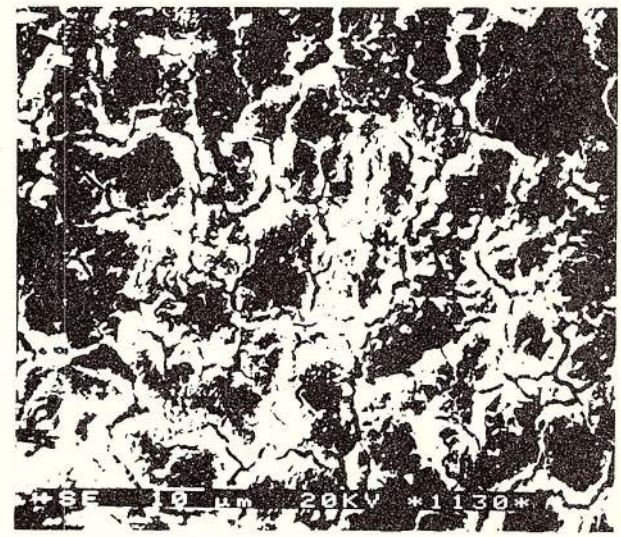

Fig. 2 — Crystals of tabular diopside (D) structured in agglomeration separated by the vitreous phase which is attacked by HF during the corroding process in the mixture (S). (SEM).

If CaF_2 is used, a very long melting interval is to be avoided to prevent fluorine losses. Masses lacking in fluor do not crystallize properly (Ciontea et al., 1977).

The X-ray diffractograms reveal a uniform composition of the samples containing diopside with a small amount of jadeite moles. (Fig. 3).

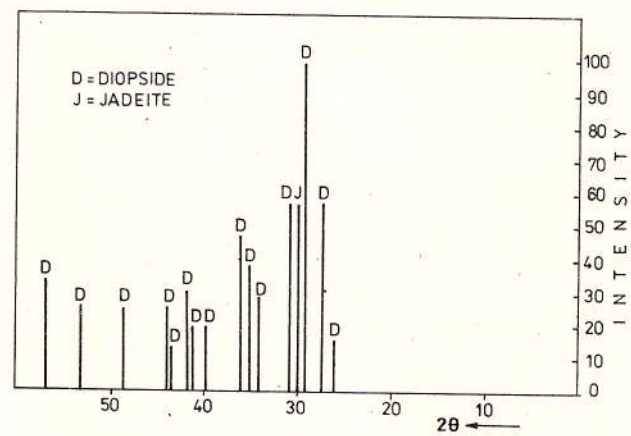

Fig. 3 — X-ray diffractograms of samples from synthetic pyroxene rocks (CuK_α radiation).

The tabular habit of the diopside is a consequence of improper crystallizing conditions. The exotherm peak

of DTA curves proves the existence of a network with a lower degree of ordering through the large bases and the diffuse peak of 945° C (Fig. 4).

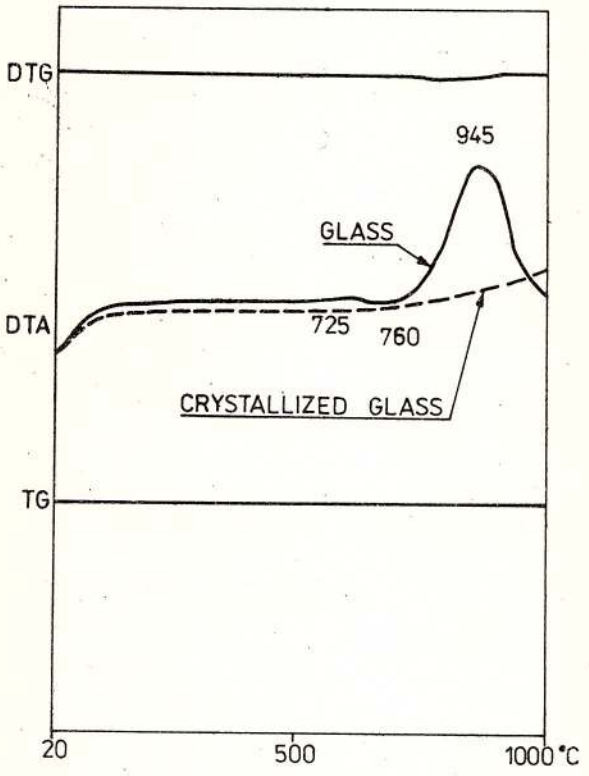

Fig. 4 DTA analysis performed on glass and crystallized glass (dashes).

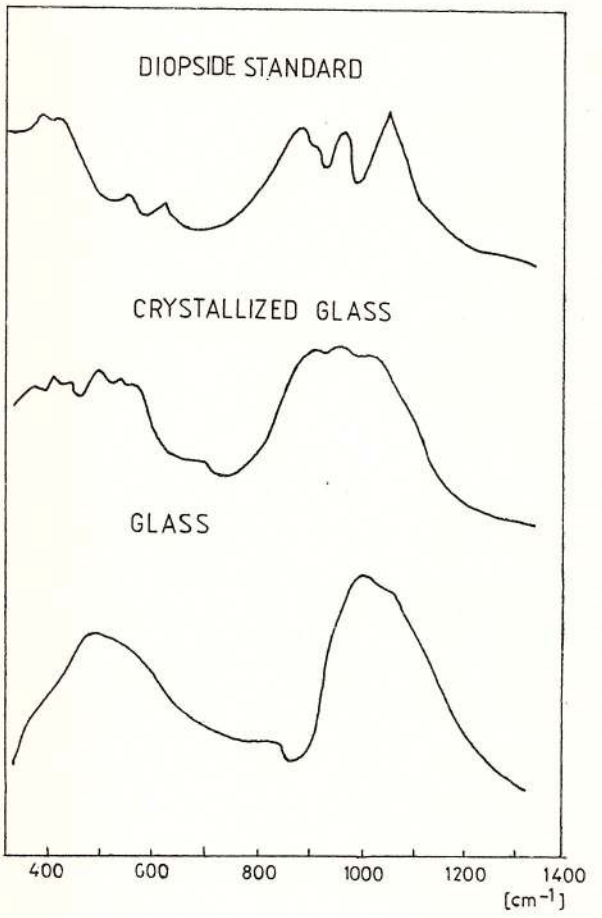

Fig. 5 IR spectra of glass, crystallized glass and standard diopside from Băiţa-Bihor.

The IR spectrophotometry demonstrates that structural glass elements form a network with certain deviations from the standard (diopside from Băiţa-Bihor) during the crystallizing process (Fig. 5).

The obtained microstructure and the presence of diopside as a crystalline phase confers the obtained masses a good chemical resistance (R=0, 35 % after boiling for 3 hours in an 1N HCl solution) and a relatively high hardness H_v=720.

Conclusions

Synthetic pyroxene masses belonging to the CaO-MgO-Al_2O_3-SiO_2 system contain more than 90 % microcrystals, the rest being residual glass. The crystalline phase consists of diopside with a low jadeite content.

Experimental samples have a good chemical resistance and mechanical characteristics which enable us to consider that they may be successfully used in producing isolators, agate substitutes, etc.

References

Ciontea N., Roşca I., Duca V. (1977) Consideraţii asupra vitroceramului de tip Transilvanit. *Materiale de Construcţii*, VII, 3, p. 130–135, Bucureşti.

Han H. C. (1963) Kataliziravanie Kristalizaţia stekla. M-L, p. 3–12, Biblioteca CERO Cluj-Napoca (traducere).

Hietannen A. (1971) Diopside and actinolite from skarn, Clearwater County, Idaho. *Amer. Mineralogist*, 56, 1-2, p. 234–236, Washington.

Kalinina A. M. (1963) Kataliziravanie kristalizaţia stekla. M-L, p. 28–36, Biblioteca CERO Cluj-Napoca (traducere).

Lipovski I. E., Dorofeev V. A. (1972) Osnovî petrurghii. Izd. "Metalurghia", 320 p., Moskva.

Rankama K., Sahama Th. G. (1970) Geochimia. Edit. Tehnică. 791 p., Bucureşti.

*** (1968) Phase diagrams for Ceramists. vol. II, The Amer. Ceram. Soc., Columbus, Ohio, USA, 601 p.

Rom. J. Mineralogy, 1993, 76, 1, p. 133–135

SOME ASPECTS REGARDING THE SYNTHESIS OF PYROXENIC AGGREGATES WITH SPODUMENE

Voicu DUCA

Babeş-Bolyai University, Department of Mineralogy. Str. Kogălniceanu 1, 3400 Cluj-Napoca.

Mihaela DUCA

Research Institute for Glass and Fine Ceramics. Str. T. Laurean 1, 3400 Cluj-Napoca.

Lelia CIONTEA

Technical University, Department of Chemistry. Str. C. Daicoviciu 15, 3400 Cluj-Napoca.

Key words: Chain silicates. Spodumene. Synthetic materials. Glass materials.

Abstract: The paper presents the synthesis of several pyroxenic aggregates in the system Li_2O-MgO-Al_2O_3-SiO_2 using TiO_2 as crystallization stimulator. The product obtained consists of a crystalline phase with more than 90 % spodumene, associated with "silica O". The residual glass covers the crystal as thin films of less than 1 μm in thickness. The thermal expansion coefficient is $3.66.10^{-6}$ C^{-1}.

Introduction

Glass-ceramics represents a group of materials with special properties for various industrial uses. Li_2O-bearing pyroxenic aggregates have been synthetically obtained using a natural starting material (Conţu spodumene) and then sistematically studied.

The product obtained shows a low thermal expansion coefficient.

Experiments and Results

The experimental samples belong to the Quaternary system Li_2O-MgO-Al_2O_3-SiO_2 with compositions ranging within the limits indicated in Table.

Collective concentrate of rutile-anatase extracted from the heavy minerals fraction resulted from the Surduc sand (Sălaj district) was used as crystallization stimulator.

The mixture was melted at 1430–1460^0 C and the obtained glass was subsequently crystallized.

The crystallized samples have a violet colour due to the absorption in the visible domain, produced by the transition Ti^{IV}-Ti^{VI} at 600^0 C (Junina et al., 1974). The oxygen defficiency has appeared as a result of the Al^{VI}-Al^{IV} transition, which enables the aluminium silicates to instabilize. Pavluskin (1979) noticed the mentioned modifications as specific for the glasses with Al_2O_3/Li_2O in which Al-Ti compounds have formed even in the first phase.

SiO_2	Al_2O_3	Fe_2O_3	CaO	MgO	Na_2O+K_2O	Li_2O	TiO_2
62–66	10–15	0.5–0.8	0.4–0.7	3.5–4.9	2.0–5.3	4.0–4.8	2.0–4.8

The raw materials include Cerişor-Lelese steatite, Surduc or Miorcani sand and Conţu spodumene. In order to raise the Li_2O weight percent of the mixture, Li_2CO_3 was added in different quantities.

Generally, the opinions regarding the evolution of nucleation in glasses with Li_2O and TiO_2 are divergent. Authors such as Bezborodov (1982) sustain the appearance of rutile directly from the cooling melt,

whereas Kirsch (1990) notices the formation of the secondary rutile as a result of the decomposition of a solid solution MAT (magnesium alumino-titanate) at 900^0 C. Lee and Davis (1967), cited by Bezborodov (1982), describe the formation of acicular nuclei of $Al_2O_3.TiO_2$ on which spodumene is directly deposited. However, some experimental data show that eucryptite or metasilicate and Li-bisilicate may form prior to spodumene (Pavluskin, 1979; Veisfeld and Seliubski, 1972 cited by Bezborodov, 1982).

Analysing the causes of the initiation of a crystallization process, the existence of defects on the corners and edges of the nuclei is generally accepted. Amato (1973) remarks a migration of the vacancies towards the zones exposed to a compression stress at the boundary between crystal and glass.

The different thermal expansion coefficient is responsible for this type of stress. As a result, the stressed zones within glass become the sites of several crystallization centers (Duca, Duca, 1990 unpubl. data).

Such an explanation may perhaps by extended to the separation limit between glass and the areas with a different composition segregated in drops as a result of the liquation process.

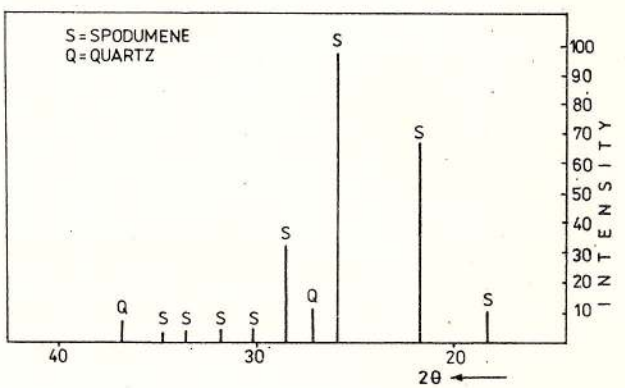

Fig. 1 X-ray diffraction pattern of the pyroxenic synthetic rock (CuK_α radiation).

In the examined sample the high viscosity of the glassy phase has maintained a relict liquated structure (Pl., Fig. 1). The deffects associated with a high viscosity played an important role in crystallization process (Junina et al., 1974). The presence of TiO_2 lowered the value of the surface tension thus facilitating the formation of the crystals (Fedorovski, 1963). Most of the samples present a structure characterized by a uniform crystal size (Pl., Fig. 2).

The X-ray diffraction patterns of the crystallized samples are identical, confirming the presence of spodumene as a main phase, associated with the so-called "silica O". The last one is actually high temperature quartz, fixing Mg^{2+} and Li^+ ions in the presence of Al_2O_3, so that the structure becomes stable upon cooling. One of the peaks corresponding to 2.5 Å has not been identified (Fig. 1). The thermal expansion coefficient of the "silica O" is of 5.10^{-6} C^{-1} (Bezborodov, 1982).

Figure 2 presents the dimensional change of both glass and crystalline sample as function of the temperature, the glass-ceramics has a thermal expansion coefficient of $3.66.10^{-6}$ C^{-1}, for temperature ranging between $20–700^0$ C. The sample with 65 % has the melting point at 1160^0 (Fig. 3).

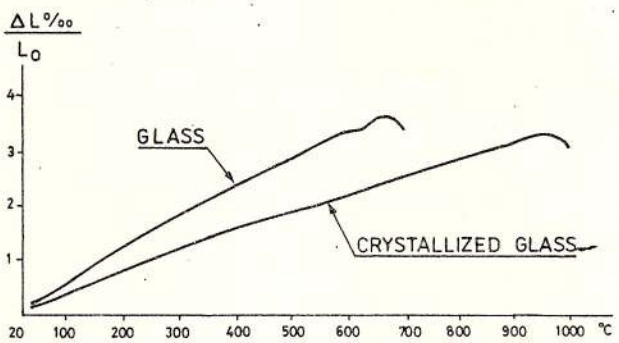

Fig. 2 Dimensional changes for glass-ceramics as a function of temperature.

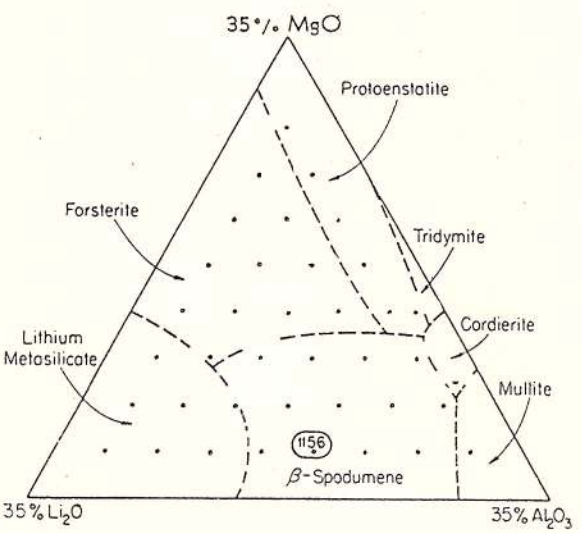

Fig. 3 Melting temperatures of several compositions in the system Li_2O-MgO-Al_2O_3-SiO_2 corresponding to the plane with 65 % SiO_2 (Prokopowicz and Hummel, 1956 cited in "Phase Diagrams for Ceramists" (1968) vol. II, The Amer. Ceram. Soc., Columbus, Ohio, 601 p.)

The infra-red absorption spectrum indicates the existence of structural elements, ordered during crystal-

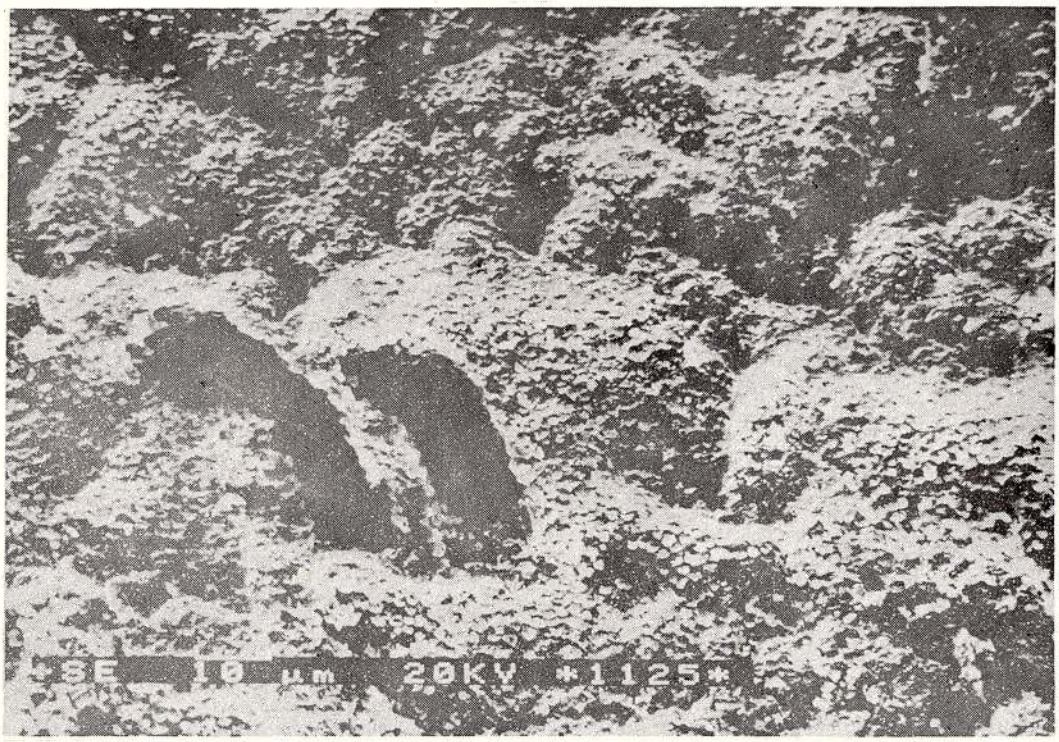

1

2

Plate

Fig. 1 – Crystallized area in the frame of a relict liquated structure, SEM picture.

Fig. 2 – Isometric crystals with maximum size of 2 µm. The glassy thin film has been disolved by corrosion with HF sample preparation, SEM picture.

lization so that their appearance is similar to that of standard (Fig. 4).

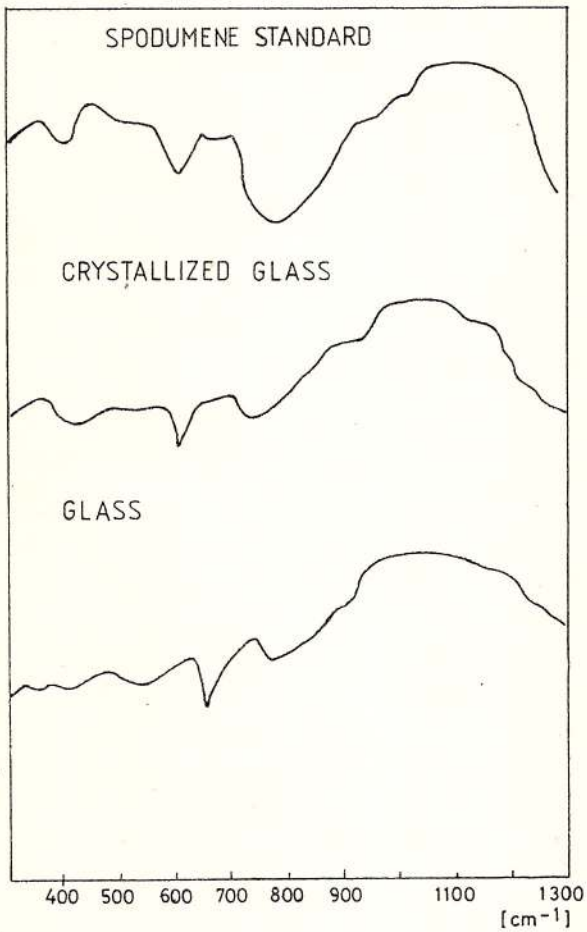

Fig. 4 IR absorption spectra of glass, crystallized-glass and standard (Conțu spodumene, Sibiu district).

Conclusions

The obtained synthetic rocks belong to the system Li_2O-MgO-Al_2O_3-SiO_2 and contain spodumene and "silica O" as crystalline phases. Pure TiO_2 was added as a crystallization stimulator in amounts varying between 2 and 4.8 %. The resulted product consists of isometric crystals of maximum 2 μm in size and a glassy thin film of less than ≤ 1 μm in thickness. By their reciprocical displacement and dimensions the two phases have a positive influence on the physical and mechanical properties of the glass-ceramic material. As a consequence, these results are the premises for future practical applications.

References

Amato S. (1973) La sinterisationne. *Ceramurgia*, 2, p. 68–72, Faenza, Italia.

Bezborodov M. A. (1982) Steklocristalinîe materiali. Izd. Nauka i tehnika, 254 p., Moskva.

Fedorovski I. A. (1963) Katalizirovanie kristallizatia stekla M-L (translated from russian – CERO reference library, Cluj-Napoca).

Junina I. A., Kuzmenkov M. I., Iaglov B. M. (1974) Pirocsenie sitalli. Izd. BGU "V. I. Lenin", 222 p., Minsk.

Kirsch M. (1990) Rutile Vitroceramics - a Novel Material for Microwawe Substrates. *Interceram*, 29, 2, p. 16–17, Freiberg.

Pavluskin N. M. (1979) Osnovî tehnologhii sitalov. Stroizdat, 260 p., Moskva.

*** (1968) Phase Diagrams for Ceramists, vol. II, 601 p. The Amer. Ceram. Soc., Columbus, Ohio, USA.

INSTRUCŢIUNI PENTRU AUTORI

ROMANIAN JOURNAL OF MINERALOGY publică contribuţii ştiinţifice originale în domeniile mineralogiei, cristalografiei, geochimiei mineralelor etc.

Vor fi acceptate numai lucrările care prezintă concis şi clar informaţii noi. Manuscrisul va fi supus lecturii critice a unuia sau mai multor specialişti; după a doua revizie nesatisfăcătoare din partea autorilor va fi respins definitiv şi nu va fi înapoiat.

Manuscrisele trebuie prezentate, de regulă, în engleză sau franceză; cele prezentate în limba română trebuie să fie însoţite de un rezumat, în engleză sau franceză, de maximum 10 % din volumul manuscrisului.

Lucrările trebuie depuse, în două exemplare, la secretariatul Comitetului de redacţie, inclusiv ilustraţiile în original. Manuscrisul trebuie să cuprindă: textul (cu o pagină de titlu, care este şi prima pagină a lucrării), bibliografie, cuvinte cheie, abstract, ilustraţii, explicaţii ale figurilor şi planşelor, şi un sumar cu scop tehnic.

Se va adăuga o filă separată cu un sumar, în care se va indica ierarhia titlurilor din text în clasificarea zecimală (1; 1.1; 1.1.1), care nu trebuie să depăşească patru categorii.

Textul va fi dactilografiat la două rînduri (31 rînduri/pagină şi 64 semne/rînd), pe o singură parte a colii, cu un spaţiu liber de 3–4 cm în partea stîngă a paginii şi nu trebuie să depăşească 20 pagini dactilografiate (inclusiv bibliografia şi figurile).

Prima pagină a textului va cuprinde: a) titlul lucrării (concis, dar informativ), cu un spaţiu de 8 cm deasupra; b) numele întreg al autorului (autorilor); c) instituţia (instituţiile) şi adresa (adresele) pentru fiecare autor sau grup de autori; d) colontitlu de maximum 60 semne. Notele de subsol se vor numerota consecutiv.

Citările din text trebuie să includă numele autorului şi anul publicării. Exemplu: Ionescu (1970) sau (Ionescu, 1970). Pentru doi autori: Ionescu, Popescu (1969) sau (Ionescu, Popescu, 1969). Pentru mai mult de doi autori: Ionescu et al. (1980) sau (Ionescu et al., 1980). Pentru lucrările care se află sub tipar, anul publicării va fi înlocuit cu "in press". Lucrările nepublicate şi rapoartele vor fi citate în text ca şi cele publicate.

Abstractul, maximum 20 rînduri, trebuie să fie în limba engleză şi să prezinte pe scurt principalele rezultate şi concluzii (nu o simplă listă cu subiecte abordate).

Cuvintele cheie (maximum 10) trebuie să fie în limba engleză sau franceză, corespunzător limbii în care este lucrarea (sau abstractul, dacă textul este în română), prezentate în succesiune de la general la specific şi dactilografiate pe pagina cu abstractul.

Bibliografia se va dactilografia la două rînduri, în ordine alfabetică şi cronologică pentru autorii cu mai mult de o lucrare. Abrevierile titlului jurnalului sau ale editurii trebuie să fie conforme cu recomandările respectivelor publicaţii sau cu standardele internaţionale.

Exemple:

a) jurnale:

Giuşcă, D. (1952) Contributions à l'étude cristallochimique des niobates. *An. Com. Geol.*, XXIII, p. 259–268, Bucureşti.

– , Pavelescu, L. (1954) Contribuţii la studiul mineralogic al zăcămîntului de la Muşca. *Comm. Acad. Rom.*, IV, 11–12, p. 658–991, Bucureşti.

b) publicaţii speciale:

Strand, T. (1972) The Norwegian Caledonides. p. 1–20. In: Kulling, O., Strand, T. (eds.) Scandinavian Caledonides, 560 p., Interscience Publishers.

c) cărţi:

Bălan, M. (1976) Zăcămintele manganifere de la Iacobeni. Ed. Acad. Rom., 132 p., Bucureşti.

d) hărţi:

Ionescu, I., Popescu, P., Georgescu, G. (1990) Geological Map of Romania, scale 1:50,000, sheet Cîmpulung. Inst. Geol. Geofiz., Bucureşti.

e) lucrări nepublicate sau rapoarte:

Dumitrescu, D., Ionescu, I., Moldoveanu, M. (1987) Report. Arch. Inst. Geol. Geofiz., Bucureşti.

Lucrările sau cărţile publicate în rusă, bulgară, sîrbă etc. trebuie menţionate în bibliografie transliterînd numele şi titlurile. Exemplu:

Krasheninnikov, V. A., Basov, I. A. (1968) Stratigrafiya kainozoia. Trudy GIN, 410, 208 p., Nauka, Moskow.

Ilustraţiile (figuri şi planşe) trebuie numerotate şi prezentate în original, pe coli separate (hîrtie de calc), bune pentru reprodus. Dimensiunea liniilor, a literelor şi simbolurilor pe figuri trebuie să fie suficient de mare pentru a putea fi citite cu uşurinţă după ce au fost reduse. Dimensiunea originalului nu trebuie să depăşească suprafaţa tipografică a paginii: lăţimea coloanei 8 cm, lăţimea paginii 16,5 cm, lungimea paginii 23 cm, pentru figuri, iar pentru planşele liniare nu trebuie să depăşească dimensiunile unei pagini simple (16,5/23 cm) sau duble (23/33 cm) şi trebuie să fie autoexplicativă (să includă titlul, autori, explicaţie etc.). Scară grafică obligatorie.

Ilustraţiile fotografice (numai alb-negru) trebuie să fie clare, cu contrast bun şi grupate pe planşe de 16/23 cm. In cadrul fiecărei planşe numărătoarea fotografiilor se repetă (de. ex. Pl. I, fig. 1, Pl. II, fig. 1).

Tabelele vor fi numerotate şi vor avea un titlu. Dimensiunea originală a tabelelor trebuie să corespundă dimensiunilor tipografice menţionate mai sus (8/16,5 sau 16,5/23).

Autorii vor primi un singur set de corectură, pe care trebuie să-l înapoieze, cu corecturile corespunzătoare, după 10 zile de la primire. Numai greşelile de tipar trebuie corectate; nu sînt acceptate modificări.

Autorii vor primi gratuit 30 de extrase pentru fiecare lucrare.

Comitetul de redacţie

INSTRUCTIONS TO AUTHORS

ROMANIAN JOURNAL OF MINERALOGY publishes original scientific contributions dealing with any subject in the field of mineralogy, crystallography, mineral geochemistry etc.

Only papers presenting concisely and clearly new information will be accepted. The manuscript will be submitted for critical lecture to one or several advisers. Papers will be definitely rejected after a second unsatisfactory revision by the authors. The manuscripts will not be returned to the authors even if rejected.

Manuscripts are prefered in English or French. Manuscripts submitted in Romanian will be accompanied by an abstract in English or French (maximum 10 per cent of the manuscript volume).

Papers should be submitted in duplicate to the secretary of the Editorial Board, including the reproduction ready original figures. The manuscript should comprise: text (with a title page which is the first page of it), references, key words, abstract, illustrations, captions and a summary for technical purposes.

The author(s) should add a separate sheet with a summary indicating the hierarchy of headings from the text listed in decimal classification (1; 1.1; 1.1.1) but not exceeding four categories.

The text should be double-spaced typed (31 lines/page with 64 strokes each line) on one side of the paper only, holding an empty place of 3–4 cm on the left side of the page. The text cannot exceed 20 typewritten pages (including references and figures).

The front page (first page of the text) should comprise: a) title of the paper (concise but informative) with an empty space of 8 cm above it; b) full name(s) of the author(s); c) institution(s) and address(es) for each author or group of authors; d) short title (colontitle) of maximum 60 strokes. Footnotes should be numbered consequtively.

Citations in the text should include the name of the author and the publication year. Example: Ionescu (1970) or (Ionescu, 1970). For two authors: Ionescu, Popescu (1969) or (Ionescu, Popescu, 1969). For more than two authors: Ionescu et al. (1980) or (Ionescu et al., 1980). For papers which are in course of print the publication year will be replaced by "in press". Unpublished papers or reports will be cited in the text like the published ones.

Abstract, of maximum 20 lines, must be in English, summarizing the main results and conclusions (not a simple listing of topics).

Key words (max. 10 items), in English or French, following the language used in the text (or the Resumé if the text is in Romanian), given in succession from general to specific, should be typed on the abstract page.

References should be typed in double-line spacing, listed in alphabetical order and chronological order for authors with more than one reference. Abbreviations of journals or publishing houses should be in accordance with the recommendations of the respective publications or with the international practice.

Examples:

a) journals:

Giuşcă, D. (1952) Contributions à l'étude cristallochimique des niobates. *An. Com. Geol.*, XXIII, p. 259–268, Bucureşti.

– , Pavelescu, L. (1954) Contribuţii la studiul mineralogic al zăcămîntului de la Muşca. *Comm. Acad. Rom.*, IV, 11–12, p. 658–991, Bucureşti.

b) special issues:

Strand, T. (1972) The Norwegian Caledonides. p. 1–20. In: Kulling, O., Strand, T. (eds.) Scandinavian Caledonides, 560 p., Interscience Publishers.

c) books:

Bălan, M. (1976) Zăcămintele manganifere de la Iacobeni. Ed. Acad. Rom., 132 p., Bucureşti.

d) maps:

Ionescu, I., Popescu, P., Georgescu, G. (1990) Geological Map of Romania, scale 1:50,000, sheet Cîmpulung. Inst. Geol. Geofiz., Bucureşti.

e) unpublished papers or reports:

Dumitrescu, D., Ionescu, I., Moldoveanu, M. (1987) Report. Arch. Inst. Geol. Geofiz., Bucureşti.

Papers or books published in Russian, Bulgarian or Serbian etc. should be mentioned in the references transliterating the name and titles. Example:

Krasheninnikov, V. A., Basov, I. A. (1968) Stratigrafiya kainozoia. Trudy GIN, 410, 208 p., Nauka, Moskow.

Illustrations (figures and plates) must be numbered and submitted as originals on separate sheets (tracing papers), ready for reproduction. The thickness of the lines, lettering and symbols on figures should be large enough to be easily read after size-reduction. The original size should not extend beyond the print area of the page: column width 8 cm, page width 16.5 cm, page length 23 cm for figures; the width of line drawings should not extend over a single (16.5/23) or double (23/33 cm) page area and must be selfexplanatory (including title, authors, legend etc.). The graphic scale is obligatory.

Photographic illustrations (black-and-white only) must be of high quality and should be grouped into plates 16/23 cm in size. Each plate should have the photos numbered, i.e. Pl. I, Fig. 1; Pl. II, Fig. 1.

Tables should be numbered and entitled. Original size of the tables should correspond to the above mentioned (8/16.5 or 16.5/23) dimensions of the printing area.

Author(s) will receive only one set of preprint proofs which must be returned, with corrections, 10 days after receiving them. Only printing errors should be corrected, no changes in the text can be accepted.

Thirty offprints of each paper are supplied to the author(s) free of charge.

The Editorial Board

(Contents continued from front cover)